Technische Universität München

TUM School of Engineering and Design

Metabolic Engineering in *Halomonas elongata* for enhanced production of compatible solutes

Karina Anna Hobmeier

Vollständiger Abdruck der von der TUM School of Engineering and Design der Technischen Universität München zur Erlangung einer Doktorin der Ingenieurwissenschaften (Dr.-Ing.) genehmigten Dissertation.

Vorsitz: Prof. Dr. rer. nat. Sonja Berensmeier

Prüfer der Dissertation:
1. TUM Junior Fellow Dr. Alberto Marin Sanguino
2. Priv. Doz. Dr. rer. nat. habil. Hans-Jörg Kunte
3. Prof. Dr.-Ing. Andreas Kremling

Die Dissertation wurde am 03.11.2022 bei der Technischen Universität München eingereicht und durch die TUM School of Engineering and Design am 15.03.2023 angenommen.

Why do you limit your choices? -Abel

Danksagung

Diese Dissertation konnte durch drei Jahre aktive Forschungsarbeit an der Professur für Systembiotechnologie an der TUM und anschließend einer weiteren (großzügigen) Zeit zur Ausarbeitung der gewonnenen Erkenntnisse entstehen. Zu Beginn meines Studiums wäre mir nicht im Traum eingefallen, einmal an diesem Punkt zu sein. Auf meine Zeit am Lehrstuhl schaue ich mit etwas Wehmut zurück, da es sich für mich rückblickend wirklich um einen der schönsten Abschnitte in meinem bisherigen Leben gehandelt hat. Dies zum einen durch die spannende und sehr abwechslungsreiche Arbeit, aber natürlich besonders durch all die Menschen, die ich währenddessen sehr ins Herz geschlossen habe.

Allen voran meinen Doktorvater Dr. Alberto Marin Sanguino. Vielen Dank für den Nachdruck, bevor ich diese Arbeit überhaupt angenommen habe, für das Vertrauen, dass ich den Aufgaben gewachsen bin, und den großen Rückhalt und die Unterstützung nicht nur in der Zeit am Lehrstuhl, sondern auch darüber hinaus. Für mich war es ein Glücksgriff, einen Betreuer zu haben, der mir an der Stelle die Freiheiten gegeben hat, wo ich sie brauchte, und die Anleitung gegeben hat, wo ich sie nötig hatte. Immer ein offenes Ohr, gefühlt 24/7, und stets mit guter Laune bist du mit mir in eine für mich ganz neue Welt der Wissenschaft hineingerutscht von der ich mich bis heute nicht trennen kann. Nuestro trabajo en conjunto me ha significado mucho.

Herzlich bedanken möchte ich mich auch bei Prof. Dr.-Ing. Andreas Kremling und Dr. Katharina Pflüger-Grau (Kathi), die mich fachlich unterstützt haben, aber auch dafür gesorgt haben, dass ich mich nicht in der Wissenschaft verlaufe und zur Promotion auch Bürokratie und Deadlines gehören. Ohne wäre es eventuell nicht zu dieser schriftlichen Ausarbeitung gekommen.

Ein weiteres herzliches Dankeschön an das ganze HOBBIT Team und speziell an Dr. Hans-Jörg Kunte und Prof. Dr. Sonja Berensmeier - danke für das Übernehmen der Prüfungsfunktionen. Die Zusammenarbeit während der Dissertation und weiterhin schätze ich sehr. Außerdem (demnächst Dr.) Lea Martin, mit der die unschlagbare *Halomonas* USP/DSP-Kombo entstand, und Dr. Martina Cantone, die mich innerhalb dieser drei Jahre in eine (mehr oder weniger) gute Coderin verwandelt hat. Mit euch beiden habe ich Freunde fürs Leben gefunden.

Weiterhin möchte ich mich bei allen meinen SBT/STT/BVT Kollegen für die gute Zusammenarbeit und das unglaublich gute Arbeitsklima bedanken. Auch wenn die Versuche manchmal nicht so wollten, bin ich immer gerne nach Garching gefahren. Danke für den Spaß und die lockere Atmosphäre, die Diskussionen und Ratschläge, das Gründen der Jogging-Gruppe, die Waffeln und den Espresso. Namentlich erwähnen muss ich dabei meine lieben STTler Stefan, Basti und Tobi. Meine Kollegen vom SBT dürfen dabei aber auch nicht zu kurz kommen. Die alte Riege - Hannes, Sabine und Sayuri-Chan - die für mich als SBT-Küken auch zum Mentor wurden, und die neue Generation - Ana, Thi und Franzi - die ich als lange Zeit einzige SBTlerin sehnlichst erwartet hatte. Ein besonderes Dankeschön gebührt meinem Lieblings-TA Stefan Darchinger. Auch hier kann ich sagen, dass wir uns bestimmt nicht das letzte Mal gesehen haben. Eine weitere Person, die nicht vergessen werden darf: Marie Goess. Ohne dich wäre die anfängliche Zeit nie so schön gewesen und ich hätte fix nicht als Doktorandin angefangen.

Ich möchte mich auch bei alle meine Studenten und Studentinnen für ihre Arbeit bedanken: Nadja Sommer, Quynh Anh Nguyen, Natalie Stasinski, Stephan Liefeldt, Martin Oppermann und Eva Weiland. Es freut mich, dass wir mit einigen eurer Daten bereits Paper veröffentlichen konnten.

Furthermore, many thanks to my friends from the UDL: Rui, Ester, Abel, Oriol, Marti, Ricardo and Jordi. I went to Spain not knowing what to expect but the time with you makes me consider Alberto's suggestion for a Post Doctorate. Thank you for being so welcoming and making my stay there unforgetable.

Zu guter Letzt bedanke ich mich bei meiner Familie und Freunden. Es war bestimmt nicht immer leicht mit mir - den Stimmungsschwankungen je nach Erfolg im Labor geschuldet. Danke euch, dass ich immer auf euch zählen konnte und kann.

Abstract

The moderate halophilic γ-proteobacterium *Halomonas elongata* isolated from solar salterns shows a remarkably wide range of salt tolerance, growing well above concentrations of 10 % NaCl. Central to its osmoadaptation mechanism is the *de novo* synthesis of ectoine – a highly soluble organic compound of low molecular weight. Even though this microbe follows the organic osmolyte strategy to achieve its salt tolerance, there are implications that there is more to it than solely the accumulation of ectoine. A closer look at the regulation of the *H. elongata* metabolome, especially in the context of varying salt concentrations, revealed some of its special features. Its OAA decarboxylase OAD was found to be a reversible membrane-bound Na^+-pump, which is actively involved in the anaplerotic flux if the salt gradient is high enough. This constitutes a parallel pathway to the conventional PEP carboxylase PEPC reaction. Both pathways share the anaplerotic role with the distribution dependent on the salt conditions. At low salt concentrations, OAD is rendered inviable due to the diminished sodium gradient. The previous suggestion of the Entner-Doudoroff pathway as the main pathway for glucose catabolism in this microbe was further supported by results obtained by RNA-Sequencing (RNA-Seq). It further revealed the possibility of a great variety of metabolic modes in *H. elongata*. At low salt conditions, indications for major problems in the membrane potential and membrane depolarization were found, hinting towards an issue with the proton gradient. A likely assumption is that the sodium gradient created across the membrane complements the proton motive force (pmf) via the Na^+/H^+-antiporters. At low salt concentrations the cytoplasmic sodium concentration is not low enough to create the necessary sodium motive force (smf) to complement the pmf adequately. This implies that the cytoplasmic sodium concentration of *H. elongata* is higher compared to regular non-halophiles, which is also supported by the higher acidity of its proteome. Interestingly, no salt-related protein folding or oxidative stress response was found in the RNA-Seq. The biggest impact at the transcriptomic level was found for motility-related genes. The expression of chemotaxis and flagellar genes were severely downregulated at low salinity. Peculiarly, this behavior for motility-related genes was also observed in two modified strains *H. elongata* Δ*teaABC* Δ*doeA* (Leaky Mutant) and *H. elongata* Δ*teaABC* Δ*doeA* Δ*pckA*. Both of these mutant strains were generated to feature favorable modifications towards ectoine production and excretion. The deletion of the *tea* operon leads to the secretion of ectoine into the extracellular space and the deletion of *doeA* abolishes its break down. The additional removal of the PEP carboxykinase gene *pckA* leads to a higher anaplerotic flux towards precursors in the biosynthetic pathway resulting in an increased extracellular ectoine titer by about 45 %. But not only the secretion of ectoine was affected. In *H. elongata* Δ*teaABC* Δ*doeA* Δ*pckA* and another further modified strain *H. elongata* Δ*teaABC* Δ*doeA* Δ*pckA* Δ*ppc* a higher concentration is accumulated in the cytoplasm compared to the parental strain *H. elongata* Δ*teaABC* Δ*doeA*. In general, intracellular ectoine levels are strictly controlled. The fact that all of these strains differ significantly from each other indicates that the control mechanisms are disrupted, which supports the hypothesis of a circulating ectoine feedback regulation. A concept like this with ectoine cycling between the cytoplasm and periplasm has already been proposed in the literature. A complementary attempt to increase the secretion was achieved by overexpression of the transmembrane proteins of the TeaABC transporter in *H. elongata* Δ*teaABC* Δ*doeA*. Essentially, without the substrate binding protein TeaA the expression of the transmembrane modules TeaBC facilitates the increased excretion of ectoine leading to a higher ectoine yield of 57 - 70 % depending on the expressed protein. Another big potential for improving an ectoine producer strain was identified in regards to nitrogen assimilation. The GS/GOGAT pathway was determined to be the only available pathway for ammonium assimilation in *H. elongata* using a *gltDB* (GOGAT) knockout mutant. By replacing the energy-intensive GS/GOGAT reaction with a glutamate dehydrogenase (GDH) reaction the mutant strains *H. elongata* Δ*gltDB*::Sm^R Δ*gdh*::*gdhA* and *H. elongata* Δ*teaABC* Δ*doeA* Δ*gltDB*::Sm^R Δ*gdh*::*gdhA* were generated. Another investigated modification was the deletion of the ectoine synthase gene *ectC* in the wild type generating strains that accumulate the ectoine

precursor Nγ-acetyl-L-2,4-diaminobutyric acid (γ-NADA). These γ-NADA producers exhibit a reduced salt tolerance which is already apparent at moderate concentrations of 6 % NaCl. But in contrast to the wild type, the compatible solute content increases over time. This again supports the hypothesized mechanism of ectoine regulation which links the regulation directly to ectoine as a molecule itself.

Contents

Acronyms

$B(t)$ Biomass.

K_S Michaelis-Menten constant.

$S(t)$ substrate.

T temperature.

$Y_{\frac{S}{X}}$ Biomass yield coefficient.

$\Delta \boldsymbol{G}_{D,water-cs}$ Change in ΔG from water to in presence of compatible solutes for denatured proteins.

$\Delta \boldsymbol{G}_{N,water-cs}$ Change in ΔG from water to in presence of compatible solutes for native proteins.

$\Delta \boldsymbol{G}_{cs,den}$ ΔG for denaturation in presence of compatible solutes.

$\Delta \boldsymbol{G}_{water,den}$ ΔG for denaturation in water.

$\Delta \boldsymbol{H}_W$ Change in enthalpy.

$\Delta \boldsymbol{S}_W$ Change in randomness.

ΔG Gibbs free energy.

α-NADA Nα-acetyl-L-2,4-diaminobutyric acid.

γ-NADA Nγ-acetyl-L-2,4-diaminobutyric acid.

$\mu(t)$ Specific growth rate.

μ_W Chemical potential of the water.

μ_{max} Maximum specific growth rate.

A. calcoaceticus *Acinetobacter calcoaceticus*.

A. succiniproducens *Anaerobiospirillum succiniproducens*.

B. subtilis *Bacillus subtilis*.

B. thuringiensis *Bacillus thuringiensis*.

C. glutamicum *Corynebacterium glutamicum*.

C. necator *Cupriavidus necator*.

C. salexigens *Chromohalobacter salexigens*.

E. coli *Escherichia coli*.

E. halochloris *Ectothiorhodospira halochloris* (now: *Halorhodospira halophila*).

E. hirae *Enterococcus hirae*.

H. beimenensis *Halomonas beimenensis*.

H. campaniensis *Halomonas campaniensis*.

H. elongata *Halomonas elongata.*

H. halochloris *Halorhodospira halochloris.*

H. isrealensis *Halomonas isrealensis.*

H. mediterranei *Haloferax mediterranei.*

H. salina *Halomonas salina.*

M. mazei *Methanosarcina mazei.*

M. smegmatis *Mycobacterium smegmatis.*

P. acidophila *Pseudomonas acidophila.*

P. aeruginosa *Pseudomonas aeruginosa.*

P. extremaustralis *Pseudomonas extremaustralis.*

P. putida *Pseudomonas putida.*

R. capsulatus *Rhodobacter capsulatus.*

R. sphaeroides *Rhodobacter sphaeroides.*

S. cerevisiae *Saccharomyces cerevisiae.*

S. costicola *Salinivibrio costicola.*

S. ruber *Salinibacter ruber.*

T. aquaticus *Thermus aquaticus.*

T. thermophilus *Thermus thermophilus.*

V. alginolyticus *Vibrio alginolyticus.*

V. aliginolyticus *Vibrio aliginolyticus.*

V. cholerae *Vibrio cholerae.*

V. parahaemolyticus *Vibrio parahaemolyticus.*

2-KGT 2-ketoglutarate.

2K3D6PG 2-keto-3-deoxy-6-phosphogluconate.

3-CB 3-chlorobenzoic acid.

3-MB 3-methylbenzoic acid.

4-MB 4-methylbenzoic acid.

6PG 6-phosphogluconate.

ABR Antibiotic resistance.

AcCoA Acetyl-CoA.

AFDW Ash-free dry weight.

Am Ampicillin.

ANR transcriptional regulator.

ASA Aspartate-β-semialdehyde.

ATP Adenosine triphosphate.

BAM Bundesanstalt für Materialforschung und -prüfung.

bitop Company developing and distributing products based on ectoine.

bp Base pair.

cDNA Complementary DNA.

CRISPR-Cas9 Genome editing tool for alteration of specific DNA sequences.

cs compatible solutes.

D denatured.

$\mathbf{D}_{cs}$ denatured proteins in environment with compatible solutes.

$\mathbf{D}_{water}$ denatured proteins in water.

DABA 2,4-diaminobutyric acid.

DHP Dihydroxyacetone phosphate.

DNA Deoxribonucleic acid.

DoE Design of experiment.

DW Dry weight.

ectoine (S)-2-Methyl-1,4,5,6-tetrahydropyrimidine-4-carboxylic acid.

ED Entner-Doudoroff.

eGFP Enhanced green fluorescent protein.

EMP Embden-Meyerhof-Parnas.

ETC Electron transport chain.

F6P Fructose-6-phosphate.

FAD Flavin adenine dinucleotide.

FAD-GADH flavin adenine dinucleotide-gluconate dehydrogenase.

FBA Flux balance analysis.

FBP Fructose-1,6-bisphosphate.

FC Fold change.

FDA United States Food and Drug Administration.

FNR transcriptional regulator.

FPKM Fragments per kilo-base million.

G3P Glyceraldehyde-3-phosphate.

G6P Glucose-6-phosphate.

GC guanine-cytosine content.

GDH Glutamate dehydrogenase.

Gm Gentamicin.

GOGAT Glutamate synthase.

GOI Gene of interest.

GS Glutamine synthetase.

GSSG glutathion, oxidized form.

HGM *Halomonas* growth medium.

HPF Hibernation promoting factor.

HPLC High-Performance Liquid Chromatography.

HS High salinity.

IR Infrared radiation.

KDPG 2-keto-3-deoxy-6-phosphogluconate.

Km Kanamycin.

LB lysogeny broth.

LM Leaky Mutant.

LS Low salinity.

MAL Malate.

Mass% Mass percent.

MCS Multiple cloning site.

MDH MAL dehydrogenase.

ME malic enzyme.

Met-R-SO methionine-(R)-sulfoxide.

Met-S-SO methionine-(S)-sulfoxide.

MM63 minimal medium 63.

MS Mass Spectrometry.

N native.

$\mathbf{N}_{cs}$ native protein in environment with compatible solutes.

N_{water} native protein in water.

NAD nicotinamide adenine dinucleotide.

NAD-ME NAD-dependent malic enzyme.

NADP nicotinamide adenine dinucleotide phosphate.

NADP-ME NADP-dependent malic enzyme.

NGS Next generation sequencing.

NO nitric oxide.

NQR Na^+-translocating NADH-quinone reductase.

O-GlcNAc O-linked N-acetylglucosaminyl.

$O2^-$ superoxide radicals.

OAA Oxaloacetate.

OAD OAA decarboxylase.

OD600 Optical density at wavelength 600 nm.

OPT Salt optimum.

ORF Open reading frame.

oriV origin of replication.

PC Pyruvate carboxylase.

PCR Polymerase Chain Reaction.

PEP Phosphoenolpyruvate.

PEP-PYR-OAA node Phosphoenolpyruvate-Pyruvate-Oxaloacetate node.

PEPC PEP carboxylase.

PEPCK PEP carboxykinase.

PHA Poly-hydroxyalkanoate.

PHB Poly-hydroxybutyrate.

pmf Proton motive force.

PP_i Inorganic pyrophosphate.

PPP Pentose-phosphate pathway.

PQQ pyrroloquinoline-quinone.

pSEVA Plasmid of Standard European Vector Architecture.

PTS^{Fru} Fructose-specific phosphotransferase transport system.

PYR Pyruvate.

RBS Ribosoal binding site.

RLU relative light unit.

RMF Ribosomal modulation factor.

RNA-Seq RNA-Sequencing.

ROS Reactive oxygen species.

RP-HPLC Reverse-Phase High-Performance Liquid Chromatography.

RPKM Reads per kilo-base million.

rRNA Ribosomal RNA.

RT room temperature.

SARS-CoV-2 Severe acute respiratory syndrome coronavirus type 2.

SBP Substrate binding protein.

Sm Streptomycin.

smf Sodium motive force.

STA Simultaneous Thermal Analysis.

TCA Tricarboxylic acid.

TGA Thermogravimetry Analysis.

TPM Transcripts per million.

TRAP Tripartite ATP-independent periplasmic transporter.

tRNA Transfer RNA.

USD US Dollar.

UVA Ultraviolet A rays.

UVB Ultraviolet B rays.

YK-R (reduced) Yano-Koga substrate inhibition model.

1 Introduction and objective

We are living in times in which our knowledge is increasing faster and faster. In his 1982 book *Critical Path*, R. Buckminster Fuller first proposed the *'Knowledge Doubling Curve'*, stating that until 1900 human knowledge doubled every 100 years and by 1945 it was doubling every 25 years. Nowadays, in 2020, it is approximated that human knowledge doubles every 12 hours. With this in mind, it seems that in the 21^{st} century, knowing how to learn has become as important as the knowledge itself.
With the digital revolution starting by the end of the 20^{th} century and the improvements made possible by digitalization, especially in connection to other fields, possibilites of new and unknown potential were opened up. Within the concept of *'Industry 4.0'* digitalization and industry were interconnected. For biotechnology this entailed the incorporation of digital systems in biotechnological research and production, which allowed development and commercialization of techniques without precedent such as Next generation sequencing (NGS) and metabolome studies. For years, people have been inspired by technological and scientific advances letting their imagination run wild while envisioning the possibilities for our future. The ideas expressed in science fiction have always been ahead of science in real life. However, looking back at fictional works of the last century, modern day biotechnology is catching up, closing the gap between fiction and reality rapidly. Things that were once deemed impossible are now within reach.
Back in 1997, the movie *'Gattaca'* portrayed a future in which editing the human genome for eugenic purposes is commonplace. Children born without such intervention are seen as inferior and prevented from taking on higher employment opportunities, being reduced to take only menial jobs. Today, genome sequencing has become much more accessible to the point where various companies are focusing on genetic tests targeted at private individuals. They can be done at home and are mostly used for reviewing genealogy, but some also determine the health risks for hereditary cancers and other conditions. Also, the groundbreaking discovery of CRISPR-Cas9 as a genome editing tool in the last decade enabled tremendous possibilities in the engineering of genes. The case of the first CRISPR-edited infants in China surfacing in 2018, however, raised massive discussions about the ethical implications of such practices. Certainly, this technique can be used to prevent devastating diseases but the red line between the prevention of serious illnesses and generating *'designer babies'* is not easily defined. In any case, recently biotechnology is moving so fast that the science fiction of yesterday is becoming the reality of today.
Another example is the well known movie, *'Jurassic Park'* from 1993, based on the 1990 novel. The topic of genomics and genetic engineering is addressed here as well. In this fictional work, dinosaur DNA is discovered from preserved blood fossilized in amber. With the DNA samples, scientists are able to clone various dinosaur species, effectively bringing these creatures, which went extinct 65 million years ago, back to life. Granted, we have not yet revived dinosaurs and no genetic information can survive for more than a million years, making it practically impossible [44, 214]. But in 2003, the first extinct animal – the Pyrenean ibex - was resurrected by cloning. In the end, the newborn died only minutes after birth due to respiratory issues. However, similar ambitions have not been deterred from bringing back extinct species, and there are already proposals to revive the woolly mammoth, whose DNA sequence was reconstructed nearly completely in 2008. The Harvard University geneticist George Church has long since been working on bringing back the species by manipulating the genome of elephant embryos. But apart from the advances done in resurrecting extinct species, genetic engineering is widely applied in all kinds of fields, for instance, in medicine or agriculture. In medicine, the microbe *Escherichia coli* is used as a producer for insulin or human serum albumin and about 30 % of the FDA approved biopharmaceuticals are produced in bacterial hosts [164]. In agriculture, a prominent example is the development of *'Bt corn'* which also lead to some ethical discussion about such artificial manipulations. Essentially, the insecticidal protein Cry1Ab discovered in *Bacillus thuringiensis* confers insect resistance to corn plants. With the plants exhibiting a higher insect resistance farmers need to

apply less insecticide to their crops.
The manipulation of microbes for our benefit has been done in many different forms: from using yeasts for the manufacturing of beer to recombinant DNA technologies production of various proteins in *E. coli* like insulin, monoclonal antibodies, and many others. Another such example is the production of the compatible solute ectoine in the extremophilic bacterium *Halomonas elongata*. This naturally synthesized amino acid derivate has many possible applications from medicinal to cosmetical use. In medicinal products, ectoine treats the disruption of epithelial barriers like skin or mucosal epithelial cells. The stabilizing effect of ectoine alleviates the symptoms of such ailments and can be administered in various application forms like transdermal or inhalation preparations. In cosmetics, ectoine shows its effectiveness as a skin protectant against many environmental stresses, most prominently UVA/UVB and IR radiation. However, it is not merely a protectant but also promotes the repair and moisturization of the natural skin barrier. Another positive quality of ectoine was found for its effect on other biomolecules as a stabilizer against denaturation. In the presence of ectoine, the loss of activity for enzymes or antibodies is strongly diminished. Its positive effects as a stabilizer and protectant have already been recognized in an industrial setting and led to the production of this attractive biomolecule by the company bitop in a scale of tons each year [120].
Most recently, in the face of the COVID-19 pandemic, which has been ongoing on a global scale since 2019, it was also claimded that ectoine inhibits the COVID-19 respiratory SARS-CoV-2 infection [17]. In the first step of the infection process, the spike protein (S-protein) attaches to the ACE2 receptor found abundantly on the outside of human throat and lung cells. After the binding of the virus's spike protein, the fusion of the viral membrane with the host cell is mediated. In *in vitro* studies, it was shown that a concentration of 1.25 – 5 % ectoine efficiently inhibits the binding of the S-protein to cells presenting the ACE2 receptor. By accumulating around both the cell membrane and the virus protein, ectoine creates a hydrate envelope. This has a stabilizing effect on the folded protein and reduces the accessibility of the receptor-binding domain in the process. Thus, ectoine is not only a highly valuable product in its regular application forms but also shows great potential as a tool in the fight against COVID-19 related diseases.
A compound closely related to ectoine but with a distinctly different structure is Nγ-acetyl-L-2,4-diaminobutyric acid (γ-NADA). As the direct precursor in the biosynthetic pathway for ectoine, this molecule shows up in the ectoine production process and in rare cases has been reported as an osmolyte on its own [131]. In the context of expanding the product spectrum and finding novel compounds with special properties γ-NADA is of special interest due to its similarities to ectoine as an aspartate amino acid derivate but with a linear structure. The typical structure of the ectoine carboxamidine heterocycle is only created by condensation of the linear γ-NADA. Due to these differences, there is a genuine potential of this novel compound in similar applications or others like polymerization.

The goal of this work is to examine various possibilites for the improvement of a ectoine producer strain targeting different key points in the *H. elongata* metabolic network and streamlining it towards ectoine synthesis. For this, it is necessary to examine and characterize the *Halomonas elongata* wild type and the regulation of its metabolism to understand the inner workings of its osmoadaptation, which is inevitably interconnected with the *de novo* synthesis of ectoine and other products derived thereof. With the knowledge gained from the underlying basic organization of its metabolism, the natural compatible solute accumulation in this microbe can be artificially enhanced by genetic modification to maximize its product yield.

2 Theoretical Background

2.1 Extremophilic organisms and halophiles in particular

Microbes were the first living beings on earth and dominated life on the planet nearly three billion years ago. Around this time, earth was not in its current habitable state. It is assumed that the temperature in the oceans was elevated and the atmosphere was strictly anoxic due to frequent volcanic eruptions. These environments are considered extreme in today's point of view, but high temperatures or pressures might have once been the norm [1, 65]. Therefore, the emergence of extremophiles, which are adapted to such harsh living conditions, should not be surprising. Extreme environments are defined by an extreme value of one or more physiochemical parameters like temperature, pressure, pH, or salinity. Today, microorganisms adjusted to such conditions are only found in special niches in the environment. For example, thermophiles adapted to high temperatures can be found in hot springs, piezophiles growing under high hydrostatic pressure exist in deep-sea habitats, or the combination of the two with thermo-piezophiles, which have been isolated at deep-sea hydrothermal vents. In general, the biggest hurdles for microorganisms in these harsh environments are energy acquisition and the stability of their biomolecules. To allow the operation of biological processes, their enzymes also need to be adapted to the extreme conditions [65, 224]. One of the most prominent examples in this regard is the discovery *Thermus aquaticus* by Thomas D. Brock [29]. With the stability of its DNA polymerase (Taq DNA polymerase) at high temperatures, the development of the Polymerase Chain Reaction (PCR) technique was made possible, which revolutionized DNA research at the time.
Another type of extremophiles - halophiles - are especially adapted to high salinity. 70 % of the earth's surface is covered by oceans, containing seawater with a salinity of approximately 3.5 % ($\approx$ 0.6 M NaCl). Therefore, it is not surprising that microbes living in this niche build their metabolism to work most efficiently in saline conditions. This osmoadaptation needs to be clearly separated from osmoregulation, which can also be observed in non-halophilic microorganisms like *Escherichia coli*. True osmoadaptation manifests itself distinctly in physiological and genetic adjustments [65]. But seawater is not the limit. There are halophiles growing in hypersaline conditions like salt lakes and salterns with concentrations of up to the NaCl solubility limit. Depending on the preferred range for optimal growth halophiles are classified into groups: slightly (0.2 – 0.5 M), moderately (0.5 – 2.0 M), borderline extremely (2.0 – 3.0 M), and extremely halophilic (3.0 – 4.0 M). However, an upper limit can hardly be defined. Even in saturated NaCl conditions growth of extremely halophilic microorganisms has been observed [224, 243]. The most important objective in hyperosmotic conditions is to prevent water loss by compensating osmolarity. For the biotechnological industry, halophiles are of great interest because of the special properties of their enzymes or the production of special metabolites counteracting the salt-induced stress but also because they grow efficiently at high pH and high NaCl concentrations, at which most other microorganisms cannot survive. In a continuous cultivation even under unsterile conditions this easily prevents contamination. It is commonly known that in direct comparison to the chemical industry, biotechnological processes have high production costs. In order to compete with chemical synthesis on an industrial scale, production costs including expensive substrates or large amounts of fresh water need to be kept as low as possible. Thus, the potential of halophilic organisms in biotechnology growing in open, unsterile, and continuous fermentation processes with abundantly available seawater, in contrast to fresh water and energy-intensive sterilization steps in common bioprocesses, is an intriguing concept [243]. In this context, the biotechnological cultivation of halotolerant bacterial strains of the genus *Halomonas* has been conducted successfully before. Johnson *et al.* [94] carried out a 3-year fermentation process for the production of poly-hydroxyalkanoates (PHA) in a mixed culture of dominantly γ-proteobacteria. Another open process for bioplastic production was performed by Yue *et al.* [246] with the strain *Halomonas campaniensis* LS21 for 65 days. The advantages of traditional industrial workhorses in biotechnology

like *E. coli* are largely connected to their well characterized genetics and cellular functions. The easy genetic manipulation contributed to the development of methods and tools for modifications. As of late, genetic manipulation methods are also being developed for halophiles in particular [64]. The CRISPR-Cas9 technology, which has revolutionized genome editing [177] has also been employed in *Halomonas* ssp. by Qin *et al.* [175]. With continuous advances in this respect, eventually, the potential of halophiles in biotechnological processes can be successfully utilized.

2.2 The chemistry of saline environments

To understand the special ability of halophilic organisms to thrive in saline environments, it is necessary to discuss why non-halophiles are hampered by salt. The presence of NaCl drastically changes the characteristic properties of water like the freezing point or the osmotic pressure. This is caused by the decrease in chemical potential of the water μ_W, which can be calculated using the change in enthalpy ΔH_W, the temperature T, and the change in entropy ΔS_W with the equation:

$$\mu_W = \Delta H_W - T \cdot \Delta S_W \tag{2.1}$$

With the impact of the second term $T \cdot \Delta S_W$ being stronger, the chemical potential is mainly determined by the entropy of the water [202]. The introduction of NaCl in the ordered water structure increases the randomness ΔS_W and, therefore, reduces the chemical potential of the water μ_W. With this in mind, in a saline environment, the free water in a cell, from which NaCl is deterred from by biological membranes and active export, has a higher potential than the water in the extracellular space. In a gradient, chemical species flow towards the lower potential and, consequently, the higher intracellular water potential causes the water to diffuse through the water-permeable cytoplasmic membrane out of the cell. This loss of cytoplasmic water leads to the cells shriveling up and experiencing other effects of dehydration like molecular crowding and reduced diffusion rates. In Figure 2.1, the impact of the solute concentration in the environment on cells is illustrated. Ideally, the environment is isotonic with the same concentration of solutes in the intracellular and extracellular space. As described above, in hypertonic conditions, when the solute concentration is higher in the surroundings, the lower extracellular water activity outside of the cell leads to dehydration. In contrast, in a hypotonic environment, the reverse effect is happening and water from the extracellular space is drawn into the cell, effectively inflating them and eventually causing them to burst [65, 77, 119].

2.3 Salt-in vs. organic-osmolyte strategy

In a saline environment, the loss of cytoplasmic water due to the differences in water potential needs to be prevented by reducing μ_W in the cytoplasm. There are two strategies employed by halophiles: the salt-in and the organic-osmolyte strategy [65, 77, 119, 163].

Salt-in strategy. In the salt-in strategy, the water potential is adjusted by increasing the concentration of KCl in the cytoplasm. Because of this, the intracellular salt concentration of halophiles using this strategy can reach even molar levels. To keep up cellular functions, the whole protein chemistry is adapted to these elevated salt concentrations and the proteome of such halophiles is highly acidic, especially the protein surfaces, to improve their solubility. Other observed changes are a reduction in hydrophobic residues and serine residues, in particular, which preferably interacts with water [224]. The salt-in strategy is a low-energy cost strategy since no additional expenses are added and the whole metabolism is altered. The downside is the narrow nature of this adaptation. Because it is highly specialized for high salt concentrations halophiles employing this strategy can only grow in these extreme environments and their enzymes are not functional without salt. Typically, archaea use this adaptation mechanism but some exceptions in bacteria do exist with *Salinibacter ruber* and a special group of *Halanaerobiales* [77, 163].

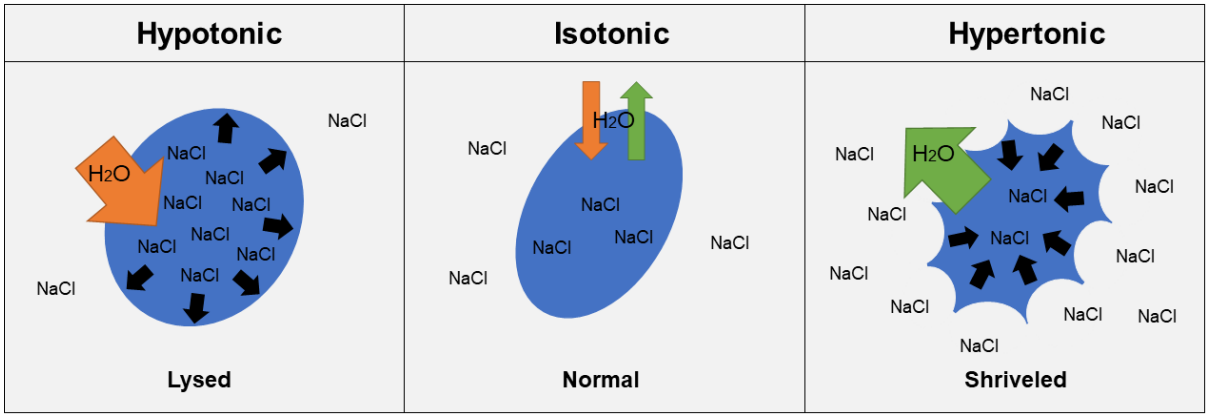

Figure 2.1: Overview of different solute environments and the consequences for the cell turgor caused by an imbalance of the water potential. In a hypotonic environment (left) the solute concentration on the outside is lower causing an influx of water and an increase of turgor pressure which poses the risk of bursting of the cell. In an isotonic environment (center) the solute concentration is balanced. In an hypertonic environment (right) the solute concentration on the outside is higher, which is representative of a high salinity environment. The imbalance in water potential causes an efflux of cytoplasmic free water and dehydration of the cell.

Organic osmolyte strategy. The alternative organic-osmolyte strategy is, on the other hand, widespread among bacteria and methanogenic archaea. It is also the most common solution to osmoadaptation [65]. In contrast to the salt-in strategy, the organic-osmolyte strategy is more energy-expensive [163] but its distinct advantage is its flexibilty to different salt levels. The reduction of the water potential μ_W is achieved by the intracellular accumulation of osmoprotective compounds. These are organic highly water soluble polar solutes with no net charge. For simplicity, they are called *'compatible solutes'* due to their compatibility with the cell's metabolism, showing no negative effect even at high concentrations. This is explained by the preferential exclusion model, which states that due to the structurally dense water bound to the proteins, compatible solutes are absent from protein surfaces. They prefer the free water portion in the cytoplasm and avoid interaction [119]. By accumulating these osmolytes, the cytoplasm stays free of ions and the interior of the cell and the enzymatic machinery remain similar to non-halophiles. So far, many osmolytes have been identified: sugar polyols like glucosyglycerol, zwitterionic trimethyl ammonium and dimethyl sulfonium compounds like betaines, natural amino acids like proline and glutamine, some glutamine amide derivatives (Nα-carbamoylglutamine amide, Nα-acetyl-glutaminyglutamine amide), N-acetylated diamino acids (Nδ-acetylornithine, Nϵ-acetyllysine), and ectoines like ectoine itself and β-hydroxyectoine. The most common compatible solutes found in halophilic bacteria are the amino acid derivatives glycine betaine and ectoine [219], which are easily able to exceed concentrations of 0.5 mM in the cytoplasm [65, 77, 119].

2.4 The compatible solute ectoine

As already mentioned, the most widespread compatible solutes are glycine betaine, and ectoine [219]. Ectoine was first discovered by Galinski *et al.* [66] in the phototrophic sulfur bacterium *Ectothiorhodospira halochloris* (now: *Halorhodospira halophila*). Some halophiles like *E. halochloris* or *Vibrio parahaemolyticus* are able to synthesize both ectoine and glycine betaine *de novo* [67, 158]. In fact, most halophiles preferably use mixtures of osmolytes, by taking up various compatible solutes from their

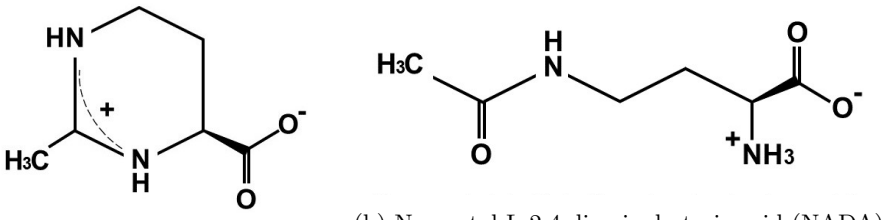

(a) Ectoine

(b) Nγ-acetyl-L-2,4-diaminobutyric acid (NADA)

Figure 2.2: Chemical structure of the (a) compatible solute ectoine, which is a cyclic aspartate derivate, and its (b) linear precursor Nγ-acetyl-L-2,4-diaminobutyric acid (NADA).

surroundings if available. Compared to the *de novo* synthesis this is not only much more energy-efficient but the sharing of compatible solutes has also been suggested to be a mechanism for cooperation in microbial communities [98, 119]. In general, glycine betaine is predominantly produced by halophilic photoautotrophs, while ectoine is mainly synthesized by halophilic chemoheterotrophs [77].

In the following, the primary focus is put on the compatible solute ectoine.

2.4.1 What is ectoine?

Ectoine is an amino acid derivate based on aspartate. The trivial name *'ectoine'* stems from its first discovery in *Ectothiorhodospira halochloris* (now: *Halorhodospira halophila*) by Galinski *et al.* [66] and is commonly used instead of its more complex systemic name (S)-2-Methyl-1,4,5,6-tetrahydropyrimidine-4-carboxylic acid. As a typical compatible solute, it is a small molecule with an atomic composition of $C_6H_{10}N_2O_2$, thereby resulting in a low molecular mass of 142.16 g/mol. The melting point is at approximately 280 °C. It is highly soluble in water with a solubility of about 4 mol/L at 20 °C [247] while in methanol it is only soluble up to 0.3 mol/L, and in ethanol even less. Due to its zwitterionic nature, it shows non-ionic characteristics at a physiological pH. The general structure as depicted in Figure 2.2a is a cyclic amidine with the ring structure responsible for its good stability. In its function as an osmolyte, it not only balances the chemical potential of the water but also protects the cytoplasmatic enzymes against the reduced water activity [66, 119].

2.4.2 Biotechnological relevance of ectoine: properties as a protectant

The activity of ectoine as an osmolyte is not its only interesting feature for biotechnological application. It has been shown numerous times that ectoine exhibits properties as a protectant and stabilizer of proteins and other biomolecules against a wide range of adverse environmental factors that are commonly causing denaturation. These include denaturants like salt but also heat, desiccation, freezing, or thawing. The stabilization occurs due to a solvophobic effect, meaning an unfavorable interaction between the osmolytes and the protein peptide backbone and was, therefore, termed *'osmophobic effect'* [21]. The osmolytes are excluded from the immediate vicinity of both native and denatured proteins and prefer to occupy the free water in the cytoplasm. Like this, a hydration cluster is formed around the proteins. This phenomenon is called *'preferential exclusion'* due to solvophobic interactions. The hydration cluster causes thermodynamic changes for the proteins making unfolding and denaturation more unfavorable. In Figure 2.3, a schematic of the changes in the Gibbs free energy ΔG caused by the presence of compatible solutes (cs) and the resulting water shell is depicted. Due to the bigger surface of denatured proteins (D) compared to the native state (N), more solvophobic interactions with the compatible solutes are happening. Thus, the difference in ΔG between water and an environment with solutes is more positive for denatured compared to native proteins: $\Delta G_{N,water-cs}$ (2) > $\Delta G_{D,water-cs}$ (4). The thermodynamic cycle requires that the difference in ΔG from denatured to native protein in the presence of compatible

solutes is the same as the difference in ΔG of the denaturation with compatible solutes and in water:

$$\Delta G_{N,water-cs}(2) - \Delta G_{D,water-cs}(4) = \Delta G_{cs,den}(3) - \Delta G_{water,den}(1) \tag{2.2}$$

Consequently, the ΔG with compatible solutes $\Delta G_{cs,den}$ (3) is more positive than in water $\Delta G_{water,den}$ (1), making the denaturation less thermodynamically favorable in the presence of compatible solutes. In short, osmolytes raise the ΔG of proteins in the denatured state more than that of native proteins [21, 188].
Apart from the positive effect of ectoine on proteins as mentioned before, a stabilizing effect was also observed on whole cells against stresses like cytotoxins or ionizing and UV radiation [43, 119, 185, 188, 243]. Further, Hahn *et al.* [82] investigated the protective capabilities of ectoine against damage caused by ionizing radiation on DNA. An effective protection was reported due to the reduction of biological damage like single strands breaks. This was attributed to the kosmotropic effect of ectoine on the water structure, displacing it in the extended hydration shell of the DNA. These beneficial characteristics make ectoine a valuable compound from a biotechnological standpoint in the pharmaceutical and cosmetics industry [16, 43, 95, 181, 188].

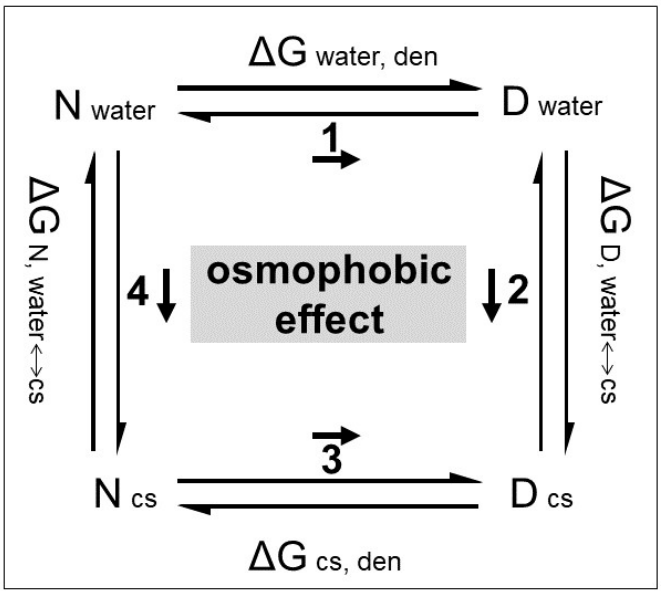

Figure 2.3: Thermodynamics of the *'osmophobic effect'*, explaining the stabilizing effect of ectoine on protein folding. The basis for the *'osmophobic effect'* are solvophobic interactions between ectoine and the protein backbone. The ΔG for denatured proteins is raised due to the presence of the osmolyte, causing protein denaturation to be less thermodynamically favorable.
D_{water}: denatured proteins in water, D_{cs}: denatured proteins in environment with compatible solutes, N_{water}: native protein in water, N_{cs}: native protein in environment with compatible solutes, $\Delta G_{water,den}$ (1): ΔG from denatured to native protein in water, $\Delta G_{N,water-cs}$ (2): ΔG between water and an environment with solutes for denatured proteins, $\Delta G_{cs,den}$ (3): ΔG from denatured to native protein in the presence of compatible solutes, $\Delta G_{D,water-cs}$ (4): ΔG between water and an environment with solutes for native proteins. Picture adapted from Bolen & Baskakov [21].

2.5 The moderate halophile *Halomonas elongata* DSM 2581

In biotechnology, *Halomonas* ssp. are used for generating a diverse range of products including bioplastics like Poly-hydroxybutyrate (PHB) or Poly-hydroxyalkanoate (PHA), alkaline enzymes, biosurfactants and -emulsifiers, and especially the compatible solute ectoine [243]. As of today, ectoine is produced on a scale of tons by the company Bitop (Witten, Germany) using the halophilic strain *Halomonas elongata* as a cell factory for production [120, 243]. Ectoine is priced at over 500 USD/kg [132]. The conversion of glucose to ectoine is highly efficient in *H. elongata* with a maximum theoretical yield of one glucose molecule needed for one molecule of ectoine [163]. In cells grown at 3 M NaCl, an ectoine content of 2.5 μmol(mgDW)$^{-1}$ (equals 355 mg(gDW)$^{-1}$) was reported [163]. Additionally, Sauer & Galinski [183] developed a biotechnological process for ectoine production using *H. elongata* called *'bacterial milking'*. For this process, *H. elongata* is initially grown in a high salinity medium (2.57 M NaCl) up to a high cell density for the intracellular accumulation of ectoine. Then the cells are transferred to a low salinity medium while retaining the cells causing an osmotic downshock. Due to the changes in solute concentration, the environment is now hypotonic, leading to an influx of water into the cells. This increases the turgor pressure, which triggers the mechanosensitive channels to open. Through these unspecific channels cytoplasmic content is released into the surroundings [216]. The ectoine-containing medium is withdrawn and is again replaced with a high salinity medium. Like this, the process can be run in continuous cycles if the cells are retained. With this method, a final ectoine yield of 155 mg(gDW^{-1}) was achieved per cycle [183]. As a comparison, another strain of *Halomonas* ssp. *Halomonas salina* is reported to excrete ectoine naturally at elevated salinities. With this strain, 220 mg(gDW^{-1}) of extracellular ectoine was produced at a moderate salt concentration of 0.5 M NaCl [243, 251]. Another close relative of *H. elongata* is *Chromohalobacter salexigens* belonging to the same family of *Halomonadaceae*. Fallet *et al.* [57] carried out a process for ectoine production using an adapted *'bacterial milking'* method with *C. salexigens* while utilizing two continuously operated bioreactors. In the first bioreactor, *C. salexigens* was grown up to a high cell density under high salinity and temperature to produce ectoine. In the second bioreactor, an osmotic downshock was applied to the cells by adding distilled water. With a stable cell density of up to 61 g/L cell dry weight, an intracellular ectoine content of up to 540 mg(gDW^{-1}) was achieved with this method [57, 243].

H. elongata is next to *Salinivibrio costicola* and *Halomonas isrealensis* one of the most extensively studied organisms regarding their mechanisms of osmoadaptation [219]. *H. elongata* was first isolated by Vreeland *et al.* [221] at a solar salt facility on Bonaire, Netherlands Antilles. Placed in the family of *Vibrionacea*, the gram-negative γ-proteobacterium has an extremely wide range of salt tolerance, being able to grow at concentrations from 0.05 M to saturation. However, optimal growth is achieved between 0.5 M and 1 M NaCl, placing it into the category of moderately extreme halophiles [219, 243]. It was described in 1980 as rod-shaped, with curved and straight form, appearing as single cells or in pairs during the logarithmic growth phase. But the shape changes in the stationary phase into elongated flexuous filaments of varying lengths (Figure 2.4). The cells are motile with predominantly polar oriented flagella. It is able to grow in a broad temperature range from 4 – 45 °C with an optimum for salt tolerance at 30 °C, at which a pH range of 5 – 9 was determined [221].

H. elongata was shown to be facultative anaerobic with catalase and Kovac's oxidase activity but also able to grow anaerobically reducing nitrate as an electron acceptor. Even though the Kovac's oxidase test was positive, which determines that a cytochrome c oxidase is present in its respiratory chain, a further cytochrome oxidase test was negative. [221]. It was reported to grow fermentatively on glucose and oxidizing sucrose, glycerol, mannose, and cellobiose. However, this glucose fermentation was not confirmed in later studies [219]. Furthermore, it was found to decarboxylate ornithine and lysine, but there was no deamination activity for phenylalanine [221].

The genome annotation of *Halomonas elongata* DSM 2581 done by Schwibbert *et al.* [188] (revision and reannotation Pfeiffer *et al.* [171]) revealed a single chromosome of 4 061 296 bp with an average GC content of 63.6 % and 3473 predicted protein coding genes. There are four rRNA operons with the 16S and 5S rRNA sequences being identical. The 23S rRNA sequence has nine polymorphic sites. *H. elongata* possesses a complete set of ribosomal proteins and tRNA ligases for 19 of the 20 canonical amino acids.

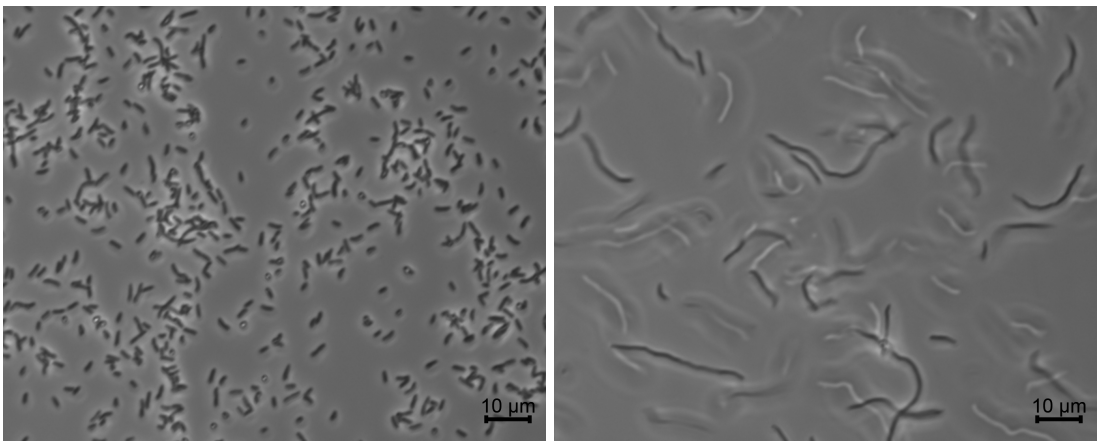

(a) Cell shape in the exponential phase (b) Cell shape in the stationary phase

Figure 2.4: Microscopy pictures of *H. elongata* DSM 2581 wild type cultures in the (a) exponential phase as rod-shaped single cells and in the (b) stationary phase showing the characteristic elongated filaments.

Its osmoadaptation is achieved by the *de novo* synthesis of ectoine conferred by the ectoine synthesis genes encoded in the *ect* operon *ectABC* [31]. Another identified operon connected to ectoine in the *H. elongata* genome is the *teaABCD* operon, encoding a specific TRAP-type transporter for the uptake of ectoine [188].
All genes needed for a complete PHB biosynthesis pathway are present in *H. elongata*: *phbA* (HELO_4131), *phbB* (HELO_3876), and *phbC* (HELO_3394). However, a depolymerase for the mobilization of this carbon storage compound has not been annotated so far and, interestingly, the genes are not clustered in an operon as it is often the case as, for instance, in *Cupriavidus necator* or *Pseudomonas acidophila*, [134]. Each gene is located apart from the others. But the separation in transcriptional units is also not unusual [134]. PHB synthesis starts with two acetyl-CoA molecules being condensed to acetoacetyl-CoA, which is catalyzed by the β-ketothiolase (*phbA*). Next, the NADPH-dependent acetoacetyl-CoA dehydrogenase (*phbB*) reduces acetoacetyl-CoA to (R)-3-hydroxybutyryl-CoA. The last step is the polymerization of these monomers into PHB by the P(3HB)-polymerase (*phbC*) [90].

2.5.1 The *H. elongata* central metabolism

H. elongata is an organism with great potential for the biotechnological industry, in particular, due to its natural ability to synthesize the compatible solute ectoine. Therefore, understanding its basic metabolic organization is essential not only to elucidate osmoadaptation in halophiles in general but also to optimize the strain's performance as an industrial producer. The metabolism of an organism describes a set of highly organized chemical reactions used for its growth. An overview of the *H. elongata* central metabolic pathways and ectoine synthesis is given in detail in the following chapters.

Glycolysis and gluconeogenesis

Glycolysis. As in many marine bacteria, *H. elongata* possesses the genes for three different ways to metabolize glucose [188], namely the Embden-Meyerhof-Parnas (EMP), the Entner-Doudoroff (ED), and the Pentose-phosphate pathway (PPP). A rough outline of these is depicted in Figure 2.5.
The EMP used, for instance, by *E. coli* as its main glycolytic pathway starts by converting glucose to Glucose-6-phosphate (G6P) using a hexokinase (*glk*, HELO_3629). Subsequently, G6P is transformed to Fructose-6-phosphate (F6P) by the enzyme phosphohexose isomerase (*pgi*, HELO_1718, HELO_4245) and is then converted to Fructose-1,6-bisphosphate (FBP) by a 6-phosphofructokinase (*pfkA*, HELO_2186). Both phosphorylation steps catalysed by hexokinase and 6-phosphofructokinase are irreversible because

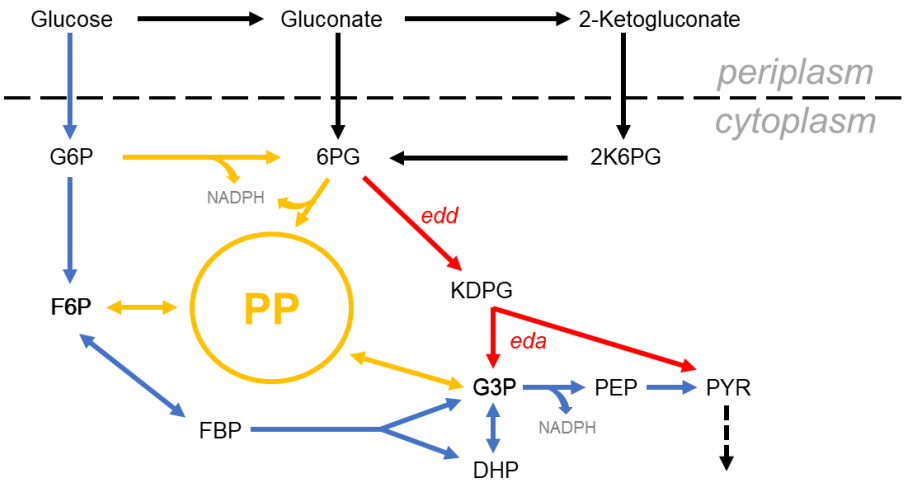

Figure 2.5: Upper carbon catabolism with reactions of the Embden-Meyerhof-Parnas (EMP) pathway (blue), the Entner-Douderoff (ED) pathway (red), and the Pentose-phosphate pathway (PPP, yellow). In Kindzierski *et al.* [107] it is proposed that *H. elongata* uses the ED pathway (red) exclusively for metabolizing glycolytic substrates.
G6P: Glucose-6-phosphate, F6P: Fructose-6-phosphate, FBP: Fructose-1,6-bisphosphate, G3P: Glyceraldehyde-3-phosphate, DHP: Dihydroxyacetone phosphate, PEP: Phosphoenolpyruvate, PYR: Pyruvate, 6PG: 6-phosphogluconate, KDPG: 2-keto-3-deoxy-6-phosphogluconate, 2K6PG: 2-keto-6-phosphogluconate, PP: Pentose-phosphate, *edd*: phosphogluconate dehydratase, *eda*: KDPG aldolase.

ATP is used as a substrate, donating a phosphate group. FBP is then divided into Glyceraldehyde-3-phosphate (G3P) and Dihydroxyacetone phosphate (DHP) by the enzyme aldolase (*fba*, HELO_1180, HELO_1183). Both trioses are in equilibrium, which is maintained by triosephosphate isomerase (*tpi*, HELO_4141). Further, G3P is converted in several subsequent steps to Phosphoenolpyruvate (PEP) and, finally, to Pyruvate (PYR) [233].
For the ED pathway, essentially, glucose needs to be converted to 6-phosphogluconate (6PG), which is the branching point between the ED and PPP [42, 54]. It is produced either via a cytoplasmic pathway using the first reaction of the pentose phosphate pathway or a periplasmic oxidation route, also called *gluconate shunt*. For the cytoplasmic pentose phosphate shunt, glucose is taken up and phosphorylated by a glucokinase (*glk*, HELO_3629), G6P and is subsequently converted to 6PG by a G6P dehydrogenase (*zwf*, HELO_3637) and a 6-phosphogluconolactonase (*pgl*, HELO_3636). The periplasmic gluconate shunt, involves the direct oxidation of glucose to gluconate in the periplasm catalyzed by quinoprotein glucose dehydrogenase (*gcd*, HELO_4006). This enzyme is a membrane-bound protein with a pyrroloquinoline-quinone (PQQ) prosthetic group to reduce ubiquinone. The cofactor PQQ is water-soluble, in contrast to the membrane-soluble quinones (ubiquinone or menaquinone), and donates electrons gained from glucose directly to the quinones of the Electron transport chain (ETC) [47]. In *Acinetobacter calcoaceticus*, this interconnection has been investigated in detail, demonstrating that quinoprotein glucose dehydrogenase supplies the same ETC as NADH dehydrogenases [12, 54]. The resulting gluconate is then either taken up and phosphorylated to 6PG catalyzed by a gluconate kinase (*gntK*, HELO_1782) or oxidized a second time in the periplasm yielding 2-ketogluconate. This reaction is catalyzed by another membrane-bound dehydrogenase (flavin adenine dinucleotide-gluconate dehydrogenase, FAD-GADH) [139, 225], which consists of three subunits: a FAD-containing dehydrogenase (HELO_3277), a subunit containing heme c (HELO_3278), and a small subunit γ of unknown function (HELO_3279). It interacts similarly with the ETC by transferring electrons to ubiquinone [139, 206, 225]. With the gluconate shunt, the rate-limiting

enzyme G6P dehydrogenase (zwf, HELO_3637) can be bypassed.
Kindzierski *et al.* [107] reported that for *H. elongata* the EMP pathway is most likely not active in a glycolytic sense. Its 6-phosphofructokinase uses PP_i as a phosphate donor instead of the more commonly found ATP-dependent version of this enzyme. In the EMP pathway, this reaction is an irreversible key step due to the ATP hydrolysis. But if the enzyme catalyzing this reaction uses PP_i as a cofactor the reaction is reversible under physiological conditions [193]. Because of this, it was proposed that in *H. elongata* the EMP route could be used in a gluconeogenetic direction and glucose degradation takes place solely via the ED pathway like in its close relative *C. salexigens* [107, 165]. The ED pathway starts with the dehydration of 6PG to 2-keto-3-deoxy-6-phosphogluconate (2K3D6PG or KDPG) catalyzed by phosphogluconate dehydratase (*edd*, HELO_3628). KDPG is further split into G3P and PYR by KDPG aldolase (*eda*, HELO_3635). Compared to the EMP pathway, only half of the ATP is produced in the ED pathway but the thermodynamic driving force is higher allowing high fluxes with less protein [6].
Gluconeogenesis. In *E. coli*, reactions linked to gluconeogenesis include the PEP carboxykinase PEPCK and, as an alternative, the combination of malic enzyme ME with the PEP synthase. In *H. elongata*, both pathways are available with PEPCK encoded by *pckA* (HELO_1685), PEP synthase encoded by *ppsA* (HELO_2433), and two isoenzymes for malic enzyme: *maeA* (NADH-dependent, HELO_3817) and *maeB* (NADPH-dependent, HELO_3763). Also active during gluconeogenesis is the glyoxylate shunt, which bypasses the decarboxylation steps of the Tricarboxylic acid (TCA) cycle, producing Malate (MAL) and succinate from isocitrate. By funneling the carbon flux through this shortcut, the amount of carbon atoms is maintained at the expense of electron carriers available for the respiratory chain [2, 157]. In *H. elongata*, these bypassing reactions are catalyzed by the isocitrate lyase encoded by *acnA* (HELO_3070) and MAL synthase encoded by *glcB* (HELO_4288).

The anaplerotic node

There are two main parts of the central carbon metabolism of chemotrophic aerobic or facultative anaerobic bacteria. First, the upper glycolytic pathways described by the EMP, ED, and PPP described above conclude with the 3-carbon intermediates PEP and PYR. The second part constitutes the TCA cycle, in which these intermediates provided by the upper glycolysis are used to create energy precursors for cellular respiration and carbon precursors for biosynthetic purposes. Both modules are connected via the PEP-PYR-OAA node – also called the anaplerotic node - which distributes the carbon flux in the whole metabolic network [184]. In general, aerobes possess a pyruvate kinase HELO_4343, HELO_1605) and a pyruvate dehydrogenase complex (HELO_3571, HELO_3572) for the conversion of PEP to PYR and, subsequently, to acetyl-CoA. Acetyl-CoA then enters the TCA cycle reacting with OAA and H_2O yielding the 6-carbon intermediate citrate. The genes comprising the anaplerotic node, specifically, are the PEP carboxylase PEPC (HELO_3010), PYR carboxylase PC (no homolog annotated), PEP carboxykinase PEPCK (HELO_1685), OAA decarboxylase OAD (HELO_3734, HELO_3735, HELO_3736), and malic enzyme ME (HELO_3817, HELO_3763). In most bacteria, the first two enzymes PEPC and/or PC take over the anaplerotic role of replenishing OAA during glycolytic growth. The latter three - PEPCK, ME, and OAD - are generally attributed to gluconeogenesis. PEPCK generates PYR directly by decarboxylation of OAA. OAD and ME produce PYR working together with a second reaction catalyzed by PEP synthase (HELO_2433), which converts PYR to PEP. But in case these reactions are reversible [238], an anaplerotic function is possible. For example, even though PEPCK is in general a gluconeogenetic enzyme it has been shown to work in an anaplerotic direction under glycolytic conditions in some bacteria like *C. necator*, anaerobic bacteria like *Anaerobiospirillum succiniproducens* or in *B. subtilis* PYR kinase deletion mutants [27, 124, 248].
Normally, different species have only a subset of the possible anaplerotic reactions. For instance, *E. coli* only possesses a PEPC, PEPCK, and ME isoenzymes. The existence of ME isoenzymes is quite common [184]. In *H. elongata*, this is also the case. The ME isoenzymes NAD-dependent malic enzyme and NADP-dependent malic enzyme both catalyze the decarboxylation of MAL to PYR. The NAD-dependent version is thought to be used in gluconeogenesis, while the NADP-dependent malic enzyme is used as a NADPH generating system. For both enzymes a OAA-decarboxylating activity has been

reported, meaning OAA can also be used as a substrate for these enzymes [63, 147]. Regarding the remaining anaplerotic reactions, *H. elongata* possesses all enzymes except for a Pyruvate carboxylase. But OAD of *H. elongata* could potentially replace the reaction. There are two versions of this enzyme. One is a cytoplasmic strictly irreversible enzyme [113]. The second version – which is present in *H. elongata* – is a membrane-bound sodium-pump also found in enterobacteria. Every decarboxylation is linked to the extrusion of 2 Na^+ [156, 234] linking this reaction and also its direction to the sodium gradient [50]. Generally its function is linked to gluconeogenesis together with PEP synthase but also the maintenance of OAA during growth on glucose [14].
The role of OAD as an anaplerotic enzyme in parallel with the commonly used PEPC has been proposed for *H. elongata*. The PEP-PYR-OAA node and the TCA in *H. elongata* with the potential anaplerotic pathways marked in color are illustrated in Figure 2.6.

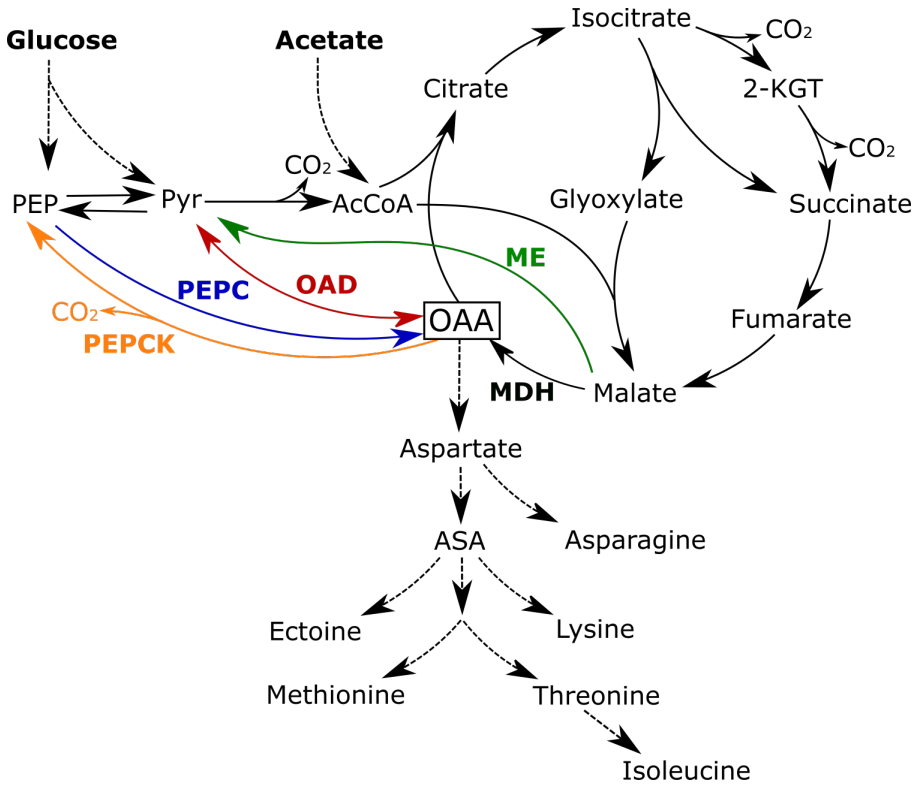

Figure 2.6: Overview of all reactions involved in the PEP-PYR-OAA node (anaplerotic node) specifically in *H. elongata*, which is used to replenish TCA intermediates (picture adapted from Hobmeier *et al.* [86]). OAA is not only a precursor for biomass synthesis, but also for ectoine *de novo* synthesis. Four enzymes can potentially take over an anaplerotic role: PEP carboxylase (PEPC), PEP carboxykinase (PEPCK), OAA decarboxylase (OAD), and malic enzyme (ME).
PEP: Phosphoenolpyruvate, PYR: Pyruvate, OAA: Oxaloacetate, Acetyl-CoA: Acetyl-CoA, MDH: Malate dehydrogenase, 2-KGT: 2-ketoglutarate, ASA: Aspartate-β-semialdehyde

Electron transport chain (ETC) and ATP synthesis

In general, the electron transport chain (ETC) can be described as the transfer of electrons from several electron donors (mainly NADH) through various membrane protein complexes and mobile carriers to an electron acceptor (for aerobes mainly oxygen) while translocating ions across the membrane. The basic function is most easily explained with the mitochondrial ETC. Initially, electrons are transferred from

NADH to Complex I or from $FADH_2$/Succinate to Complex II. The difference between these two complexes is that Complex I translocates protons directly across the membrane while Complex II does not. The electrons that are taken up are used to reduce the mobile carrier ubiquinone in the intermembrane space to ubiquinol. The resulting ubiquinol is then oxidized at Complex III (cytochrome bc_1 complex) and in the process the electrons are transferred from ubiquinol to the mobile carrier cytochrome c. In the last step (Complex IV) the electrons carried by cytochrome c are used to reduce molecular oxygen O_2.
The ETC in the mitochondria of eukaryotes is a relatively linear process and is not substantially influenced by changing environmental conditions. This is not the case for the ETCs found in prokaryotes, which are generally made up of a branched electron flow designed to adjust to different environmental situations. Prokaryotes are usually equipped to deal with additional electron donors and acceptors and different dehydrogenases are often active simultaneously. An example for this is *E. coli*'s overflow metabolism. Here, aerobic respiration occurs simultaneously with acetate fermentation. This apparent waste of energy has been explained as a short-term strategy to boost the growth rate [203, 212]. A general depiction of the bacterial respiratory chain is shown in Figure 2.7. Especially after the quinone level, the bacterial respiratory chain has various possibilities. Since the ratios of proton per electron differ between the branches, the route taken determines the efficiency of energy conservation [192, 196, 212].

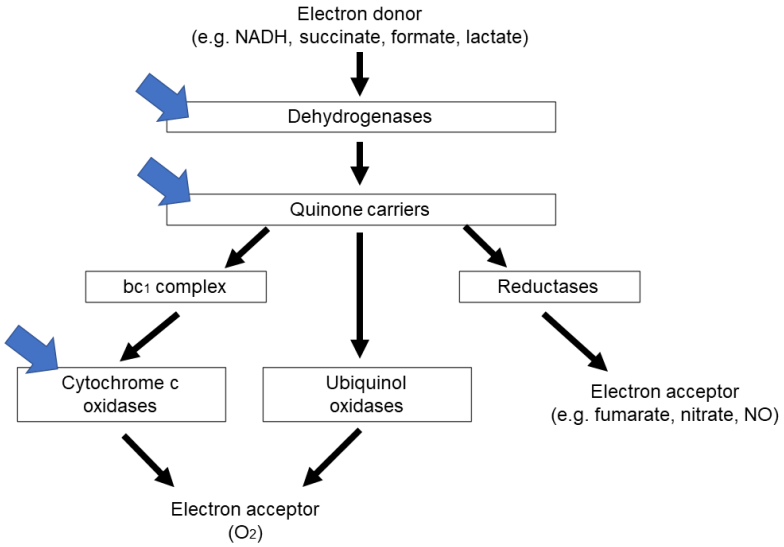

Figure 2.7: Overview of the bacterial respiratory chain adapted from Shepherd & Poole [192]. The various entry points for electrons are marked with blue arrows. NO: nitric oxide.

Aerobic respiration in *H. elongata*. The ETC in *H. elongata* specifically shares many elements with the best-studied examples of ETCs (mitochondrial and *E. coli* [96]). But it also includes additional options. At the dehydrogenase level, *H. elongata* differs from the two models pointed out because it lacks a proton-translocating NADH dehydrogenase (Complex I). Instead, it has a Na^+-translocating complex NQR (*nqrABCDEF*, HELO_2215-20). In general, there are three types of NADH dehydrogenases with different mechanisms and evolutionary origins – NDH-1, NDH-2, and NQR. NDH-1 is an ortholog to Complex I. On the other hand, NQR is a unique redox-driven Na^+-pump that is only found in prokaryotes [103, 143]. Comparing the ion translocation of NDH-1 and NQR with stoichiometries of 3 proton/2 electron and 1 Na^+/electron, respectively, NQR is either less efficient or the sodium gradient is larger than the proton gradient [8, 235]. The second dehydrogenase NDH-2 encoded by *ndh*

(HELO_3377) present in *H. elongata* is a single small membrane protein unlike the large NDH-1 or NQR complexes containing multiple subunits. Also, NDH-2 does not contribute to the pumping of ions [170]. Additional dehydrogenases found in *H. elongata* include, for example, the Complex II ortholog succinate dehydrogenase (*sdhABCD*, HELO_3113-6), a formate dehydrogenase (HELO_1895-9, formerly annotated as *nuo*), or a lactate dehydrogenase (*lldD*, HELO_1406). After the quinone level, there are four alternative branches available for *H. elongata* leading towards the final electron acceptor oxygen. Two of these branches channel the electrons through the cytochrome bc_1 complex (*petABC*, HELO_1943-5) equivalent to Complex III. From here, the electrons are transferred to one of two cytochrome c oxidases (equal to Complex IV): either *ctaCDE* (HELO_2502-5), or *ccoNOPQ* (HELO_3536-9). This is similar to the mechanism found in the mitochondria but is not available to *E. coli*. In *E. coli*, the electrons are channeled through cytochrome b quinol oxidases. Of these, *H. elongata* has two alternatives: a bo' quinol oxidase (*cyoABCD*, HELO_3152-5) and a bd quinol oxidase (*cydAB(CD)*, HELO_2456-9). In *E. coli*, the bo' quinol oxidase is used under aerobic conditions. This membrane protein is a proton-pump with a proton/electron ratio of 2. The second option, the bd quinol oxidase, is linked to growth in microaerobic conditions and has a lower proton/electron ratio of 1, generating the proton motive force (pmf) by releasing protons from quinol oxidation into the periplasm while taking protons from molecular oxygen in the cytoplasm [196]. Its expression is regulated by the transcription factor FNR [51, 192]. But it has also been linked to low oxygen availability and other stress conditions like high temperature, high pH, or membrane de-energization [72].

Oxygen sensing and respiration in anaerobic conditions. To ensure that the most efficient pathway is used bacteria apply a strict hierarchy. Oxygen allows for the biggest difference in voltage between electron donor and acceptor and is the preferred acceptor substrate. In its presence alternative pathways are repressed [80, 92]. Under anaerobic conditions, other final electron acceptors like nitrate are used. This reaction is catalyzed by a nitrate reductase encoded by the *nar* operon (*narGHIJ*, HELO_2851-5) with a proton/electron ratio of 1. In *E. coli*, the switch between aerobic and anaerobic metabolism is regulated by the transcription regulator FNR. This regulator is described as a redox-sensor, which is activated by reduced levels of ATP to recover energy metabolism [10, 41, 213]. FNR is strictly inactivated under aerobic conditions due to its iron-sulfur cluster acting as an O_2-sensor. Under anaerobic conditions, FNR exists as a homodimer with one $[4Fe–4S]^{2+}$ per subunit. Under this state, it binds DNA at specific promoters to initiate transcription. But in aerobic conditions, the oxygen converts the iron-sulfur cluster into its $[2Fe–2S]^{2+}$ form, which causes the dimers to dissociate and lose the ability to bind DNA [79, 191]. Though its re-activation has been observed *in vitro* with glutathione as a reducing agent [128, 213]. *H. elongata* has a similar transcriptional regulator ANR (HELO_1634) that is homologous to *E. coli*'s FNR.

ATP synthesis. The genome annotation revealed that *H. elongata* possesses the genes coding for two potential ATP synthases: an F-type and a V-type ATPase. One of the first prokaryotes discovered to possess two functionally expressed ATPases simultaneously was *Enterococcus hirae*. In this bacterium, a proton gradient dependent F-type ATP synthase provides ATP while the Na^+-translocating V-type ATPase is used for sodium homeostasis as a Na^+ pump [148, 204]. Another microbe using two ATP synthases simultaneously is *Methanosarcina mazei*. In this archaeon, a F-type ATP synthase is translocating Na^+, while an A-type ATP synthase is linked to H^+ as the coupling ion [13]. V-type ATPases are normally known as ion-pumps but can also act in the reverse direction as synthases. An example for this is *Thermus thermophilus*, which uses a V-type ATP synthase driven by a proton gradient to facilitate ATP production [149].

Redox homeostasis and oxidative stress responses

During aerobic respiration, reactive oxygen species (ROS) are created. At either extreme of the redox potential, meaning the ratios of the redox couples $NADH/NAD^+$ and $NADPH/NADP^+$ are shifted either far towards the oxidized or reduced form, ROS cannot be taken care of adequately. In an environment with a reduced potential, the amount of ROS produced is increased due to respiratory processes and exceed ROS scavenging. In contrast, with an oxidizing potential, the rate of ROS scavenging is low and

can be easily overwhelmed [5]. Both NAD^+ and $NADP^+$ are electron carriers but play different roles in cell metabolism. NAD^+ is involved in catabolic pathways for respiration and energy homeostasis. $NADP^+$ on the other hand, is used in anabolism for the biosynthesis of fatty acids and nucleic acids as well as the balancing of the redox state. Because of their different roles, the preferred state is also the opposite. NAD^+ needs to be in the oxidized state to accept electrons and transfer them to the ETC, thus, the $NADH/NAD^+$ ratio is preferably low. In contrast, $NADP^+$ is preferably present in its reduced form NADPH to perform its role as an electron donor in anabolic processes and the $NADPH/NADP^+$ ratio is high. But even though the NAD^+ pool is in general much larger than the $NADP^+$ pool the intracellular concentrations of the reduced forms are similar [18, 244]. For environmental aerobic bacteria, a potent response to oxidative stress is essential and can explain the preference of catabolizing glycolytic substrates via the ED pathway over the EMP. This was shown, for instance, in *Pseudomonas putida* by Chavarría *et al.* [35]. When comparing the net yields of both pathways, less ATP is generated using the ED. It generates 1 ATP, 1 NADH, and 1 NADPH whereas the EMP alternative produces 2 ATP and 2 NADH. But the additional NADPH gained from the ED at the cost of 1 ATP and 1 NADH was found to be essential in *P. putida* to counter oxidative stress.
$NADP^+$ is synthesized from NAD^+ and, NAD^+ is formed, in prokaryotes, from the amino acid aspartate and dihydroxyacetone phosphate. In eukaryotes, NAD^+ is generated from tryptophan. The tryptophan biosynthetic route was widely believed to be unique to eukaryotes but several bacteria have been found that utilize this pathway as well [121]. In the *H. elongata* genome annotation, all genes for NAD^+ synthesis via aspartate are present. The biosynthesis pathway via tryptophan, also called the kynurenine metabolic pathway, is incomplete. In the current genome annotation, only 2 homologs of the 5 needed enzymes can be found: the tryptophan-2,3-dioxygenase encoded by *kynA* (HELO_1509) and the kynureninase encoded by *kynU* (HELO_1508).
The sensing and maintenance of the redox state of the cell is a complex process and involves various mechanisms. Redox homeostasis is tightly linked to iron metabolism because one of the first targets of ROS are iron-containing proteins. ROS oxidize the iron in iron-sulfur clusters, thus, damaging the protein and releasing Fe^{2+}. This leads to the production of even more radicals. Many redox-sensors rely on iron-sulfur clusters or heme-based sensors in their cofactors to detect ROS [191]. Others are non-metalated thiol-based switches like glutathione, mycothiol, bacillithiol, or trypanothinone. Glutathione, for instance, modifies cysteine residues and protects them from oxidation. It is used as a protectant against ROS and for peroxide scavenging in eukaryotes and many mostly gram-negative bacteria. Similar to $NADPH/NADP^+$ it cycles between two species: the reduced GDH and the disulfide bonded GSSG form [111]. To perform its role, it is most abundantly present in the cell in the reduced form GDH. In *H. elongata*, thiol-based redox regulators are encoded by HELO_3167, HELO_2745, and HELO_2540 for glutaredoxins and a thioredoxin encoded by HELO_1735.
Strategies for protection against oxidative stress and ROS include superoxide dismutases (HELO_2574 and HELO_3311) removing superoxide radicals ($O2^-$), catalases (HELO_1513) removing hydrogen peroxide, and alkyl hydroperoxide reductases (HELO_4329 and HELO_4330) which are also scavenging peroxides. Despite the removal of the ROS, repairing the damage is an essential part of the oxidative stress response. *H. elongata* has several peptide methionine sulfoxide reductases that repair oxidized methionine residues. After oxidization, the methionine sulfoxides exist either as methionine-(S)-sulfoxide (Met-S-SO) or methionine-(R)-sulfoxide (Met-R-SO). For each form, a specific reductase exists encoded by *msrA* (HELO_2578 and HELO_3076) and *msrB* (HELO_2015 and HELO_1686). Additionally, *H. elongata* possesses a third type of methionine sulfoxide reductase – *msrC* (HELO_3000) – which is specific for the repair of free methionine sulfoxide [48, 195, 229].

Nitrogen metabolism

Not only carbon but also nitrogen is essential for the growth of all organisms. There are two amino acids that are the immediate products of NH_4^+ assimilation: glutamate and glutamine. They are used as essential nitrogen donors throughout the whole metabolism instead of using NH_4^+ directly because it traps NH_4^+ metabolically. Glutamine, for example, is the main amide donor for the synthesis of nu-

cleotides and, therefore, DNA and RNA. But normally, the flux into glutamate is much higher than into glutamine. Glutamate provides approximately 72 % of the nitrogen for cellular processes while glutamine provides the remaining 28 %. In general, there are two central nitrogen assimilating routes, GS/GOGAT and GDH (Figure 2.8) able to synthesize glutamate [178, 215].

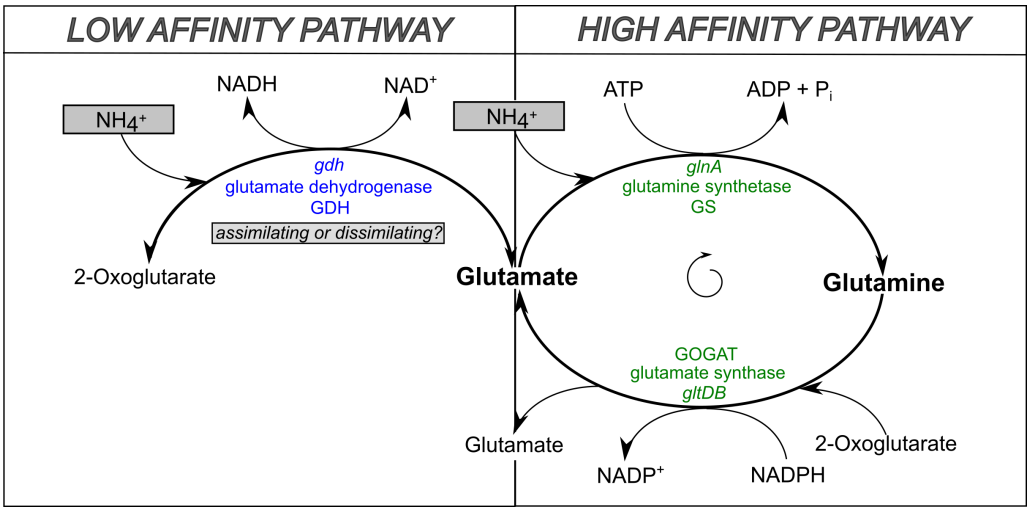

Figure 2.8: Overview of the possible pathways of ammonium assimilation in *H. elongata*. The high-affinity pathway catalyzed by two enzymes GS/GOGAT (green) operates in a loop and uses an additional ATP compared to the low-affinity pathway which is catalyzed by a single enzyme GDH (blue).
GS: glutamine synthetase, GOGAT:glutamate synthase, GDH: glutamate dehydrogenase.

GS/GOGAT. In the GS/GOGAT route, the first reaction is catalyzed by the enzyme Glutamate synthase (also called glutamine-2-oxoglutarate amidotransferase, GOGAT). GOGAT transfers the glutamine amide group to 2-oxoglutarate forming two glutamate molecules while oxidizing NADPH to $NADP^+$ [215]. In *H. elongata*, the two subunits of GOGAT are encoded by *gltDB* (HELO_3752, HELO_3753) with the small subunit GltD and the large subunit GltB [142, 188]. In tandem with the only glutamine synthesizing enzyme Glutamine synthetase (GS, HELO_1126), which catalyzes the amination of glutamate to glutamine while hydrolyzing one ATP, the assimilation of ammonium forms a cycle going from glutamate to glutamine and back.
Glutamate dehydrogenase GDH. The second route for glutamate synthesis is the Glutamate dehydrogenase (GDH) catalyzing the reductive amination of 2-oxoglutarate to glutamate oxidizing its cofactor [178]. There are different versions of GDH with different cofactor specificities – either NADH-dependent, NADPH-dependent or non-specific. In prokaryotes, the assimilation of NH_4^+ is generally linked to the NADPH-dependent version of this enzyme. The NADH-specific versions are mainly attributed to a catabolic function. But studies have shown that there are strong sequence similarities and no sharp evolutionary division between NADH-GDH and NADPH-GDH have been found which makes a separation into an assimilatory and dissimilatory category difficult, leaving their physiological role ambiguous. For instance, the archaeon *Haloferax mediterranei* possesses a NADH-specific GDH with a very low catabolic activity determined in *in vitro* assays hinting towards an anabolic role for this enzyme [49]. The same was found for an NADH-dependent GDH in *Mycobacterium smegmatis*, which showed a nitrogen assimilating function [84]. *H. elongata* possesses a NADH-dependent GDH (HELO_3049).
Either GOGAT or an assimilatory GDH can facilitate ammonia assimilation but a closer look at the enzymes reveals different substrate affinities [178]. Comparing the substrate affinities of the homologs found in *E. coli*, GOGAT shows a much higher affinity towards NH_4^+ with a saturation constant Km of 0.1 mM versus Km of 1.0 mM for GDH. Stoichiometrically with the more complex GS/GOGAT cycle one net glutamate is produced using two enzymes one ATP for each NH_4^+. The single enzyme reaction

via GDH yields one net glutamate without ATP consumption. In conclusion, the GS/GOGAT pathway is a high-affinity pathway adapted to low nitrogen availability and is preferred at low NH_4^+ concentrations or when energy is not a limiting factor. The assimilation via GDH, on the other hand, is only a viable alternative if NH_4^+ concentrations are high enough [178, 215].

2.5.2 Ectoine synthesis pathway and regulation in *H. elongata*

Ectoine synthesis. For *H. elongata* as a moderate halophile, the *de novo* synthesis of its compatible solute, ectoine, is essential for growth in elevated salinites. The intracellular ectoine content in the cell is highly regulated [52] depending on the salt concentration in the environment, but the regulation itself is not entirely elucidated so far. Peters *et al.* [169] proposed the possible synthesis steps but the organization in a cycle with a connection to the degradation pathway has been proposed by Göller *et al.* [74] after the genome annotation of *H. elongata*. In Figure 2.9 this cyclic ectoine synthesis pathway is illustrated. As mentioned before, ectoine is an amino acid derivate synthesized from aspartate, which is connected to the central metabolism via the TCA intermediate OAA. The glutamate-dependent transamination catalyzed by aspartate transaminase converts OAA to aspartate [178]. Ectoine synthesis from aspartate-β-semialdehyde takes three consecutive steps [159, 169, 188]. In the first step, aspartate-β-semialdehyde is transaminated by 2,4-diaminobutyric acid (DABA) transaminase EctB using glutamate as amino group donor and producing DABA. Subsequently, an acetyl group from acetyl-CoA is transferred to DABA by the DABA Nγ-acetyltransferase EctA yielding the linear molecule Nγ-acetyl-L-2,4-diaminobutyric acid (γ-NADA). The final step is the cyclic condensation of γ-NADA catalyzed by the ectoine synthase EctC, creating the ectoine ring structure. In certain conditions – especially at elevated temperatures – ectoine is converted to 5-hydroxyectoine by ectoine hydroxylase EctD [188].
The *ect* operon comprising the synthesis genes in *H. elongata* was elucidated by transposon studies with salt-sensitive strains [74, 117]. The operon consists of the genes *ectABC* (HELO_2588, HELO_2589, HELO_2590) while the gene *ectD* (HELO_4008) encoding the ectoine hydroxylase is located apart. The transcriptional regulation revealed its organization as an operon with two promoters found in front of *ectA* and one in front of the *ectC* gene. The promoters for *ectA* include one housekeeping promoter σ70 which is 25 bp upstream of the START codon and one σ38 which is 92 bp upstream identified as osmotically induced. The additional promoter for *ectC* is located 47 bp before its START codon and was determined as a σ54 promoter which is normally attributed to genes involved in ammonia and glutamate assimilation [188]. However, this is not unreasonable since it was shown that in *Corynebacterium glutamicum* and *Halorhodospira halochloris* compatible solute synthesis is not only linked to the salinity of the environment but also the nitrogen supply [67, 237].
Ectoine degradation. Ectoine can also be utilized as a source of carbon and nitrogen [119]. In *H. elongata* the enzymes needed for ectoine catabolism are encoded by the degradation genes organized in two clusters. The genes *doeAB* (HELO_3665, HELO_3664) are separated from the remaining *doeCD* genes (HELO_3662, HELO_3661) by *doeX* (HELO_3663). Ectoine degradation takes place with the initial hydrolysis of ectoine by the ectoine hydrolase DoeA creating Nα-acetyl-L-2,4-diaminobutyric acid (α-NADA). Like this, the synthesis and degradation of ectoine involves two forms of NADA with the acetyl group either at the α or γ position of the carboxylic acid. It was proposed that DoeA is able to form either structure, but it is also possible that another acetyltransferase step is involved by converting the isomers. However, it is clear that the next degradation step catalyzed by α-NADA deacetylase DoeB is specific for α-NADA as a substrate [188]. α-NADA is deacetylated by DoeB forming DABA with acetate as a side product. For DABA, two options arise with either the reincorporation into the synthesis cycle or the further break down by transamination to aspartate-β-semialdehyde catalyzed by the DABA transaminase DoeD and, finally, the oxidation to aspartate by the aspartate semialdehyde dehydrogenase DoeC. Due to the nature of the degradation pathway as a cycle structure incorporated into the synthesis pathway, a possible cycle with the continuous synthesis and degradation of ectoine takes place. Such cyclic structures are not uncommon as, for example, also found for the synthesis of the carbon storage polymer Poly-hydroxyalkanoate (PHA). The simultaneous activities of PHA synthase and depolymerase are used to balance the storage and use of carbon as energy source [173]. Regarding ectoine synthesis,

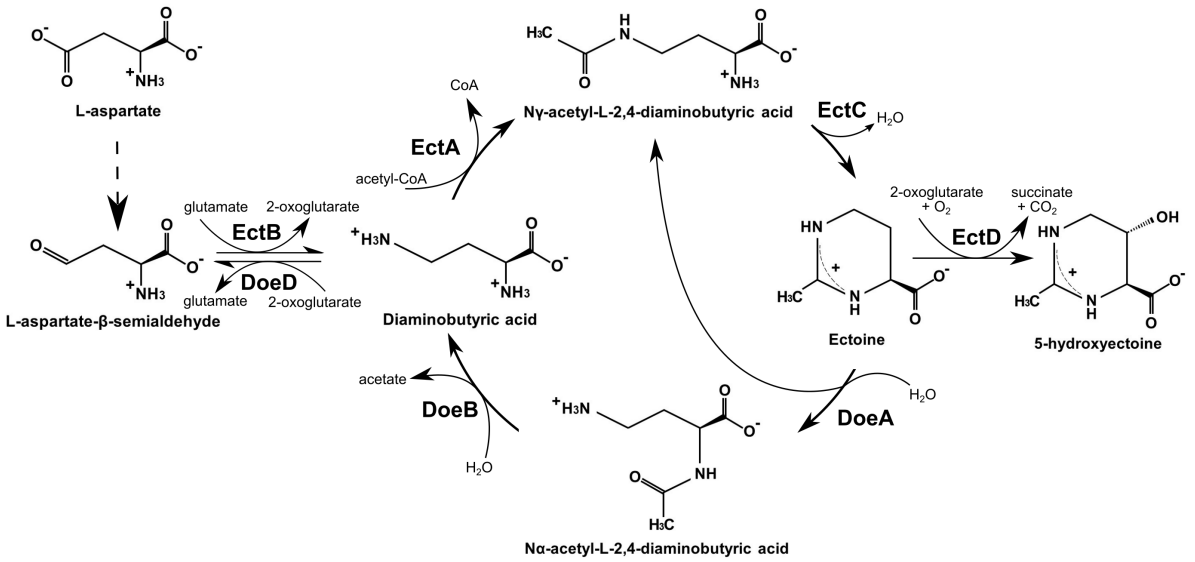

Figure 2.9: The cyclic *de novo* synthesis pathway of ectoine in *H. elongata*; picture adapted from Schwibbert *et al.* [188]. Ectoine is based on the amino acid L-aspartate and is synthesized mediated by the *ect* operon gene products EctB, EctA, and EctC in this order. In certain stress environments, ectoine is further converted to 5-hydroxyectoine catalyzed by EctD. The degradation pathway of ectoine is catalyzed by the enzymes DoeA, DoeB, DoeD, and DoeC in this order for the full conversion to L-aspartate. After the degradation to Diaminobutyric acid, the cycle allows this intermediate to either be further broken down or re-enter the synthesis cycle.

the cycle would allow a fast regulation of internal ectoine content depending on extracellular changes in the salt concentration [120, 188].

Ectoine specific transport. The *de novo* synthesis of ectoine is not the only way of acquiring compatible solutes. Many halophiles use mixtures comprised of different compatible solutes that are taken up from the surroundings. *H. elongata* has several transporters for glycine betaine but also takes up ectoine from the environment if it is available. The biosynthesis is far more energetically demanding than the uptake [119]. The ectoine-specific TRAP transporter TeaABC (HELO_4274, HELO_4275, HELO_4276), in *H. elongata* identified by Grammann *et al.* [77], is a tripartite ATP-independent periplasmic transporter (TRAP or TRAP-T). This kind of transporter uses a periplasmic substrate binding protein (SBP) which is typical for unidirectional transport but the translocation is not mediated by the hydrolysis of ATP but instead driven by an electrochemical gradient [180]. The ectoine uptake by TeaABC specifically is coupled to the symport of Na^+ or H^+. The SBP encoded by *teaA* shows a high affinity to ectoine and to a lesser extent hydroxyectoine [115]. The remaining genes *teaBC* encode the transmembrane proteins TeaC, which is the larger membrane protein suggested to be responsible for the translocation itself, while the smaller membrane protein TeaB might be involved in the interaction with the SBP TeaA. This type of transport was first found for glutamate uptake in *Rhodobacter sphaeroides* and *Rhodobacter capsulatus* [61, 93]. The TeaABC transporter is the second TRAP transporter described on a molecular level and the first one that is osmoregulated [119]. It was observed that the deletion of transporter genes generates mutant strains excreting ectoine, which led to the conclusion that the primary function of this ectoine-specific transporter is to promote the maintenance of the internal ectoine concentration by salvaging ectoine that is leaking through the membrane [77, 120]. It was further proposed that the loss of ectoine is not an entirely uncontrolled process but involved in a regulatory loop for the cytoplasmic solute concentration. An abundance in intracellular ectoine leads to an influx of water into the cells and an increased turgor pressure. To avoid bursting of the cells ectoine is released through an efflux channel.

The periplasmic ectoine is then recovered by TeaA and transported back into the cytoplasm causing a downregulation of the synthesis pathway. This negative regulation of the synthesis is needed because the *de novo* synthesis is reduced if osmolytes are available in the surroundings. Like this, cycling of ectoine between the cytoplasm and periplasm could have a regulatory function, with ectoine serving as a signal for its own synthesis [77, 120].
Adjacent to the *teaABC* operon, a fourth Open reading frame (ORF) was found to be co-transcribed along with the transporter genes. This ORF named *teaD* was determined to bind ATP and form a dimer-dimer complex with one ATP for each monomer. Its deletion enhances the ectoine uptake by the TeaABC transporter, which suggests a role as a negative regulator but no transcriptional regulation of the *teaABC* genes via DNA binding of TeaD could be found. The exact role and function of this protein in the regulation of ectoine uptake is not elucidated so far [120, 186].

2.6 Growth behavior of halotolerant microbes with changing salinities

The two main factors determining the impact of increased salinity on the growth of a halophilic microbes are the amount of energy generated and its osmotic adaptation strategy. Processes with little energy yields like methanogenesis or dissimilatory sulfate reduction are not found in these environments. The expected metabolisms at high salt include either ones that are not energy-limited like in phototrophs or chemotrophs using highly exergonic reactions for energy generation. This is achieved for aerobic respiration with oxygen or dissimilatory nitrite reduction using nitrate as an electron acceptor. With the salt-in adaptation strategy, which is the low energy cost approach of osmoadaptation, also processes generating less energy up to a limit are possible [163].
With increasing salt concentrations, an impact on the medium properties is noticeable. At high salt conditions, more ions are present which interact with the water molecules. This leads to a decrease in the partial molar volume of water with a negative impact on oxygen solubility [208]. Dötsch *et al.* [52] constructed a mathematical model for the prediction of growth and osmoregulation representing halophiles based on data from *H. elongata* as a model organism. The model includes substrate utilization and salt dependence of the growth rate, the uptake of potassium and ectoine, and ectoine synthesis. The gradual decrease of growth rate with an increasing salt concentration was represented mathematically using substrate inhibition kinetics. The growth optimum for *H. elongata* is a salt concentration of slightly above 0.5 M NaCl (Figure 2.10a). At lower concentrations, the growth rate decreases rapidly and at higher concentrations, the growth rate is negatively impacted as well, but the reduction in growth rate is not as prompt. At an extremely high salt concentration of 3.6 M NaCl, *H. elongata* is still able to grow, which illustrates its broad range of tolerance. Dötsch *et al.* [52] identified two already established substrate inhibition models that show a good fit with the same degree of determination ($R^2 = 0.966$). One of these is a reduced version of the substrate inhibition model developed by Yano & Koga [241]:

$$\mu_N = \mu_{max,N} \cdot \frac{N}{k_N + N + \frac{N^3}{{k_2}^2}} \tag{2.3}$$

with:

N = salt concentration $[M]$
μ_N = specific growth rate at salt concentration N $[h^{-1}]$
$\mu_{max,N}$ = maximum specific growth rate at salt concentration N $[h^{-1}]$
k_N = Salt Monod constant $[mM]$
k_2 = Salt inhibition constant $[mM]$

The exact cause of the growth inhibition apart from the increased energy demand is not entirely clear. But Dötsch *et al.* [52] concluded that the changes in cytoplasmic free water due to the increased salinity does not directly respond to the decrease in growth rate. The (reduced) Yano-Koga substrate inhibition

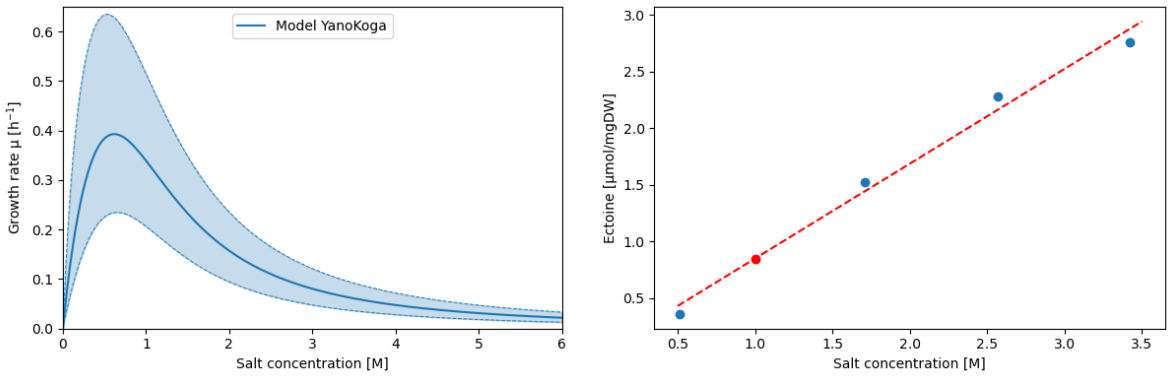

(a) (reduced) Yano-Koga substrate inhibition model

(b) Intracellular ectoine content

Figure 2.10: Impact of the salt concentration on the growth rate and intracellular ectoine content. (a) Depiction of the maximum specific growth rates predicted by the (reduced) Yano-Koga substrate inhibition model [52] depending on the salt concentration. (b) Correlation between the intracellular ectoine content in *H. elongata* depending on the extracellular salt concentration based on data (blue) from Dötsch *et al.* [52]. The predictions at 1 M (and 2 M) NaCl in this work are done using this linear fit indicated in red.

model (YK-R) was established to describe the substrate inhibition by the formation of enzyme inhibitor complexes. Derived from this, the reason for the reduction in growth could be linked to interactions with ionic groups of the enzymes or transport systems exhibiting an ion-pairing effect.
Furthermore, Dötsch *et al.* [52] created a formula for the prediction of the intracellular ectoine content based on the osmotic pressure using the data points in Figure 2.10b. To simplify this complex prediction for the intracellular ectoine content in this work it was roughly approximated using a linear fit as illustrated with the dashed red line. The linear equation for this fit is as follows:

$$Ectoine\ [\frac{\mu mol}{mgDW}] = 0.837 \cdot NaCl\ [M] + 0.012 \tag{2.4}$$

Table 2.1: Model parameters published by Dötsch *et al.* [52] which were determined for the substrate inhibition models to fit the growth behavior of the *H. elongata* salt dependency.

Model based on	$\mu_{max,N}$ [h^{-1}]	k_N [M]	k_2 [M]
YK-R inhibition model	0.88±0.24	0.51±0.24	0.96±0.19

2.7 Principles of Metabolic Engineering

Metabolic engineering is described as the improvement and optimization of cellular properties using genetic modifications guided by the systemic analysis of metabolic pathways [106, 110]. With the emergence of recombinant DNA techniques, the precise manipulation of specifically targeted enzymes was made possible, which in turn enabled the application of *in silico* modeling and predictions to help guide these modifications [25]. Among the different modeling techniques, stoichiometric models are one of the most popular, because they can easily be formulated just from the information on metabolic pathways. In this context, a pathway is defined as the sequence of biochemical reaction steps that are connecting a set of input and output metabolites. The flux is the rate at which the input metabolites are processed to form the output metabolites. After the analysis and the determination of targets in the metabolic

network, like enzymatic reactions, transport, or regulatory functions, these are implemented using molecular biological techniques. This is why the aspect of being target-oriented is a major part of Metabolic Engineering. After the introduction of the genetic change, the effects are analyzed and incorporated as the basis for further improvements. Like this, iterative cycles of modeling and genetic modification alternate [110].
An example of successful strain engineering using Flux balance analysis (FBA) – a technique based on stoichiometric models – is the production of formic acid in *Saccharomyces cerevisiae*. Here, an advantageous combination of gene deletions was predicted to achieve an increased production of formic acid [102]. In *C. glutamicum*, the L-histidine synthesis was optimized using systems metabolic profiling and flux balance analysis. The tight connection of energy metabolism and histidine biosynthesis could be made clear by employing computational tools and was then targeted to balance the energy state of the cell [187].
In a holistic approach for the biotechnological optimization of a microorganism, the whole metabolic network needs to be considered. There are three underlying principles in how the cellular metabolism can be tuned instead of merely introducing heterologous genes [6]. The first way is the decrease or completely abolishing competition for metabolic fluxes. The flux towards the desired product needs to be maximized; thus, any other synthesized byproducts are wasting resources. A well-known example of this is the acetate production of *E. coli* or ethanol production by yeasts during overflow metabolism [9, 218]. A second strategy is to increase the availability of direct precursors used in the biosynthetic pathways of the desired product. This can be achieved by tuning endogenous enzymes or potentially also by the introduction of heterologous enzymes. Here, various modifications are possible, like adjusting the GC content or codon usage in heterologous genes [176]. Additionally, the amount of enzyme can be impacted by adjusting promoters or ribosomal binding sites (RBS) [26, 249]. The last principle is providing sufficient energy in the producer cells mainly via ATP and redox equivalents. In general, the aim is to increase ATP levels and the availability of energy carriers by constructing ATP efficient pathways. If the synthesis pathway includes a reaction with a low thermodynamic driving force, the consequences are either low reaction rates or a high energy investment to drive the reaction forward. Because of the complexity and multifaceted interactions of the cellular metabolism, these optimization tactics truly are dependent on the guidance of computational tools [6].

3 Materials and Methods

3.1 Strains and general procedure for growth experiments

All strains used in this work are summarized in Table A.1. *H. elongata* DSM 2581 and mutant strains derived from this wild type were grown at 30 °C either in lysogeny broth LB complex medium [141] or MM63 minimal medium [126] containing a variable concentration of NaCl (Table A.6). *E. coli* strains were used during molecular cloning either as transformation host (*E. coli* DH5α λpir) or during bacterial mating for horizontal gene transfer (*E. coli* DH5α λpir, *E. coli* HB101 (pRK600)) into *H. elongata*. These *E. coli* strains were routinely grown at 37 °C in LB complex medium. To assure adequate aeration all liquid cultures were incubated in a rotary shaker at 220 rpm and supplemented with antibiotics (Table A.2) if needed for plasmid maintenance or selection purposes.

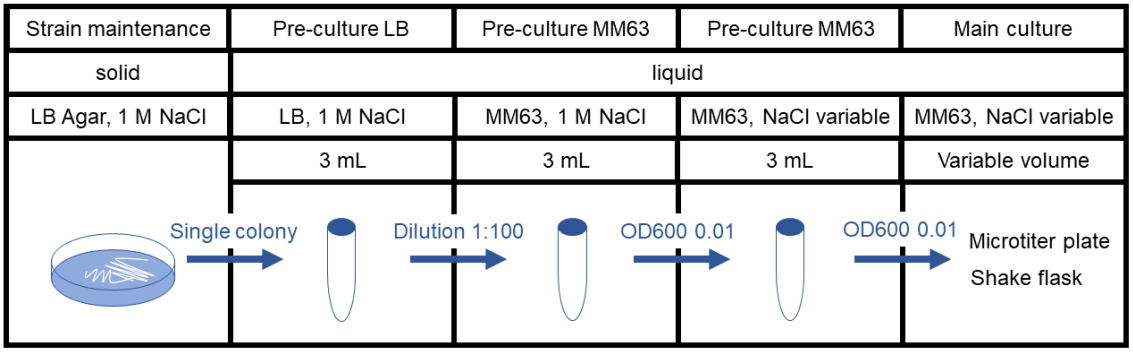

Figure 3.1: Routine procedure of performing growth experiments in this work. Routinely, 2 to 3 pre-cultures were used depending on the main culture medium. Per pre-culture a single colony from a plate is picked. The first pre-culture is grown in complex LB medium. Consecutively, a second pre-culture in MM63 minimal medium with 1 M NaCl and 27.75 mM of the same carbon source as used in the main culture medium is grown. For the inoculation the initial LB culture is diluted 1:100. Unless stated otherwise, a third pre-culture is grown using the exact same medium as also used in the consecutive main culture. The inoculum volume is adjusted to a starting OD600 of 0.01. Most experiments were performed in microtiter plate or shake flask scale.
LB: lysogeny broth complex medium [141], MM63: minimal medium 63 [126].

Routine pre-culture steps until inoculation. Unless stated otherwise, for each tested strain, growth condition, or combination thereof, three biological replicates were grown in parallel to determine statistical averages. Also, as stated before, all liquid cultures were incubated at 30 °C in a rotary shaker at 220 rpm. In the following, the general procedure for the inoculation of a microbial growth experiments is explained. The individual steps are also visualized in Figure 3.1. A single colony was picked from an agar plate and a 3 mL overnight culture was grown in LB medium with 1 M NaCl. Subsequently, an aliquot of this overnight culture was used to inoculate 3 mL of MM63 minimal medium with 1 M NaCl in a ratio 1:100. This culture was then used to inoculate a last pre-culture step using the same medium as in the main culture. The inoculum volume here was adjusted to result in an OD600 of 0.01 in the new medium. This third pre-culture step was especially important for experiments in which the main culture medium differed from the routinely used MM63 minimal medium with 1 M NaCl (Table A.6). If the main culture employed the MM63 minimal medium with 1 M NaCl, the third pre-culture step was omitted at times. The inoculum volume for the main culture was adjusted to a starting OD600 of 0.01

unless stated otherwise.

3.1.1 Microtiter plate screenings

The main cultures were carried out in sterile 96-well plates (Greiner, Germany) with a filling volume of 0.2 mL per well. The experiment was performed in an automated microplate reader (Tecan, Austria) at 30 °C with regular shaking (30 sec orbital shaking) and OD600 measurements every 10 min. The OD600 evolution in the main culture was followed for approximately 16 – 24 h or until the stationary phase was reached. Additionally, to the inoculated wells, for every screening wells filled with the sterile main culture medium was also measured as sterile controls and blanks. In the following, any changes from the routine procedure are listed for specific screening experiments.

For **salt tolerance growth screenings**, in the third pre-culture step, four cultivation tubes with MM63 medium containing the four different tested salt concentrations 0.17 M (low salt), 0.5 M (lower salt optimum), 1 (upper salt optimum), and 2 M (high salt) NaCl were inoculated from the same culture of the second pre-culture step. From each of these a single well in the microtiter plate main culture was inoculated.
In the **fluorophore expression screening** via the XylS/Pm promoter using the plasmids pSEVA438-eGFP and pSEVA438-mCherry the third pre-culture step was omitted. To test four different inducer concentrations (0 mM, 0.1 mM, 1 mM, 2 mM) for 3-methylbenzoic acid (3-MB) and two induction times (immediately upon inoculation and after 4 h) using the eGFP expression plasmid pSEVA438-eGFP eight wells were inoculated for each biological replicate. While examining different types of benzoate-derived inducers (0 mM uninduced, 0.1 mM 3-MB, 1 mM 3-MB, 1 mM 4-methylbenzoic acid 4-MB, 1 mM 3-chlorobenzoate 3-CB) using both expression plasmid pSEVA438-eGFP and expression plasmid pSEVA438-mCherry five wells were inoculated and immediately induced after the inoculation for each biological replicate. To rule out any impact of the solvent ethanol (EtOH), in which the inducers are dissolved, the same end volume of ethanol was added to every culture well. The automated microplate reader (Tecan, Austria) measured the fluorescence for eGFP (excitation: 485 nm, emission: 520 nm) and mCherry (excitation: 585 nm, emission: 620 nm) additionally to the OD600.
In the **Design of Experiment (DoE) growth medium screening**, the third pre-culture step was omitted. The main culture was comprised of 15 different media detailed in Table A.8. For each medium composition, two technical replicates were grown in parallel. As a carbon source, a higher glucose concentration of 110 mM was added and 3 μg/mL Nile-red stain (stock solution of 3 mg/mL in acetone) was added into one of the two replicates to approximate the intracellularly accumulated PHB. The Nile-red fluorescence was measured with an excitation wavelength of 535 nm and emission at 605 nm. The measurements for OD600 and fluorescence took place every 20 min.
In the **carbon source screening** the MM63 pre-culture was supplied with 27.75 mM glucose and 1 M NaCl. The third step was omitted and the main cultures in the microtiter plate were inoculated directly from the 1 M MM63 (glucose) medium. A list of the carbon sources used in the microtiter plate main culture can be found in Table 4.2. For each medium, four replicates were grown in parallel and of these two were supplemented with 3 μg/mL Nile-red stain (stock solution of 3 mg/mL in acetone) to follow the intracellular PHB accumulation. Every 20 min the OD600 and Nile-red fluorescence (excitation: 535 nm, emission: 605 nm) was measured.

3.1.2 Routine shake flask experiments

Experiments in shake flasks were prepared according to the procedure shown in Figure 3.1. In general, a 1 M NaCl MM63 minimal medium and 27.75 mM glucose in a flask scale of either 100 mL, 250 mL, or 500 mL and a filling volume of 10 % was used unless stated otherwise. The external NaCl concentration or the carbon source was varied between 0.17 M, 0.5 M, 1 M, 2 M NaCl and glucose, fructose, and acetate (always 27.75 mM), respectively. Changes to the routine MM63 minimal medium (Table A.6) were specified in the individual experiments. The biomass evolution was followed by regularly mea-

suring the OD600 in a spectrometer (Eppendorf, Germany) or a microtiter plate reader (Tecan, Austria).

3.1.3 Mathematical analysis

Monod model for biomass evolution

To describe the microbial growth of *H. elongata* mathematically, the experimental data for growth gained during the batch cultivations were applied to the classical Monod equation. This equation follows the Michaelis-Menten enzyme kinetics and connects the specific growth rate $\mu(t)$ to a single growth-limiting substrate $S(t)$ using three parameters: the maximum specific growth rate μ_{max}, the saturation constant K_S, and the yield coefficient $Y_{\frac{S}{X}}$ [200]. Like this, the growth rate $\mu(t)$ is defined in:

$$\mu(t) = \mu_{max} \frac{S(t)}{S(t) + K_S} \tag{3.1}$$

Biomass production $B(t)$ is calculated using:

$$\frac{dB}{dt} = \mu(t)\ B(t) \tag{3.2}$$

And substrate utilization is given by:

$$S(t) - S_0 = Y_{\frac{S}{X}}\ (B_0 - B(t)) \tag{3.3}$$

Determination of average growth rates using linear regression

Small-scale growth experiments in microtiter plates were carried out as screening experiments to compare different strains growing in varying growth conditions and for monitoring the production of fluorescent proteins during growth. They were performed in MM63 medium with 27.75 mM of different carbon sources. The growth rate of each well was calculated by determining the maximum value of linear regression of the logarithm of the OD600 along a sliding window of at least 29 points with a coefficient of determination of at least 0.9. Using biological replicates for each condition, a mean growth rate was calculated.

3.2 Plasmids and construction of plasmids

The plasmids used and created in this work are summarized in the annex in Tables A.3 and A.4, respectively. The created plasmids were cloned either by traditional cloning using digest and ligation or by Gibson Assembly [71] cloning.

General cloning routine. PCR amplification of inserts was carried out using the Q5 High-Fidelity DNA Polymerase (New England Biolabs, USA) with the reaction mixture (25 μL scale) and the PCR cycle protocol applied as suggested by the manufacturer. For purification of the PCR fragments purification kits of Macherey Nagel (NucleoSpin Gel and PCR Clean up Mini kit, Macherey Nagel, Germany) or NIPPON Genetics (FastGene GEL/PCR Extraction Kit, NIPPON Genetics, Japan) were used according to the manufacturer protocol. Plasmids, mostly from the pSEVA line [194], used as backbones were isolated from a bacterial culture with plasmid purification kits from either Macherey Nagel (NucleoSpin Plasmid EasyPure Mini kit, Macherey Nagel, Germany) or NIPPON Genetics (FastGene Plasmid Mini Kit, NIPPON Genetics, Japan). Generally, the instructions for plasmid preparation of low-copy plasmids were followed. The enzymes for restriction digests were provided by NEB (New Englands Biolabs, USA) and the digestion reaction was prepared and performed as suggested by the manufacturer with a minimum incubation time of 1 h. Separation of the digested backbone fragments

was done by gel extraction and subsequent purification of the desired fragments from the agarose gel was carried out using purification kits from either Macherey Nagel (NucleoSpin Gel and PCR Clean up Mini kit, Macherey Nagel, Germany) or NIPPON Genetics (FastGene GEL/PCR Extraction Kit, NIPPON Genetics, Japan) again according to the manufacturer protocol. For ligations, the T4 DNA Ligase (New England Biolabs, USA) was used with the suggested reaction mixture by the provider and routinely carried out as an overnight reaction at 16 °C and under shaking (300 rpm). Gibson Assembly cloning was performed with the Gibson Assembly Cloning Kit from NEB (New England Biolabs, USA) as instructed by the reaction protocol. For both cloning types, the *NEBioCalculator* application by NEB was employed to determine the molar insert:vector ratio of 3:1 for a reaction containing 50 ng vector DNA to determine the concentration of backbone and insert for the ligation or assembly reaction. Colony PCRs for the verification of the successfully assembled plasmid were done using the oneTaq DNA polymerase and more specifically the oneTaq (2x) Master Mix with Standard Buffer from NEB (New England Biolabs, USA) (primers: SW18, SW17 designed by Wagner [223]). The reaction preparations (25 μL scale) and PCR cycles were carried out according to the suggested protocol and the template DNA applied in these colony PCR amplifications was either by directly resuspending a single colony in the reaction mixture or by using 1 μL of a single colony resuspended in 20 μL sterile demineralized water. All cloned plasmids were further verified by sequencing performed by Eurofins Genomics (Germany).

The expression plasmids **pSEVA438-eGFP and pSEVA438-mCherry** were created by removing the multiple cloning site (MCS) including a constitutive promoter lacIp, a synthetic ribosomal binding site (RBS, 5' aggaggaaaaacat 3'), and an eGFP or mCherry encoding gene from the plasmids pSEVA237R-32 and pSEVA237R-31 [223] and transferring this transcription unit into the MCS of the plasmid pSEVA438. This was achieved by restriction digest with the restriction enzymes PstI and SpeI. The linearized backbone pSEVA438 and the transcription unit taken from the MCS of pSEVA237R-32 and pSEVA237R-31 were separated and purified by agarose gel extraction. After purification of the desired fragments, their concentration was approximated based on the fluorescent signal of a DNA stain on an agarose gel. The ligation of the new plasmid backbone pSEVA438 and either the eGFP insert or the mCherry insert was carried out in three different concentration ratios in parallel. Initially, the molar insert:vector ratio of 3:1 for a reaction containing 50 ng vector DNA was determined with the *NEBioCalculator* application. For each expression plasmid, one reaction with this 3:1 ratio was used. Additionally, two more ligation reactions were prepared with half and double the volume of insert used in the 3:1 ratio reaction while keeping the backbone concentration the same. After ligating overnight, the reactions were transformed into TSS-competent *E. coli* DH5α λ*pir* cells.
The expression plasmids **pSEVA438-*teaBC*, pSEVA438-*teaB*, and pSEVA438-*teaC*** were cloned by Gibson Assembly. The primers were designed with the *NEBuilder Assembly Tool* (New England Biolabs, USA) with a minimum overlap length of 20 nt and a minimum primer length of 18 nt. The restriction sites on either end were set to be regenerated with the minimum number of bases (option 'Min') in order to retain the restriction sites used to linearize the plasmid pSEVA438. For expression plasmids pSEVA438-*teaBC* and pSEVA438-*teaC* the linearization was done using *Sac*I and *Hind*III while for pSEVA438-*teaB* the restriction enzymes *Sac*I and *Pst*I were used. The respective insert DNA fragments containing the transcription unit including a synthetic RBS (5' aggaggcttcat 3') and the coding genes for *teaBC*, solely *teaB* or solely *teaC*, were generated by PCR amplification with the primers specified in Table A.5. For the insert containing both genes *teaB* and *teaC* the primers 438-teaBC-fwdP and 438-teaBC-revP were used. For amplification of only *teaB* the reverse primer was exchanged for 438-teaB-revP and similarly for only *teaC* the forward primer was switched to 438-teaC-fwdP. The Gibson Assembly reaction was prepared as suggested, for a 2 – 3 fragment assembly with 50 ng plasmid DNA and the amount of insert adjusted to a molar insert:vector ratio of 3:1. After the assembly, the reaction mixtures were transformed into TSS-competent *E. coli* DH5α λ*pir* cells.
The construction of the **integration vectors** used in genome modifications pSEVA212S-Δ*pckA*::SmR, pSEVA212S-Δ*pckA*, pSEVA212S-Δ*maeB*::SmR, pSEVA212S-Δ*maeB*, pSEVA212S-Δ*gltDB*::SmR, pSEVA511CS Δ*gdh*::*gdhA* used for the modification of the *H. elongata* genome is described in detail later while explaining the homologous recombination method. As an exception to the other vectors,

the integration vector pSEVA212S-Δ*gdh*::*gdhA* was generated based on pSEVA511CS-Δ*gdh*::*gdhA* by restriction and ligation and is thus described here. To transfer the needed sequences for the integration and substitution from the pSEVA511CS backbone to pSEVA212S, a PCR amplification of the flanking regions with the *gdhA* and its promoters σ38 and *lacIp* situated in between the flanks, was carried out with the primers SW16 and X11 31 *Avr*II rev. The resulting PCR fragment has an *Avr*II cut site on either end, which were used to insert the fragment into pSEVA212S. The new backbone pSEVA212S was linearized with the restriction enzymes *Xba*I and *Spe*I. Cutting with *Avr*II creates cohesive ends, which are also compatible with *Xba*I and *Spe*I, but naturally the cut sites are destroyed when ligating these ends. Since the *Xba*I and *Spe*I sticky ends are also compatible with each other, the backbone was dephosphorylated using an arctic phosphatase (New England Biolabs, USA) to avoid religation of the backbone without the insert. The dephosphorylation was done directly after the restriction digest in the same reaction mixture. The phosphatase buffer and enzyme were added as suggested by the manufacturer, and the reaction was incubated under shaking at 350 rpm and 37 °C for 30 min before inactivation of the phosphatase at 90 °C for 2 min. Here, both the insert and backbone DNA were purified by gel extraction after the restriction digest and dephosphorylation of the backbone. For the ligation, a molar insert:vector ratio of 3:1 for a reaction containing 50 ng vector DNA was used. The appropriate amount of insert DNA was determined with the *NEBioCalculator* application and an approximation of the DNA concentration for the insert and backbone. The ligation was done with the Quick Ligation Kit from NEB (New England Biolabs, USA) with the reaction mixture prepared according to the Kit protocol and incubation at RT for 5 min. After the incubation, the reaction mixtures were transformed into TSS-competent *E. coli* DH5α λ*pir* cells.
To improve the methodology of the genome modification in *H. elongata*, a new plasmid **pSEVA511CS (and pSEVA211CS)** based on the plasmid pSEVA212S, which was routinely used as the basis for the integration vector, was created. In this new default integration vector, the recognition sequence (5' CAAAACGTCGTGAGACAGTTTGGT 3') for a second homing endonuclease I-*Cre*I was inserted encompassing the MCS like the I-*Sce*I cut sites in the following order: I-*Cre*I site, I-*Sce*I site, MCS, I-*Cre*I site, I-*Sce*I site. Additionally, the fluorescent protein mCherry under the regulation of a constitutive promoter *lacIp* (taken from pSEVA237-31) is inserted into the backbone to allow easier detection of the presence of the integration vector in cointegrates. For this, initially, two sequences were amplified by PCR: the MCS of pSEVA212S using the primers SP Cre-Sce MCS FWD and SP MCS Cre-Sce REV, and the mCherry transcription unit including the *lacIp* promoter, a synthetic RBS (5' aggaggaaaaacat 3'), and the mCherry encoding gene using the primers SP Cre Spe 31/32 FWD and SP 31/32 Spe REV. Details about the primers are found in Table A.5. The reverse primer for the amplification of the pSEVA212S MCS and the forward primer for the mCherry transcription unit were designed with overlapping regions to allow joining of the two PCR fragments in a second overlap-extension PCR. This was carried out in a 50 μL reaction with 1 μL of both cleaned up PCR fragments used as templates. Also, the first 15 cycles in this overlap extension PCR were done without any primers. Following these 15 cycles, the primers SP Cre Spe 31/32 FWD and SP 31/32 Spe REV were added, and 35 further cycles were run. This joined PCR fragment was then used as the insert in a restriction/ligation cloning. The plasmid(s) pSEVA512S (and in parallel pSEVA212S) and the overlap extension fragment were digested with the restriction enzymes *Pac*I and *Spe*I. These restriction enzymes are generally located at the ends of the MCS in the pSEVA plasmid organization effectively removing the default MCS from pSEVA512S (and pSEVA212S) to allow insertion of the modified MCS created by the overlap-extension PCR. After purification of the desired fragments, the two fragments were ligated overnight and subsequently transformed into TSS-competent *E. coli* DH5α λ*pir* cells.
Both complementation plasmids for the *gltDB* Knockout mutant KHN1, **pSEVA338-*gltDB*** and **pSEVA237-*gdhA***, were generated using Gibson Assembly. The primers were designed with the *NEBuilder Assembly Tool* (New England Biolabs, USA) with a minimum overlap length of 20 nt and a minimum primer length of 18 nt. For pSEVA338-*gltDB*, which is based on the pSEVA vector pSEVA338, the cut sites *Hind*III and *Spe*I were used and both recognition sequences were retained in the finished construct (option 'Min'). The insert consisting of the *gltDB* gene segment from the *H. elongata* genome was PCR-amplified using the primers 338-gltDB-F and 338-gltDB-R (Table A.5).

The linearized backbone and the PCR fragments were purified and the concentration of either was approximated using fluorescent DNA staining on an agarose gel. The Gibson Assembly reaction was performed with 50 ng vector DNA and the amount of insert was adjusted to achieve a molar ratio of 3:1 for insert:vector. For these calculations the *NEBioCalculator* application was used. The Gibson Assembly reaction was prepared as suggested for a 2 – 3 fragment assembly and transformed into TSS-competent *E. coli* DH5α λ*pir* cells. In the plasmid pSEVA237-*gdhA* only one of the restriction sites for the linearization of the backbone (*Sac*I) was set to be regenerated (option 'Min'). The plasmid used as a backbone was pSEVA237-31, which was digested with the restriction enzymes *Sac*I and *Spe*I to remove the synthetic RBS and the mCherry encoding gene but leaving the constitutive promoter *lacIp*. The insert was generated by PCR amplification of the *gdhA* from *P. putida* KT2440 with the primers 237-gdhA-NEB-fwd and 237-gdhA-NEB-rev specified in Table A.5. After purification of the fragments and approximation of their concentration via fluorescent DNA staining on an agarose gel, the molar insert:vector ratio of 3:1 for a reaction containing 50 ng vector DNA was determined with the *NEBioCalculator* application. The Gibson Assembly reaction was prepared as suggested for a 2 – 3 fragment assembly and transformed into TSS-competent *E. coli* DH5α λ*pir* cells.
The complementation plasmid **pSEVA037-*gdhA*** was created based on plasmid pSEVA237-*gdhA*. Initially, pSEVA237-*gdhA* was used as a template in a PCR, which amplified the complete plasmid using the primers SynthP_Hind_F and SynthP_Hind_R (Table A.5) but leaving out the KmR gene *neo*. The primers were designed with overhangs including a *Hind*III cut site in each primer. After clean up of the PCR fragment, it was digested using the restriction enzyme *Hind*III to create complementary sticky ends on each side of the fragment. The cut fragment was once again purified and subsequently ligated overnight to form a cyclic plasmid structure. After ligation, the DNA in the ligation reaction was purified by ethanol precipitation. For this, 1/10 of the reaction volume of 5 M Ammonium acetate, 5 μg glucose, and 2.5 times the reaction volume of ethanol was added. The reaction was mixed and frozen at -20 °C for 30 min. Then the mixture was centrifuged (15000g, 5 min, room temperature (RT) and the supernatant was carefully removed. The pellet was dried at RT to evaporate any remaining ethanol. Finally, the DNA pellet was resuspended in 10 μL of sterile demineralized water and the DNA concentration and purity were checked in a spectrophotometer (Eppendorf, Germany) at a wavelength of 260 nm and the ratio at 260 nm/280 nm. The ligated DNA was then electroporated into electro-competent *H. elongata* Δ*gltDB*::Sm^R cells.
The plasmid **pSEVA238-eGFP/lacIp-*gdhA*** used to examine the plasmid loss in *H. elongata* Δ*gltDB*::Sm^R was created based on plasmid pSEVA237-*gdhA* by restriction and ligation. The eGFP transcription unit from pSEVA438-eGFP, including the XylS/Pm promoter system, a synthetic RBS (5' aggaggaaaaacat 3'), and the eGFP encoding gene was cut out by restriction digest with the enzymes *Pac*I and *Spe*I. Plasmid pSEVA237-*gdhA* was linearized using the restriction enzymes *Pac*I and *Xba*I. *Xba*I was used because *Spe*I was eliminated during the insertion of the *gdhA* gene by Gibson Assembly and cutting with *Xba*I creates compatible cohesive ends which can be ligated with a *Spe*I cut site. After gel extraction of the eGFP transcription unit and the pSEVA237-*gdhA* backbone with the *gdhA* insertion of the two fragments, the DNA concentration was determined using a fluorescent DNA stain. The ligation was performed with 50 ng vector DNA and a molar insert:vector ratio of 3:1 which was approximated with the *NEBioCalculator* application. The ligation reaction was transformed into TSS-competent *E. coli* DH5α λ*pir* cells.

3.3 Transformation and transfer

Cloned plasmids were transformed into TSS-competent *E. coli* and were then transferred to *H. elongata* through tri-parental mating or electroporation.

3.3.1 TSS-Transformation into *E. coli*

All cloned plasmids were routinely transformed into TSS-competent *E. coli* DH5α λ*pir* cells as described by [38]. To prepare these cells first, a single colony is used to inoculate a 3 mL LB overnight culture.

A 400 μL aliquot of this preculture is then diluted with 40 mL LB medium in a 500 mL flask and again incubated until an OD600 of 0.4 is reached. At this point, the biomass is separated from the liquid LB medium by centrifugation (Centrifuge 5418, Eppendorf, Germany) (882g, 10 min, 4 °C) and resuspended in 2 mL cold TSS medium. Aliquots of 200 μL of this TSS cell suspension are then used for transformation into *E. coli* DH5α λ*pir*. After transferring 200 μL of TSS cell suspension onto the ligation or the Gibson Assembly preparation, it is incubated for 30 min on ice before adding 2 mL of TSS medium and further incubation at 37 °C in the rotary shaker (220 rpm) for 1 h. After this, the biomass is separated again by centrifugation (Centrifuge 5418, Eppendorf, Germany) (882g, 10 min, 4 °C) and the cell pellet is plated on solid LB agar plates with the respective antibiotic for selecting for the transformed plasmid. The plates are incubated overnight at 37 °C and the presence of the plasmid in the colonies formed on the solid medium is checked using PCR using the oneTaq (2x) Master Mix with Standard Buffer (New England Biolabs, USA).

3.3.2 Tripartental mating into *H. elongata*.

To transfer plasmids from *E. coli* to *H. elongata*, bacterial mating, either in a triparental (one donor strain) or quattroparental (two donor strains) form is used. For this, liquid overnight cultures of the acceptor strain (*H. elongata* or derivative strain), the helper strain *E. coli* HB101 (pRK600), and the donor strain(s) harboring the plasmid(s) which need to be transferred are prepared in their respective growth media. These overnight cultures with similar OD600 values are then mixed in a 1:1 ratio with volumes ranging from 0.2 – 1 mL. To separate the biomass from the liquid medium, the mixture is centrifuged (Centrifuge 5418, Eppendorf, Germany) (882g, 10 min, RT) and the concentrated cell pellet is pipetted onto a solid LB agar plate with 0.5 M NaCl. After the cells are slightly dried on this agar plate, it is incubated at 30 °C for 6 – 8 h and finally using an inoculation loop, the cells are transferred again to a new LB agar plate with 1 M NaCl and the respective antibiotic(s) for the selection of the plasmid(s) taken up by *H. elongata*. The plates are then incubated overnight at 30 °C and the presence of the plasmid in the formed colonies is verified by PCR using the oneTaq (2x) Master Mix with Standard Buffer (New England Biolabs, USA).

3.3.3 Electroporation into *H. elongata*.

Electroporation of plasmids and ligation preparations of plasmids into *H. elongata* or derivative strains was performed using a protocol established by the Bundesanstalt für Materialforschung und -prüfung (BAM, Prof. Dr. Hans Jörg Kunte, personal communication) adapted from [85]. First, a 3 mL overnight culture in a low ionic strength medium (HGM) is prepared. The HGM consists of 10 g/L tryptone, 5 g/L yeast extract, and 3.5 % NaCl (pH 7.5). An aliquot of the overnight culture is subsequently used to inoculate 50 mL HGM in a 500 mL shake flask, which is incubated as per usual in a rotary shaker at 220 rpm and 30 °C. After reaching an OD600 of 0.5, the biomass is harvested by centrifugation (5000g, 10 min, 23 °C) separated into two aliquots of 25 mL each. After removal of the HGM, the cells are washed in 25 mL 300 mM sucrose solution. This centrifugation and washing step is repeated again, but with 0.5 % of the volume (12.5 mL), and again with only 0.01 % of the volume (0.25 mL). After this final wash step, the two aliquots are pooled, resulting in a total volume of 0.5 mL of *H. elongata* cells in 300 mM sucrose solution for use in the electroporation. 0.1 mL of the *H. elongata* cell suspension is mixed with approximately 100 ng of plasmid DNA and transferred into a 2 mm gap parallel electrode cuvette. The electroporation in the GenePulser Xcell electroporator (Bio rad Laboratories, USA) was carried out under the following conditions: 2.1 kV, capacitance 50 μF, resistance 150 Ω. After the application of the electric pulse, the cell suspension is mixed with 0.9 mL of 1 M NaCl LB medium directly in the cuvette and transferred into a 2 mL tube. To recover the cells, they are incubated at 220 rpm and 30 °C for at least 2 h. After this, the cells are separated from the liquid medium (Centrifuge 5418, Eppendorf) (centrifugation at 775g, 3 min, RT) and plated on agar plates with the respective solid medium needed

for the selection and maintenance of the respective plasmid. The plates are then incubated overnight at 30 °C and growing colonies are tested for the uptake of the desired plasmid using PCR.

3.4 Targeted gene modification in *H. elongata* via homologous recombination

3.4.1 Conceptualizing and generating the integration vector

In order to modify (substitution or deletion) the *H. elongata* genome at specifically targeted genes, an integration vector needs to be generated. In this work, the used integration vectors are either based on the pSEVA212S from the pSEVA line [194] or the created pSEVA511CS. In Figure A.2(a), the general organization of the integration vectors for substitutions (A, C) and deletions (B) is illustrated. To make the integration into the genome possible homologous regions of 500 – 800 bp length upstream (up, green) and downstream (down, dark blue) of the gene of interest (GOI) are inserted into the MCS of the integration vector. In the case of clean deletions, these flanking regions of the GOI are seamlessly joined. If the GOI is to be substituted by another gene, for instance, an antibiotic resistance like *aadA* (streptomycin resistance gene) the gene and its promoter is put in between the flanking upstream and downstream region.
The integration vectors were routinely generated using Gibson Assembly cloning with the reactants provided by the Gibson Assembly Cloning Kit from NEB (New England Biolabs, USA). The insert DNA fragments for the assembly were generated by PCR using the Q5 High Fidelity DNA Polymerase (New England Biolabs, USA) with the primers (Table A.5) and the procedure as suggested by the manufacturer protocol. The backbone of the integration plasmid was isolated from a bacterial culture using plasmid purification kits from either Macherey Nagel (NucleoSpin Plasmid EasyPure Mini kit, Macherey Nagel, Germany) or NIPPON Genetics (FastGene Plasmid Mini Kit, NIPPON Genetics, Japan) according to the manufacturer protocol. Opening of the cyclic plasmid DNA was achieved by restriction digest with the respective restriction enzyme. The purification of PCR fragments and the digested backbone was carried out using purification kits from either Macherey Nagel (NucleoSpin Gel and PCR Clean up Mini kit, Macherey Nagel, Germany) or NIPPON Genetics (FastGene GEL/PCR Extraction Kit, NIPPON Genetics, Japan) again according to the manufacturer's protocol. The plasmids put together by Gibson Assembly were transformed into TSS-competent *E. coli* DH5α λ*pir* cells as described previously.

3.4.2 Cointegration of integration vectors

The integration vectors were integrated into the *H. elongata* genome by transfer from *E. coli* DH5α λ*pir* to *H. elongata* by bacterial mating as described above. The origin of replication (oriV) R6K of the integration plasmids requires the π protein which initiates DNA replication and is encoded by the *pir* gene [91, 198]. Since *E. coli* DH5α λ*pir* possesses the *pir* gene, it is able to replicate the integration vectors as plasmids, but *H. elongata* does not have this gene and can, therefore, also not replicate them. When applying selection pressure using the antibiotic resistance in the backbone of these vectors, the only option for *H. elongata* is the co-integration of the vectors into the genome by using the complementary flanking regions (up or down). This is indicated in Figure A.2(b) for the integration of a vector used for the substitution of a gene of interest (GOI) by a streptomycin resistance cassette (left) and the integration of a vector used for a clean deletion (right).

3.4.3 Orientation of the integration

Since there are two complementary flanks present in the integration vector, the integration event can occur via either one. In Figure A.2(c), both possible ways of integrating the vector into the genome are outlined for the substitution of a gene of interest (GOI). The GOI is either located before or after the integrated vector and the integration, as well as its orientation, was determined by PCR using the

oneTaq (2x) Master Mix with Standard Buffer (New England Biolabs, USA). For this, one primer outside of the complementary flanking region and another within the integrated plasmid backbone were utilized with the PCR reaction and procedure carried out according to the manufacturer's instruction.

3.4.4 Induction of double-strand break and its repair by homologous recombination

The recombination event is triggered by a deliberate double-strand break in the genome at the target site. This is achieved using the homing endonuclease I-*Sce*I, which recognizes the two 18 bp cut sites within the backbone of the integration vector pSEVA212S (or pSEVA511CS). The double-strand break is induced by the expression of the I-*Sce*I endonuclease from plasmid pSW-2, which was introduced into *H. elongata* by bacterial mating either simultaneously with the integration vector (quattroparental mating) or in succession (triparental mating twice). The pSW-2 plasmid is an expression vector for the I-*Sce*I endonuclease under the regulation of the XylS/Pm promoter and for *H. elongata*, slightly lower inducer concentrations were applied compared to the concentration originally used by [136] in *P. putida*. To induce the recombination event in the co-integrates harboring the pSW-2 plasmid, a single colony was picked and an overnight culture in 3 mL LB medium with 1 M NaCl and the respective antibiotics was grown. The applied antibiotics varied depending on the type of modification and the integration vector used. In general, the medium was supplied with Am 500 μg/mL to select for *H. elongata*, ruling out a carry over of *E. coli* from the previous mating steps and Gm 50 μg/mL to maintain the pSW-2 plasmid. Additionally, for substitutions with a Sm^R cassette Sm 200 μg/mL and for clean deletions with pSEVA212S Km 50 μg/mL were applied. During the substitution of *gdh* by *gdhA* in KHN1 specifically, the fact that the integration of *gdhA* recovers the ability to grow in minimal medium was taken advantage of and was used in this instance as a selection condition instead of additional antibiotics. The next day the cells from the overnight culture were harvested by centrifugation (3000*g*, 5 min, RT) and the pellet was routinely washed in LB medium with 1 M NaCl but in case of the *gdh* substitution MM63 with 1 M NaCl was used. In 3 mL new medium (LB or MM63 with 1 M NaCl) the OD600 values were adjusted to OD600 of 1 and the previously mentioned antibiotics for the overnight culture were added at the same concentrations except for antibiotics, for which the resistance is conferred by a resistance cassette located in the integration plasmid backbone. This only applies to clean deletions where Km 50 μg/mL was initially applied to select for co-integrates. In these cultures, the resolution of the co-integrates was induced by the expression and activity of the I-*Sce*I endonuclease by the addition of an inducer concentration of 3-methylbenzoic acid ranging from 1 – 10 mM (in general 10 mM). The cultures were further incubated at 220 rpm and 30 °C for 3 – 8 h depending on the specific modification that was performed. After incubation an aliquot was plated on solid LB agar plates with 1 M NaCl supplied with Am 500 μg/mL and for substitutions with a Sm^R cassette, additionally, with Sm 200 μg/mL. As mentioned before, the substitution of *gdh* by *gdhA* in KHN1 constituted a special case in which MM63 medium with 1 M NaCl was used instead in order to directly select for complemented strains. These plates were incubated at 30 °C for 48 h and the single colonies formed were picked and gridded on LB plates with different antibiotics to identify clones that lost the integration plasmid backbone and, thus, also the antibiotic resistance conferred with it.

After the successful resolution of the cointegrates, the integration vector backbone is lost due to the I-*Sce*I endonuclease cut and the double-strand break is repaired by homologous recombination resulting in two possible outcomes. These are illustrated for a substitution of a GOI with a Sm^R cassette in Figure A.2(d). Either it is reverted to the wild type, or the introduced modification is incorporated. In either case, the backbone antibiotic resistance is lost, but only the modified strain shows a phenotype that is able to grow with streptomycin. For a deletion, only the loss of the integration vector can be verified using its phenotype. The successful deletion needs to be proven by PCR. However, if the GOI, which is to be removed, happens to be an antibiotic resistance cassette, the deletion can be found in its phenotype by the loss of its antibiotic resistance. Single colonies from the solid agar plates were picked and gridded on LB plates with different antibiotics to identify clones that lost the integration plasmid backbone and, thus, also the antibiotic resistance conferred with it. Clones showing growth for the

desired phenotype were further tested by PCR using the oneTaq (2x) Master Mix with Standard Buffer (New England Biolabs, USA). The primers used for this verification of the modifications were situated on either end of the targeted area but outside of the used flanking regions. Additionally, the modification was confirmed by sequencing of the complete PCR fragment (Eurofins Genomics, Germany).

3.5 OD600 to biomass correlation

The OD600 to biomass ratio for the *H. elongata* wild type was determined in an OD600 range of 0.2 – 1.2 using simultaneous thermal analysis (STA) as described in Hobmeier *et al.* [86] and detailed in Chapter 4.1.1.
The OD600 to biomass ratios for both NADA producers *H. elongata* Δ*ectC* and *H. elongata* Δ*ectC* σ38 RBS were established using the same STA method but for a far wider OD600 range of 0.7 – 19.0 and 0.6 – 16.0, respectively. For both modified strains the determining key points during combustion - the complete removal of residual water at 160 °C and that only inorganic salts remain after 1000 °C) - were applied to calculate the ash-free dry weight as well.

3.6 Overexpression of transmembrane proteins TeaB and TeaC

Ectoine excretion via the transmembrane proteins TeaB and TeaC was tested in the Leaky Mutant strain (*H. elongata* Δ*teaABC* Δ*doeA*). For this, the inducible (XylS/Pm) expression plasmids pSEVA438-*teaBC*, pSEVA438-*teaB*, and pSEVA438-*teaC* were used.

3.6.1 Influence of inducer and solvent

The influence of inducer 3-methylbenzoic acid (3-MB) (dissolved in EtOH) and the solvent ethanol (EtOH) on ectoine excretion was tested on the Leaky Mutant without plasmids in the routine MM63 minimal medium supplemented with 1 M NaCl and 27.75 mM glucose. Pre-cultures were done according to the general procedure but the third pre-culture step was omitted. Also, from each pre-culture three 100 mL flasks filled with 10 mL medium were inoculated to a starting OD600 of 0.01 to determine changes in the ectoine excretion due to the supplements in the same biological replicate. Together with the inoculum in one of the three flasks 0.1 mM 3-MB inducer was added, in another only the volume of EtOH solvent, which was added in the first flask with the inducer, was added, and in the third flask no additional supplements were added. The cultures were grown routinely up to an OD600 of 1, at which 1 mL samples for the quantification of extracellular ectoine were taken.

3.6.2 Induction of *teaBC*, *teaB*, and *teaC* overexpression

The ectoine excretion via the transmembrane proteins was investigated in two experiments. Initially, a growth experiment with the plasmid pSEVA438-*teaBC* was performed. In a second experiment the plasmids pSEVA438-*teaB* and pSEVA438-*teaC* expressing the proteins individually were tested. The routine MM63 minimal medium supplemented with 1 M NaCl and 27.75 mM glucose was used and the pre-cultures were done as described in the general procedure but without the third pre-culture step. The main cultures were carried out in 250 mL shake flasks with 25 mL filling volume, which were inoculated to a starting OD of 0.01. From each pre-culture two flasks were inoculated to compare the effects of induction or rather membrane protein expression in the same biological replicate. The OD600 was measured regularly in a photometer (Eppendorf, Germany). The main cultures were induced after reaching an OD600 of approximately 0.1, which resulted in an adaptation period of about 7 h. After reaching an OD600 of 1, 1 mL samples for the detection of extracellular ectoine were taken. In the first experiment with pSEVA438-*teaBC*, sampling was done at three time points in the late exponential phase after reaching OD600 1 in order to calculate ectoine excretion rates. In the second experiment with pSEVA438-*teaB* and pSEVA438-*teaC*, one sample was taken after reaching OD600 1 and samples

for the final ectoine titer after more than 24 h of process time were taken. The extracellular ectoine concentration was measured using HPLC.

3.7 Ectoine production in SO_4^{2-}-limited MM63 medium

The ectoine production of the two modified strains, *H. elongata*-PCK (*H. elongata* Δ*teaABC* Δ*doeA* Δ*pckA*) and *H. elongata*-PCKMAE (*H. elongata* Δ*teaABC* Δ*doeA* Δ*pckA* Δ*maeB*) on glucose compared to the Leaky Mutant (*H. elongata* Δ*teaABC* Δ*doeA*) was determined in a flask experiment in slightly altered SO_4-limited MM63 minimal medium (detailed composition in annex Table A.7). The general procedure was followed but an additional fourth pre-culture step was performed, which was done exactly like the previous third step, meaning in SO_4-limited medium. The main culture was carried out in 500 mL shake flasks with 10 % working volume. After reaching the end of bacterial growth, 1 mL samples for the determination of the extracellular ectoine titer were taken.

3.8 Adaptive laboratory evolution and growth experiments with the obtained mutants

3.8.1 Periodic transfer of cultures

The adaptive laboratory evolution of *H. elongata* Δ*gltDB*::Sm^R Δ*gdh*::*gdhA* was performed in the regular MM63 minimal medium with 1 M NaCl and 27.75 mM glucose. As a starting point, the flask cultures of the three biological replicates used to compare the growth rates of wild type, the plasmid-based complementation *H. elongata* Δ*gltDB*::Sm^R (pSEVA237-*gdhA*), and the strain of interest *H. elongata* Δ*gltDB*::Sm^R Δ*gdh*::*gdhA* were taken. After reaching the stationary phase in the growth experiment aliquots of two of these cultures (flask 1: clone 1, flask 2: clone 2) were used to inoculate two culture tubes with 5 mL new minimal medium diluting the cultures 1:100. After 24 h of incubation at 30 °C and under shaking (220 rpm) as usual, an aliquot was transferred again 1:100 to new culture tubes containing 5 mL of new minimal medium. After three transfers, aliquots were taken from each tube and plated on solid MM63 minimal medium plates. The plates were incubated at 30 °C for 48 h and 5 single colonies of each plate were picked and tested in a microtiter plate screening. Based on this screening, one clone of the tested 10 clones (clone 8) was added as a third culture for the periodic transfer into new medium after 24 h of incubation. After 10 transfers of the original two cultures, a second screening with three clones each was performed as described for the first screening. The transfers continued until 20 transfers were done in total for the two original lines 1 and 2. The additional line 8 was transferred 15 times. Eventually, aliquots of the liquid cultures were plated on solid MM63 minimal medium plates with 200 μg/mL and incubated at 30 °C for 48 h. A colony for each of the three plates was tested by PCR using the oneTaq (2x) Master Mix with Standard Buffer (New England Biolabs, USA) for the two substitutions: *gltDB* with a streptomycin resistance cassette and *gdh* with *gdhA* (from *P. putida*). After verification of the genotype, the tested single colony was then used to create a glycerol stock.

3.8.2 Growth of the adaptive laboratory evolution stains in MM63 minimal medium

With colonies from these stocks, growth experiments were carried out in 100 mL flasks (working volume 10 %). The pre-cultures were done according to the general procedure but the third pre-culture step was omitted since the growth experiment was carried out in the regular MM63 minimal medium with 1 M NaCl and 27.75 mM glucose. However, in the first experiment, only two biological replicates were used to compare the three evolved mutants (DE1, DE2, DE8) to the wild type. The experiment was repeated in a second flask experiment, with three biological replicates but as a reference the original strain *H. elongata* Δ*gltDB*::Sm^R Δ*gdh*::*gdhA* was used instead of the wild type.

3.9 Batch cultivation in 2 L bioreactor scale

The *H. elongata* wild type and the γ-NADA producer *H. elongata* ΔectC σ38 RBS were grown in a Labfors 5 stirred tank bioreactor (InforsHT, Switzerland) in a 2 L batch to identify the specific growth yields and generate models for the growth and product formation in these strains. The cultivation parameters were controlled at a fixed temperature of 30 °C, 1000 rpm stirrer speed, a pH of 7.0 regulated with 5 M NaOH, and a constant aeration of 1.25 L/min. The media used in these batch cultivations were modified versions of the routinely used MM63 minimal medium with 27.75 mM glucose as substrate. The wild type was grown in 1 M NaCl while *H. elongata* ΔectC σ38 RBS was grown in 0.5 M NaCl. Further, a supplement of 68 μM $CaCl_2$ and 1 mL/L trace element solution (EDTA 5 mM, $MnSO_4$ ·2 H_2O 3 mM, $ZnSO_4$ ·7 H_2O 1 mM, $CoCl_2$ · 6 H_2O 1 mM, $CuSO_4$ ·5 H_2O 40 μM, $KAl(SO_4)_2$ ·12 H_2O 4 μM, H_3BO_3 162 μM, Na_2MoO_4 ·2 H_2O 41 μM, $NiCl_2$ ·6 H_2O 105 μM) was added.
For the inoculum, initially, a single colony was picked from a solid agar plate and grown overnight in 3 mL LB medium supplemented with 1 M NaCl. The next day, pre-cultures comprised of four 500 mL flasks with 20 % filling volume with the above described modified MM63 medium were inoculated from the LB culture to an OD600 of 0.01 . After incubation of these pre-cultures the main culture inoculum was prepared using all four flasks. The cultures were centrifuged (3200*g*, 15 min, RT) to concentrate the biomass and the supernatant was discarded. The cell pellet was resuspended in 20 mL modified MM63 minimal medium (10 % of reactor working volume). After inoculation with the concentrated cell suspension, sampling (1 - 2 mmL) took place regularly under sterile conditions for OD600 measurement in a photometer (Eppendorf, Germany) and glucose analysis via HPLC. For the wild type specifically the evolution of the ammonium concentration was determined using an enzymatic assay from R-Biopharm (Germany). The exhaust gas was gathered continuously using a BlueSense Exhaust Gas Analyzer (BlueSense Gas Sensor GmbH, Germany). For the γ-NADA producer 1 mL samples for the quantification of intracellular γ-NADA were taken after 7 h of process time. Cell disruption was achieved by freeze/thaw cycle at -20 °C and RT. The released γ-NADA concentration was then measured by HPLC as described in but the HPLC samples were prepared similar to extracellular ectoine samples by 1:10 dilution in mobile phase. The exhaust gases were gathered continuously using a BlueSense Exhaust Gas Analyzer (BlueSense Gas Sensor GmbH, Germany).

3.10 Plasmid maintenance in *H. elongata*

The plasmid maintenance was investigated in *H. elongata* Δ*gltDB*::SmR, harboring the plasmid pSEVA238-eGFP/*lacIp-gdhA*. To monitor its presence during growth, eGFP expression from this plasmid was induced (XylS/Pm) and with the fluorescent signal the amount of plasmid loss was inferred.

3.10.1 Plasmid loss in non-selective medium and fluorescent imaging

H. elongata Δ*gltDB*::Sm^R (pSEVA238-eGFP/lacIp-*gdhA*) was inoculated from a selective agar plate directly in 10 mL complex LB medium supplied with 1 M NaCl. The induction of eGFP expression was done immediately with inoculation (0.1 mM 3-MB). After reaching the stationary phase, an aliquot plated on a non-selective LB agar plates with 1 M NaCl and 0.1 mM 3-MB inducer. The plates were incubated at 30 °C until single colonies were formed. Using fluorescent imaging of the plates in a laser scanner (Amersham Typhoon, GE Healthcare Europe GmbH, Germany) the emitted eGFP and, thus, presence of the plasmid within the single colonies was detected. Additionally, from each plate, 50 single colonies were tested regarding growth on solid MM63 minimal medium without supplemented glutamate.

3.10.2 Plasmid loss in minimal medium with different selection pressures

Baseline experiments for plasmid loss

Preparation and execution of the plasmid loss experiments in 100 mL shake flasks was done as described in the general procedure. For the main cultures, five different media based on the default MM63 minimal medium with various supplements as described in Table 3.1 were used. The baseline experiments in medium (1) and (2) were done individually while media (3), (4), and (5) were tested simultaneously in one experiment. In all media except for medium (1), in which the GOGAT knockout strain without plasmid pSEVA238-eGFP/*lacIp-gdhA* was used, the induction of eGFP expression was done immediately upon inoculation of the main culture medium. Because different strains and media compositions were used the pre-culture media were also slightly altered in respect to each main culture experiment. In the initial 1 M NaCl LB overnight culture, for all except the main culture medium (1) 50 μg/mL kanamycin was supplied. In the subsequent 1M NaCl MM63 minimal medium, for the main culture medium (1), only 1.25 g/L glutamate was added while for all others 1.25 g/L glutamate and 50 μg/mL kanamycin was added. The third pre-culture step was omitted for all. The 10 mL main culture media were inoculated with the inoculum volume adjusted to a starting OD600 of 0.01. Except for main culture medium (1) eGFP synthesis was induced with 0.1 mM 3-MB immediately upon inoculation. The OD600 and eGFP fluorescence (excitation λ 485 nm, emission λ 520 nm) were measured in an automated microplate reader (Tecan, Austria). Fresh sterile cultivation medium was used as a blank for each new measurement.

Plasmid loss in the early exponential phase of *H. elongata* Δ*gltDB*::SmR

H. elongata Δ*gltDB*::Sm^R shows a bi-phasic growth when grown in batch with a decreased growth rate after reaching an OD600 of 0.2. The plasmid loss experiments in media (3), (4), and (5) (details in Table 3.1) within the first exponential phase was tested in a prolonged initial phase. The pre-cultures and main cultures were prepared as described in the baseline experiments. After reaching the critical OD600 of 0.2 the cultures were diluted in fresh medium, respectively medium (3), (4), or (5), to a starting OD600 of 0.01.

Plasmid	Description	Glutamate [g/L]	Kanamycin [μg/mL]	Medium
-	Baseline for autofluorescence	1.25	0	(1)
+	Baseline both selection pressures	0	50	(2)
+	No selection pressure	1.25	0	(3)
+	Seletion via kanamycin	1.25	50	(4)
+	Selection via GDH	0	0	(5)

Table 3.1: Overview of all media used in determining the plasmid maintenance in *H. elongata*. The presence of the plasmid pSEVA238-eGFP/*lacIp-gdhA* in *H. elongata* Δ*gltDB*::Sm^R in the specific experiment is indicated with + for present and - for not present. With medium (1), the autofluorescence of *H. elongata* to identify the fluorescent signal caused by the presence of the plasmid. In medium (2), both selection pressures are applied, while in medium (3) the opposite with no selection pressure is tested. Finally, in the media (4) and (5) the antibiotic resistance and complementation of ammonium utilization are used as selection markers, respectively.

3.11 Transcriptomic analysis

3.11.1 Strains and growth conditions for RNA sampling

The strains analyzed via RNA-Seq were the *H. elongata* wild type in varying conditions and two modified strains, the Leaky Mutant (*H. elongata* Δ*teaABC* Δ*doeA*) and *H. elongata*-PCK (*H. elongata* Δ*teaABC* Δ*doeA* Δ*pckA*) in 1 M NaCl MM63 minimal medium with glucose. A summary of all combinations of

conditions and strains is listed in Table 3.2. Two batch experiments were performed with the wild type grown in the salt extremes in one and the remaining cultivations at 1 M NaCl with different carbon sources and strains in the other. The cultures were grown following the general procedure for shake flask cultivation (500 mL volume) described before in 50 mL scale. But in the third pre-culture step 5 mL medium instead of 3 mL was used. In this step always the same medium as the main culture is used.

Condition	Strain	Salt [M]	Carbon source	Batch
Low salt	Wild type	0.17	Glucose	1
High salt	Wild type	2.0	Glucose	1
Salt optimum	Wild type	1.0	Glucose	2
Gluconeogenesis	Wild type	1.0	Glucose	2
Modified strain	Leaky Mutant	1.0	Glucose	2
Modified strain	PEPCK knockout	1.0	Glucose	2

Table 3.2: Overview of all combinations of investigated growth conditions and *H. elongata* strains used in the RNA-Seq analysis.

3.11.2 RNA isolation, sequencing method, and data processing pipeline

Samples for the RNA-Seq taken in the exponential phase at an approximate OD600 of 0.5. For the first batch, 10 mL samples were taken and mixed 2:1 with RNAprotect reagent (Qiagen, Germany), which is used to stabilize the RNA and preserve the expression profile. The biomass was separated by centrifugation (Heraeus Megafuge 16R Centrifuge, Thermo Fisher Scientific, USA) for 5 min at $4752g$ and RT. In the second batch, RNAprotect reagent (Qiagen, Germany) was applied in a ratio of 1:1 to 4 mL samples except for the acetate cultures for which 6 mL samples were taken. The samples were centrifuged for 7 min to separate the biomass. The total RNA was extracted with the Macherey-Nagel NucleoSpin RNA kit (Macherey Nagel, Germany) as described by the manufacturer and sent to GATC Biotech (Germany) for strand-specific cDNA library generation and RNA sequencing. The company performed RNA-Seq on either the Illumina HiSeq 4000 (first batch) or the Illumina NovaSeq 6000 S4 XP (second batch). The obtained reads for the first batch were single-end read and 50 bp long, and for the second batch paired-end reads and 150 bp long. The quality of the FASTQ files was checked using FastQC and no trimming or filtering was necessary. Alignment of the reads to the genome was done with Bowtie2. The number of reads per gene was calculated using SAMtools. Normalization of the raw counts regarding the GC content was performed using EDASeq. The obtained counts were then converted to TPM (transcript per million) and analyzed using a Python script.

3.12 Nile-red staining of poly-hydroxybuytrate (PHB) granules

The formation of PHB granules was detected via Nile-red staining as demonstrated by Gorenflo *et al.* [75]. The Nile-red stain, due to its lipophilic nature, is able to bind to the PHB-polyesters which are accumulated as insoluble inclusion bodies in the cytoplasm. Using the emitted fluorescent signal from the Nile-red stain, the presence and amount of PHB can be assessed. For the staining, living *H. elongata* cells were treated with a 1 mg/mL Nile-red stock solution (in acetone) to an end concentration of 3 μg/mL. The cells were examined under an Olympus IX70 microscope (Olympus, Japan) using a 60X objective and the Nile-red fluorescence was excited with a polychromator at a wavelength of 560 nm.

3.13 Quantification of substances via high-performance liquid chromatography

3.13.1 Glucose quantification

Glucose was measured via high-performance liquid chromatography (HPLC) in an Agilent 1100 series machine (Agilent, USA) using a Shodex SH 1011 column (Showa Denko Europe GmbH, Germany). The column was kept at a constant temperature at 60 °C. The mobile phase was 0.5 mmol/L H_2SO_4 with a flow rate of 0.45 mL/min. 20 μL per sample was injected.

3.13.2 PHB detection by conversion to crotonic acid

PHB quantification via HPLC analysis was performed by conversion of PHB to crotonic acid [99]. The biomass of 0.9 mL of the sample culture was digested in 0.25 mL concentrated sulfuric acid. After incubation for 1 h at 90 °C, the PHB is depolymerized forming crotonic acid, which can be detected by HPLC at 210 nm. For the separation, a reverse phase column was used (Kinetex 5 μm EVO C18 150/3, Phenomenex, USA) applying a 0.007 mol/L H_2SO_4 solution as mobile phase. The digested PHB samples were diluted 1:10 with the mobile phase.

3.13.3 Quantification of intracellular and extracellular compatible solutes

Intracellular ectoine content [g/gDW]

The quantification of intracellular ectoine using RP-HPLC was described in Hobmeier *et al.* [86]. The ectoine extraction was done using a two-phase protocol developed by Bligh & Dyer [19] and modified by Galinski & Herzog [67]. For this, the biomass was separated by centrifugation (15000g, 5 min, RT) and the supernatant was carefully removed. The cell pellet was then treated with 250 μL extraction solution comprised of methanol, chloroform, and bidestilled water in a 10:5:4 ratio. The mixture was incubated for 30 min at RT and under shaking (300 rpm, Thermomixer Comfort Typ 5, Eppendorf). Subsequently, 65 μL chloroform and bidestilled water were added followed by a second incubation period of 10 min under the same conditions as previously. The phase separation was achieved by centrifugation (8000g, 5 min, RT). From the upper aqueous phase (theoretical volume: 0.25 mL) 0.1 mL was removed and diluted in 0.9 mL acetonitrile/phosphate (71/29) mobile phase. The separation of ectoine was achieved with a reverse phase column (Nucleodur 100-5 NH2-RP CC 125/4, Macherey Nagel, Germany) and detected at 210 nm using a UV-detector [86, 114]. The ectoine concentration measured via HPLC an corrected by the dilution was then used to deduce the mass of ectoine in the taken sample. With the biomass inferred by the OD600 to biomass correlation the ectoine per dry weight was determined.

Extracellular ectoine concentration [g/L]

First, the biomass in the samples was separated by centrifugation (15000g, 5 min, RT) and the supernatant was carefully removed. Then either 0.1 or 0.05 mL of the supernatant was diluted in 0.9 or 0.95 mL (1:10 or 1:20 dilution) acetonitrile/phosphate (71/29) mobile phase. The separation of ectoine was achieved with a reverse phase column (Nucleodur 100-5 NH_2-RP CC 125/4, Macherey Nagel, Germany) and detected at 210 nm using a UV-detector [86, 114].

Intracellular γ-NADA content [g/gDW]

γ-NADA quantification was performed similarly to ectoine quantification using the same reverse phase HPLC method. As a linear molecule, the UV signal for γ-NADA was detected at a wavelength of 198 nm. The presence of extracellular γ-NADA was checked with samples taken directly from the supernatant after separation from the biomass. The supernatant was diluted at 1:10 with the mobile phase acetonitrile/phosphate (71/29). The intracellular content was routinely determined as described

in Kuhlmann & Bremer [114] and Hobmeier *et al.* [86] by extraction with chloroform. 0.1 mL of the aqueous phase was diluted with 0.9 mL mobile phase and used as the sample for HPLC analysis. As an exception to this, for the batch cultivation in a bioreactor at 2 L scale (Labfors 5 fermenter, InforsHT, Switzerland) the intracellular ectoine was released via freeze thawing. 1 mL of culture broth was frozen at -20 °C for 24 h and, after thawing, the biomass was separated by centrifugation (15000 *g*, 10 min, RT). The γ-NADA concentration in the supernatant was then determined by diluting it 1:10 with the mobile phase and analyzing the diluted sample with the previously described HPLC method.

4 Results

4.1 Characterizing the *H. elongata* wild type

4.1.1 OD to Biomass correlation via Simultaneous Thermal Analysis

One of the most important parameters to monitor and control a biotechnological process is undoubtedly the available biomass of the organism in question. Methods to determine the actual dry weight (DW) of the biomass directly from the cultivation medium, however, are lengthy since it is necessary to completely remove the water in the sample. Therefore, it has been well established to use other more easily and quickly measured parameters to lead back to the DW, like the optical density at 600 nm (OD600) allowing the swift monitoring of a biological process. The OD600, on the other hand, is dependent on the absorbance of the measured subject. Changes in cell composition of a microbe due to growth conditions let alone different strains will result in changes in the correlation between OD600 and DW.
To identify the specific correlation for *H. elongata*, the actual DW of samples with known OD600 values ranging from 0.2 to 1.2 during the exponential growth was determined. Regarding the medium composition, the most abundantly analyzed salt concentration in this work was chosen: 1 M NaCl with glucose as the sole carbon source. However, the high salt content of the medium creates difficulties for the conventional determination of the dry weight, where inorganic components are often neglected. Especially for marine organisms, the ash-free dry weight (AFDW) which separates the organic biomass from the inorganic components, is a better option to use [179]. The practical measurement of separating the organic and inorganic parts in a biomass sample was carried out using simultaneous thermal analysis (STA) coupled with mass spectrometry (MS). The *H. elongata* biomass samples were obtained by growing several shake flask cultures inoculated from the same pre-culture in parallel. For these, an average growth rate of 0.360 h^{-1} ($R^2 = 0.997$) was determined. At five different OD600 values during exponential growth – more precisely at OD600 0.2, 0.4, 0.8, 1.0, and 1.2, – material for the STA was gathered. The procedure is described in detail in Hobmeier *et al.* [86]. In Figure 4.1a the progression of the thermogravimetry analysis (TGA) signal in Mass% of these samples during combustion is depicted. All samples showed the same pattern with four distinct steps. Together with the MS signal (Figure 4.1b, exemplary for one sample) monitoring the emitted ion current, it is possible to estimate what happened in each stage. Initially, the residual water evaporated. Within all five samples, the evaporation of free remaining water was found to be concluded after reaching a temperature of 160 °C. After that, there was a gradual production of CO_2 and H_2O by combustion. The different steps are likely due to the combustion of different types of molecules at different temperatures. Afterwards, at 800 °C, another loss of mass was observed without the release of CO_2 and H_2O illustrating that all organic components had already been burned at this point. By determining the amount of water content at the beginning of the combustion and the portion of inorganic components left after 1000 °C, the AFDW can be assessed. Like this, the correlation between AFDW and OD600 for the *H. elongata* wild type grown in MM63 minimal medium with 1 M NaCl and glucose as substrate was determined:

$$AFDW\ \frac{g}{L}\ [H.\ elongata\, wildtype] = 0.485 \cdot OD_{600} - 0.026,\ R^2 = 0.971 \tag{4.1}$$

The OD600 to AFDW correlation was also performed via STA for the modified *H. elongata* strains *H. elongata* Δ*ectC* and *H. elongata* Δ*ectC*σ^{38} RBS in an OD600 range of approximately 0.5 to 18:

$$AFDW\ \frac{g}{L}\ [H.\ elongata\, \Delta ectC] = 0.268 \cdot OD_{600} + 0.031,\ R^2 = 0.993 \tag{4.2}$$

$$AFDW\ \frac{g}{L}\ [H.\ elongata\, \Delta ectC\ \sigma^{38}\ RBS] = 0.284 \cdot OD_{600} + 0.144,\ R^2 = 0.998 \tag{4.3}$$

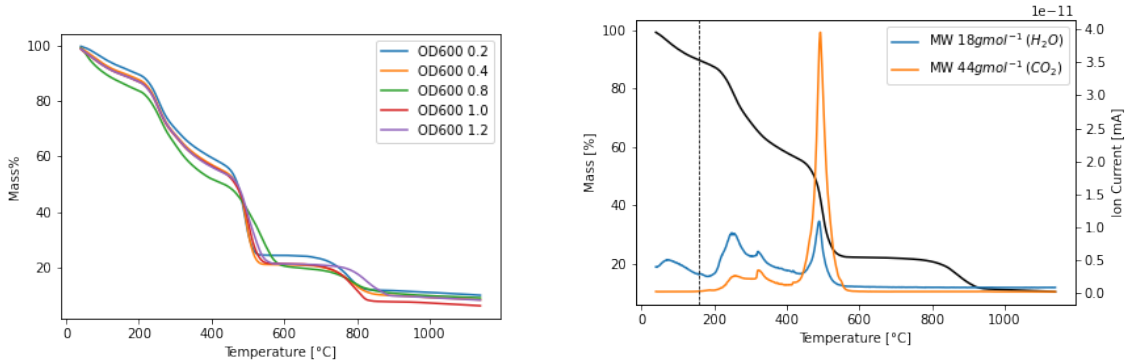

(a) All TGA signals

(b) TGA signal and MS signals (H_2O and CO_2) exemplary for one sample

Figure 4.1: TGA and MS signals gained by STA reveal several combustion steps with the biomass combustion taking place between 400 and 600 °C. (a) Evolution of the TGA signals with increasing temperature for each sample of the wild type taken at a different OD600 during culture growth. Combustion and the resulting mass reduction takes place in three steps. At 1000 °C, only inorganic components remain. (b) TGA signal (black) and MS signals for molecular weight of 18 g/mol corresponding to H_2O (blue) and molecular weight of 44 g/mol corresponding to CO_2 (orange) for one representative sample. The dashed vertical line indicates 165 °C, at which free remaining water is evaporated. Biomass combustion takes place at around 500 °C indicated by the peak observed for thee CO_2 MS signal.
TGA: thermogravimetry analysis, MS: mass spectrometry, STA: simultaneous thermal analysis.

All three OD600/DW correlations are also illustrated in Figure 4.2. The correlations for the modified strains *H. elongata* Δ*ectC* and *H. elongata* Δ*ectC*σ^{38} RBS showed a very different relationship compared to the wild type but were very similar to each other. With drastically different correlations like this, a similar OD600 for cultures of wild type and the modified strains translates to a much lower actual AFDW for the latter.

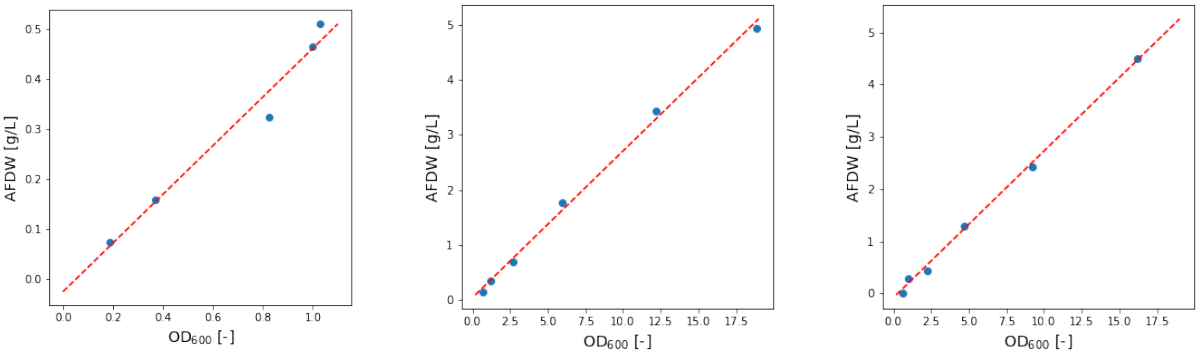

(a) wild type

(b) Δ*ectC*

(c) Δ*ectC*σ38*RBS*

Figure 4.2: Correlations of OD600 and AFDW determined via STA for (a) the *H. elongata* wild type and the two γ-NADA producers (b) *H. elongata* Δ*ectC* and (c) Δ*ectC*σ38*RBS*.
AFDW: Ash-free dry weight, STA: Simultaneous Thermal Analysis.

4.1.2 Growth of *H. elongata*: nutrient demand

Maximum growth rate in complex medium

In a rich (complex) medium, the cell can focus its metabolism on protein synthesis and transport of precursors in order to reach its maximum growth rate [45, 89, 254]. To find its maximum growth rate, *H. elongata* was grown in a complex medium enriched with 1 M NaCl. Here, an average rate of $0.878 \pm 0.022\ h^{-1}$ was obtained (Figure 4.3). As a comparison, the same cultures were inoculated in 1 M NaCl MM63 minimal medium with glucose as the sole carbon source. Here, all amino acids needed to be synthesized by the cells themselves, which resulted in a decrease in growth rate. In minimal medium the obtained growth rate was $0.479 \pm 0.027\ h^{-1}$, which is only about half of the growth rate achieved in complex medium.

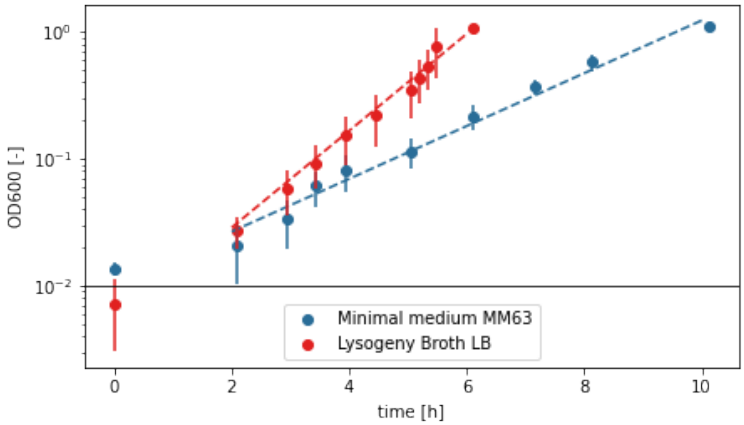

Figure 4.3: Average growth rate found in LB complex medium in contrast to minimal medium MM63 for the *H. elongata* wild type. Depicted is the OD600 over time for three shake flask cultivations per medium in a semi-logarithmic plot. With the average slopes representing the growth rates illustrated with dashed lines a faster growth in LB complex medium compared to MM63 is evident.
Red: LB complex medium, Blue: minimal medium MM63.

Composition of minimal medium

To study the behavior of the *H. elongata* wild type and modified strains derived from it, growth experiments were carried out exclusively in minimal medium with clearly defined conditions. To identify which compounds of the minimal medium have an impact on the growth rate and biomass formation, three essential salts were varied: NaCl, NH_4^+, and PO_4^+ (raw data from Nguyen [152]). As a moderate halophile, the sodium concentration is one of the major factors determining its growth, which has been mathematically approximated by Dötsch *et al.* [52] using substrate inhibition kinetic models. An optimum with the highest growth rates achieved was found at moderate sodium concentrations of 0.5 to 1 M NaCl, while either below or above this range the rates decrease. Additionally, the oxygen solubility in the medium decreases with an increasing salt concentration [208]. Calculations of the solubility showed that at high salt (2 M NaCl) it is only about half of that at low salt conditions (0.17 M NaCl). For aerobic halophiles, this might have an impact on growth. Further, the nitrogen concentration is inevitably linked to biomass and ectoine synthesis since it is part of their empirical elemental formulas. Finally, the phosphate in the medium can be used in cellular functions but is generally used in media to control the pH due to its high buffering capacity. To avoid performing a vast number of experiments while testing each compound individually, the medium composition was evaluated using a central composite

design experiment. This systematic method additionally allows conclusions about possible interactions between the examined input factors. With the three factors NaCl, NH_4^+, and PO_4^+, the corners of a cube in a three dimensional space are defined (full factorial design), with every point representing an iteration of a low and high setting for each combination of each factor [230]. A visualization of this is shown in Figure 4.4. This can also be represented as a matrix with low and high settings described by -1 and 1, respectively. Translating this into a function the influence of each factor individually and their interactions was assessed:

$$y = intercept + \beta_A x_A + \beta_B x_B + \beta_C x_C + \beta_{AB} x_A x_B + \beta_{AC} x_A x_C + \beta_{BC} x_B x_C + \beta_{ABC} x_A x_B x_C \quad (4.4)$$

To increase the accuracy and detect non-linear behavior, supplementary points at the extreme ends of each factor (star points) as well as a central point were also observed. This setup is referred to as central composite design which is illustrated in Figure 4.4. The distance of the star points to the center can be calculated using the following equation.

$$\alpha = (2^k)^{0.25} \quad (4.5)$$

With three factors (k = 3) the distance α is —1.682— for the extreme star points. The design space covers the central point at 0, the factorial design cube points located at -1 and 1, and the star points at -1.682 and 1.682. Thus, in a central composite design, each factor is described at five levels (Table 4.1) which allows the estimation of curvature compared to a linear approximation with only the factorial design [15]. An overview of all 15 experiments is summarized in Table A.8 together with the two observed effects growth rate μ and biomass formation reflected by the maximal achieved OD600 (OD_{max}) in the stationary phase.

Taking a closer look at the achieved growth rates, two conditions lead to slower growth than the average. This includes medium M14 (specified in Table A.6), which was the star point for low sodium (-1.682, 0, 0), and medium M10 (specified in Table A.6), the factorial point for the single effect of sodium (1, -1, -1). Here, growth rates of 0.332 ± 0.035 h^{-1} and 0.304 ± 0.055 h^{-1} were observed. In between these two, no statistical difference was observed (p = 0.715) suggesting a similar decrease for both conditions. Remarkably, the growth rate of only one of the two extreme star points for sodium was

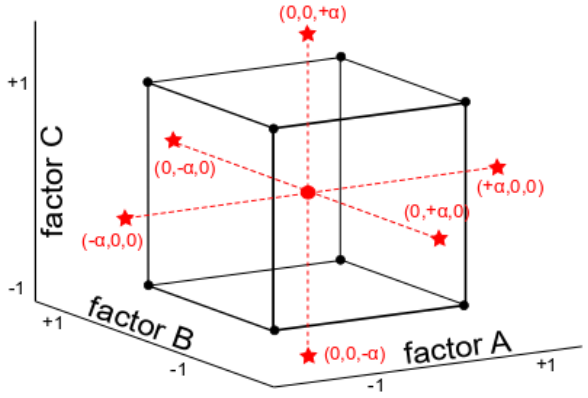

Figure 4.4: Schematic for the investigated design area in a central composite design experiment with three factors A, B, and C. The factors chosen for the investigation of the medium composition are the components NaCl, NH_4^+, and PO_4^+. The edges of the black design cube represent the conditions for the 8 factorial experiments. The red circle in the center of the factorial design cube represents the center point of the central composite design, and the remaining red stars are also part of the central composite design representing the extreme star points. The coordinates of the star points respective to the central point are given in parentheses with α according to equation 4.5.
Factor A: NaCl concentration, factor B: NH_4^+ concentration, factor C: PO_4^+ concentration.

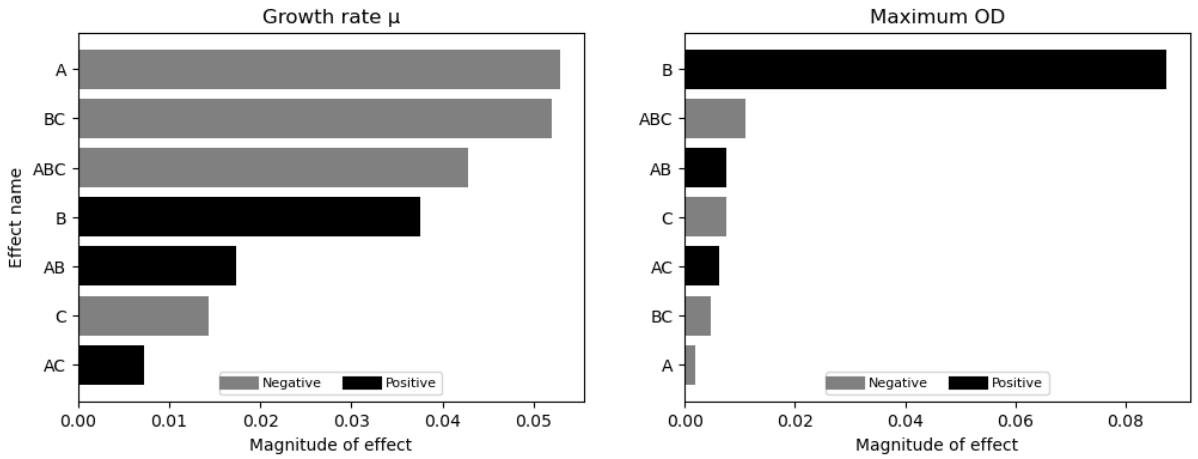

Figure 4.5: Bar charts depicting the magnitude of effect of each factor and all possible interactions on the following two responses: the growth rate (left) and the maximum OD (right). The magnitude of effect is determined by predicting the coefficients (absolute values) for equation 4.6 using linear regression. Positive coefficients representing a positive effect on the response are colored black while negative coefficients a negative effect on the response are grey. The growth rate is impacted by a variety of factors including negatively by the NaCl concentration (A), the interaction of NH_4^+ and PO_4^+ concentration (BC), the interaction of all three medium components NaCl, NH_4^+, and PO_4^+ concentration (ABC), and positively by the NH_4^+ concentration (B). In contrast, the maximum OD is only impacted by one factor: positively by the NH_4^+ concentration (B).
A: NaCl concentration, B: NH_4^+ concentration, C: PO_4^+ concentration, AB: interaction of NaCl and NH_4^+ concentration, BC: interaction of NH_4^+ and PO_4^+ concentration, AC: interaction of NaCl and PO_4^+ concentration, ABC: interaction of NaCl, NH_4^+, and PO_4^+ concentration.

decreased - specifically the point at higher salinity. However, the drop in growth rate for a higher sodium concentration in combination with lower amounts of nitrogen and phosphate suggests interactions that are more prevalent at high salt levels.

Using function 4.4, the coefficients for each factor and its interactions were predicted for the growth rate data as follows:

$$y_\mu = 0.500 - 0.053x_A + 0.038x_B - 0.014x_c + 0.017x_Ax_B + 0.007x_Ax_C - 0.052x_Bx_C - 0.043x_Ax_Bx_C \quad (4.6)$$

Level of factor	**NaCl [M]**	**NH_4^+ [mM]**	**PO_4^+ [mM]**
$-\alpha$, extreme low	0.17	0.66	11.70
-1, low	0.54	1.34	23.52
0, center	1.09	2.33	40.85
$+1$, high	1.63	3.33	58.18
$+\alpha$, extreme high	2.00	4.00	70.00

Table 4.1: Schematic for the investigated area regarding the three minimal medium components A = NaCl, B = NH_4^+, and C = PO_4^+. The black circles represent the conditions for the 8 factorial experiments. The red circle in the center of the factorial design cube represents the center point of the central composite design, and the remaining red stars are also part of the central composite design representing the extreme star points.

In Figure 4.5, the absolute values of the predicted coefficients were listed according to their value reflecting the importance of the respective factor for the effect in question. The two most relevant factors for the growth rate with a negative relation were the sodium concentration (A) as well as interactions between nitrogen and phosphate (BC). Next, interactions between all three factors (ABC) seemed to have an influence. Overall, there were several different factors and interactions that impacted the growth rate in a similar magnitude hinting towards a rather diverse interplay of all factors. This was also indicated by the low coefficient of determination for the linear regression of only $R^2 = 0.576$. A comparison with the maximum OD600 revealed a much simpler relationship for the biomass accumulation. The only important factor here was the nitrogen concentration (B) with a positive correlation to the achieved OD600 values. Nitrogen is generally one of the main components of biomass with about a fourth of the nitrogen atoms needed for every carbon atom [11]. Thus, without the needed building blocks, no biomass can be generated. A linear fit for the OD600 data against the NH_4^+ concentration gives a positive correlation ($R^2 = 0.909$) of:

$$OD_{600}[-] = 0.081 \cdot NH_4[mM] + 0.061 \tag{4.7}$$

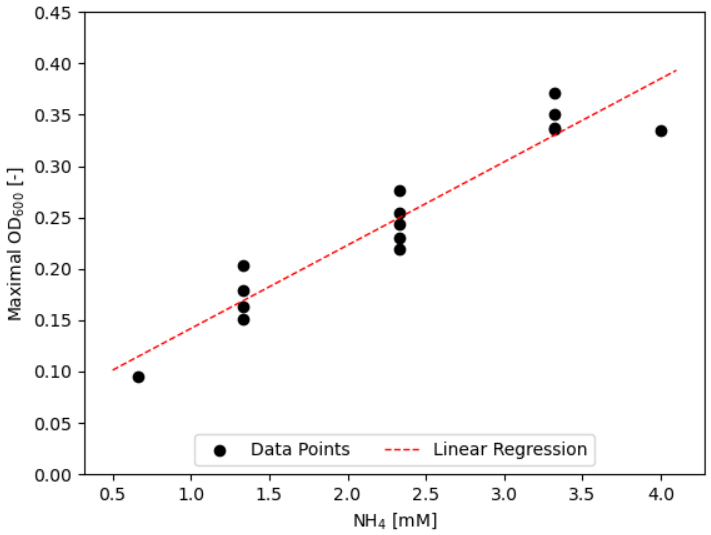

Figure 4.6: Linear correlation of the NH_4^+ concentration available in the medium and the amount of biomass accumulated represented by the maximum achieved OD600. Regarding the biomass increase only the component NH_4^+ concentration was found to have a major influence. The linear fit (equation 4.7) is illustrated by the dashed red regression line.

There is one unfavorable combination in particular in the tested media that resulted in a significantly lower growth rate as well as less biomass formation. In this composition (M10, specified in Table A.6) the sodium concentration was high while the concentrations of the other components are low. As mentioned before, for increasing NaCl concentrations above 1 M, the growth rate is known to decrease steadily [52]. Due to the higher osmotic pressure, a greater amount of compatible solute ectoine needs to be synthesized which is likely responsible for the higher nitrogen demand. On the other hand, even though the growth rate was also reduced at the other extreme in low osmolarity, the impact of the other two components was minor in comparison to the high NaCl condition. The highest growth rate was achieved with high NH_4^+ and low PO_4^+ concentrations, which was also the case for growth in high salt. But here a second maximum was observed for exactly the opposite composition with high PO_4^+ and low NH_4^+ concentrations. As depicted in the 3D plot in Figure 4.7a, an area of moderately fast growth is spanned diagonally across the design space with maxima on either end forming a saddle. In contrast, a 3D plot for low salt depicted in Figure 4.7b with the same scaling resembles a slightly upturned plane towards

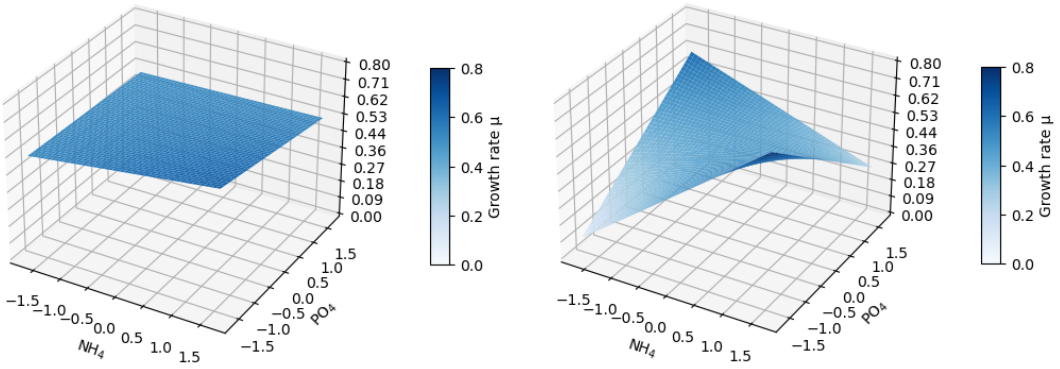

(a) Low NaCl (Factorial design: -1)

(b) High NaCl (Factorial design: +1)

Figure 4.7: 3D plot comparing the impact of varying the NH_4^+ and PO_4^+ concentration in (a) low NaCl and (b) high NaCl conditions on the growth rate. (a) At a low NaCl concentration an inclined plane with a maximum in one corner is observed. Fastest growth is observed for the combination of a high NH_4^+ and a high PO_4^+ concentration. (b) At a high NaCl concentration a saddle forms. The fastest growth is observed for either a low NH_4^+ in combination with a high PO_4^+ concentration or for a high NH_4^+ in combination with a low PO_4^+ concentration. If the NH_4^+ and PO_4^+ concentrations are both high or low drastically slower growth was observed. Overall, compared to the changes in growth rate at high NaCl concentration, the impact at low NaCl concentration is minor.
Low NaCl: 0.54 M, high NaCl: 1.63 M, low NH_4^+: 1.34 mM, high NH_4^+: 3.33 mM, low PO_4^+: 23.52 mM, high PO_4^+: 58.18 mM.

high NH_4^+ and low PO_4^+ concentrations.

Going back to the schematic of the design space in Figure 4.4 with all investigated points for the full factorial design and the central composite design, the design space is shown in Figure 4.8 with color-coded points representing the achieved growth rates. Looking at the color gradient directly in the design space like this, it is evident that an area with high growth rates was found for the low NaCl points of the factorial cube and only at extremely lower sodium concentrations at the negative star point growth was notably reduced. This is reasonable since these low sodium points represent a NaCl concentration of 0.54 M, which is still considered within the growth optimum of *H. elongata*. The highest growth rates were observed with high nitrogen but low phosphate concentrations with either high or low sodium. Also, in agreement with this, considerably fast growth for the extremely low phosphate star point hints towards a good distribution of these three medium components in this area. Remarkably, however, the star point with an extremely high phosphate concentration which is not connected to the area described before, showed a high growth rate as well. This suggests that there are local maxima for the optimum growth speed.

Variation of carbon sources at low salinity

Next to the overall salt composition of the medium, another major influential factor for bacterial growth is the available carbon source. In natural environments, a wide fluctuation of the available resources is to be expected. Because carbon is the main component of biomass, microorganisms are generally able to utilize a great range of different types. Depending on the used carbon source, entirely different uptake mechanisms and catabolic pathways may be activated. In the majority of experiments in this work, glucose is supplied as the only available carbon source. Glucose is most likely metabolized via the Entner-Doudoroff (ED) pathway in *H. elongata* as described in detail before [107]. However, *H. elongata* is able to utilize a great variety of other carbon compounds as well. To explore the different pathways available to *H. elongata* and to characterize the impact on the global phenotype, growth on a variety of carbon sources was examined. In the following, the growth rates and biomass accumulation using the

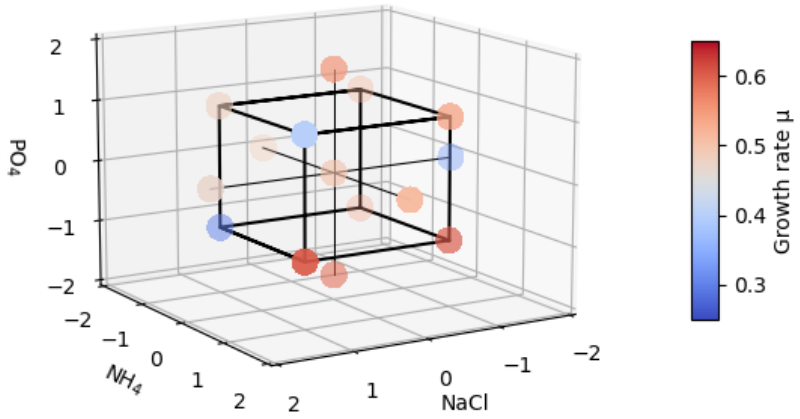

Figure 4.8: Design space for the central composite design experiment with the observed growth rate μ color-coded at the investigated conditions (edges of the factorial design cube, central and star points of the central composite design). On the colorscale high growth rates are shown in red colors, while slower growth rates are blue. There is not a linear gradient across the design space or even a single definite area at which the highest growth rates were observed. The profile is more complex with a local high for high NH_4^+ (3.33 mM) and low PO_4^+ (23.52 mM) concentrations between NaCl concentrations of 0.54 M and 1.63 M.

carbon substrates fructose, sucrose, acetate, citrate, succinate, and D-lactate are described (raw data from Nguyen [152]). Similar to the screening regarding the medium composition, the achieved growth rate in the exponential phase (μ_{max}) and the biomass accumulation after reaching the stationary phase (OD_{600}) were observed. Since it was indicated previously that the medium composition has the least impact on the growth rate at lower salinities, the influence of the carbon sources was tested in low salt condition at 0.17 M NaCl to minimize other effects other than the changing carbon sources.
The published genome annotation revealed that all genes for a fructose-specific phosphotransferase transport system (PTS^{Fru}) are present in *H. elongata* [188]. This includes genes for the membrane translocation machinery *fruAB* (HELO_3696, HELO_3698) and a 1-phosphofructokinase *fruK* (HELO_3697). In its close relative *C. salexigens*, two possible pathways for fructose catabolism exist. There are homologs for the mentioned PTS^{Fru} resembling an Embden Meyerhof Parnas (EMP) pathway, in which Fructose-1,6-bisphosphate (FBP) generated by FruK is further split by an aldolase into Glyceraldehyde-3-phosphate (G3P) and Dihydroxyacetone phosphate (DHP) [166]. However, even though the intermediates for the PTS^{Fru} seem to be EMP-like, it cannot be determined which path is taken after generating FBP. In *P. putida*, for instance, fructose is taken up via the PTS^{Fru} exclusively, but the carbon flux is split between the EMP, ED, and the pentose phosphate pathway (PPP) with a preference for the ED pathway [34]. Furthermore, in *C. salexigens* a second alternative to the PTS^{Fru} is available using an unidentified non-PTS sugar transporter and a soluble fructokinase converting fructose to fructose-6-phosphate (F6P) [166]. In *H. elongata*, a putative fructokinase (HELO_3631) is annotated, suggesting a similar arrangement.

The disaccharide sucrose is made up of one glucose and one fructose molecule. In order to utilize sucrose as a carbon source, it is split into its monosaccharide molecules. For this cleavage, an invertase like the CscA invertase from the *E. coli* W *csc* operon is needed, but no sequence similarities in the *H. elongata* genome could be identified. Even though the presence of a sucrose porin (HELO_3673) hints towards an existing sucrose uptake and *H. elongata* is able to grow on sucrose (this work).
Acetate is a common substrate evoking gluconeogenesis. It enters the central metabolism in *H. elongata* via acetyl-CoA after a two-step conversion catalyzed by acetyl-CoA synthetase (*acs*, HELO_3563). In *E. coli*, this is considered a high-affinity pathway with the alternative low-affinity pathway using an acetate kinase (*ackA*) and subsequently a phosphate acetyltransferase (*pta*). However, in *H. elongata*, the low-affinity pathway is not available.
Citrate and succinate both are direct intermediates of the TCA cycle. Citrate is created in the very first step by joining an acetyl-CoA with oxaloacetate (OAA) creating a six-carbon molecule. Succinate, on the other hand, is the four-carbon molecule generated after the two decarboxylation steps of the TCA cycle. Under aerobic conditions with a functioning TCA cycle, citrate and succinate utilization is solely dependent on an appropriate transport system.
Finally, the way of D-lactate utilization in *H. elongata* is not fully elucidated. L-lactate is converted to pyruvate via the L-lactate dehydrogenase encoded by *lldD* (HELO_1220). An equivalent to this enzyme for D-lactate as, for example, present in *Corynebacterium glutamicum* [100] is not known and no lactate racemase is annotated. But a homolog to a lactate dehydrogenase of unknown specificity (HELO_1046) is annotated.
Figure 4.9 summarizes the growth rates and achieved maximum OD600 values for different carbon source. On average, the growth rate was $0.164 \pm 0.039\ h^{-1}$ and the achieved OD600 value was 0.273 ± 0.049. The mixture of fructose and glucose (Frc/Glc) with one part fructose and three parts glucose did not show a diauxic growth pattern and was further found to be in the average range for either growth rate as well as the achieved OD600 values. Surprisingly, citrate turned out as the carbon source for which the highest growth rate was achieved ($\mu = 0.232 \pm 0.030\ h^{-1}$) but it led to the lowest final OD600 values (0.203 ± 0.023). Citrate formation is a competing branch to PHB synthesis since it uses acetyl-CoA as a precursor. With citrate supplied as the carbon source, the demand for acetyl-CoA to be converted to citrate for operating the TCA cycle might be lowered due to its abundance. This would allow a bigger portion of acetyl-CoA to be available for PHB synthesis, which could explain the difference in obtained biomass for citrate compared to the other carbon sources. In contrast to the fast growth with citrate, a reduced growth was observed for both acetate and D-lactate with growth rates of only $0.120 \pm 0.035\ h^{-1}$ and $0.097 \pm 0.031\ h^{-1}$, respectively.

Table 4.2: List of the carbon sources and the applied concentrations used in the microtiter plate screening to determine which carbon sources can be metabolized and their quality for the *H. elongata* wild type growing at low salinity (0.17 M) specifically.

Carbon source	Concentration [g/L]
Fructose/Glucose	0.625/1.875
Fructose	2.5
Sucrose	2.5
Acetate	2.5
Citrate	2.5
Succinate	2.5
D-Lactate	2.5

In general, bacterial growth depends on the energy content of the substrates and the molecular routes taken by these. Depending at which point the carbon enters, the central metabolism plays a major role in determining the production cost of metabolites. For instance, the metabolic cost for different amino acids is based on the proximity of the entry point to the synthesis pathway. Amino acids with precursors

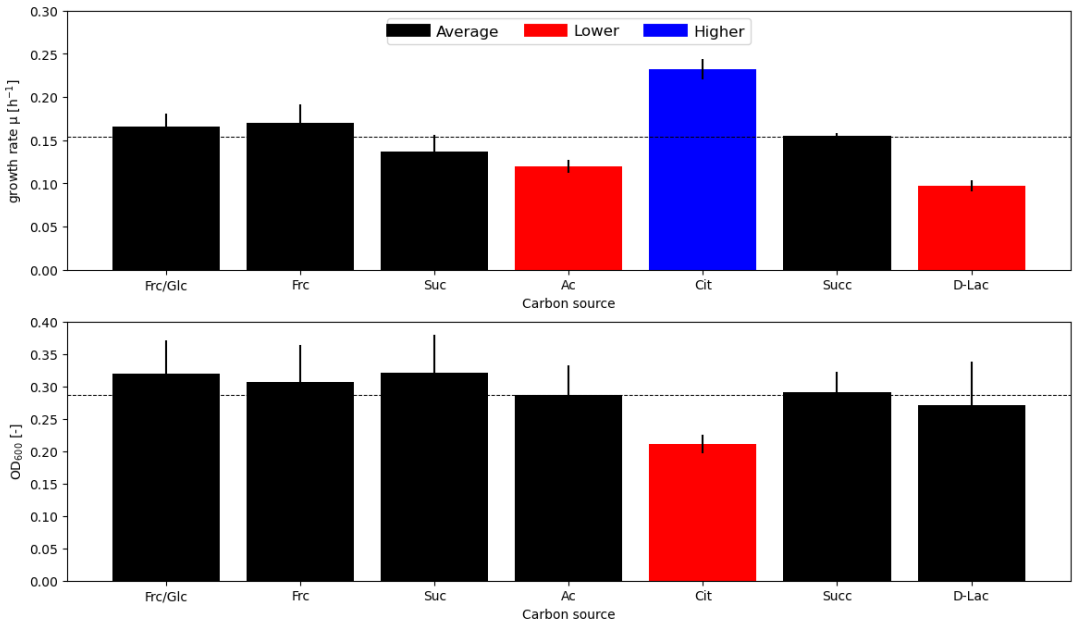

Figure 4.9: Growth rates and maximum achieved OD600 for *H. elongata* wild type growing on various carbon sources at low salinity (0.17 M). The used concentrations for each substrate are listed in table 4.2. The same total concentration (2.5 g/L) of carbon substrate was used for all. The overall average for either growth rate or maximum OD600 is depicted by a horizontal dashed line. The bars for all carbon sources falling within the average are depicted in black. Deviations from the average ($p < 0.01$) are shown in either red for less than the average or blue for higher than the average. Regarding the growth rate, there are two substrates, acetate and D-lactate, for which a lower growth rate than the average was observed. In contrast, for the substrate citrate the growth rate was higher than the average. Regarding the maximum achieved OD600, only citrate falls outside of the average range with a lesser OD600 value achieved by the end of the cultivation.
Frc: fructose, Glc: glucose, Suc: sucrose, Ac: acetate, Cit: citrate, Succ: succinate, D-Lac: D-lactate.

in glycolysis or the PPP are produced with less metabolic cost when using glycolytic substrates as a carbon source but are more expensive during gluconeogenesis. Vice versa, amino acids with precursors in the TCA cycle are cheaper in gluconeogenetic growth but have a higher biosynthetic cost for substrates metabolized via glycolysis [178]. Furthermore, several reactions are directly affected whether growing in a glycolytic or gluconeogenetic fashion with an impact on the metabolism. For example, the phosphoenolpyruvate carboxykinase PEPCK is a key reaction for gluconeogenesis which brings about an additional cost due to its consumption of ATP. Similarly, growing on glycolytic substrates, the reverse anaplerotic reaction catalyzed by phosphoenolpyruvate carboxylase PEPC needs to be active, which consumes high-energy phosphate bonds [227]. Like this, either pathway has its advantages and disadvantages regarding the metabolic cost.
For *H. elongata*, all carbon sources differing from the average in their respective growth rate represent gluconeogenetic substrates. Utilization of acetate via acetyl-CoA synthetase involves the consumption of ATP and yields two carbon molecules. To maintain the number of carbon atoms, the decarboxylation steps of the TCA cycle are circumvented via the glyoxylate shunt converting isocitrate to malate and succinate. This goes hand in hand with the expense of a reduced production of redox equivalents impacting respiration [2, 157]. Especially unfavorable conditions seem to take place for the metabolization of D-lactate exhibiting the lowest growth rate. The conversion of D-lactate to pyruvate via lactate dehydrogenase involves generating a redox equivalent. However, since no specific dehydrogenase has been

annotated, the slow growth might hint towards a longer, more complex set of reactions that might be involved in D-lactate utilization by *H. elongata*. On the other hand, TCA intermediates are also considered to be gluconeogenetic substrates. Succinate shows the same growth rate as the glycolytic substrates and citrate even exceeds them. This fast growth might be connected to the position of citrate as a six carbon molecule situated before the decarboxylation steps of the TCA cycle readily available to produce redox equivalents for the respiratory chain. In the natural PHA producer *P. putida*, which is also able to utilize citrate as a carbon source, the growth behavior compared to glucose is similar [226]. At the same time, Wang & Nomura [226] as well as Follonier *et al.* [60] showed that using citrate as the sole carbon source results in poor PHA production.

Glycolytic and gluconeogenetic carbon sources at the salt optimum

Growing with the glycolytic substrates glucose or fructose, the same growth rates were achieved (raw data from Opperman [160]), whereas with the gluconeogenetic carbon source acetate the growth rate was reduced (Figure 4.10a). Because of the similar growth rates, at a first glance, it seems reasonable to assume that similar pathways are taken for metabolizing glucose and fructose. As a comparison, in *P. putida*, the differences in carbon fluxes growing on glucose and fructose are reflected in its growth rates and biomass yields [34]. It uses the ED pathway to catabolize glucose like *H. elongata*. Fructose is taken up via the PTS^{Fru}, a fructose-1,6-bisphosphatase converts FBP to F6P [154], and ^{13}C studies showed that the flux is split between all three pathways from there. In the traditional glycolysis, the direction of this conversion goes the opposite direction catalyzed by an ATP-dependent phosphofructokinase Pfk and it is generally an irreversible reaction due to the phosphorylation. It constitutes the first committed step of glycolysis and is also its main control point. In *H. elongata*, however, the phosphofructokinase uses pyrophosphate (PP_i) as a cofactor, which makes this reaction reversible [140]. Thus, even though no apparent impact of fructose as a substrate was observed, fluxes through either the EMP, ED, or PPP cannot be excluded.
Comparing the growth rates with those obtained in the screening at low salinity, as expected, notably higher rates were achieved. Where at low salinity with fructose as the sole carbon source only a rate of 0.170 ± 0.022 h^{-1} was observed, at 1 M NaCl the growth rate was 0.439 ± 0.010 h^{-1}, marking an increase of more than 2.5 times. With acetate, the growth rate was up even 3.25-fold from 0.120 ± 0.007 h^{-1} to 0.390 ± 0.052 h^{-1} in the salt optimum. Qualitatively - regarding the substrates themselves - the same pattern was found at both salinities with fructose facilitating faster growth than acetate.
At the same time however, the growth rate of 0.413 ± 0.010 h^{-1} with glucose as the sole substrate was notably slower (about 15 % less) compared to the previously described experiment in minimal medium (Chapter 4.1.2) with the same composition. Throughout this work, it became apparent that the growth rate of *H. elongata* seems to be largely affected by the cultivation mode and volume. To filter out batch effects, experiments were always set up as a matched controls experiment, which include a control group as direct reference.
In contrast to the growth rates, the use of different carbon substrates should not have an impact on the ectoine synthesis. The amount of ectoine present in the cytoplasm is regulated and closely linked to the external salt concentration. An imbalance with either higher or lower levels would lead to water influx or efflux and, consequently, to the swelling or shriveling of the cells [52, 77]. Thus, the same amount of intracellular ectoine is to be expected for all substrates. In Figure 4.10a the measured ectoine content is depicted. No differences in ectoine content between cells growing on glucose and fructose with 0.118 ± 0.003 g Ectoine/g DW and 0.117 ± 0.006 g Ectoine/g DW, respectively. With acetate as a carbon source, a slightly higher content of 0.195 ± 0.045 g Ectoine/g DW was measured. However, this is most likely an artefact produced by the slower growth rates and the sampling. Samples were taken at the same time point meaning that for glucose and fructose more biomass was present and the cultures most likely were at different stages in growth. For glucose and fructose, the ectoine content was measured at an average dry weight of 0.484 ± 0.038 g/L while the biomass for acetate was at only 0.023 ± 0.005 g/L at the time. Since this is especially early in the growth phase, a steady state might not have been reached yet. Kraegeloh & Kunte [112] and Dötsch *et al.* [52] showed in experiments and simulations that after an

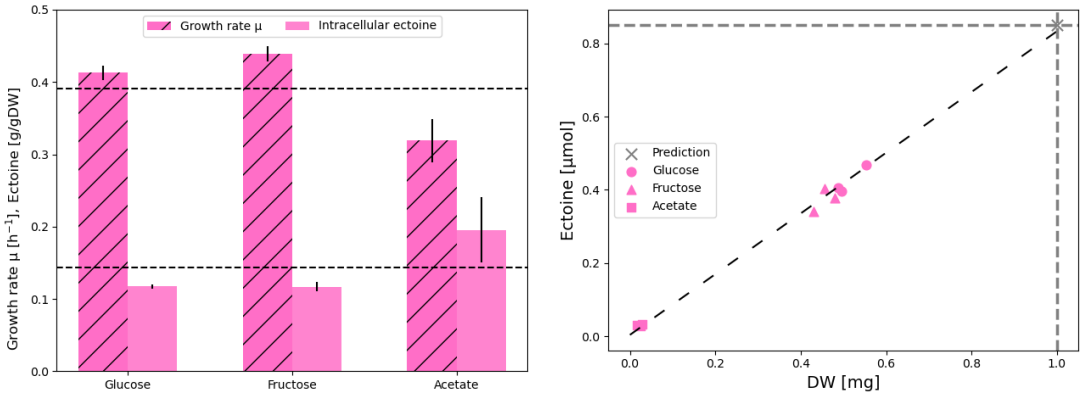

(a) Growth rates and ectoine content

(b) Intracellular ectoine content in 1 mL sample

Figure 4.10: Characteristics of the *H. elongata* wild type (a) Growth rates (left, striped) and intracellular ectoine content (right, no pattern) of the wild type grown at the salt optimum 1 M NaCl with the different carbon sources glucose, fructose, and acetate. The overall averages for all substrates for the growth rate and intracellular ectoine content are depicted in dashed vertical lines. With glucose and fructose higher growth rates than for acetate were observed. Regarding intracellular ectoine a slightly higher content for cultures growing on acetate are shown, which however is most likely an artefact due to the different cultivation stage at which the samples were taken. (b) Total ectoine content in μmol for all tested carbon sources in 1 mL sample. The theoretical prediction based on data from [52] is marked for 1 mg DW in grey. Overall, for the data points gathered regardless of carbon source in this work and the theoretical prediction a linear trend can be observed.
Glucose: circles, fructose: triangles, acetate: squares, theoretical ectoine prediction: grey X.

osmotic upshift the intracellular ectoine levels are briefly overregulated leading to a higher content than necessary. No upshift in salinity took place but the dilution during inoculation of the main culture might cause a similar response. Plotting the ectoine [μmol] against the respective DW [mg] a linear behavior can be observed overlapping with the theoretical prediction for 1 mg DW (Figure 4.10b).

4.1.3 Monod Kinetics in salt optimum: Batch cultivation of *H. elongata*

The illustration of the cellular processes in *H. elongata* as a model network allows for theoretical prediction of the *H. elongata* growth behavior in a certain environment. The known metabolic network based on the stochiometric reactions given by the available enzymes or rather genes defined in the genome annotation [188] was further refined by examining its growth parameters in a bioreactor. Here, cellular processes of biomass convertion can be viewed as a black box model with in- and outputs depicted by defined values like substrate yields and exhaust gases. In this case, the growth at optimal salt condition, at 1 M NaCl was examined in detail. As carbon and nitrogen substrates an initial concentration of 5 g/L glucose and 2 g/L ammonium sulfate was used. Relating this to a general biomass composition of $CH_{1.6}O_{0.37}N_{0.26}S_{0.006}$ [11] the nitrogen substrate was given in excess to limit growth solely by carbon. The maximum growth rate in this cultivation was 0.394 h^{-1} and after complete depletion of the carbon source approximately 8 h after inoculation a biomass concentration 3.200 g/L was achieved. The obtained growth parameters were compared to a previous batch experiment performed with the same conditions and reactor system [168]. All data is summarized in Table 4.3. The averages for the yields between both experiments, which are detailed in Table 4.3 and also illustrated in Figure 4.11a, were then used in a Monod model to allow predictions for biomass and substrate evolution over the course of the cultivation. The resulting model prediction and the experimentally obtained data (only from this work) for AFDW and glucose are illustrated in Figure 4.11b.

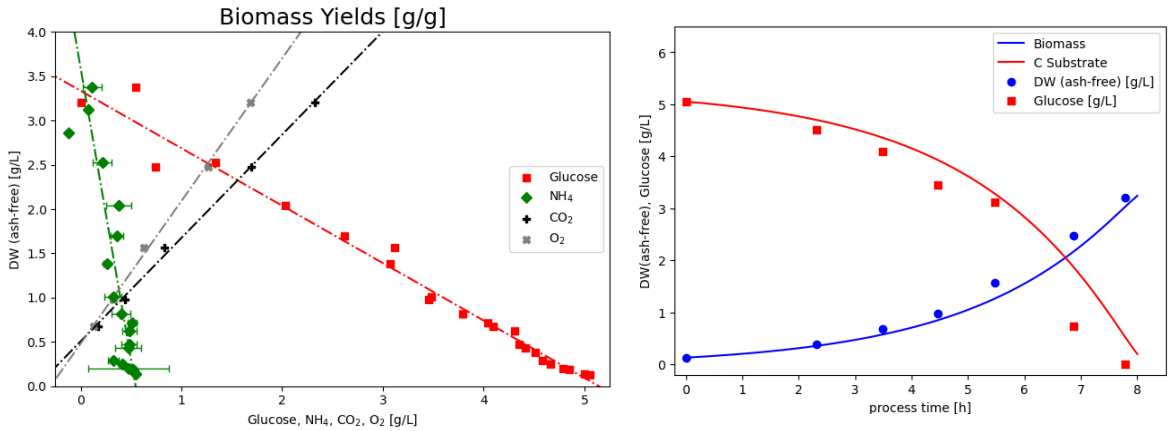

(a) Wild type growth yields

(b) Biomass and substrate prediction

Figure 4.11: (a) Overview of the experimentally determined growth yield for the *H. elongata* wild type batch cultivation which were used in a Monod model. The yields are determined for a 2 L batch cultivation (30 °C, 1000 rpm stirrer speed, 1.25 L/min) in MM63 minimal medium at 1 M NaCl with glucose as the sole carbon source. The data used stems from this work and a previous batch experiment performed with the same conditions and reactor system [168]. (b) Model prediction for biomass and the carbon substrate glucose by implementing the determined growth yields in a Monod model. The experimentally measured data points (only from this work) are overlayed as a scatter.
Biomass (AFDW via OD600): blue circles, carbon substrate glucose: red squares, nitrogen substrate NH_4: green diamonds, carbon dioxide CO_2: black diamonds, oxygen $O2$: grey squares.

The experimentally determined biomass yield $Y_{X/C}$ of 0.587 gDW/gGlc was considerably higher than the predicted theoretical growth yield of 0.466 ± 0.005 gDW/gGlc published by Dötsch *et al.* [52]. In this experiment more biomass was generated per glucose substrate than predicted. The approximation for the intracellular ectoine content based solely on the external salt concentration leads to a theoretical ectoine content of 0.386 g/L for this cultivation.

Table 4.3: Parameters used in the Monod model for the *H. elongata* wildtype growing in 1 M NaCl and with glucose as the sole carbon substrate. For growth rate and glucose yield the averages for two batch cultivations (this work and [168]) were used.

Parameter	Unit	Experimental Data	Previous Data [168]	Used in model
Growth rate μ	h^{-1}	0.395	0.394	0.395
AFDW	g/L	3.200	3.371	3.286
Glucose Yield $Y_{\frac{X}{C}}$	g/g	0.587	0.706	0.646
Ammonium Yield $Y_{\frac{X}{N}}$	g/g	-	6.574	6.574
O_2 Yield $Y_{\frac{X}{O2}}$	g/g	1.204	-	1.204
CO_2 Yield $Y_{\frac{X}{CO2}}$	g/g	1.610	-	1.610

4.1.4 Transcriptome analysis in various growth conditions and strains

Since the sequencing and annotation of its genome, the metabolic reconstruction of *H. elongata* was updated in this work. The latest incarnation of the network benefits from the information obtained by the transcriptomic analysis using experiments and also by careful manual curation of several key pathways. In the following, several updated modules relevant to the transcriptomic response observed

for growth with glycolytic vs. gluconeogenetic carbon substrates and in varying salinities are discussed [87].
The samples for RNA-Seq analysis were generated in two batches with differing library preparations and sequencing lengths. One (low salt, high salt) was sequenced in 50 nt single end reads, while the other (optimum salt, acetate, Leaky Mutant) used 150 nt paired end reads. With longer reads, the information about the specific location in the genome is more reliable, which is important for sequences that appear multiple times in the genome. Similarly, paired end reads help with mappability since not only a single read in one direction is performed like for the single end method. With reads for both directions (paired ends), the positive and negative strand can both be aligned simultaneously [40]. Needless to say, this has to be considered when comparing both datasets. Generally, there are different ways of normalizing the raw reads, accounting for the total number of reads (library size) and transcript length. The RPKM (reads per million) uses the total reads in a sample divided by a million as a scaling factor. The read counts for a transcript are normalized using this scaling factor and the gene length in kilobases [145]:

$$RPKM = 10^9 \frac{Reads\ mapped\ to\ transcript}{Total\ reads\ times\ transcript\ length} \tag{4.8}$$

RPKM is used for single end reads. The FPKM (fragments per million) are made for paired end reads and are calculated like RPKM but taking into account that two reads can stem from one fragment. A problem with comparing RPKMs and FPKMs is that the total number of reads varies between samples. Another normalization – TPM (transcripts per million) – was proposed to solve this issue [130, 222]:

$$TPM = 10^9 \frac{\frac{Reads\ mapped\ to\ transcript}{transcript\ length}}{Sum\ \frac{Reads\ mapped\ to\ transcript}{transcript\ length}} \tag{4.9}$$

The essential difference for TPM is that the normalization for gene length is done before the normalization for sequencing depth. The read counts for a transcript are divided by the transcript length in kilobases, yielding the reads per kilobase (RPK). As a scaling factor, all RPKs are summed up and divided by a million. The TPM for each gene is then calculated, by dividing the RPK by the scaling factor. With this normalization, the sum of all TPMs in a sample is the same [252]. The RNA-Seq results of *H. elongata* in different growth conditions discussed in the following chapters are based on the TPM counts. Statistically relevant changes in the expression of a gene between the samples in different conditions or of different strains (after the normalization to TPM) are described as differentially expressed genes, which were determined using a cut off of |1.5| for the log2 fold change (FC) between two compared conditions or strains [253]. The relevant differentially expressed genes are depicted in heat maps with the columns depicting the genes (locus tag, gene name) and the rows detailing the compared conditions: low salt against high salt (LS/HS), low salt against salt optimum (LS/OPT), high salt against salt optimum (HS/OPT), and acetate against glucose (AC/GLC). Genes shown in red (log2 FC > 1.5) with a positive fold change are upregulated in the condition given in the numerator compared to the denominator and genes shown in blue (log2 FC < -1.5) are downregulated. A log2 FC between -1.5 and 1.5 describes genes that are not differentially expressed which are shown in a greyish color.

Expression correlating to growth

For fast-growing cultures, the expression of many genes correlates with the growth rate [189] though this relation differs for slow growing cultures. For the *H. elongata* wild type growing in different conditions including three salt concentrations (0.17 M, 1 M, and 2 M NaCl) with glucose and one (1 M NaCl) with acetate as carbon source, only 22 genes showed a coefficient of determination greater than 0.6 when relating the TPM linearly to the growth rate. With growth rates for *H. elongata* in defined media generally are below 0.5 h^{-1}, these findings are consistent with those in slow growing cultures. In optimum salt conditions, growth on the glycolytic substrate glucose drastically facilitates faster growth compared to the gluconeogenetic alternative acetate. With a growth rate of 0.244 ± 0.037 h^{-1} on acetate, the growth is reduced almost by half compared to glucose with a growth rate of 0.443 ± 0.039 h^{-1} representing the

slowest growth rate analyzed within the RNA-Seq. All growth rates calculated for the cultures used in RNA-Seq are summarized in Table 4.4. The salt dependence of the growth rate has been mathematically

Strain	Carbon source	Salt [M]	Growth rate μ [h^{-1}]
Wild type	Glucose	0.17	0.353 ± 0.005
Wild type	Glucose	2.0	0.304 ± 0.011
Wild type	Glucose	1.0	0.443 ± 0.039
Wild type	Acetate	1.0	0.244 ± 0.037

Table 4.4: Overview of the growth conditions, carbon source and salt condition, and the respective growth rates for the cultures used in the RNA-Seq analysis.

approximated by Dötsch *et al.* [52]. The reduced version of the model by Yano & Koga [241] predicts growth rates of 0.218 h^{-1} with 0.17 M NaCl, 0.339 h^{-1} in the salt optimum 1 M, and 0.157 h^{-1} with 2 M NaCl. The growth rates achieved experimentally with the cultures used for RNA-Seq analysis are clearly considerably higher. But except for the high salt condition, the obtained growth rates still lie within given variance of the model. When calculating an average for all performed growth experiments at said conditions throughout this work, the average growth rates for the extreme salt conditions are slightly slower while the growth rate at the optimum is higher (0.17 M: 0.267 ± 0.011 h^{-1}, 1 M: 0.426 ± 0.017 h^{-1}, 2 M: 0.238 ± 0.014 h^{-1}). These averages all lie within the variances for the model prediction. It has been shown for *E. coli* that in unlimited growth the priority is given to synthesis of ribosomal

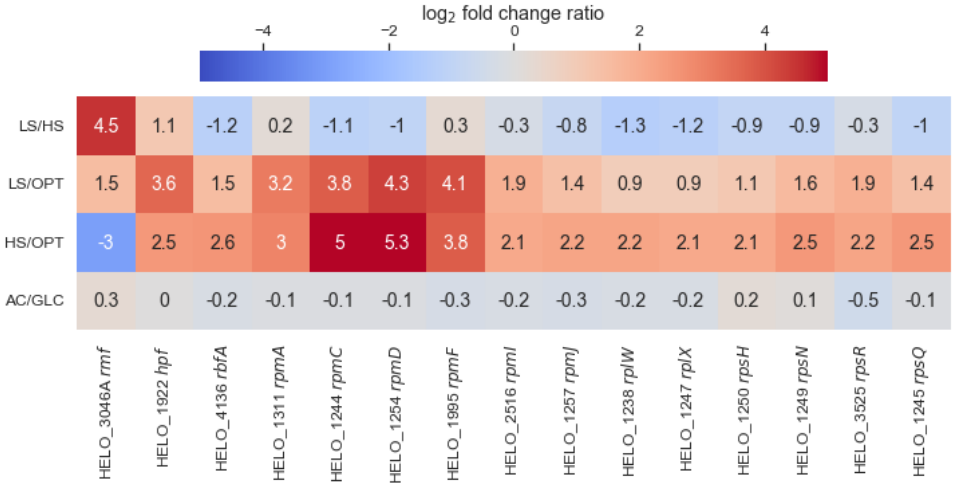

Figure 4.12: RNA-Seq results: ribosomes. Heat map depicting the log2-FC between the extreme salt conditions low salt against high salt (LS/HS), low salt against optimum (LS/OPT), HS against optimum (HS/OPT), and acetate against glucose (AC/GLC) for genes involved in ribosome regulation or ribosome biosynthesis. Genes shown in red (positive fold change) are upregulated in the condition specified in the numerator compared to the one in the denominator while blue (negative fold change) signifies a downregulation. With a change in the salt concentration several genes of the ribosomal machinery show differential expression. Apart from the ribosome modulation factor RMF, which is downregulated with increasing salt concentration, the other affected genes are downregulated in the salt optimum specifically. No differences for the glycolytic and gluconeogenetic substrates were observed. The growth rates in the different growth conditions are summarized in Table 4.4.

proteins. Ribosomes can be described as the machinery to translate the genetic code into proteins and there is a positive correlation between the growth rate and the amount of ribosomal proteins relative to

the total amount of protein. Like this, the distribution of the cellular macromolecule fractions changes depending on the growth rate. In contrast, while facing growth-limiting conditions an allocation towards metabolic proteins at the cost of ribosomal proteins takes place [45, 89, 254]. In *H. elongata*, some ribosomal genes exhibit a salt-dependent expression (Figure 4.12) comparing either of the salt-induced stress conditions with growth in the salt optimum. Naturally, a comparison of the stress conditions and the salt optimum is accompanied by a change in the growth rate. This was taken into consideration by choosing concentrations on either side of the salt tolerance range, which leads to similar growth rates (0.17 M and 2 M NaCl) in *H. elongata*, thus minimizing the growth rate effect.
Three of the differentially expressed ribosome-related genes are part of regulatory processes: *rmf* (HELO_3046A), *hpf* (HELO_1922), and *rbfA* (HELO_4136). The ribosome modulation factor RMF, which is characteristic for γ-proteobacteria and has been linked to the stationary phase and slow growth, seems to correlate linearly with the salt concentration with an increased expression at lower salinity. The hibernation promoting factor HPF is upregulated in both salt stresses compared to the salt optimum. RMF and HPF together initiate the formation of translationally silent 100S ribosomes called ribosome hibernation. This is a strategy applied by cells growing under adverse conditions to modulate and suppress protein synthesis [174, 209, 210]. Another regulatory gene, the ribosome binding factor A (HELO_4136), involved in ribosome biogenesis [76] was similarly upregulated in low and high salt condition. The overexpression of RbfA has been shown to counteract deleterious deletions like the cold sensitive mutation in 16S rRNA [46] or the slow growth and translational deficiency of a *rimM* deletion mutant [30]. The same salt related expression was observed for a set of genes of the 50S (*rpmA* HELO_1311, *rpmC* HELO_1244, *rpmD* HELO_1254, rpmF HELO_1995, *rpmI* HELO_2516) and 30S (*rpsN* HELO_1249, *rpsR* HELO_3525) ribosomal protein. Other genes of the 50S (*rpmJ* HELO_1257, *rplW* HELO_1238, *rplX* HELO_1247) and 30S (*rpsH* HELO_1250, *rpsQ* HELO_1245) ribosome showed only an upregulation in high salt (Figure 4.12).
No changes in expression when comparing growth on glucose and acetate could be detected. The growth rates achieved with glucose are distinctly higher, differing about 30 %. This indicates that the observed expression patterns in different salinities are indeed related to the salt concentration and not an artifact due to changes in the growth rate.

Glycolysis and gluconeogenesis

For a majority of organisms, glucose is preferred over other carbon sources [62]. It can either be metabolized by phosphorylation or directly by oxidation to gluconate [12] depending on the available pathways and regulation of the organism. Many *Halomonadaceae* including *C. salexigens* – a close relative of *H. elongata* – were found to exclusively use the ED pathway for glucose utilization. Kindzierski *et al.* [107] showed a salt-related regulation of proteins of the ED pathway for *H. elongata* using proteomics. For instance, both the phosphogluconate dehydratase Edd and the KDPG aldolase Eda are upregulated during growth at high salt. In contrast, none of the EMP or PPP enzymes exhibited clear changes in expression. Another peculiarity was found regarding the cofactor specificity of its phosphofructokinase *pfkA*. Instead of the commonly used ATP, the cofactor in the enzyme from *H. elongata* uses pyrophosphate (PP_i) as a phosphate donor, making the reaction reversible and, thus, opening up a potential function in gluconeogenesis [107].
The transcriptome analysis provides further evidence for the primacy of the ED/PPP branch (Figures 4.13) The expression of *pfkA* was very consistent with both glycolytic and gluconeogenetic substrates as well as in the different salinities. No apparent regulation of this enzyme on a transcriptomic level was observed. Other genes in the central pathway of carbon metabolism are upregulated growing on glucose: *zwf* (HELO_3637), *pgl* (HELO_3636), and the ED-pathway genes *edd* (HELO_3628) and *eda* (HELO_3635). Further two isoenzymes for the glucose-6-phopshate isomerase *pgi1* (HELO_4245) and *pgi2* (HELO_1718), as well as one of the pyruvate kinase isoenzymes *pykA1* (HELO_4243) and the alcohol dehydrogenase *adh2* (HELO_2818) are upregulated on glucose. In contrast, a glyceraldehyde-3-phosphate dehydrogenase homolog (HELO_2214) is upregulated on acetate. The two isoenzymes available in *H. elongata* for the utilization of acetate – the acetyl-CoA synthetase (*acsA*, HELO_3563

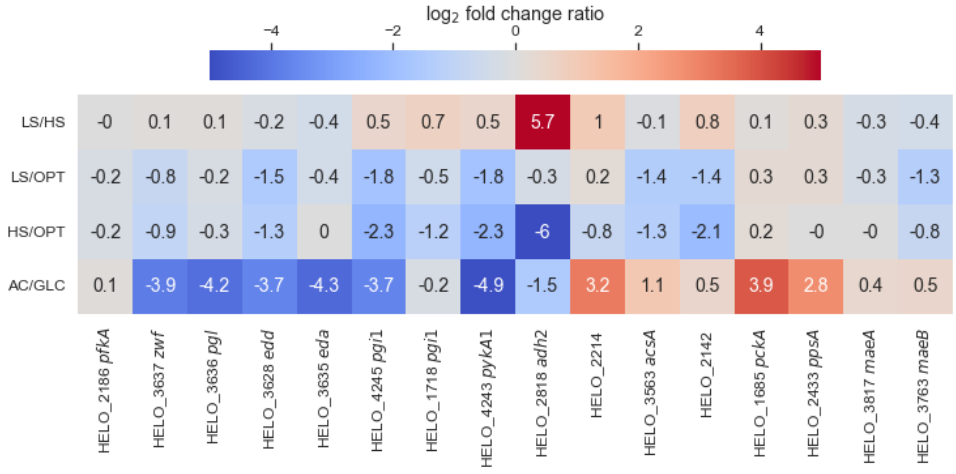

Figure 4.13: RNA-Seq: carbon catabolism (1). Heat map depicting the log2 fold change between the extreme salt conditions low salt against high salt (LS/HS), low salt against optimum (LS/OPT), HS against optimum (HS/OPT), and acetate against glucose (AC/GLC) for selected genes involved in glycolysis or gluconeogenesis. Genes shown in red (positive fold change) are upregulated in the condition specified in the numerator compared to the one in the denominator while blue (negative fold change) signifies a downregulation. There are several genes affected mainly by the used carbon source like the ED pathways genes *edd* and *eda* or genes linked to gluconeogenesis like *pckA* and *ppsA*. The alcohol dehydrogenase *adh2* shows a surprising expression profile with a severe downregulation at high salinity.

and the isoenzyme HELO_2142) – show no changes in expression between the carbon sources used. Metabolization of acetate via acetyl-CoA synthetase is considered a high-affinity pathway used at low substrate concentrations in *E. coli*. However, as indicated, no homologs for the low-affinity alternative [116] are present in *H. elongata*. The expression of PEPCK (HELO_1685) was strongly upregulated growing on acetate as expected, but showed relation to salinity. PpsA (HELO_2433) was found to be upregulated in acetate as well. Similarly, the glyoxylate shunt reactions for the circumvention of the TCA cycle, *aceA* (HELO_3070) encoding the isocitrate lyase and *glcB* (HELO_4288) encoding the malate synthase, and the glyoxylate carboligase *gcl* (HELO_1601), the hydroxypyruvate isomerase *hyi* (HELO_1602), and *glxR1* (HELO_1603) are upregulated during growth on acetate. In contrast, the $NADP^+$-dependent malic enzyme encoded by *maeB* was downregulated with acetate. Apart from this, neither malic isoenzyme – *maeA* (NAD^+, HELO_3817) nor *maeB* ($NADP^+$, HELO_3763) - showed significant changes in expression in any other tested condition. Naturally, when comparing the transcriptomes growing with either glucose or acetate a variety of sugar transporters are differentially expressed. They comprise transporters and porins for glucose, maltose, and trehalose which are upregulated on glucose. The tricarboxylic acid transport protein encoded by HELO_1043 and HELO_1044 is also upregulated on glucose. Transporter-related genes upregulated on acetate include the substrate binding protein HELO_1625 for tricarboxylic acid substrates, the Na^{2+}/proline symporter HELO_3259, and a similar symporter HELO_3085 with unknown substrate.
Other genes impacted by glycolytic and gluconeogenetic growth are the nitrate reductase genes *narGH* (HELO_2853-4), a transporter HELO_2857 also related to nitrogen metabolism, the cytochrome bd ubiquinol oxidase *cydAB* (HELO_2456-7), the bifunctional proline dehydrogenase *putA* (HELO_1802), and three genes involved in the metabolism of aliphatic amino acids (*mmsA1* HELO_1515, *mmmsB* HELO_2425, HELO_2317), which are all upregulated on acetate. In contrast, the tryptophan synthase encoded by *trpA1* and *trpB1* (HELO_4326-7) are upregulated on glucose.

Apart from the changes in the transcriptome in carbon catabolism caused by the different sub-

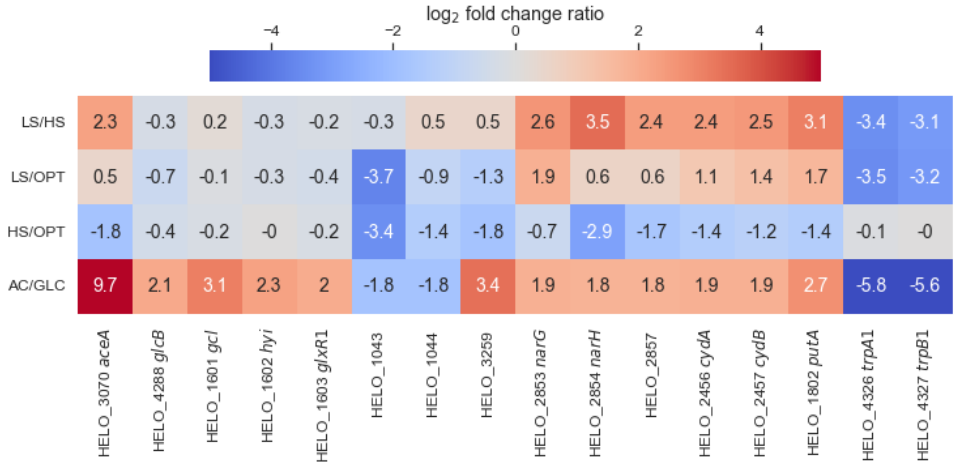

Figure 4.14: RNA-Seq: carbon catabolism (2). Heat map depicting the log2 fold change between the extreme salt conditions low salt against high salt (LS/HS), low salt against optimum (LS/OPT), HS against optimum (HS/OPT), and acetate against glucose (AC/GLC) for selected genes involved in glycolysis or gluconeogenesis and further genes impacted by the change in carbon substrate. Genes shown in red (positive fold change) are upregulated in the condition specified in the numerator compared to the one in the denominator while blue (negative fold change) signifies a downregulation. The most drastic changes in expression are observed for the isocitrate lyase *aceA* catalyzing the first step of the glyoxylate shunt, which is strongly upregulated growing under gluconeogenetic conditions but is also slightly downregulated at high salinity. Further the tryptophan synthase genes *trpA1* and *trpB1* are strongly downregulated growing on acetate and at low salinity. Further, there are some genes impacted by the choice of carbon source and the salinity (HELO_1043, HELO_1044, HELO_3259, *narG*, *narH*, HELO_2857, *cydA*, *cydB*, *putA*) and others only affected by the carbon source (*glcB*, *gcl*, *hyi*, *glxR1*).

strates, some genes showed a salt-related expression. The quinoprotein glucose dehydrogenase Gcd has already been identified to be upregulated in low salinity via proteomic analysis [107]. However, no distinct difference on a transcriptomic level was observed. Rather, the transcription of enzymes for the reactions following Gcd namely *gnl* (HELO_1553) and an isoenzyme HELO_1490A, which both produce gluconate, and the first gene encoding the three membrane-bound gluconate-2-dehydrogenase subunits (HELO_3279) were found to be upregulated. Further, two genes of the EMP pathway, *glk* (HELO_3629) and *pgi1* (HELO_4245) were downregulated in both salt extremes. As mentioned before, 6PG is an important intermediate for the PPP and the branching point between the ED and PPP. At this bifurcation, the expression profile might therefore be of relevance to the partitioning of the carbon flux. Kindzierski *et al.* [107] observed an upregulation of the ED pathway enzymes Edd and Eda in high salt. However, on a transcriptomic level, no salt-related expression was found.
Furthermore, some reactions involved in carbon catabolism have various isoenzymes for the same reaction which show different expression profiles depending on the tested conditions. For instance, there are three isoenzymes for the conversion of glyceraldehyde-3-phosphate to glycerate-1,3-biphosphate encoded by *gapA1* (HELO_4242), *gapA2* (HELO_2131), and HELO_2214. *GapA1* and HELO_2214 seem to be counterparts with *gapA1* being expressed preferentially during growth on glycolytic substrates, while the isoenzyme encoded by HELO_2214 shows higher expression during gluconeogenesis. For the third version, *gapA2*, no distinct changes could be observed. Another set of genes (*pykA1* HELO_4243 and *pykA2* HELO_1605) encoding for pyruvate kinase isoenzymes catalyzing the synthesis of PYR from PEP is active in different conditions. *PykA2* is downregulated in high salt while *pykA1* seems to be related to growth on glycolytic substrates but might also simply correspond to the growth rate.

Salt adaptation processes

Low salt vs. high salt stress response. To understand how *H. elongata* changes its expression profile for the adaptation to different salt concentrations, first, the RNA-Seq results for cultures growing with low salt stress and high salt stress (0.17 M vs 2 M NaCl) were compared. The specific concentrations were selected based on the growth rate to achieve approximately the same amount of growth rate reduction even though caused by different stress factors.
Within the expression profiles an asymmetry in the high and low datasets (asymmetry of -0.95) was found. Based on the TPM count, in total, 555 genes were differentially expressed with 419 genes upregulated and 136 genes downregulated in respect to the low salt condition. In Hobmeier *et al.* [87] this asymmetry is analyzed in greater detail. A quick overview of the main modules impacted by the salinity is shown in Figure 4.15.

PHB synthesis. In *H. elongata*, PHB accumulation during growth in low salt conditions has been observed by Nile-red staining and, additionally, PHB could be detected by HPLC analysis via the conversion to crotonic acid [99]. The transcriptomic analysis backs up this observation with all three PHB synthesis genes *phbABC* (HELO_4131, HELO_3876, HELO_3394) being upregulated in low salinity.

Compatible solute synthesis. The changes in the transcriptome, especially at high salt, showed a series of well-known osmoregulatory responses. Consistent with the RNA-Seq results for other halophiles like *Chromohalobacter salexigens* [182] or *Halomonas beimenensis* [36] as well as with the previously performed proteomic analyses in *H. elongata* [107], the ectoine and hydroxyectoine synthesis pathway encoded by *ectABC* (HELO_2588-90), and *ectD* (HELO_4008) are generally more transcribed in high salt conditions. The first two genes *ectAB* encoding the enzymes needed for two initial steps in ectoine synthesis were downregulated at low salt specifically. The ectoine synthase EctC was directly positively correlated to the salt concentration and the ectoine hydroxylase EctD was upregulated only at high salt. In contrast to the ectoine synthesis genes, the first two steps of the ectoine degradation pathway encoded by *doeAB* (HELO_3665, HELO_3664) were downregulated at high salt, which is also consistent with previous reports [107, 188]. However, the transcriptomic analysis did not show an osmoregulation for the remaining degradation genes *doeCD* (HELO_3662, HELO_3661) on the level of transcription.
Further, the transporter genes *teaABC* (HELO_4274-6) encoding the TRAP transporter specific for the uptake of ectoine from the periplasm [77] were found to be downregulated at low salt. After the operon *teaABC*, another open reading frame *teaD* (HELO_4277) encoding a regulator protein has been identified before. It has been proposed by Schweikhard *et al.* [186] that it might be involved in the regulation of the transporter TeaABC and potentially ectoine uptake. Other differentially expressed transporters related to compatible solute transport are the BCCT family transpoters encoded by *betG* (HELO_1580) and *betH* (HELO_3358) which were found to be salt-regulated with the first one correlating negatively and the latter positively to the medium salinity. Apart from these, another BCC transporter HELO_3694 was downregulated in the low salt condition. However, its substrate is not yet identified.

Motility: chemotaxis and flagellar genes. A clear salt-dependent regulation could be observed for genes related to motility, namely chemotaxis and flagella. So far, it has already been reported in other *Halomonas* strains that flagella-related genes are upregulated in environments with high osmolarity [36]. Flagella expression is regulated by the motility sigma factor *fliA* (HELO_4331), which was found to correlate negatively to the salt concentration in *H. elongata*. At least 42 genes related to flagella could be identified in the genome annotation overall. In comparison, in *E. coli* or *Salmonella enterica* sv. *Typhimurium*, there are more than 50 genes involved in biosynthesis and function. A minimum core set of 24 genes determined to be essential for assembly and operation was proposed by Liu & Ochman [133] and this core set is upregulated at high salt when comparing the low salt and high salt stress conditions (LS/HS) Figure 4.16). Some of the genes are directly related to the high salt condition like the sigma factor *fliA* or the flagellar biosynthesis proteins *fliPRQ* (HELO_4368-70). This is apparent in the log2-FC between the low salt condition and the salt optimum (LS/OPT) and the log2-FC between the high salt condition and the salt optimum (HS/OPT). *FliA* is only differentially expressed in the latter.

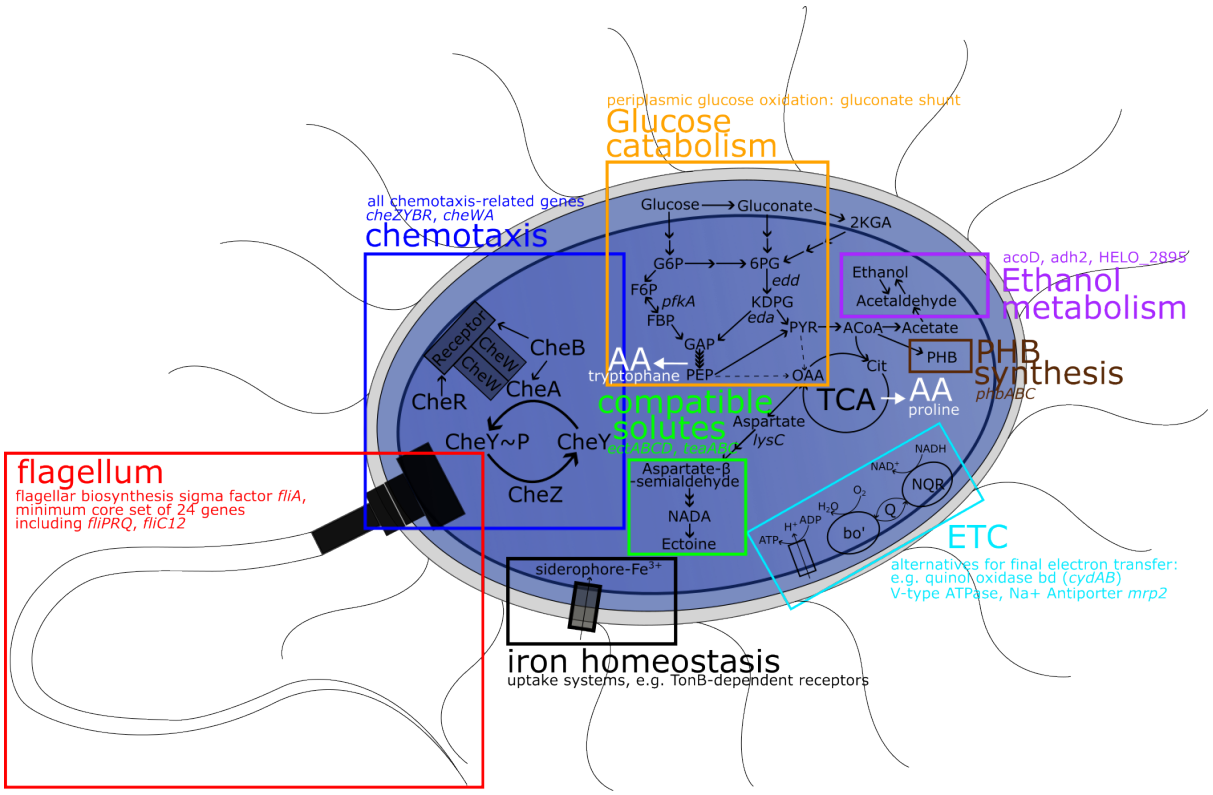

Figure 4.15: Overview of the modules which are affected by a shift in the medium salinity and some of their associated functions or genes. Motility-related functions, the flagellum (red) and chemotaxis (blue), are downregulated in low salinity. Pathways related to compatible solute synthesis (green) like the ect operon are increasingly expressed at high salinity while the degradation pathway (*doeAB*) naturally is upregulated in low salt conditions. For glucose utilization (orange) no paramount changes were identified regarding changes due to the salinity but the increased periplasmic oxidation of glucose channeling the substrate through the gluconate shunt before its uptake into the cytoplasm. Amino acids (AA, white) affected the most are proline and tryptophane. In low salt condition, the put operon for proline utilization is upregulated. In contrast, tryptophane synthesis (*trpA1*, *trpB1*) is downregulated. Many genes involved in respiratory functions (cyan) and iron homeostasis (black) are upregulated in low salinity. Especially the impact on the electron transport chain (ETC) is needs to be noted since various alternatives for are expressed simultaneously. Further, ethanol metabolism (purple) and PHB synthesis (brown) genes are upregulated at low salinity.

Other genes like the genes encoding flagellin *fliC1* and *fliC2* (HELO_4352-3) behave the opposite: only a differential expression is determined between the low salt condition and the salt optimum (LS/OPT), linking them to a low salt response.
Further, genes involved in chemotaxis (*cheZYBR* HELO_4335-7 and *cheWA* HELO_4341-2) were found to be universally downregulated in low osmolarity. Between high salt condition and salt optimum (HS/OPT), except for *cheY*, no change in expression was observed. The upregulation of motility in high salt is in accordance with other halophilic organisms like *C. salexigens* or *H. beimenensis* [36, 182]. The flagellar motion is linked to the ion gradient across the membrane. Thus, an impact of changes in the external ion concentration on motility related genes is reasonable. In *E. coli*, it is powered by the influx of protons. In contrast, in the marine bacteria *Vibrio aliginolyticus*, *Vibrio parahaemolyticus*, and *Vibrio cholerae*, it is entirely sodium-specific. However, experiments with *Halomonas* spp. showed

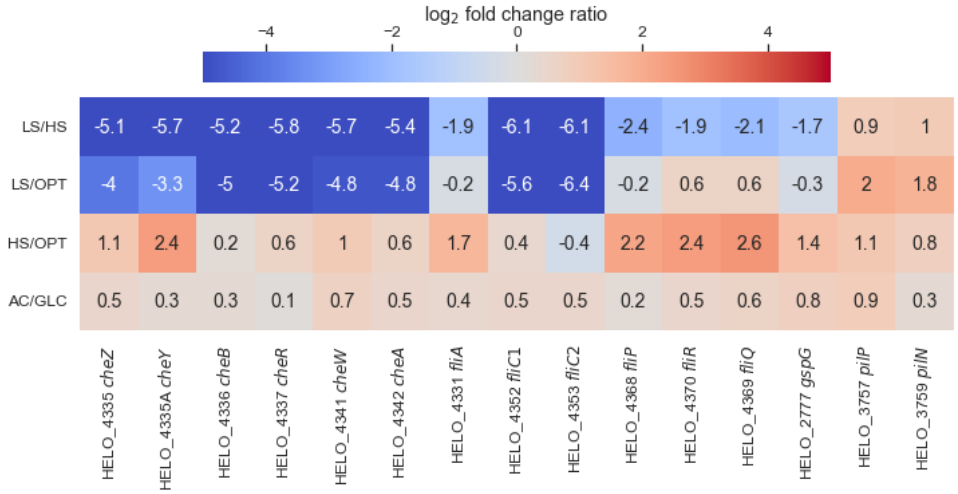

Figure 4.16: RNA-Seq: motility. Heat map depicting the log2 fold change between the extreme salt conditions low salt against high salt (LS/HS), low salt against optimum (LS/OPT), and HS against optimum (HS/OPT) for motility-related genes. This includes chemotaxis, flagella assembly, and pili/fimbrae. Genes shown in red (positive fold change) are upregulated in the condition specified in the numerator compared to the one in the denominator while blue (negative fold change) signifies a downregulation. In general, motility-related genes like chemotaxis and flagellar genes are downregulated at salinity.

a link to both ions [108, 182]. This bimodal nature of motility might be an indication that the proton and sodium gradient in *H. elongata* are intrinsically connected.
Additionally, some genes involved in pili and fimbrae formation were found to be differentially expressed due to the changes in salinity. For instance, the genes *gspG* (HELO_2777), *gspL* (HELO_2773), and *gspE* (HELO_2779) which are part of the general secretion pathway were transcribed more in the high salt condition. However, pili and fimbrae related genes had varying transcription patterns. Most of these genes were upregulated at low salinity including *pilP* (HELO_3757), *pilN* (HELO_3759), and loci HELO_2151A-C.

Energy metabolism. The RNA-Seq results showed an upregulation of ANR (HELO_1634) in *H. elongata* at low salt. Other genes related to the respiratory system were also identified to be upregulated with low osmolarity. Overall, the *cyoABCD* (HELO_3152-5) genes were highly expressed regardless of salinity. Therefore, it sees that in agreement with *E. coli* growing aerobically, the quinol oxidase bo' constitutes the main pathway for electron flow among the four alternatives present in *H. elongata*. In low salt, a clear upregulation of two genes of the bd quinol oxidase (*cydAB*, HELO_2456-7) was observed. This type of response is associated with decreasing oxygen (microaerobic) and other forms of stress in *E. coli*. Additionally, genes of both of the available cytochrome c oxidases, aa_3 (*ctaCDEG*, HELO_2502-5) and ccb_3 (*ccoNOPQ*, HELO_3536-9), were upregulated at low salinity as well, namely HELO_3538 and HELO_2502-3 (Figure 4.17). All experiments for the transcriptome analyses took place under aerobic conditions with oxygen readily available as an electron acceptor. But the oxygen solubility of the medium might be impacted by the salt concentration to a certain extent: with an increase in salt concentration, the solubility decreases [208] to a point, where at 30 °C the oxygen solubility at 2 M NaCl (high salt condition) drops by approximately 50 % compared to a medium with 0.17 M NaCl (low salt condition). Therefore, an effect related to oxygen limitation due to the influence of salt in the medium, if any, would be expected rather at high salinity. Nevertheless, another remarkable finding in this context was the upregulation of genes of the nitrate reductase at low salt despite the absence of nitrate in the medium. If oxygen is present, other final electron acceptors are normally repressed. Vice versa, under anoxic con-

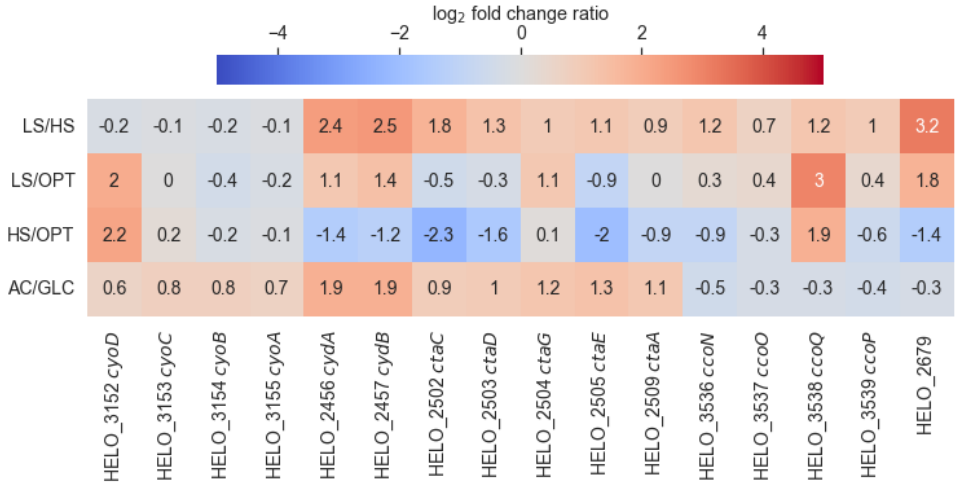

Figure 4.17: RNA-Seq: cytochrome oxidases. Heat map depicting the log2 fold change between the extreme salt conditions low salt against high salt (LS/HS), low salt against optimum (LS/OPT), and HS against optimum (HS/OPT) for genes encoding for cytochrome b (*cyo, cyd*) oxidases and the cytochrome c (*cta, cco*) oxidases. Additionally, the UPF0057 family protein encoded by HELO_2679 indicating a membrane depolimerization is also shown. Genes shown in red (positive fold change) are upregulated in the condition specified in the numerator compared to the one in the denominator while blue (negative fold change) signifies a downregulation. The expression of one of the cytochrome b oxidases bd, encoding by *cydAB*, is downregulated with the salt concentration and regarding carbon substrates upregulated with acetate. Apart from these genes, the change in carbon substrate shows no impact on the expression of the other listed genes. For the other cytochrome oxidases single genes of the respective operons show salt-induced changes in expression. The expression of HELO_2679 exhibits a negative relation to the salt concentration.

ditions and nitrate reduction as the next best alternative, repression of both quinol oxidases bo' and bd takes place [196]. The *nar* operon has been reported to be directly controlled by ANR. Apart from ANR, these genes which normally associated with microaerobic conditions are regulated by a two component system RegAB (HELO_2707, HELO_2706). RegB detects the ubiquinone pool in the membrane and responds accordingly by auto-phosphorylation and phosphorylation of the response regulator RegA. It is best described in the phototrophs *R. capsulatus* and *R. sphaeroides* but RegAB homologs were found to be highly conserved in photosynthetic and non-photosynthetic bacteria hinting towards a redox regulating role in many bacterial species. RegB (HELO_2706) was continuously less transcribed with a decreasing salt concentration. ANR activity is directly linked to no oxygen, while RegB is responding to the absence of a terminal electron acceptor and the resulting accumulation of quinol. *HemN* (HELO_2849), typically an alternative to *hemF* (HELO_1379) during growth in microaerobic conditions was also upregulated at low salinity. Both genes encode a coproporphyrinogen-III-oxidase, which is used in the biosynthesis of the tetrapyrrole ring of hemes. In *E. coli*, HemN has been identified as an oxygen-independent version of the oxygen-dependent HemF [127, 153]. Many of the involved genes in the low salt expression profile seemingly respond to a shift in oxygen availability. In *Pseudomonas extremaustralis*, heme synthesis genes and the cytochromes *cioA*, *ccoN*, and *ccoO* are controlled by ANR [207] and in *P. aeruginosa*, the expression of high-affinity oxidases has also been linked to an energy conservation function under microaerobic conditions [101]. Further in a high pH environment, cytochrome c has been proposed to function as an electron storage due to its electron retaining ability [138]. Another noteworthy gene here was HELO_2679 which is a UPF0057 family protein and was also found to be increasingly expressed at low salinity (Figure 4.17). These type of proteins are ubiquitous in all domains of life and are highly

related to a decrease in the membrane potential [123]. Interestingly, only the latter part of the ETC is involved in the transcriptional response. Even though the Na^+-translocating NADH oxidoreductase NQR of *H. elongata* is directly coupled to sodium no regulation of the *nqr* genes on a transcriptomic level was observed.
No genes related to ROS-scavenging (expressing catalases or superoxide dismutases) were found to be differentially expressed for *H. elongata*. This is in contrast to the findings made in *C. salexigens* [182]. In *H. elongata*, two peroxiredoxin candidates (HELO_1409 and HELO_4301) were upregulated in low salt similar to two peptide methionine sulfoxide reductases *msrA2* (HELO_3076) and *msrB2* (HELO_1686) were upregulated at low salt. Despite their function to counteract oxidative stress, MsrA and MsrB are not normally part of antioxidant regulons [56]. This has been explained due to their nature as post-damage repair as opposed to a detoxifying function. Another set of enzymes *msrA1* (HELO_2578), *msrB1* (HELO_2015), and *msrC* (HELO_3000) are present in *H. elongata* but the corresponding genes did not show differential expression based on salt-related stress. The glyoxalase HELO_3670 and three glyoxalase-like genes (HELO_3433, HELO_3142, HELO_2032) were downregulated in high salt. Other differentially expressed genes related to oxidative stress include the recombination mediator DprA (HELO_1377) and the thiol-disulfide interchange protein DsbA (HELO_4264) which are less transcribed the higher the salt concentration.
The sigma factor RpoH (HELO_3832) regulating protein folding stress was found to be upregulated at low salt. However, only one heat shock protein, *ibpA* (HELO_1663) showed the same behavior. Further, some genes encoding for proteases *htpX* (HELO_2012), *degP1* (HELO_3026), and a S49 family protease were differentially expressed. For the first two a negative correlation to salinity was found while the S49 family protease was downregulated at low salt. Additionally, two chaperones HELO_2151D and HELO_1078 were also overexpressed at low salt.

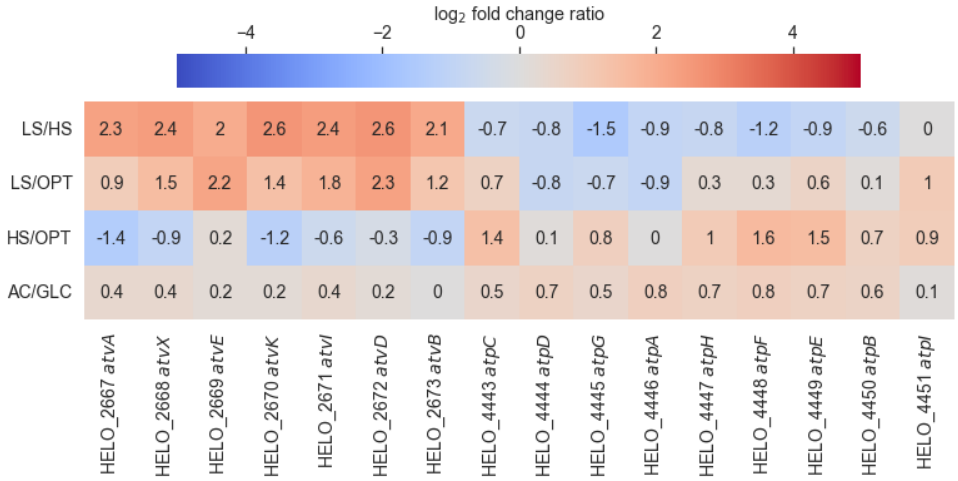

Figure 4.18: RNA-Seq: ATPases. Heat map depicting the log2 fold change between the extreme salt conditions low salt against high salt (LS/HS), low salt against optimum (LS/OPT), and HS against optimum (HS/OPT) for genes encoding the F-type (*atp*) and V-type (*atv*) ATPase. Genes shown in red (positive fold change) are upregulated in the condition specified in the numerator compared to the one in the denominator while blue (negative fold change) signifies a downregulation. The expression of the genes encoding the V-type ATPase is negatively impacted with the salt concentration and is upregulated at low salinity.

Iron homeostasis. Several genes related to iron homeostasis were found to be affected by the medium salinity. The TonB-dependent receptor *irgA* (HELO_3349) was downregulated at high salt while

showing a similar transcription at the salt optimum and low salt condition. Other TonB-dependent receptors HELO_1153, HELO_2827, HELO_3304, HELO_3316, and HELO_3326 were most transcribed at the salt optimum and less in either salt-stress condition while the TonB-dependent receptors HELO_3038 behaved the exact opposite. The transporter genes HELO_3347 and *futA* (HELO_4001) for ABC transporter systems related to iron uptake were downregulated especially at high salinity. The same was found for the ferric siderophore reductase HELO_1154, a variety of genes involved in siderophore synthesis (HELO_3332-6), and a probable siderophore uptake system (HELO_3344-8). The UDP-glucose/iron transport system encoded by *futAB* (HELO_2138-9) was also more transcribed in low salinity.

ATPases. In Hobmeier *et al.* [87], the two potential ATP synthases present in *H. elongata*, F-type and V-type, were evaluated regarding their ion specificities based on the protein sequence similarities of their translocating c subunits (*atpE* and *atvK*) compared to other known ATPases. The F-type c subunit of *H. elongata* showed the highest sequence similarity to the H^+-translocating equivalent in *E. coli*. In contrast, the V-type c subunit of *H. elongata* possesses many similarities to the essential binding residues found in Na^+-translocating V-type ATPases. However, a direct comparison with both Na^+- and H^+-coupled V-type ATPases revealed that *H. elongata* takes on a position in between, partially showing binding ligands for Na^+ and H^+ at the same time. With these findings, the most probable scenario is a H^+-translocating F-type ATPase and a Na^+-translocating V-type ATPase.
Regarding their roles in the metabolism either ATP synthesis or ATP hydrolyzation activity linked to ion extrusion is possible. The RNA-Seq results (Figure 4.18) showed that the F-type ATPase is highly expressed in all tested salt conditions and shows a tendency to be increasingly expressed at high salinity. In comparison, the V-type ATPase behaves the opposite. All genes are clearly upregulated in low salt condition. Three of the genes are upregulated in low salt specifically while the other three genes are directly correlating negatively with the salt concentration. Both ATPase types are expressed simultaneously. The working direction of either enzyme cannot be predicted explicitly but the most reasonable solution is a H^+-translocating F-type ATP synthase providing ATP equivalents while the presumably Na^+-translocating V-type ATPase works as a sodium pump, removing sodium ions from the cytoplasm. Initially, this is a counter-intuitive behavior to increase the expression of a sodium pump in a low salinity environment. However, it can be explained as a result of the failing membrane gradient in these conditions. As demonstrated in Hobmeier *et al.* [87], there are indications in the transcriptomic profiles, which suggest a depolarization of the membrane in low salinities leading to a shift of the ETC towards a lower efficiency. The overexpression of a Na^+-pump can, therefore, be interpreted as an attempt to achieve a higher membrane gradient. Furthermore, V-type ATPases are generally described as ion pumps in the literature but a synthase activity in *H. elongata* cannot be discarded completely. There are some examples of V-type ATP synthases as for example in *T. thermophilus* [149].

Na^+/H^+ antiporters and outer membrane proteins. *H. elongata* has several cation/proton antiporters with different structures and possibly different stoichiometries. Na^+/H^+ exchangers are important to extrude Na^+ ions that enter the cell due to symport or other processes like the operation of the anaplerotic enzyme OAD [86]. *H. elongata* possesses the genes for two Mrp systems. These are monovalent cation/proton antiporters which catalyse the efflux of monovalent sodium, potassium, or lithium ions, energized by the electrochemical proton gradient. Its stoichiometry is supposed to transport more protons than Na^+ [201]. Intererstingly, both antiporters are located at the same site on the *H. elongata* genome but in different directions with the Na^+-specific version on the negative strand and the K^+-specific version on the positive strand. In the RNA-Seq analysis, the Na^+/H^+ exchanger (*mrp1*, HELO_3507-13) all genes encoding its subunits were upregulated in low salinity. One subunit in particular, *mrpF1* (HELO_3508), was upregulated in both salt-stress conditions. In contrast, for the K^+/H^+ exchanger (*mrp2*, HELO_3514-9) only two genes were differentially expressed: *mrpC2* (HELO_3515) and *mrpF2* (HELO_3518). But these were upregulated in both salt-related stress conditions. Additionally, in the genome annotation, one NhaC (HELO_1557) and two NhaD transporters (*nhaD1*, HELO_1427 and *nhaD2*, HELO_2323) were found. Nha antiporters have been reported to play an important role in pH and Na^+ homeostasis and for the NhaD-type an importing activity for osmoregulatory purposes was proposed [122]. In *H. elongata* one of NhaD-type antiporters,

nhaD1 was downregulated in both salt-stress conditions. Also, a K^+ uptake protein TrkI (HELO_1450) was found to be downregulated at high salt specifically.
In the outer membrane two proteins encoded by HELO_1459 and HELO_1799 both annotated as OmpW were found to be differentially expressed. In *V. alginolyticus*, the proteins OmpV and OmpW are responsive to osmotic stress. They act as counterparts with OmpV expressed in high and OmpW in low osmolarity [239]. Both proteins of *H. elongata* show similarities to the low salt related OmpW from *V. alginolyticus* (HELO_1459: 45 % identity, HELO_1799: 31 % identity) but no homolog to OmpV could be found. But even though a higher sequency identity to the *V. alginolyticus* OmpW was determined for HELO_1459, only HELO_1799 showed a clear salt-regulated behavior with direct negative correlation to an increase in salt concentration. HELO_1459 expression was slightly upregulated at low salinity; however, a much bigger impact was observed for gluconeogenetic growth on acetate.
Another differentially expressed gene with an unusual expression pattern is HELO_2403. It shows a drastic increase in expression in the salt optimum. But this gene is not solely linked to a fast growth rate because a similar behavior was observed during growth on acetate with a considerably lower growth rate. Unfortunately, the function of the HELO_2403 gene product is unknown. A screening for conserved protein sequences revealed an existing HINT domain. Regarding associated proteins only one related protein encoded by HELO_2402 was identified. However, the expression pattern of HELO_2402 does not mimic HELO_2403. It is downregulated only in high osmolarity and regarding its function, a glycosyltransferase domain was identified in the sequence. Therefore, HELO_2402 and HELO_2403 might potentially work together in processes maintaining the membrane.

4.1.5 Anaplerosis in *H. elongata* and its role in ectoine synthesis

In most aerobic and facultative anaerobic bacteria, carbon catabolism and the TCA cycle, which are connected via the PEP-PYR-OAA node (Figure 2.6), constitute the basic central metabolism. Intermediates of this interconnecting node have important functions in energy metabolism due to oxidation to CO_2 but also as precursors for carbon metabolites. Therefore, it has a special position in the central metabolism, being responsible for distributing carbon fluxes as a main switching point [184]. Growing under glycolytic conditions, the TCA cycle is entered via acetyl-CoA. A second way to supply the TCA cycle with carbon compounds is by carboxylation of a three carbon molecule, like PEP or PYR, to form OAA. This route is commonly referred to as anaplerosis and is needed to replenish the carbon molecules used in biosynthetic processes. The anaplerotic flux is possible through carboxylation of PEP by the PEP carboxylase PEPC or, as an alternative route, carboxylation of pyruvate by pyruvate carboxylase PC. Both reactions are essentially irreversible, and while PEP carboxylase is widely distributed in prokaryotes and plants, pyruvate carboxylase is mostly found in vertebrates and yeast. Only a few prokaryotes have been found to use pyruvate carboxylase as an anaplerotic enzyme exclusively like, for instance, *B. subtilits*. In many cases, both enzymes have been detected, however, their distinct role and the division of the flux between them is not clear [184].
The PEP-PYR-OAA node is even more important for *H. elongata* due to the *de novo* synthesis of ectoine, which is derived from the amino acid aspartate. Its precursor stemming from the TCA cycle is OAA [159]. Because of ectoine, the amount of carbon which is withdrawn from the TCA cycle is even higher in *H. elongata* compared to other organisms. The demand for OAA, which is not only higher but also responds to different triggers, was investigated in detail in Hobmeier *et al.* [86]. The essential findings of this work are summarized in the following.

In *H. elongata*, OAA is used not only for amino acid synthesis but also as precursor for ectoine. Thus, the overall demand for OAA can be approximated by determining the content of OAA-derived amino acids and the ectoine content [86], (supplementary material). OAA-derived amino acids are aspartate, asparagine, threonine, isoleucine, methionine, and lysine. Based on the composition established for *E. coli* [150], which is commonly used for gram-negative cells in general, the content for these amino acids was estimated in mmoles/gDW and the demand for OAA was calculated using this amino acid content times the growth rate. The second OAA consumer, ectoine, is strictly dependent on the salinity

of the medium to maintain the osmotic balance. Additionally, during cell growth, ectoine synthesis needs to compensate the dilution due to cell growth. With the ectoine concentration determined by the salinity of the environment, the dilution term is equal to the ectoine concentration times the growth rate [52, 86]. In order to relate this to the salt concentration, functions giving the ectoine content and growth rate in relation to the salt concentration from [52] were applied. In Figure 4.19, the OAA demand with the share of the two fractions is shown over a NaCl concentration ranging from 0 to 3 M. At low NaCl concentrations below 0.17 M NaCl, the OAA demand in *H. elongata* is very similar to other non-halophilic bacteria. With an increasing NaCl concentration, the demand for ectoine rises rapidly. For the overall OAA demand, a maximum between 0.5 and 1 M NaCl is reached, which corresponds to the optimal range for growth. Within this range, the amount of OAA used for amino acid synthesis starts decreasing again, while the fraction for ectoine synthesis takes over a bigger portion. For sodium concentrations over 1 M NaCl, the overall OAA demand decreases again due to the reduction in growth rate. For high salt conditions, the portion of OAA used for ectoine synthesis exceeds the amount used for amino acid synthesis [86]. The four potential anaplerotic enzymes include a phosphoenolpyruvate

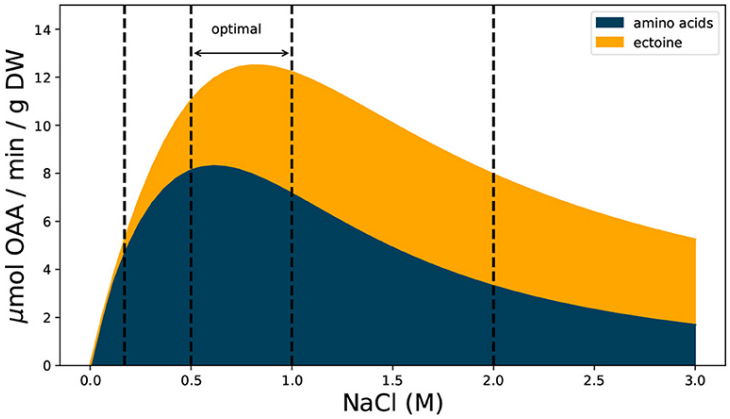

Figure 4.19: In *H. elongata* the OAA demand is split into two fractions: use as a building block for amino acid synthesis (dark blue) or for ectoine synthesis (orange). The demand itself depends on the amount of biomass and the amount of ectoine produced which is both linked to the salinity (NaCl) of the medium. The demand for OAA for biosynthetic purpose was calculated using the molar fractions published by [150], as an approximate for the general composition of gram negative bacteria, for OAA-derived amino acids. The molar fractions were converted to mmoles/gDW, summed up, and to estimate the consumption of OAA multiplied times the growth rate. The OAA demand for ectoine synthesis was calculated using the correlation of ectoine content and salt concentration (equation 2.4) and similarly multiplying the content times the growth rate. The highest total OAA demand is observed in the growth optimum between 0.5 and 1 M NaCl. While initially at low NaCl concentrations, the fraction for ectoine synthesis is far smaller its share gets bigger with an increasing NaCl concentration. This image is published in Hobmeier *et al.* [86] in Frontiers in Microbiology.
OAA: oxaloacetate, optimal: salt range at which the fastest growth is generally observed (also: salt optimum).

carboxylase PEPC, a phosphoenolpyruvate carboxykinase PEPCK, an oxaloacetate decarboxylase OAD, and two isoenzymes for the malic enzyme ME. Growing on glucose, glycerol, and pyruvate, *E. coli* channels the anaplerotic flux through PEPC and no alternative pathway from PYR to OAA is available. The reverse reaction, decarboxylating OAA to PEP by PEPCK is traditionally a key step for gluconeogenetic growth. In case the reaction is thermodynamically reversible, a flux towards an anaplerotic direction is in principle possible as well. In *H. elongata*, a Pyruvate carboxylase (PC) converting PYR to OAA is not present like in *E. coli*. However, its OAD is a membrane-bound complex translocating sodium ions [86, 184]. Depending on the sodium concentration, this membrane-pump is

reversible and can potentially work in an anaplerotic direction. ME activity is also normally associated with gluconeogenesis by circumventing the thermodynamically rather unfavorable reaction catalyzed by malate dehydrogenase MDH. In *H. elongata*, two isoenzymes with different cofactor specificities are present. Most organisms typically only have a subset of all possible reactions around the PEP-PYR-OAA node [184]. Interestingly, *H. elongata* possesses a great variety of these enzymes, solely missing a PYR carboxylase. This reaction could in theory be substituted by the membrane-bound reversible sodium pump OAD.
As mentioned before, in most bacteria the anaplerotic flux is directed through PEPC. All other alternatives available in *H. elongata* apart from PEPC are in general considered thermodynamically unfavorable in an anaplerotic direction within realistic framework conditions. With reference values for the Gibbs free energy $\Delta G^{0'}$, the likelihood of each enzyme working in an anaplerotic sense can be evaluated. Only OAD is involved in the sodium gradient due to its translocating activity and is directly impacted by a changing external sodium concentration. But even in high osmolarity conditions, the calculated $\Delta G^{0'}$ for OAD is still positive. For the reaction to take place, the free energy must be not only negative but also negative enough to result in an efficient use of the enzyme. The $\Delta G^{0'}$ calculated for PEPCK and both ME isoenzymes are positive as well, suggesting that an anaplerotic flux is unlikely. In contrast, as expected, PEPC has the most negative $\Delta G^{0'}$, hinting towards a main role of this enzyme for the anaplerotic flux. However, since standard conditions do not account for membrane gradients, the prediction for OAD needs to be handled with some caution.
To get a clearer picture of their feasibilty *in vivo*, a model based on stoichiometric and thermodynamic constraints was applied [86]. This model includes the basic metabolic network like the respiratory chain, ATPase, and other processes related to sodium transport. Stoichiometrically, PEPCK and ME are the preferred reactions for the anaplerotic flux but taking thermodynamics into account, no viable flux distribution for PEPCK and ME is achieved. To work in an anaplerotic direction, the required concentrations for substrate and product for both enzymes are not compatible with the rest of the network. The ED glycolytic pathway results in a 1:1 ratio of PEP and PYR. PYR gained from glycolysis needs to be phosphorylated to form PEP, before the flux can be channeled towards OAA via PEPC. This phosphorylation is catalyzed by the phosphoenolpyruvate synthase Pps, which is an energy-expensive reaction consuming a pyrophosphate (PP_i) from ATP in the process. If PEPC is the only anaplerotic option, this ATP demand results in as low yields as in operating without anaplerosis at all. With a high enough sodium gradient, OAD can convert PYR directly to form OAA, circumventing the ATP consuming step to PEP. Based on the metabolic model, PEPC and OAD are most likely to be involved in carrying the anaplerotic flux. To figure out which enzyme is truly responsible and how the fluxes are partitioned *in vivo*, a deletion mutant for each reaction was created: *H. elongata* PEPC with the knockout of the PEPC gene *ppc* and *H. elongata* OAD with the knockout of the OAD operon. Both were grown at a range of salt concentrations from 0.17 to 2 M NaCl, with either glucose or acetate as the sole carbon source. For gluconeogenetic growth on acetate, anaplerosis is irrelevant. Therefore, any problems of *H. elongata* PEPC or *H. elongata* OAD during growth on glucose should disappear growing on acetate.

For either deletion mutant strain, growth screenings in microtiter plate scale showed a phenotype with severely impeded growth. The deletion of PEPC causes an impaired growth at low salt conditions (0.17 M NaCl), while the loss of the *oad* operon brings about defects on the opposite end at high salt (2 M NaCl). For both strains, the deficient phenotypes only appear for glycolytic growth. When grown under gluconeogenetic conditions, the same growth rates as the wild type are achieved. These observations were further confirmed in shake flask experiments. With acetate as the carbon source, the *H. elongata* PEPC knockout mutant showed a similar growth rate of $0.16 \pm 0.02\ h^{-1}$ to the wild type with a rate of $0.19 \pm 0.004\ h^{-1}$ in low salt conditions (0.17 M NaCl). But with glucose, its growth was drastically decreased by almost a fifth to a growth rate of $0.06 \pm 0.04\ h^{-1}$, in contrast to the wild type with $0.28 \pm 0.007\ h^{-1}$. Likewise, the observed drop in growth rate for the second knockout strain, *H. elongata* OAD, in high salt conditions (2 M NaCl) was reproduced in shake flasks. In comparison to the wild type with a growth rate of $0.25 \pm 0.01\ h^{-1}$, the *H. elongata* OAD mutant achieved only approximately a third of this with a rate of $0.09 \pm 0.004\ h^{-1}$ growing on glucose. Notably, the growth

of the other mutant strain, *H. elongata* PEPC, was also found to be slightly decreased in high salt condition to a growth rate of 0.13 ± 0.01 h^{-1}. In general, an increase in lag phases was observed in both deletion mutants. The impact of the PEPC deletion even at high salt conditions hints towards it being an essential part of metabolism in glycolytic growth, which manifested itself in higher fluctuations in the growth rates as well [86].
Any insufficiencies regarding the OAA demand due to a deficient anaplerotic flux can lead to a reduction in biomass synthesis, as reflected in the growth rates, but can also potentially impact ectoine biosynthesis. Thus, in addition to the growth rates of *H. elongata* PEPC and *H. elongata* OAD, the intracellular ectoine concentrations were examined in high salt conditions at 2 M NaCl as well (Figure 4.20). The equivalent cultures at low salt condition were not included because the amount of ectoine produced at 0.17 M NaCl is negligibly low. Regardless of strain and carbon source, a clear linear behavior of the ectoine to biomass ratio is evident. The data is also consistent with previously reported values by Dötsch *et al.* [52]. The only discrepancy is introduced by strain *H. elongata*-OAD growing on glucose, which shows consistently lower ectoine contents. However, this is also the strain that experiences the biggest impact on growth rate with a decrease to roughly 30 % compared to the wild type. The estimation of the OAA demand showed that the absence of the Na^+-pump OAD causes a drastic reduction in anaplerotic flux. In high salt conditions, the deletion mutant *H. elongata*-OAD only reaches 30 % of the wild type OAA flux. In contrast, without PEPC the flux is also reduced, although not as much. *H. elongata* PEPC achieves 50 % of the wild type flux. Since neither deletion mutant achieves the same flux the anaplerotic role in *H. elongata* is most likely shared between PEPC and OAD even in high salt conditions. Together, both enzymes constitute parallel pathways for anaplerosis. In general, PEPC is thermodynamically more favorable but with the direct coupling of OAD to the sodium gradient, this alternative pathway ensures a sufficient increase in anaplerotic flux for ectoine synthesis. OAD takes over the role to adjust the OAA demand dependent on the sodium concentration and PEPC can respond to the demand required for amino acid biosynthesis [86].

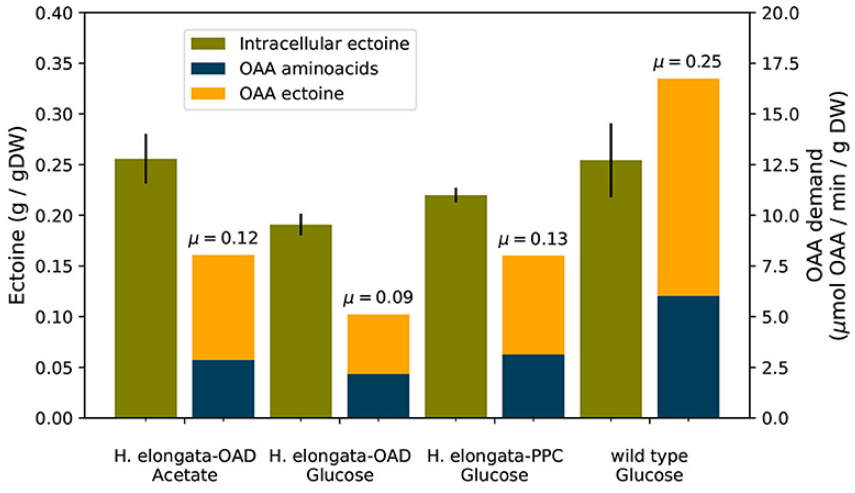

Figure 4.20: Bar chart depicting the measured intracellular ectoine content (olive green) and the respective OAA demand for amino acid (dark blue) or ectoine (orange) biosynthesis for the *H. elongata* wild type and the deletion strains *H. elongata*-PPC and *H. elongata*-OAD growing in 2 M NaCl high salt medium. The growth rates, which are indicated above the OAA demand bars, are reduced for both deletion strains compared to the wild type. The biggest negative impact in growth is observed for *H. elongata*-OAD on glucose but growing on acetate the negative effect is not as severe. Corresponding to this, only in *H. elongata*-OAD growing on glucose a lower intracellular ectoine content was found. This image is published in Hobmeier *et al.* [86] in Frontiers in Microbiology.

4.1.6 Regulated expression of heterologous genes

The gene expression of a microbe in a natural environment is governed by the ever changing conditions in its surroundings. Intending to maximize growth, microbial populations are able to deal with these changes by shifting their gene expression leading to metabolic and also morphological changes. The switch gives an advantage for growing in a specific environmental condition, but in others, it would be considered a maladaptation [70]. A prominent example of this is the lac operon of *E. coli*. The structural genes for the metabolism of lactose are located within a single operon and the expression is only activated if the substrate lactose, which is at the same time the inducer of the operon, is present while other more energetically favorable carbon sources like glucose are absent [245]. On the other hand, many metabolic genes, especially in the central metabolism, are constitutively expressed at all times and only the amount of expression might change slightly.
The clear advantage of inducible systems is the versatility of the expression level directly variable by the added inducer. It is possible to accomplish either high-level protein production or low-level expression applied in metabolic pathways. Also, cloning and expression of genes with deleterious effect are carried out more easily in a regulated system. An established regulator/promoter system applied for recombinant protein production but also Metabolic Engineering purposes is the positively regulated XylS/Pm system originating from the *P. putida* TOL plasmid, which is often featured for its tight control. In response to benzoate effectors, the transcriptional regulator XylS is activated inducing dimer formation. In turn, these dimers bind to the operator sequence inducing transcription from Pm. Inducers based on benzoic acid derivatives can be considered convenient since they are cheap and enter the cell easily by passive diffusion but are usually not metabolized [69, 105]. The application of the XylS/Pm expression system has been carried out in several gram-negative organisms and its viability was also examined in *H. elongata* using the fluorescent signal proteins eGFP and mCherry as heterologous proteins.

Expression of eGFP as a model protein

In an initial experiment, eGFP was used as a signaling molecule to show the behavior of the positively regulated XylS/Pm promoter system [69] in *H. elongata*. The genetic construct was introduced using the plasmid pSEVA438-eGFP, which consists of the *xylS* gene for the activation of the Pm promoter and the eGFP encoding gene under the regulation of Pm and a synthetic Ribosoal binding site (RBS). The induction strength was varied using 3-methylbenzoic acid (3-MB) as an inducer and concentrations ranging from 0 mM (uninduced) to 2 mM.

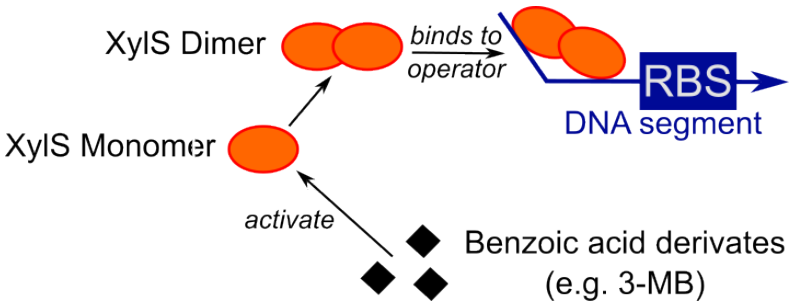

Figure 4.21: Schematic of transcription activation via the XylS/Pm promoter system. After activation by benzoic acid derivates (e.g. 3-MB) the *xylS* gene product forms dimers. These bind to the corresponding operator sequence and thereby activate the transcription (picture adapted from [69]).

The special feature of the XylS/Pm – its tight control of transcription activation in *P. putida* [69] – was also observed in *H. elongata*. The bar chart in Figure 4.22 depicts an overview of the eGFP signals. They were normed using the amount of biomass by dividing the eGFP relative lighting units (RLU)

by the respective OD600 value. Without the inducer, only a negligible amount of fluorophore could be detected regardless of the time of induction showing a very low basal expression level. This demonstrates that the characteristic tightness observed for the XylS/Pm promoter in other gram-negative bacteria is the same in *H. elongata*. At the same time, with only a minimal concentration of 3-MB, the expression was strongly activated. For the tested 3-MB concentrations, an increase in inducer concentration from 0.1 mM to 1 mM lead to a noticeable higher eGFP signal but at 2 mM the same signal as with 1 mM was observed. Thus, after approximately 1 mM 3-MB, the inducer concentration was saturated. The addition of more 3-MB did not change the level of eGFP signal and was rather inferred by that the amount of expressed protein.
Some minor differences between the two induction times were observed. For the immediate induction simultaneous to inoculation, consistently lower eGFP signals of 13 – 24 % less were detected compared to a later induction 4 h after inoculation. The eGFP signal at saturated inducer concentrations for the immediate induction with 421617 ± 32353 RLU/OD600 was slightly lower than the signal for the later induction after 4 h with 485369 ± 33273 RLU/OD600. With an inducer concentration of 0.1 mM, the eGFP signal for immediate induction only made up about 64 % of the saturation signal while for the later induction after 4 h, a 0.1 mM inducer concentration resulted in about 75 % of the saturation signal. This suggests a slightly postponed induction of protein expression with an initial adaptation period for the newly inoculated cultures might be better for protein production overall.
Corresponding to the slightly lower eGFP signals with an immediate induction, the growth rates behaved exactly the opposite. These are illustrated in Figure 4.22 with a scatter plot overlying the eGFP signal bars. Since less protein is synthesized more resources were used for growth in contrast to the later induction after 4 h. Focusing on the impact of the inducer concentration, the same pattern was found for both induction strategies. With increased inducer concentration, the growth rate droped steadily. This decrease in growth rate can be attributed to the reallocation of resources from growth to eGFP protein production. Interestingly, for the highest inducer concentration, 2 mM 3-MB, still, a decrease in growth rate was observed even though this reduction was not reflected in an increased protein synthesis compared to 1 mM 3-MB. This might be due to an adverse effect of the inducer itself or its solvent ethanol.

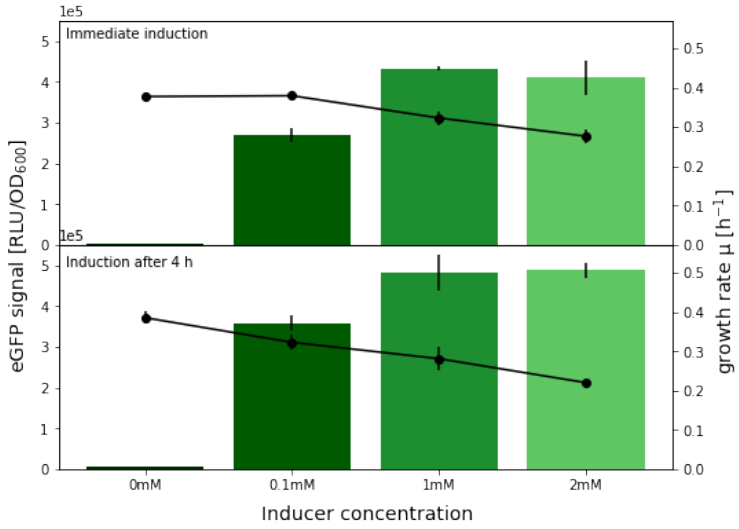

Figure 4.22: eGFP fluorescence signal in RLU per OD600 obtained with different concentrations of inducer (0 mM, 0.1 mM, 1 mM, and 2 mM 3-MB) are depicted in green bars. Two different time points of the induction were tested, with an immediate induction at the same time as inoculation (upper) and a later induction after 4 h of process time (lower). The growth rates are indicated by the scatter plot in black. With increasing inducer condition, the eGFP signal increases but the growth rate decreases.

Overall, the *P. putida* XylS/Pm promoter for regulated heterologous protein expression was transferable into *H. elongata* and fully functional without difficulties. eGFP was readily produced after induction – either immediately simultaneous with inoculation or after an adaptation period of 4 h.
The inducer saturation of the heterologous protein expression can further be described by a dose-response curve. The results for the eGFP data are shown in Figure 4.23. Since slightly lower eGFP signals were detected for the immediate induction, the data obtained for each induction strategy – immediately or after an adaptation period of 4 h – were fitted individually as well as an overall fit with both datasets. The results indicate the optimum inducer concentration to be between 0.1 mM and 1 mM 3-MB at around 0.25 mM.

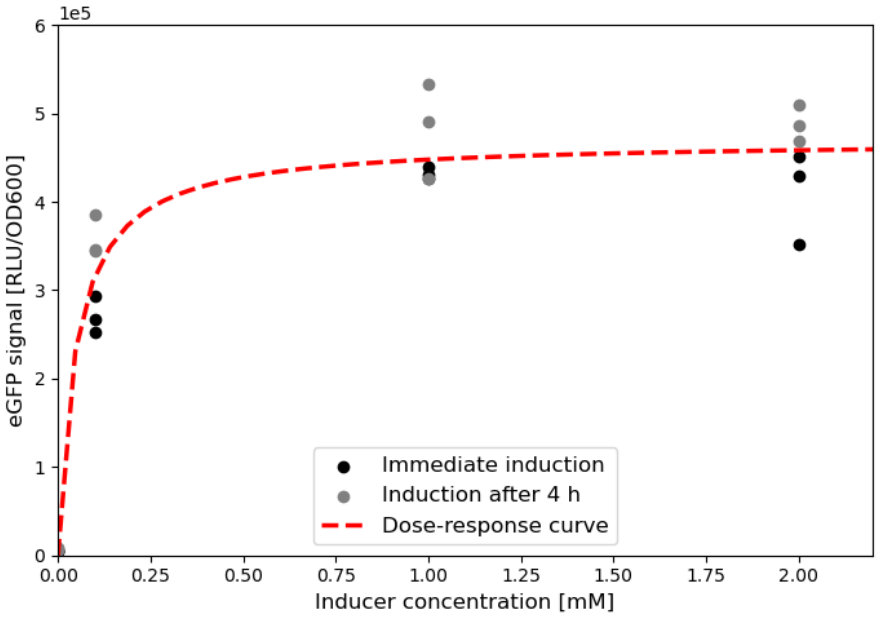

Figure 4.23: Dose-response curve showing the eGFP signal response to the 3-MB inducer concentration. With higher inducer concentrations the eGFP signal increases up until the saturation at approximately 0.25 mM 3-MB. The raw data for the immediately induced (black) and later induced (after 4 h, grey) cultures are shown in scatters. The response function (red dashed line) detailed in equation 4.10 is shown in red.

Dose-response relationship:

$$MagnitudeofresponseE = \frac{469434 \cdot c_{inducer}\ [mM]}{0.049\ [mM] + c_{inducer}\ [mM]} \tag{4.10}$$

Expression of eGFP and mCherry with different inducers

In a second experiment with the XylS/Pm promoter in *H. elongata*, another commonly used fluorescent signal protein mCherry was tested. The expression plasmid pSEVA438-mCherry is organized the same as the expression plasmid for eGFP. Additionally, different benzoic acid derivatives were checked for their properties as inducers including the previously used 3-MB, its isomer 4-methylbenzoic acid (4-MB), and 3-chlorobenzoic acid (3-CB).
In Figure 4.24, the fluorophore signal in RLU/OD600 for eGFP and mCherry is illustrated. The main

difference between the two tested fluorophores is the absolute fluorescent signal [RLU]. For eGFP, consistently 10-fold higher signals than for mCherry were measured. But the same general patterns regarding the achieved RLU/OD600 were observed. Again, without any inducer only a very minor signal was detected, reinforcing the fact that the XylS/Pm promoter has little basal expression in *H. elongata*. The highest fluorescence signal was measured with the inducer 3-MB at a concentration of 1 mM. But with only 0.1 mM 3-MB, already 60 – 65 % of the signal found for 1 mM was achieved.

Comparing the fluorescent signals of all benzoate derived inducers, 3-MB clearly facilitated the highest

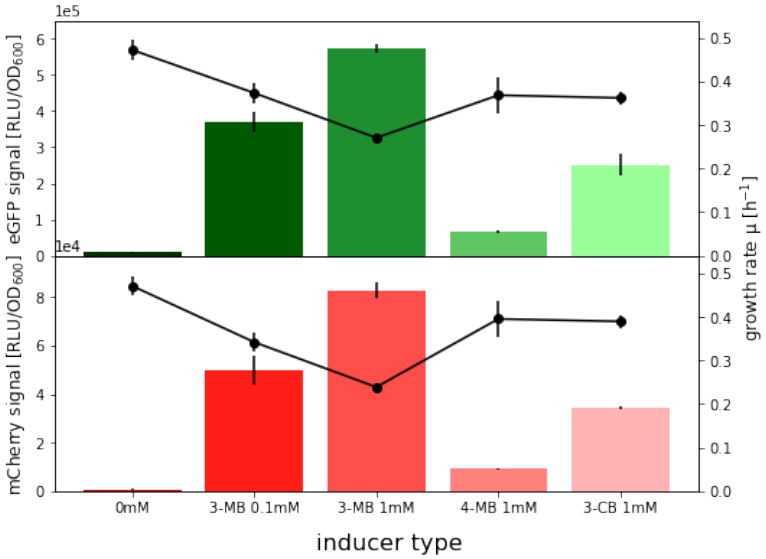

Figure 4.24: eGFP fluorescence signal (green, upper) and mCherry (red, lower) fluorescence signal in RLU per OD600 obtained with different concentrations and kinds of inducer (0 mM, 0.1 mM 3-MB, 1 mM 3-MB, 1 mM 4-MB, 1 mM 3-CB). The induction was done immediately at the same time as the inoculation of the cultures. The respective growth rates are indicated by the scatter plot in black. The expression strength for both fluorophores shows the same pattern regarding the tested inducers and inducer concentrations. For both expression systems, the strongest induction indicated by the highest RLU per OD600 signal is achieved with 1mM of 3-MB, while 1mM 4-MB was the weakest inducer.

fluorescent signal. Its isomer 4-MB barely induced protein expression at a concentration of 1 mM, at which the 3-MB concentration is already saturated. Only 11 – 12 % of the fluorophore signal compared to 3-MB at the same inducer concentration was achieved with 4-MB. The other alternative 3-CB performed better but still did not reach the same levels of protein expression at 1 mM compared to 3-MB. With 3-CB, 41 – 44 % of the fluorophore signal compared to 3-MB was achieved. Based on these results, the most efficient inducer out of all tested compounds is 3-MB. Saturation is achieved with only very low inducer concentrations almost like an on/off switch. However, weaker inducers can also have advantages. For instance, if a certain level of expression instead of a saturated induction is desired, this can be adjusted more easily and accurately with a less responsive inducer.

The average growth rate for each condition is again illustrated in Figure 4.24 by the scatter plot. For the inducer 3-MB, a consistent increase in fluorophore signal and simultaneous decrease in growth rate was observed the more 3-MB was used. This is also consistent with the first eGFP experiment. The more resources are needed for protein synthesis, the fewer resources remain for biomass production and growth, which impacts the growth rate negatively. However, for the other two inducers, 4-MB and 3-CB similar growth rates as for the induction with 0.1 mM 3-MB were obtained even though notably less signal was measured. With the inducer 3-CB, almost four times the fluorescent signal found for 4-MB was detected but the growth rates for both are the same. This discrepancy might be due to the known

adverse effects of benzoic acids on microbial growth [125, 129]. The minor differences in the chemical structures seem to have a big impact regarding microbial growth.
Regardless of the heterologous protein itself, the expression using the XylS/Pm in *H. elongata* was very reproducible. The tested inducers showed the same effects for both proteins, with 3-MB as the most efficient inducer which facilitated the production of the highest signals at a concentration of 1 mM. However, the saturation concentration for the inducer3-MB is most likely far lower.

4.2 Metabolic Engineering towards increased ectoine production targeting the anaplerotic node

The importance of the anaplerotic node for ectoine synthesis as it has already been described previously (Chapter 4.1.5; [86]) lies within its function as a key point in directing carbon fluxes towards OAA [37, 184]. Since it is inevitably intertwined with the availability of ectoine precursor molecules, this node is an excellent target for Metabolic Engineering towards a more efficient producer strain. The intracellular content of compatible solutes in halophiles like *H. elongata* as the essential feature to resist the increased turgor pressure in saline environments, is tightly controlled to accurately balance the external salt concentration [52, 77]. Like this, the distribution of carbon flux between biomass accumulation and ectoine synthesis is strictly linked to the external salt concentration and an artificial increase in intracellular ectoine content by changing the flux distribution would most likely result in a negative feedback loop downregulating the synthesis. To achieve an increase in production, this regulation needs to be uncoupled. Thus, all changes in the central metabolism aiming to redirect fluxes towards ectoine precursors were carried out in a modified strain: *H. elongata* Δ*teaABC* Δ*doeA* [118, 119].
This above mentioned strain has two modifications in its genome compared to the wild type with the deletion of the *teaABC* operon and the gene *doeA*. First, the *teaABC* genes encode for a tripartite ATP-independent periplasmic (TRAP) transporter, which has been shown to be ectoine-specific [77]. By deletion of this transporter it was observed that strains harboring this modification are secreting ectoine into the culture medium [115, 118]. This deletion mutant was thus termed *"Leaky Mutant"* because the intracellular ectoine is not properly retained in the cells but leaks out into its surroundings. This leads to an uncoupling of the regulated intracellular accumulation and ectoine production, and the yield per carbon source is increased [120]. The second modification is the deletion of *doeA*, encoding an ectoine hydrolase used for the breakdown of ectoine. *H. elongata* is able to use ectoine as a sole carbon substrate via the degradation pathway encoded by the *doe* genes (*doeABCD*) [188]. Ectoine produced in excess can be taken up again and used for biomass synthesis. This is prevented by deleting the hydrolase, the first step in the ectoine degradation pathway. Any increase in the carbon flux used for ectoine will, therefore, lead to a higher ectoine yield in this mutant.

4.2.1 The Leaky Mutant as a starting point for an ectoine producer

Since the Leaky Mutant is the precursor strain for any further modifications, its properties need to be assessed first. Even though major changes in ectoine uptake and utilization are expected in this strain, a very similar growth behavior was observed in the salt optimum. In fact, comparing the growth rates achieved by the wild type growing on glucose or fructose with 0.413 ± 0.010 h^{-1} and 0.439 ± 0.010 h^{-1}, respectively, the rates for the Leaky Mutant growing with these carbon sources were in the same range with growth rates of 0.450 ± 0.010 h^{-1} in glucose and 0.433 ± 0.006 h^{-1} in fructose (raw data from Opperman [160]). Even though a higher fraction of the available carbon needs to be channeled towards compatible solute production, to compensate for ectoine loss, this loss has no impact on the maximal growth rate. It is possible that the amount that is secreted in proportion to the cytoplasmic concentration is negligible and can easily be replaced without any major difficulties to uphold the turgor pressure. Or the Leaky Mutant can increase the flux of ectoine synthesis to keep the growth rate at the cost of getting a lower yield. Therefore, the changes in carbon flux are not as drastic as to have a noticeable impact. Interestingly, for the amount of ectoine leaked into the culture medium, the Leaky Mutant

showed significant differences when grown on glucose vs fructose (p = 0.001). The extracellular concentration of ectoine was tested in the late exponential phase at two time points between 11.5 h and 12 h of cultivation. Growing on glucose as the sole carbon source an average amount of ectoine of 0.026 ± 0.004 g/gDW while for fructose a higher content of 0.043 ± 0.006 g/gDW was detected (Figure 4.25a) making up a difference of approximately 62 %.

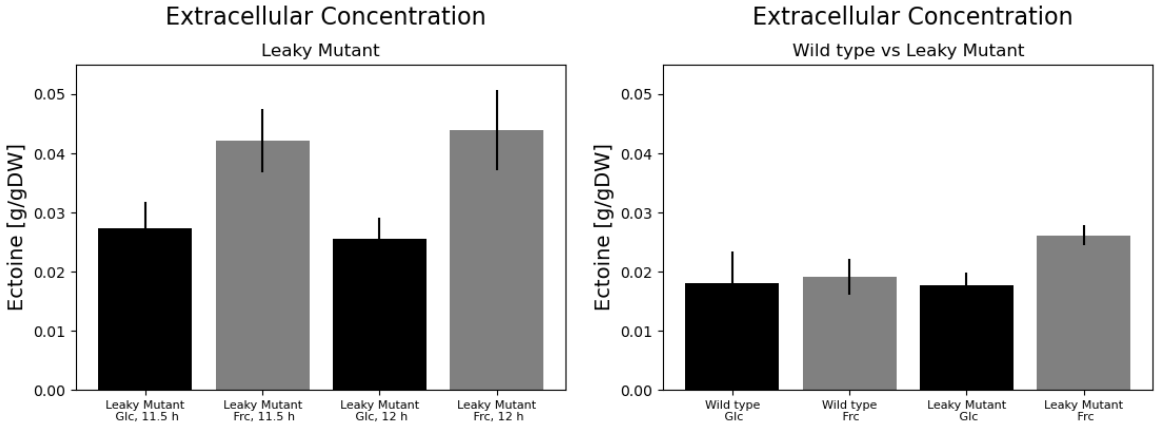

(a) Ectoine yield (extracellular) for only the leaky mutant

(b) Ectoine yield (extracellular) for the wild type and leaky mutant

Figure 4.25: Two separate experiments for measuring the extracellular ectoine yield [g/gDW] with the glycolytic substrates glucose (Glc) or fructose (Frc) are depicted. In (a) only the Leaky Mutant strain was characterized. Samples were analyzed at two time points during the cultivation process: after 11.5 h and after 12 h of process time. For both time points, a higher extracellular yield with fructose as substrate was determined. In (b) a second experiment comparing the Leaky Mutant with the Wild type is shown. For the Wild type no difference between the substrates could be determined. However, for the Leaky mutant, again, a higher extracellular yield with fructose was found. In comparison to the experiment depicted in (a) the yields for the Leaky Mutant in (b) were slightly lower. This is most likely caused by the difference in sampling times and consequently the amount of biomass.

To double check this phenomenon, in a second experiment, the ectoine concentrations achieved by the Leaky Mutant were examined again and compared to those of the wild type (raw data from Opperman [160]). The results are depicted in Figure 4.25b. Again, a difference in the extracellular concentrations when grown with either glucose or fructose as a carbon source was observed in the Leaky Mutant. Although the findings were not as clear cut as for the six replicates shown before, a higher concentration of extracellular ectoine was shown for fructose as a carbon substrate compared to glucose (p = 0.013). Remarkably, also for the wild type, ectoine could be determined to be present in the medium and even on similar levels as the Leaky Mutant. Apart from dead cells undergoing cell lysis and releasing ectoine, no major secretion should take place in the wild type. Therefore, it will be difficult to attribute the increase observed to any particular mechanisms until further experiments are done. Comparing the wild type and the Leaky Mutant, no differences are to be expected due to the tight regulation of intracellular ectoine levels. In Figure 4.26a, the intracellular ectoine content is depicted. Overall, no significant differences between both strains or the carbon sources are apparent (p > 0.05). The total average intracellular ectoine content was 0.093 ± 0.007 g/gDW. When plotting the intracellular ectoine content against the respective biomass, the data obtained for the Leaky Mutant fits with the linear relationship observed before for the wild type (Figure 4.26b). Appending this with the previously obtained data for the wild type and the theoretical prediction for 1 mg DW both match with this linear trend.
As mentioned earlier, *H. elongata* has two parallel pathways available to assimilate fructose just like *C. salexigens* [166]. These end in carbon intermediates available for either glucose catabolic pathway.

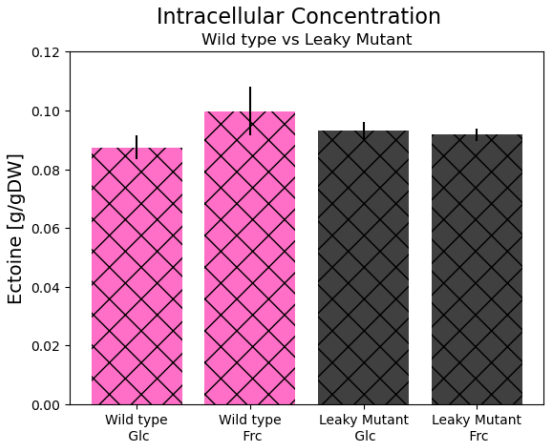

(a) Ectoine yield (intracellular) for the wild type and leaky mutant growing on glucose (Glc) and fructose (Frc)

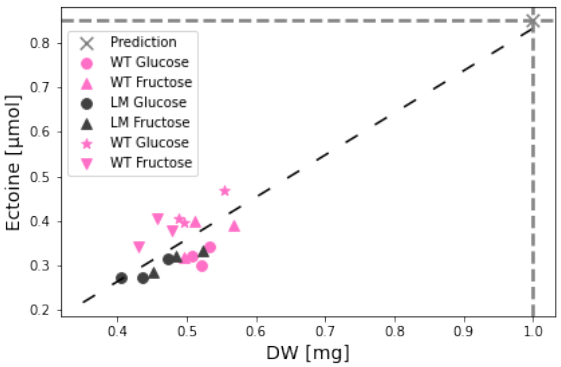

(b) Biomass vs ectoine for the wild type and leaky mutant growing on glucose (Glc) and fructose (Frc)

Figure 4.26: (a) Ectoine data for intracellular ectoine yield [g/gDW] comparing the wild type and the Leaky Mutant strain growing on glykolytic substrates: glucose or fructose. For either strain and carbon source approximately the same intracellular concentration was determined. (b) Biomass vs ectoine: The total ectoine content in μmol in 1 mL sample for the wild type (pink) and the Leaky Mutant (grey) are plotted analogous to the plot in [86] showing ectoine data achieved at 2 M NaCl. In grey, the theoretical prediction of ectoine [μmol] for 1 mg dry weight is indicated. Similar to the results for 2 M NaCl [86] a linear trend can be assumed.
Glc: glucose, Frc: fructose, WT: wild type, LM: Leaky Mutant.

Glucose is processed through the ED pathway which was substantiated in the RNA-Seq analysis (Chapter 4.1.4). Using either glucose or fructose showed no observable difference in growth rate for the Leaky Mutant. However, the extracellular ectoine concentration was significantly higher with fructose as a carbon substrate. The difference in ectoine excretion between glucose and fructose hints towards differences in the flux distribution, when using either carbon source. Based on genomic evidence, the assumed pathway for fructose uptake is through the PTS^{Fru}. This uptake pathway provides FBP, which can further be channeled through either the EMP or ED pathway. Depending on which catabolic pathway is taken, the produced metabolites from one carbon substrate changes. The EMP ends in 2 PEP, while the ED ends in 1 PEP and 1 PYR. The increased ectoine synthesis with fructose necessarily involves an increase in anaplerotic flux towards its precursor OAA. This could be achieved via either PEPC or OAD. However, to reach reliable conclusions about the flux distribution, more information is needed.

4.2.2 Impact of deletion of gluconeogenetic pathways on growth

As explained in detail before, there are four enzymes in *H. elongata* around the anaplerotic node circulating the carbon flux. The PEP carboxylase PEPC and the OAA decarboxylase OAD are collaborating to take over the anaplerotic role. PEPC constitutes the main pathway from PEP to OAA. If the salt concentration is high enough, OAD reverses its direction, carboxylating PYR to OAA. The remaining enzymes PEP carboxykinase PEPCK and malic enzyme ME are, in contrast, assigned to gluconeogenetic growth conditions, and convert OAA to PEP or MAL to PYR, respectively (Figure 2.7). The operation of PEPCK for the irreversible decarboxylation of OAA consumes ATP. *In silico* simulations based on stoichiometry predict no net flux through this reaction in glycolytic conditions. A flux through the gluconeogenetic PEPCK-mediated reaction is not needed and this reaction lowers the overall available ATP for the system [107]. But these unfavorable reactions, in fact, take place *in vivo* [32, 184]. In the case

of PEPCK, material cycles PEP and OAA in a futile cycle, which makes PEPCK an interesting target for modification to abolish a competing pathway and avoid redundant ATP consumption in glycolytic growth. Yang *et al.* [240] determined that for wild type *E. coli*, 8.2 % of the total energy flux is due to this ATP-dissipating reaction. Thus, disabling the reaction in *H. elongata* should free a notable portion of ATP molecules for other metabolic processes.
The PEPCK-encoding gene Δ*pckA* (HELO_1685) was completely replaced by a streptomycin resistance cassette in the Leaky Mutant as described in Chapter 3.4. This marker replacement mutant was called *H. elongata*-PCK::Sm^R. Based on this marker replacement mutant, subsequentially, an in-frame null mutation strain *H. elongata*-PCK was generated.

Screening of a Δ*pckA* knockout mutant

The impact of a missing PEPCK in the already modified *H. elongata* Leaky Mutant strain was initially tested in microtiter plate experiments [88], analogous to the growth screenings conducted with the strains *H. elongata*-PEPC and *H. elongata*-OAD previously (Chapter 4.1.5). *H. elongata*-PCK::Sm^R has its PEPCK gene replaced by a streptomycin (Sm) resistance cassette and its growth was characterized with different carbon sources (glucose, acetate, D-lactate) and in a range of salt concentrations spanning from 0.17 M to 2 M NaCl. The results of the growth screenings which are summarized in Figure 4.27 revealed a change in growth behavior with glucose as substrate. Even though the PEPCK-mediated reaction is designated as a gluconeogenetic reaction no significant differences in growth rate were observed between the Leaky Mutant and *H. elongata*-PCK::Sm^R growing on acetate over the whole range of tested salt concentrations ($p > 0.05$). Only at a low salt condition of 0.17 M NaCl *H. elongata*-PCK::Sm^R showed a slightly diminished growth rate, although not significantly reduced ($p = 0.029$). Growing on glucose, however, *H. elongata*-PCK::Sm^R grew slower than the Leaky Mutant in all salt concentrations but the high salt condition at 2 M NaCl. This trend proved to be significant ($p < 0.01$), except for the condition at 0.5 M NaCl, at which the standard deviations for both strains are notably higher compared to the other tested salt concentrations.
For the third substrate D-lactate, no impact of the PEPCK deletion was observed similar to the results with acetate. But not only the behavior of *H. elongata*-PCK::Sm^R in comparison to its parental strain, but also the absolute numbers for the achieved growth rates were similar to those achieved with acetate. For instance, at high salt, at which no impact of the PEPCK deletion with either substrate was found, the highest growth rate regarding the carbon source was achieved with glucose with a rate of 0.255 ± 0.026 h^{-1}. In contrast, growth on acetate or D-lactate diminished the rates by about a third to 0.163 ± 0.021 h^{-1} and 0.181 ± 0.006 h^{-1}, respectively. The reduced growth rate on gluconeogenetic carbon sources in comparison to glycolytic substrates is well known and is generally attributed to limitations of energy or monomers [33]. This suggests a similar metabolization of acetate and D-lactate as gluconeogenetic substrates. The most prevalent pathway for the utilization of L-lactate in general is the conversion to PYR via a L-lactate dehydrogenase and subsequent metabolization of the gluconeogenetic substrate PYR. *H. elongata* has an annotated L-lactate dehydrogenase *lldD* (HELO_1220). Another lactate dehydrogenase homolog was found with HELO_1046 but no substrate specificity has been associated. This might be a potential lactate dehydrogenase for the utilization of L-lactate analog to the L-enantiomer.

Screening of a Δ*pckA* Δ*maeB* double knockout mutant

The remaining enzyme involved in the PEP-PYR-OAA node, next to PEPCK and the anaplerotic enzymes PEPC and OAD, is the malic enzyme ME. In *H. elongata*, like in *E. coli*, the isoenzymes NAD-ME encoded by *maeA* (*sfcA* in *E. coli*) and a NADP-ME encoded by *maeB* are present. Both isoenzymes are annotated as OAA-decarboxylating, meaning not only MAL but also OAA can be used as a substrate to convert to PYR. Since this OAA decarboxylation would constitute a competing pathway to ectoine synthesis, ME was used as the next target for genome modification in *H. elongata*-PCK. *In vitro* enzyme assays with *H. elongata* cell lysate and either cofactor only showed a measurable activity for NADP-ME with $NADP^+$ cofactor specificity [86]. Thus, based on *H. elongata*-PCK a second modified strain was constructed, deleting the $NADP^+$-dependent ME encoded by *maeB* (HELO_3763). The *maeB*

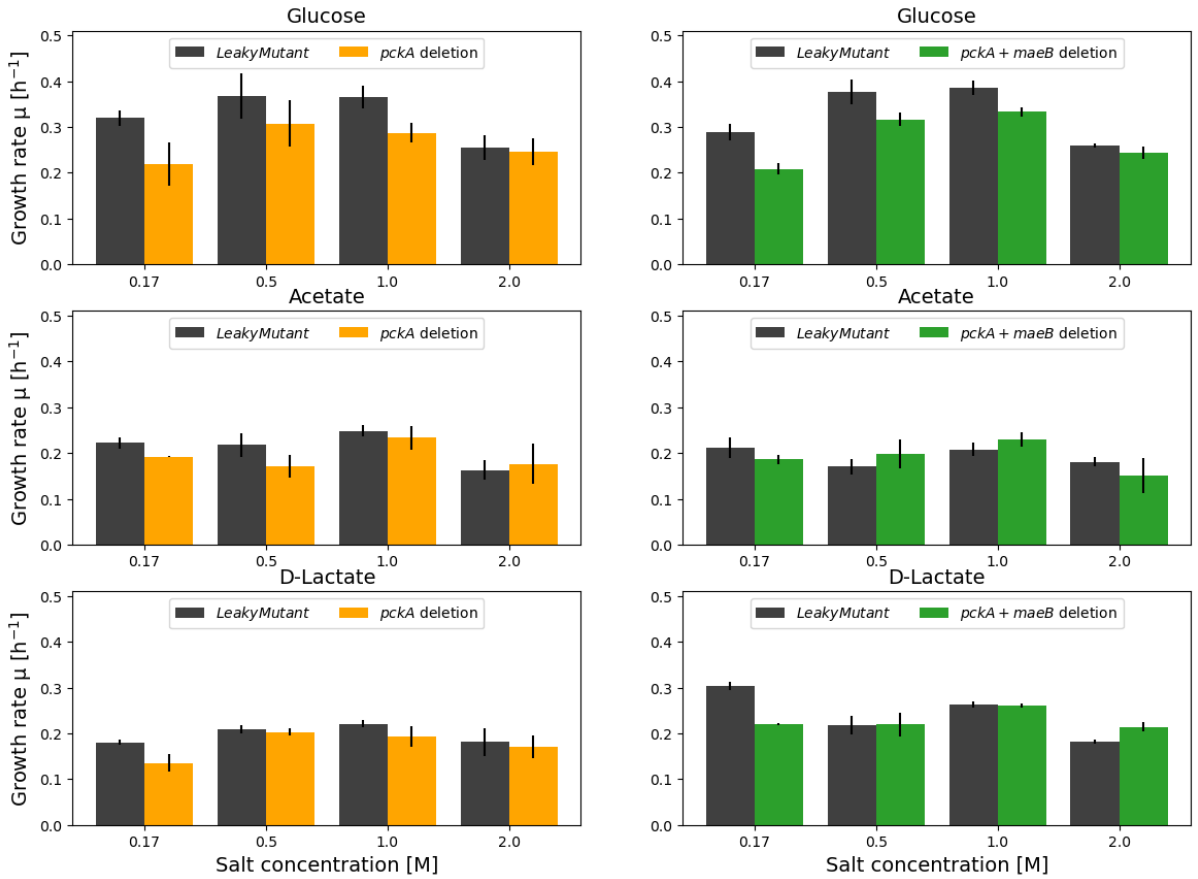

Figure 4.27: Growth rate screening of the strain *H. elongata*-PCK::Sm^R (orange) and *H. elongata*-PCKMAE::Sm^R (green) with the Leaky Mutant as a reference (black). Tested is a salt range from 0.17 M NaCl to 2 M NaCl and three different carbon sources: Glucose, Acetate, and D-Lactate.

knockout was performed in the *H. elongata*-PCK deletion strain. Like for the PEPCK knockout, *maeB* was first completely replaced by a Sm^R resistance cassette and, subsequently, the antibiotic gene was removed again. The double knockout mutants *H. elongata* Δ*teaABC* Δ*doeA* Δ*pckA* Δ*maeB*::Sm^R and *H. elongata* Δ*teaABC* Δ*doeA* Δ*pckA* Δ*maeB* are from here on referred to as *H. elongata*-PCKMAE::Sm^R and *H. elongata*-PCKMAE, respectively.
Analog to *H. elongata*-PCK::Sm^R, the second modified strain *H. elongata*-PCKMAE::Sm^R was tested in microtiter plate experiments [88] with the carbon substrates (glucose, acetate, and D-lactate) and the same salt concentrations ranging from low salt to high salt (0.17 – 2 M NaCl). The results are summarized in Figure 4.27. All in all, the growth behavior of *H. elongata*-PCKMAE::Sm^R was very similar to the single knockout strain *H. elongata*-PCK::Sm^R. Again, growth on acetate (and D-lactate) was still not only possible but just like for *H. elongata*-PCK::Sm^R no significant difference compared to the Leaky Mutant was observed. Similar to *H. elongata*-PCK::Sm^R, the biggest impact on growth occurred with glucose as a carbon substrate. A significantly lower growth rate was observed but only for the low salt (0.17 M NaCl) condition ($p = 0.007$). Interestingly, the negative effect with glucose in the salt optimum, caused by the PEPCK deletion seemed to be lessened by the additional removal of *maeB*. The reduction in growth rate for *H. elongata*-PCKMAE::Sm^R was not as drastic ($p > 0.01$) as observed for *H. elongata*-PCK::Sm^R. At high salt (2 M NaCl), the growth rate was the same as for the Leaky Mutant reference, which was also the case for the single knockout strain *H. elongata*-PCK::Sm^R.

The transcriptomic analysis showed, that both isoenzymes are transcribed in all tested conditions and strains, but no differential expression within the log2 FC threshold of |1.5| was observed and no distinct impact on the growth rates after removal of *maeB* was detected.
In Figure 4.28 the YK-R model approximation for the growth rates and the experimentally determined

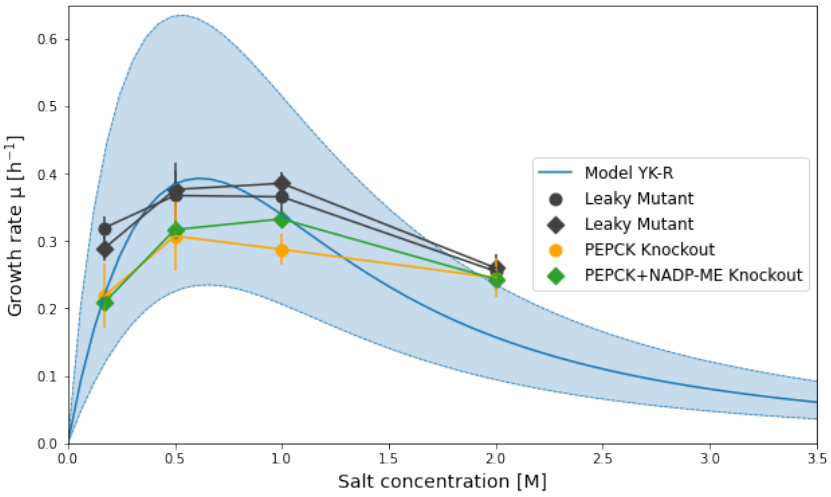

Figure 4.28: Experimentally achieved growth rates for *H. elongata*-PCK::Sm^R(orange, circles) and *H. elongata*-PCKMAE::Sm^R (green, diamonds) and the respective references (grey) for each screening experiment (circles: *H. elongata*-PCK::Sm^R screening, diamonds: *H. elongata*-PCKMAE::Sm^R screening) over the salt-dependent prediction of growth rates calculated for the YK-R model. The tinted area show the span of the 95 % confidence interval [52].
PEPCK Knockout: strain *H. elongata*-PCK, *pckA* knockout, PEPCK+NADP-ME Knockout: strain *H. elongata*-PCKMAE, *pckA* and *maeB* knockout.

growth rates for Leaky Mutant, *H. elongata*-PCK, and *H. elongata*-PCKMAE are shown. Between the salt range from 0.17 M to 1 M NaCl Leaky Mutant growth rates match well with the theoretical prediction for the wild type. At 2 M NaCl a deviation for the experimental growth rates was observed with a notably lower prediction. This underestimation at high salt was found before for the wild type growth rates in shake flask experiments (see Chapter 4.1.4). For both modified strains the reduction in growth rates at lower salinities is illustrated. At the high salt condition all growth rates converge. In general, the typical salt-dependent behavior of *H. elongata* with the plateau of maximum growth rates between 0.5 M and 1 M NaCl is still visible in both modified strains.

Growth of *H. elongata*-PCK and *H. elongata*-PCKMAE in shake flasks

To verify the results obtained from the small-scale screening, which often show a high variability, further shake flask experiments were conducted. A variety of batch experiments in the salt optimum at 1 M NaCl were conducted with both in-frame null mutation knockout strains *H. elongata*-PCK and *H. elongata*-PCKMAE. In Figure A.1b (appendix), an outline of all six experiments is depicted. Each strain was tested four times with two experiments involving all three strains. Because the Leaky Mutant exhibited a significantly faster growth rate with glucose as the substrate compared to both mutants ($p < 0.01$), two separate experiments with only the Leaky Mutant and two with only the modified strains were carried out. For the Leaky Mutant, an average growth rate of 0.467 ± 0.044 h^{-1} was determined. Both modified strains grew slower at 1 M NaCl but, interestingly, at almost identical average growth rates of 0.345 ± 0.051 h^{-1} and 0.348 ± 0.057 h^{-1} for *H. elongata*-PCK and *H. elongata*-PCKMAE, respectively. This makes up only 75 % of the Leaky Mutant growth rate. The reduction in growth speed can clearly be

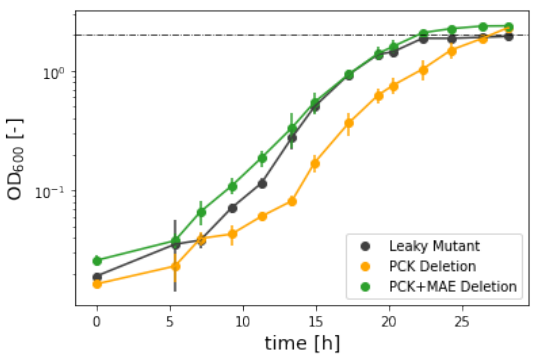

(a) Growth curves in half-log depiction

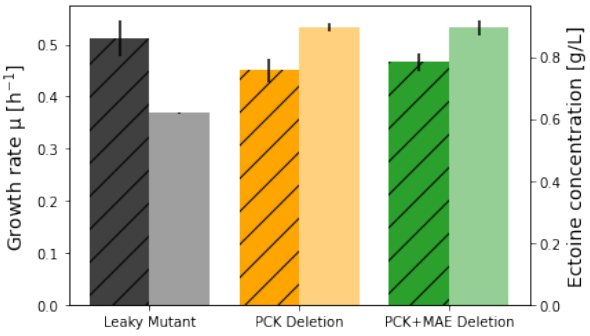

(b) Growth rates (dashed) and final extracellular ectoine concentration

Figure 4.29: (a) Growth curve of the *H. elongata* Leaky Mutant, the *pckA* knockout strain *H. elongata*-PCK, and the *pckA maeB* double knockout strain *H. elongata*-PCKMAE in a SO_4-limited medium shown in half-logarithmic depiction focusing on the exponential phase. The OD600 value of 2 is indicated by a dashed horizontal line. *H. elongata*-PCK experiences a longer lag phase compared to the other strains. These illustrations are published in Hobmeier *et al.* [88] in Frontiers in Microbiology. (b) Growth rates (left, striped bars with saturated colors) and extracellular ectoine concentrations (right, no stripes, pastel colors) in a SO_4^--limited medium (Glucose, 1 M NaCl) of the three strains Leaky Mutant (grey), *H. elongata*-PCK (orange), and *H. elongata*-PCKMAE (green). Similarly reduced growth rates for the mutant strains were determined. Ectoine samples were taken after 48 h to determine the final titer. For the mutant strains the measured ecotine titers are notably higher.
PCK Deletion: strain *H. elongata*-PCK, *pckA* knockout, PCK+MAE Deletion: strain *H. elongata*-PCKMAE, *pckA* and *maeB* knockout.

attributed to the loss of PEPCK. As explained before, even though PEPCK is generally branded as a gluconeogenetic enzyme, in *H. elongata* it seemingly plays a role in growing on glucose as well. The additional deletion of *maeB* showed no drastic changes in its phenotype, in comparison to the single knockout strain. However, in contrast to the prolonged lag phase (Figure A.1a, appendix) experienced for *H. elongata*-PCK, the double knockout strain *H. elongata*-PCKMAE seemed to be able to commence growth slightly faster after inoculation.

4.2.3 Ectoine production in *H. elongata*-PCK and *H. elongata*-PCKMAE

The original goal for the introduction of the modifications was to increase the carbon flux towards ectoine synthesis and, thereby, improving the ectoine yield. Therefore, the ectoine production of the modified strains *H. elongata*-PCK and *H. elongata*-PCKMAE was determined to identify any improvements [88]. In shake flask experiments, the amount of biomass that can be generated is limited. Additionally, the secreted ectoine by the cells into the medium is massively diluted due to the low amount of achievable biomass in comparison to the medium volume. To increase the concentration of the extracellular ectoine concentration and facilitate a more accurate detection, the regular minimal medium was slightly altered. With the *H. elongata* biomass composition known, the amount of available sulfate was appropriately reduced to only allow the biomass formation up to an OD600 value of 2. After the depletion of sulfur, the remaining resources are available for ectoine synthesis exclusively. The growth rates (Figure 4.29a) observed in this sulfate-limited minimal medium at 1 M NaCl and with glucose as the sole carbon substrate reflected the results obtained in the regular medium. The highest growth was achieved by the Leaky Mutant with a rate of 0.512 ± 0.035 h^{-1}. The growth rates of the modified strains *H. elongata*-PCK and *H. elongata*-PCKMAE were in comparison slightly reduced to 0.450 ± 0.024 h^{-1} and 0.466 ± 0.017 h^{-1}, respectively. Even though the same growth rates were obtained for both strains, *H. elongata*-PCKMAE resumed growth faster after inoculation than *H. elongata*-PCK, which had a prolonged lag

phase (Figure 4.29b). After reaching approximately OD600 2, the sulfate limitation caused a sharp bend in the growth curve for the Leaky Mutant. In contrast, both modified strains exceeded this OD600 value and showed no drastic nick. This could imply changes in the biomass composition and/or the OD600 to biomass correlation due to the deletion of PEPCK and NADP-ME.
The final extracellular ectoine titers (Figure 4.29b) determined after 48 h for the Leaky Mutant were 0.619 ± 0.002 g/L, while for *H. elongata*-PPC and *H. elongata*-PCKMAE reasonably higher titers of 0.895 ± 0.012 g/L and 0.894 ± 0.025 g/L could be achieved. This is an approximate increase of 45 % in extracellular ectoine. The additional deletion of *maeB* compared to the single knockout in *H. elongata*-PCK showed no impact in neither the growth rate nor the ectoine titer [135]. But a regulatory role for NADP-ME was suggested. In *E. coli*, the genes *ppsA*, *sfcA* (equates to *maeA* in *H. elongata*), and *maeB* are involved in the regulation of carbon source transition. The gluconeogenetic flux to PEP was found to be important for the adequate activation of the global regulatory system during the transition from glucose to acetate [97]. In *H. elongata* a similar feedback interaction might be present.

4.2.4 Transcriptomic Analysis of the Leaky Mutant and *H. elongata*-PCK

Not only the wild type transcriptome was analyzed using RNA-Seq, but also two modified strains: the Leaky Mutant (Δ*teaABC* Δ*doeA*) and *H. elongata*-PCK (Δ*teaABC* Δ*doeA* Δ*pckA*) [87, 88]. For both of these strains only one growth condition, namely the salt optimum at 1 M NaCl with the carbon source glucose was investigated. With a growth rate of 0.461 ± 0.008 h^{-1}, the Leaky Mutant grew at a similar rate as the wildtype, which was established and noted in general before in Chapter 4.2.1. This growth rate also agrees well with the growth rate of 0.467 ± 0.044 h^{-1} established for the leaky mutant in the shake flask experiments in Chapter 4.2.2. In contrast, the growth rate for *H. elongata*-PCK with the additional deletion of PEPCK was considerably lower than the previously observed growth rate (0.345 ± 0.051 h^{-1}, Chapter 4.2.2) at 0.256 ± 0.008 h^{-1}. In Table 4.5, the growth conditions and rates are summarized. Figure 4.30 shows the average transcripts for one strain plotted against the number of

Strain	Carbon source	Salt [M]	Growth rate μ [h^{-1}]
Leaky Mutant	Glucose	1.0	0.461 ± 0.008
H. elongata-PCK	Glucose	1.0	0.256 ± 0.008

Table 4.5: Overview of the growth conditions regarding carbon source and salt condition and the respective growth rates calculated for three biological replicates of the Leaky Mutant strain and strain *H. elongata*-PCK used in the transcriptomic analysis.

transcripts for another strain in order to visualize the discrepancies in the expression profiles. Each dot represents a gene in the *H. elongata* genome and genes that are transcribed in a similar amount appear on a diagonal line from the lower left end to the upper right end of the plot. Extreme changes in the transcription levels for the Leaky Mutant result in a shift away from this diagonal line. Plot A shows the Leaky Mutant in comparison to the wild type and at first glance, the transcriptomes seem to have a rather low variance. Even though major modifications have taken place in the genome of the Leaky Mutant, the transcriptome has few deviations from the wild type with the majority of genes showing up tightly packed around the diagonal line. As a comparison to the changes introduced through genome modifications, the same illustration was done for the transcriptome of the wild type in low salt (0.17 M NaCl) against the salt optimum (1 M NaCl) shown in Plot B. The salt-related stress induces vast differences in the transcriptomic expression levels shown by the more dispersed cloud of dots farther away from the diagonal. Furthermore, the transcripts of *H. elongata*-PCK against its parental strain, the Leaky Mutant, is depicted in Plot C. The single deletion of PEPCK seemingly leads to bigger changes, compared to the deletion of *teaABC* and *doeA* in the Leaky Mutant which is reflected in the larger scattering. This is not only visually recognizable but can also be put into numbers. Comparing the number of differentially expressed genes (threshold: log2-FC change of |1.5|, [253]) for the Leaky Mutant and the wild type, only 80 genes were considered to be down- and 16 genes were considered to be upregulated. In *H. elongata*-PCK on the other hand, 180 genes were down- and 103 genes were

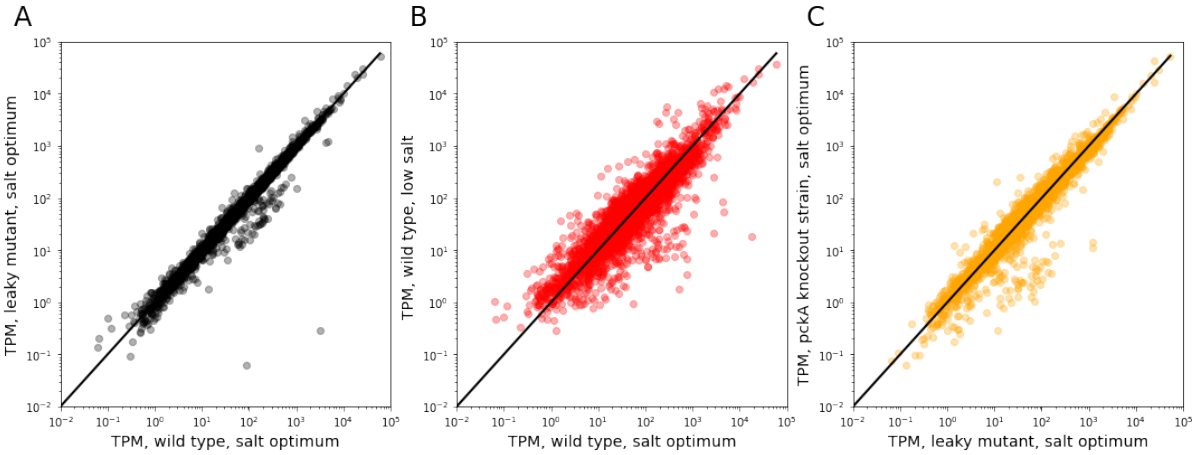

Figure 4.30: Variation of the transcriptomes for the wild type grown in different salinities and the wild type and Leaky Mutant grown at the salt optimum (1 M NaCl). In black, the transcripts per million (TPM, 4.1.4) determined for the Leaky Mutant growing in salt optimum (1 M) are plotted against the wild type in the salt optimum (1 M). In orange, the TPM determined for the *pckA* knockout mutant growing in the salt optimum (1 M) are plotted against the Leaky Mutant in the salt optimum (1 M). In red, the TPM determined for the wild type growing in low salt condition (0.17 M) are plotted against the wild type in the salt optimum (1 M). Even though there are several genes removed in the Leaky Mutant (*teaABC*, *doeA*
) the expression profile is more similar to the wild type than comparing the expression profiles of the wild type growing at low or high salinity indicated by the increased scattering.

upregulated compared to the Leaky Mutant. This equates to almost three times more genes that are changing their expression profile in the PEPCK knockout strain. For both strains, the majority of the differentially expressed genes are downregulated.
The affected genes were further clustered into their respective COG categories. In the Leaky Mutant compared to the wildtype, mostly genes involved in cell motility and signal transduction were affected including the flagellar transcriptional sigma factor *fliA* (HELO_4331). Especially genes involved in flagellar biosynthesis and genes encoding proteins, that are part of the basal body and the hook of the flagellum embedded into the membrane, are affected (*flhABC* HELO_4333-5, *fliC1C2D1D2* HELO_4352-55, *fliEFGHIJKLMNOPQR* HELO_4358-70, *flgABCDEFGHIJKL* HELO_4371-82, *motB* HELO_4343). Chemotaxis-related genes (*cheABRWZ* HELO_4334-42), which are part of the signal transduction category, are downregulated as well and also another chemotaxis sensory protein *tar1* (HELO_4356), which is located apart farther downstream. Other downregulated genes in the Leaky Mutant are all of the removed genes, *teaABC* (HELO_4274-6) and *doeA* (HELO_3665). Since no expression can take place at all, this is not surprising and provides no further information about the metabolism, but it is a good quality control for the transcriptomic data. *TeaD* (HELO_4277) which is located adjacent to the *teaABC* operon unit with the same reading direction was found to be upregulated in the Leaky Mutant. This can also be attributed directly to the removal of the *teaABC* genes. The promoters and ribosomal binding sites of the *tea* operon are still intact and, thus, *teaD* is now directly under its regulation resulting in an 'artificial' overexpression of *teaD*. Another artefact due to the genome modification is the downregulation of *doeB* (HELO_3664) and *doeC* (HELO_3662). These genes encode the enzymes catalyzing the ectoine-degrading reactions directly following the *doeA* mediated hydrolysis reaction [188]. This is most likely the direct consequence of the *doeA* deletion since no ectoine hydrolysis is taking place. Further observations are the downregulation of an O-linked N-acetylglucosaminyl (O-GlcNAc) transferase (HELO_4351) involved in the glycolysation of proteins, a

maturation protein for the cbb_3-cytochrome c-oxidase (HELO_3542A), and a TonB-dependent receptor for the uptake of siderophores (HELO_2827). But even though the iron transport was negatively affected another gene *phnD* (HELO_2137) involved in the import of the inorganic ion phosphate was upregulated. Another upregulated gene in the Leaky Mutant specifically is HELO_2071, which is described as a NLPC domain protein. Typically, proteins containing this NlpC/P60 domain have hydrolytic activity like, for example, acyltransferases, amidases, and endopeptidases [4]. The role of NlpC/P60 proteins is suggested to revolve around cell division and cell wall maintenance [7].

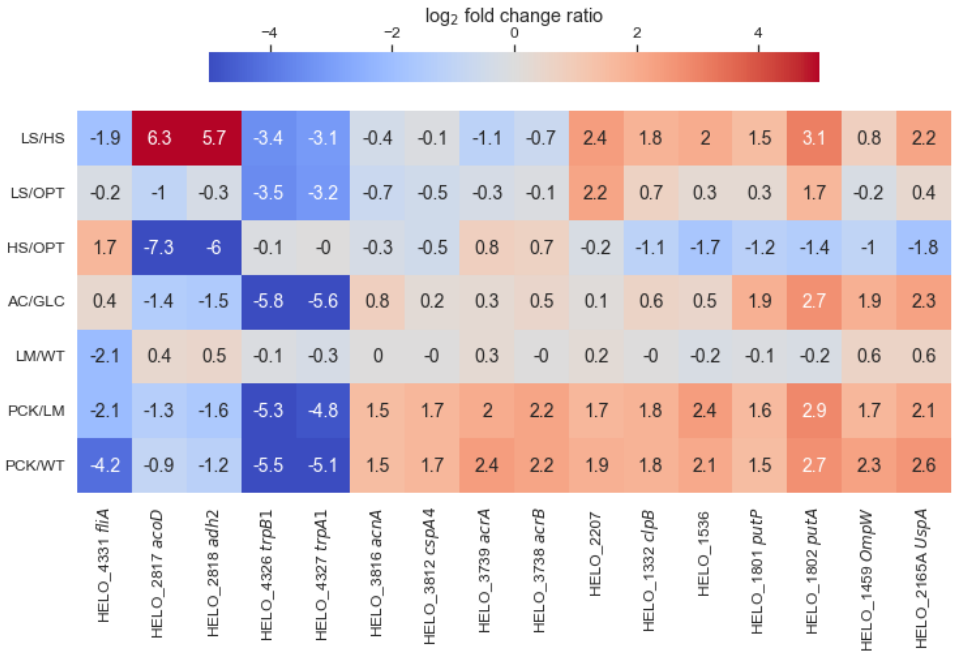

Figure 4.31: Expression profiles of selected differentially expressed genes based on the set threshold of a log2 fold change of |1.5| in the PEPCK-knockout mutant *H. elongata*-PCK compared to its parental strain the Leaky Mutant (PCK/LM). The log2 fold change for all observed strains and growth conditions are are shown: low salt against high salt (LS/HS) in the wildtype, low salt against salt optimum (LS/OPT) in the wildtype, high salt against salt optimum (HS/OPT) in the wildtype, gluconeogenetic growth against glycolytic growth (AC/GLC) in the wildtype, Leaky Mutant against the wildtype (LM/WT), *H. elongata*-PCK against the Leaky Mutant (PCK/LM), and *H. elongata*-PCK against the wildtype (PCK/WT). Genes shown in red (positive fold change) are upregulated in the condition specified in the numerator compared to the one in the denominator while blue (negative fold change) signifies a downregulation

Behavior similar to that of the Leaky Mutant is also observed in *H. elongata*-PCK. With the additional PEPCK deletion an even stronger downregulation of the motility and singal transduction modules occurs: *flhABCDE* (HELO_4332-5A), *fliTSC1C2D1D2* (HELO_4348-55), *fliEFGHIJKLMNOPQR* (HELO_4358-70), *flgBCDEFGHIJKL* (HELO_4371-81), *flaG* (HELO_4357), *motAB* (HELO_4343-4), *cheABRWZY* (HELO_4334-42), *tar1* (HELO_4356), and the transcriptional regulator of these genes, sigma factor *fliA* (HELO_4331). The behavior of *fliA* and other interesting genes for all tested conditions throughout this work is illustrated in Figure 4.31. Essentially, the expression of the flagellar sigma factor correlates positively with salinity but also the deletion of *teaABC* and *doeA* in the Leaky Mutant and further the deletion of *pckA* cause a downregulation. Apart from this, the biggest portion of differentially expressed genes in the PEPCK deletion mutant compared to either the Leaky Mutant

or the wildtype are not annotated and can thus not be categorized. However, naturally, compared to the Leaky Mutant transcriptome the downregulation of *pckA* (HELO_1685) is observed, which similar to the deleted genes in the Leaky Mutant, is directly related to the removal of *pckA* and can be taken as a control for the validity of the RNA-Seq data. Furthermore, some genes related to carbohydrate and amino acid metabolism were found to be downregulated as well. This includes two ABC-type sugar transporter permease proteins (HELO_2484-5), a TRAP malate $2H^+/Na^+$ lactate antiporter (SBP, HELO_1558), a protein with glycosyltransferase domain (HELO_3595), and an alcohol dehydrogenase *adh2* (HELO_2818) regarding carbohydrate metabolism. The expression of *adh2*, and another related gene *acoD* (HELO_2817) has been shown to also be regulated by salinity. In the mutant *H. elongata*-PCK and with an increasing salt concentration the expression is reduced. For amino acid metabolism, the tryptophan synthase genes *trpA1* and *trpB1* (HELO_4327, HELO_4326) and a histidine decarboxylase *hdc* (HELO_2826) are affected. *TrpA1* and *trpB1* were found to be strongly affected by the salinity correlating positively with the salt concentration and also the carbon source. In essence, the expression of the tryptophan synthase genes growing at low salinity, under gluconeogenetic condition, and *H. elongata*-PCK was downregulated. Other downregulated genes include the enterobactin synthase component EntE (HELO_2837), the iron-containing cbb_3-type cytochrome oxidase *ccoQ* (HELO_3538), the transcription regulator PrtN (HELO_4202), two DNA methylases (DNA-adenine methylase HELO_2662, DNA-cytosine methylase, HELO_4206), a UDP-galactopyranose mutase encoded by *rfbD*, and a hydrolase domain protein (HELO_4192) akin to N-acetylmuramoyl-L-alanine amidase AmiC in *E. coli*. Overall, there are less genes upregulated than downregulated in *H. elongata*-PCK. These include some stress response proteins like the universal stress protein UspA (HELO_2165A), the cold shock protein CspA4 (HELO_3812), the molecular chaperone ClpB (HELO_1332), and defense mechanisms like the multidrug efflux pump AcrAB (HELO_3739, HELO_3738). Some of these are unique to the *H. elongata*-PCK transcriptome like CspA4 and AcrAB, which facilitates the ATP-dependent vertical transport of diverse compounds from the cytoplasm directly into the extracellular space [53], and most interestingly, the aconitate hydratase encoded by *acnA* (HELO_3816). AcnA is an integral part of the TCA cycle and catalyzes the two-step reaction converting citrate to isocitrate. This could hint towards an increased flux through the TCA cycle in the PEPCK knockout strain. The stress response proteins CspA4 and ClpB seem to be linked to conflicting stress factors with CspA4 as a cold shock protein linked to a temperature downshift [172], while ClpB is commonly associated with high temperature stress [3]. However, it has been shown that stress proteins often correspond to a variety of stresses. In contrast to CspA4, the expression of ClpB was also influenced by salinity. Similar to two other genes, HELO_2207 and HELO_1536, they are upregulated in *H. elongata*-PCK and correlate negatively with salinity. HELO_2207 is not annotated, but was linked to lipid metabolism by sequence similarity to the poly-β-hydroxybutyrate synthase PhaC and HELO_1536 encodes an APC family transporter. The universal stress protein UspA mentioned above was found to change in *H. elongata*-PCK and also regarding the used carbon source. This was also the case for the outer membrane porin OmpW (HELO_1459) and the *put* operon comprised of the Na^+/proline symporter PutP (HELO_1801) and the bifunctional protein PutA (HELO_1802). These genes were upregulated in *H. elongata*-PCK and in the wildtype growing with acetate under gluconeogenetic conditions.

4.2.5 Further modifications: Additional deletion of PEPC

The growth behavior of *H. elongata*-PCK and *H. elongata*-PCKMAE on glucose and acetate was still not easily explained. The deletion of PEPCK did not show a phenotype growing with acetate but with glucose and this, particularly, at lower salt concentrations. We proposed that the OAA levels are finely tuned and removal of the OAA-consuming reaction offsets the intracellular ratios of the metabolites, which in turn leads to feedback inhibition [37, 161, 184]. To gain some more insights into this phenotype caused by the PEPCK knockout, another strain based on *H. elongata*-PCK was generated by additionally deleting the PEP carboxylase (*ppc*, HELO_3010). Here, the in-frame null mutation was done immediately without an initial marker replacement step. The new knockout mutant *H. elongata* $\Delta teaABC$ $\Delta doeA$

Δ*pckA* Δ*ppc* is from here on called *H. elongata*-PCKPPC.

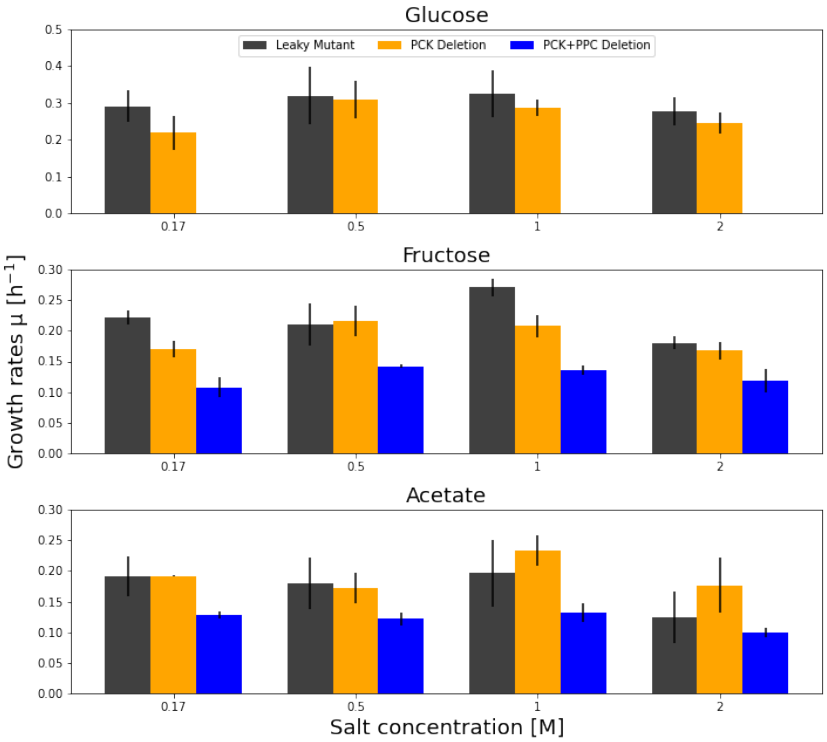

Figure 4.32: Growth screening of *H. elongata*-PCKPPC (blue) compared to the Leaky Mutant (grey) and *H. elongata*-PCK (orange). Tested is a salt range from 0.17 M NaCl to 2 M NaCl and three different carbon sources: Glucose, Fructose, Acetate. In the microtiter plate, strain *H. elongata*-PCKPPC did not show growth even though in the direct pre-culture using the exact same medium growth could be observed. Further, for either remaining carbon source, fructose and acetate, *H. elongata*-PCKPPC consistently showed the slowest growth rates over the whole range of salt concentrations.
PCK Deletion: strain *H. elongata*-PCK, *pckA* knockout, PCK+PPC Deletion: strain *H. elongata*-PCKPPC, *pckA* and *ppc* knockout.

Screening of a Δ*pckA* Δ*ppc* double knockout mutant

The results of some initial screenings of *H. elongata*-PCKPPC in microtiter plate experiments are depicted in Figure 4.32. One experiment for each carbon source – glucose, acetate, and fructose – was carried out again in a range of salt concentrations, spanning from low salt to high salt conditions (0.17 M to 2 M NaCl) with the Leaky Mutant as a reference. Only for the fructose screening all three strains including *H. elongata*-PCK were grown in the same experiment. The additional growth data with glucose and acetate for *H. elongata*-PCK was taken from the results of a previous screening. Therefore, the growth rate data for the Leaky Mutant with glucose and acetate for both batches was averaged.
Focusing on the impact of the additional deletion of PEPC, the most striking observation is, that with glucose as substrate, *H. elongata*-PCKPPC showed no growth up until 18 h after inoculation. This happened at all salt concentrations. But even though no growth was observed in the screening, the strain was able to grow in the same minimal medium during the preculture steps. As it was mentioned before, the deletion of PEPC lead to a rather unstable phenotype with high variations in lag phases and growth behavior. Since the microtiter plate experiment was carried out in only 200 μL volume the

inoculum was very small and the microplate reader itself did not provide ideal conditions for growth, like for example continuous shaking. This can result in potential problems with aeration or changes in the medium volume due to evaporation of water. Therefore, it is possible, that a delicate strain like *H. elongata*-PCKPPC is unable to commence growth after the transfer from the precultures. For growth on acetate, a slightly diminished growth rate compared to the Leaky Mutant was found for the lower salt concentrations at 0.17 M and 0.5 M NaCl ($p < 0.05$), while at higher concentrations the same rates were achieved. For the substrate fructose, a similar behavior at all salt conditions was observed for the three strains. The growth rate decreased stepwise with each additional deletion. Within the standard deviations, these steps were statistically relevant only for 0.17 M and 1 M salt concentration ($p < 0.05$), while for 0.5 M and 2 M NaCl the growth rates of Leaky Mutant and *H. elongata*-PCK were the same. The double knockout strain *H. elongata*-PCKPPC, however, consistently showed the slowest growth rates over the whole range of salt concentrations.

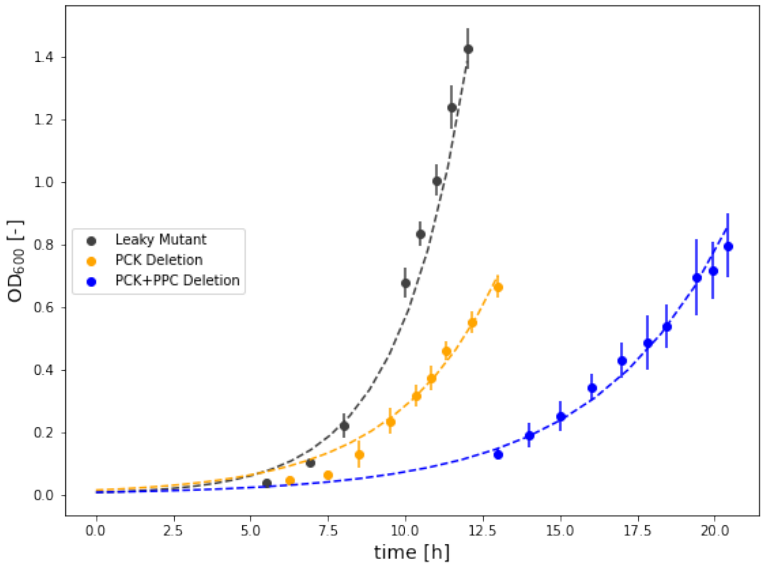

Figure 4.33: Growth curves and lag phases observed in flask experiments at 1 M NaCl with glucose as carbon source; depicted are the strains: Leaky Mutant (grey), *H. elongata*-PCK (orange), and *H. elongata*-PCKPPC (blue). An approximation of the biomass evolution for each strain is shown by the dashed curves in the respective colors. The shortest lag phase and fastest growth rate was observed for the Leaky Mutant. Compared to that, the single *pckA* knockout strain *H. elongata*-PCK has a longer lag phase and slower growth rate. Finally, with an additional knockout of *ppc* the double knockout strain *H. elongata*-PCKPPC experiences the longest lag phase and the growth rate is reduced even more.
PCK Deletion: strain *H. elongata*-PCK, *pckA* knockout, PCK+PPC Deletion: strain *H. elongata*-PCKPPC, *pckA* and *ppc* knockout.

Verification of the Δ*pckA* Δ*ppc* phenotypes in shake flasks

Since no growth of the double knockout strain *H. elongata*-PCKPPC with glucose as substrate was observed in the screening, the mutant was characterized in flask experiments with a moderate salt concentration of 1 M NaCl. In Figure 4.33, the average growth curves of the Leaky Mutant, *H. elongata*-PCK, and *H. elongata*-PCKPPC are illustrated. With the evolution of the OD600 for all three strains plotted next to each other, the differences in growth especially the increased lag phases are apparent. With each additional deletion, the growth rate gradually decreases, and the duration of the lag phase increases.

For a complete picture, flask experiments with fructose and acetate as sole carbon sources were conducted as well. All resulting growth rates are summarized in the bar plot in Figure 4.34. The data presented for the Leaky Mutant growing with glucose and fructose has already been discussed previously (Chapter 4.2.1, Figure 4.26). All in all, no difference in growth rate between cultures using glucose and those supplied with fructose could be observed in *H. elongata*-PCKPPC with growth rates of 0.450 ± 0.004 h^{-1} and 0.433 ± 0.006 h^{-1}, respectively. In contrast, with acetate as substrate, the growth rate droped by almost 50 % to 0.237 ± 0.003 h^{-1}. Comparing all three strains growing on glucose, the modification of the anaplerotic node has a negative impact on the growth rate. The growth rate of the Leaky Mutant droped from 0.450 ± 0.004 h^{-1} to 0.303 ± 0.036 h^{-1} after the first deletion of PEPCK and decreased even further to 0.238 ± 0.010 h^{-1} after the additional deletion of PEPC. However, due to the high variance in *H. elongata*-PCK no statistically significant difference was observed ($p = 0.069$). Regarding the substrate fructose, no significant changes for both modified strains could be determined from the growth rates ($p > 0.05$), although again the variation especially in *H. elongata*-PCK was notably high. With the gluconeogenetic substrate acetate, all strains showed very similar growth rates with 0.237 ± 0.003 h^{-1}, 0.227 ± 0.004 h^{-1}, and 0.222 ± 0.004 h^{-1} for Leaky Mutant, *H. elongata*-PCK, and *H. elongata*-PCKPPC, respectively. As already observed in the microtiter plate screening before, growth on acetate was not particularly impacted by the loss of PEPCK, suggesting an available alternative pathway, which can take over most of the flux. This is most likely the route via ME and PEP synthase.

During gluconeogenesis, no replenishment of OAA through the anaplerotic reactions is needed and, therefore, it is not surprising that the deletion of the anaplerotic enzyme PEPC has no drastic impact on acetate. A noteworthy observation here is the very low variance in either strain with acetate as a substrate. For both other substrates – glucose and fructose – an anaplerotic flux from PEP to OAA is expected and it seems as if an alteration of the node manifests itself in bigger deviations between replicates. Considering the standard deviations, the only statistically significant difference for the modified strains was determined for *H. elongata*-PCK growing on fructose and acetate ($p = 0.009$). Overall, the screening and shake flask experiments provided coinciding results. With acetate as a carbon source no differences in growth rates were observed for either strain. Growing on fructose, the *H. elongata*-PCKPPC mutant showed the biggest reduction in growth rate. However, due to the high standard deviations in the flask experiments no statistically significant differences were observed. Needless to say, the lack of growth on glucose during the screening experiment was disproven.

Additional to the growth data, the extracellular ectoine content in the late exponential phase was determined (Figure 4.34). As a baseline, the Leaky Mutant, which has partially been discussed before, showed similar amounts for all substrates with a slightly higher content of 0.026 ± 0.002 g/gDW growing on fructose ($p = 0.008$). Both modified strains had higher ectoine contents than the Leaky Mutant when grown with glycolytic substrates. But with acetate as a substrate, they are on the same level with ectoine contents of 0.023 ± 0.001 g/gDW for both modified strains ($p = 0.032$). Comparing *H. elongata*-PCK and *H. elongata*-PCKPPC on glycolytic substrates, no differences between the strains were determined ($p > 0.05$). This is undoubtedly due to the high variances experienced, especially for glucose as a substrate.
In general, the deletion of PEPC lead to extensively increased lag phases, and a reduced growth rate with glycolytic substrates. This is not surprising, since PEPC is one of the main enzymes for anaplerosis and the removal disturbs the flux distribution at a central part of the metabolism [37, 86, 184]. Interestingly, the adverse effect of the PEPCK deletion seemed less severe with fructose as a substrate compared to glucose, which is likely due to different flux distributions around the anaplerotic node for either carbon source. For gluconeogenetic growth on acetate, none of these effects were apparent, linking the phenotype directly to the disruption of the anaplerosis. Regarding the extracellular ectoine content, with glycolytic substrates, an increase was observed for both deletion strains, while during gluconeogenesis – when anaplerosis is irrelevant – the same ectoine concentration as for the reference was detected. Using the substrate glucose, with *H. elongata*-PCK the achieved ectoine concentrations

were higher and the additional knockout of PEPC had an adverse effect on ectoine production. However, due to the relatively high variation, an advantage of the PEPCK knockout strain could not be clearly established. With fructose as the sole substrate, no differences in the extracellular ectoine concentration between the deletion strains was found.

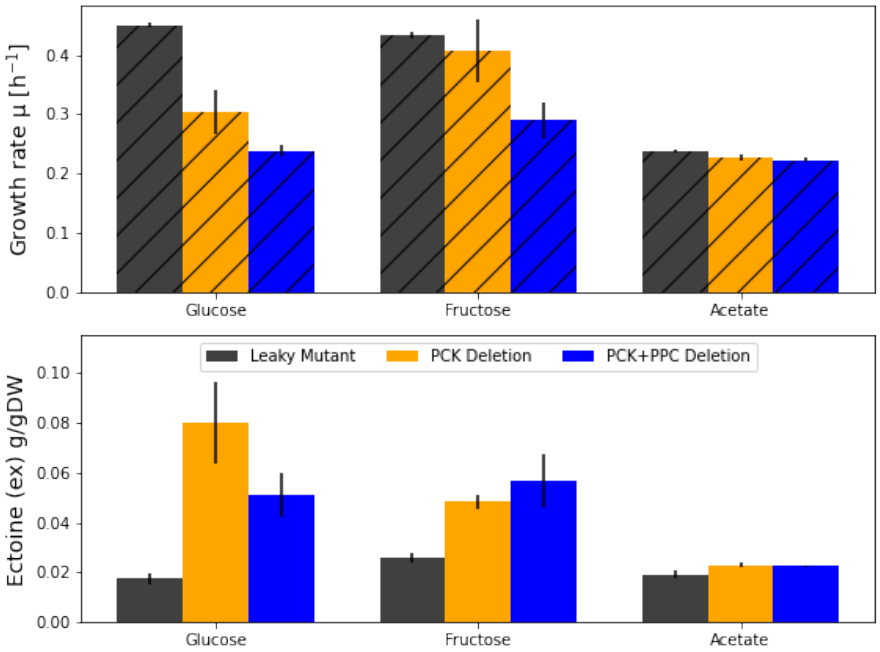

Figure 4.34: Summary for all growth rates and extracellular ectoine data measured for *H. elongata*-PCKPPC (blue) in comparison with its parental strains *H. elongata*-PCK (orange) and the Leaky Mutant (grey) in flask experiments at 1 M NaCl with glucose, fructose, and acetate as the sole substrate. A negative impact of the deletions on the growth rate is apparent for glycolytic substrates. Similarly, regarding the extracellular ectoine, higher yields for the deletion mutants growing on glycolytic substrates was observed.
PCK Deletion: strain *H. elongata*-PCK, *pckA* knockout, PCK+PPC Deletion: strain *H. elongata*-PCKPPC, *pckA* and *ppc* knockout, ectoine (ex): extracellular ectoine.

4.3 Improving the ectoine secretion of the Leaky Mutant

The strategy to increase ectoine production by pushing the metabolic flux towards the synthesis pathway by deletion of PEPCK showed great success with a 45 % increase in the ectoine titer. This improvement in *H. elongata*-PCK is only possible because of the special characteristic of this strain leaking ectoine into the medium. The central metabolism is strictly regulated and especially essential intermediates are often themselves activators or inhibitors depending on their concentration [37, 178, 184]. Upon increasing the flux towards OAA, a sufficient drain is needed to avoid accumulation and subsequent inhibitory effects. In theory, the difference in intracellular and extracellular ectoine concentration should create a gradient strong enough for ectoine secretion to be an effective drain for the carbon flux along the ectoine synthesis pathway. However, the amount that is secreted by the Leaky Mutant might not be enough to relieve the additional flux, leaving some room for improvement.
The secretion of ectoine has been observed after knockout of the whole *tea* operon but also for single transporter genes like *teaC* [77]. The mechanism of the secretion itself is not fully elucidated but it is

known that in the wild type ectoine is continuously excreted into the periplasm, where it is taken up again by the TeaABC transporter. Based on this, it was proposed that without the substrate binding protein (SBP) ectoine cannot be taken up again and the ectoine in the periplasm eventually dissipates into the extracellular space. The remaining genes of the operon, *teaB* and *teaC*, encode the small and big transmembrane unit of the TRAP transporter. Since TeaABC is an ectoine-specific transporter, the possibility of ectoine passing through the channel created by the transmembrane proteins without the SBP was evaluated. Like this, the defective transporter complex could potentially facilitate the export of ectoine into the periplasm [88].

4.3.1 Influence of 3-methylbenzoic acid on ectoine secretion in the Leaky Mutant

The XylS/Pm promoter is induced by benzoic acid derivatives [69] and was shown to be activated very efficiently in *H. elongata* with 3 -methylbenozic acid (3-MB) in Chapter 4.1.6. In food technology, benzoic acids are used as a food preservative. Their antimicrobial effect is mainly attributed to energy depletion of the living cell but for short-chain fatty acids, like benzoic acids, interaction with the cell membrane by introducing changes in the membrane fluidity or interfering with the membrane proteins was also proposed [197, 199]. Additionally, as an aromatic carboxylic acid, 3-MB is barely soluble in water but well soluble in alcohol and ether. The used 3-MB was dissolved in ethanol (EtOH), which has also been reported to alter lipid bilayers making them more fluid and permeable [167]. Like this, both substances introduced for the induction of the promoter could have interactions with the cell membrane permeability, which may have consequences for the ectoine secretion independent of the involvement of the TeaBC permeases. To exclude any effects of the inducer and its solvent and connect any improvements in ectoine secretion directly to the expression of the transmembrane proteins, a control experiment using the Leaky Mutant without any plasmids was conducted. The extracellular ectoine content in the late exponential phase of Leaky Mutant cultures treated with 0.1 mM 3-MB (in EtOH), the same volume but only solvent EtOH, or without any additives at all. In Figure 4.35, the obtained ectoine content in the samples is depicted. No significant differences between the treatments were observed ($p = 0.632$) with an overall average of 0.010 g/gDW of ectoine. The added substances during induction of XylS/Pm did not show any impact on ectoine secretion and, therefore, any changes during the expression of TeaBC can be attributed to the presence of the transmembrane proteins.

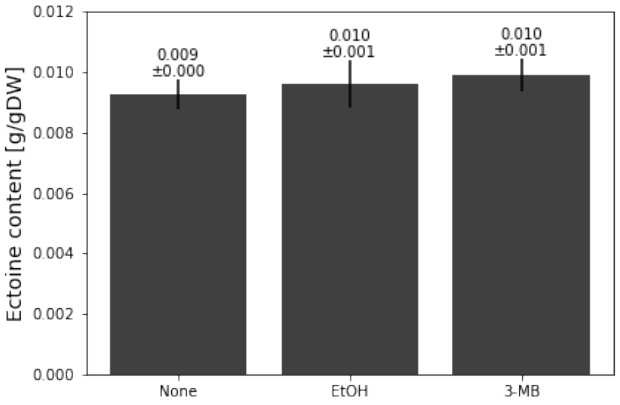

Figure 4.35: Extracellular ectoine concentrations at OD600 1.5 observed for the Leaky Mutant in a 1 M NaCl glucose MM63 minimal medium supplied with and without additives EtOH and 3-MB. No statistic difference regarding ectoine excretion between the additives is visible.

4.3.2 Overexpression of both transmembrane protein encoding genes *teaBC*

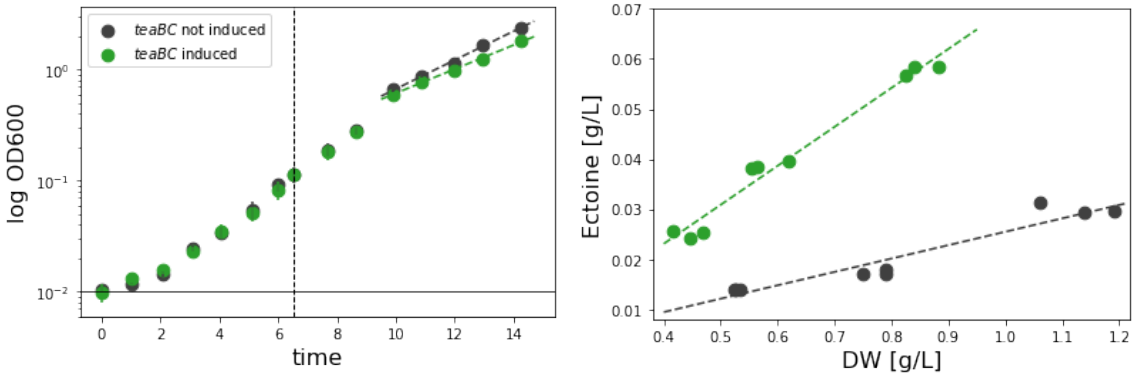

(a) Growth curves for TeaBC

(b) Extracellular ectoine concentration for TeaBC

Figure 4.36: (a) Growth curves for uninduced (grey) and induced (green, 0.1 mM 3-MB) cultures of the Leaky Mutant harboring the expression plasmid for the *teaBC* genes. Approximately 3 h after induction (indicated with a vertical dashed line), a slightly reduced growth rate for the induced cultures is visible ($\mu_{uninduced} = 0.299 \pm 0.011$ h^{-1} vs. $\mu_{induced} = 0.249 \pm 0.006$ h^{-1}). (b) Extracellular ectoine concentration for uninduced (black) and induced (green, 0.1 mM 3-MB) Leaky Mutant cultures harboring the *teaBC* expression plasmid plotted against the DW. Samples were taken at the last three time points (12 - 14 h process time) shown in the growth curves. Image 4.36b is published in Hobmeier *et al.* [88] in Frontiers in Microbiology.

Initially, the potential of TeaBC as a defective channel possibly facilitating ectoine efflux was tested with both permeases together. In Figure 4.36a, the growth curves of Leaky Mutant replicates carrying the expression plasmid pSEVA438-*teaBC* are depicted. First, all cultures were grown uninduced since it was not clear how the overexpression of the transmembrane proteins impacts the cell vitality. Faulty channels might create gaps effectively perforating the membrane, especially since they are not expressed at their normal physiological level but in a much higher amount. The overexpression was induced after reaching an OD600 of approximately 0.1. All cultures showed the same growth behavior with an average growth rate of 0.468 ± 0.010 h^{-1} up until about 3.5 h after induction. After reaching the late exponential phase, the growth rates of the uninduced and induced cultures diverged from each other ($p < 0.01$). Without induction, they continued at an average growth rate of 0.299 ± 0.011 h^{-1}, while the rate of induced cultures was slightly slower with 0.249 ± 0.006 h^{-1}. A reduced growth rate in comparison to the uninduced cultures could hint towards resources used for synthesis of the membrane proteins TeaBC at the expense of growth speed in the induced replicates. The extracellular ectoine concentration was determined at three time points near the end of the cultivation, after 12 - 14 h process time. In Figure 4.36b, the measured concentrations are plotted against the respective DW of the culture. At all three time points, for the induced cultures expressing the TeaBC transmembrane channel, a significantly higher ectoine content was detected than for the uninduced controls ($p < 0.01$). This is also reflected in the different slopes representing the secretion rates (see Figure 4.36b). For the induced replicates, the slope of 0.078 was almost three times as high compared to only 0.027 for the negative control. These results show, that the joint overexpression of both transmembrane proteins TeaB and TeaC successfully facilitated the excretion of ectoine into the medium. It allowed the secretion at a rate approximately three times higher than observed in the Leaky Mutant.

4.3.3 Overexpression of the transmembrane protein encoding genes *teaB* and *teaC* individually

Since both transmembrane proteins together were shown to have a positive effect on ectoine excretion, each protein was tested individually as well. In this way, it is possible to determine whether only one is responsible for the observed increase in excretion or if both are needed for the translocation through the membrane. The growth for the Leaky Mutant with either pSEVA438-*teaB* or pSEVA438-*teaC* are depicted similarly to the previous experiment in Figure 4.37a. Again, the overexpression was induced after an initial growth phase up to an OD600 of 0.1 (Figure 4.37a). During this part of the cultivation, the evolution of biomass observed was comparable for all cultures regardless of the expression plasmid ($p > 0.05$). The growth rate averaged for all replicates was 0.545 ± 0.040 h^{-1}. Approximately 3 h after induction, an impact on the growth curves was observed. The induced cultures harboring plasmid pSEVA438-*teaC* started to diverge from the others with a notable decrease in growth rate. It drastically droped to only 0.189 ± 0.047 h^{-1}, while the uninduced controls with the same plasmid continued at a much faster rate of 0.381 ± 0.024 h^{-1}. A similar growth rate was determined for the uninduced controls for pSEVA438-*teaB* with 0.380 ± 0.013 h^{-1}. In contrast to the impact of *teaC* expression, for the induced *teaB* expressing cultures the growth rate was closer to the control cultures but slightly reduced with a rate of 0.328 ± 0.021 h^{-1} ($p = 0.014$).
For the last timepoint, 13 h after inoculation and 6 h after induction, the detected extracellular ectoine concentration is shown in Figure 4.37b (right). The concentration is plotted against the DW of the respective culture at the sampling time. The highest ectoine content was found in the cultures expressing the bigger subunit TeaC. On average, an ectoine content of 0.079 ± 0.013 g/gDW was determined for TeaC, while the expression of TeaB yielded 0.021 ± 0.002 g/gDW – only about a fourth of this. Both uninduced controls for TeaB and TeaC showed a very similar ectoine content regardless of the plasmid with 0.006 ± 0.001 g/gDW and 0.007 ± 0.001 g/gDW, respectively. In comparison to the cultures expressing *teaC*, this is not even 10 %, while compared to the cultures expressing *teaB*, the controls reach about 30 % of the ectoine content. For either permease individually, an increased ectoine content compared to the uninduced samples was detected. This shows that either protein can facilitate the translocation of ectoine. By the end of the exponential phase, the ectoine excreted via the large subunit

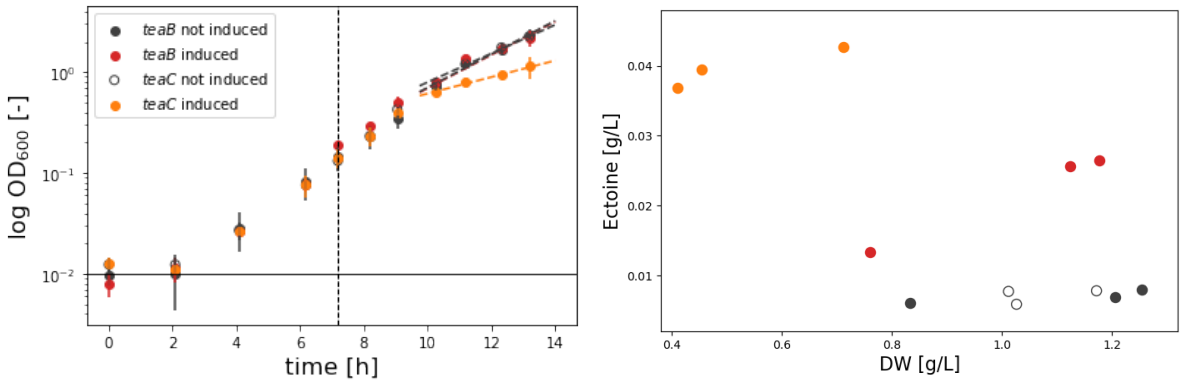

(a) Growth curves for TeaB and TeaC

(b) Extracellular ectoine for TeaB and TeaC

Figure 4.37: (a) Growth curves for uninduced (grey), induced *teaB* (red, 0.1 mM 3-MB), and induced *teaC* (orange, 0.1 mM 3-MB) expressing cultures of Leaky Mutant. A while after induction (indicated with a vertical dashed line), a negative impact on the growth is only apparent for the strains overexpressing *teaC*. (b) Extracellular ectoine concentration for uninduced (grey), induced *teaB* (red, 0.1 mM 3-MB), and induced *teaC* (orange, 0.1 mM 3-MB) expressing Leaky mutant cultures plotted over the DW. Samples in this experiment were only taken at one time point in contrast to Figure 4.36 for which three time points were investigated.

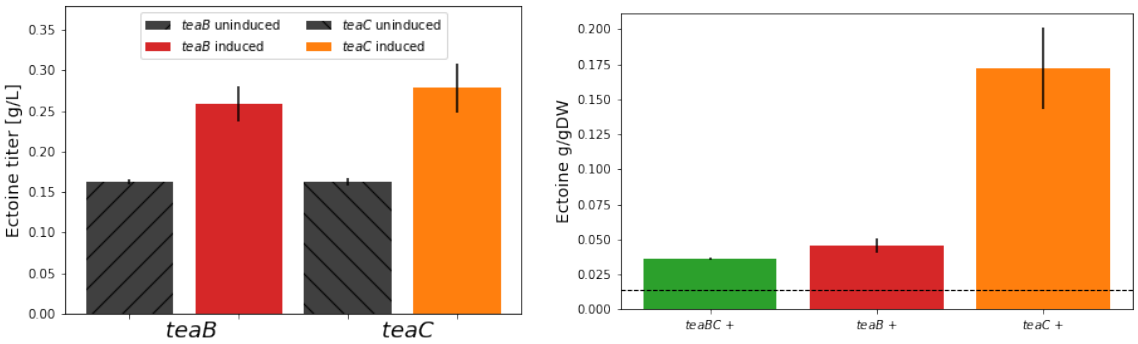

(a) Ectoine titers for TeaB and TeaC

(b) Comparison of TeaBC, TeaB, and TeaC

Figure 4.38: (a) Final ectoine titers for the expression of *teaB* (red) and *teaC* (orange) in the Leaky Mutant with the uninduced plasmids as a reference (grey). Both transmembrane proteins improve the excretion. (b) Extracellular ectoine concentration in the late exponential phase normed by the DW and the respective references to allow a comparison in between the batch experiments. Overexpression of *teaBC* in green, *teaB* in red, and *teaC* in orange. Image 4.38b is published in Hobmeier *et al.* [88] in Frontiers in Microbiology.

TeaC was 10 fold higher. In comparison, the small subunit TeaB also showed a higher content than the control, although only 3.5 times higher.
In this experiment, additionally, the final ectoine titers after 30 h of process time were analyzed. Because measurements of the OD600 after the stationary phase decrease again, it is not possible to reliably approximate the biomass via the OD600 at this stage. At this point in the process, the carbon substrate was fully depleted and since the Leaky Mutant strain is unable to break down ectoine due to the deleted ectoine hydrolase gene *doeA*, all of the synthesized and excreted ectoine during the process was detected. Therefore, the total concentration in the culture medium was determined as the ectoine titer. In Figure 4.38a, the final ectoine concentrations are plotted next to each other. The uninduced controls regardless of the plasmid showed the same concentration of 0.163 ± 0.003 g/L for the *teaB* and 0.163 ± 0.005 g/L for the *teaC* plasmid. Surprisingly, even though the ectoine content in the *teaB*-expressing replicates after the exponential phase was lower than that for the *teaC* counterparts, the titers were at the same level with 0.259 ± 0.022 g/L for TeaB and 0.278 ± 0.03 g/L for TeaC. This might be due to the dramatic decrease in growth rate observed for the cultures expressing *teaC*. In contrast to TeaB, which grew almost as fast as the uninduced replicates the growth of the induced cultures harboring pSEVA438-*teaC*, declined after reaching only an OD600 of 1. It is possible that the reduction in growth rate not only reflects an increased protein synthesis, but it could also mean that the overexpression of *teaC* is detrimental for the cells. Since only one of the two needed proteins of the ectoine-specific transmembrane complex was present, the substrate specificity might be reduced. If the TeaC channel lost its specificity, various solutes may have been able to pass through into the periplasm. In the worst case, it might have impacted membrane integrity negatively to an extent of perforating the membrane and leaking the cytoplasm into the extracellular space, which basically equates to cell lysis. This could explain the major differences in ectoine content after 14 h and the ectoine titer after 30 h of process time. In this case, in the *teaC* cultures biomass would accumulate mainly up to the induction point. After expression of *teaC* cell lysis would take place spilling the cytoplasm into the surrounding medium. Like this, the extracellular ectoine content would increase very fast in a short amount of time after induction but the amount of biomass in these conditions is limited. In contrast, the *teaB* cultures, seemingly unaffected by the overexpression of the transmembrane protein, seemed to secrete ectoine slower but continuously. By reaching a higher biomass, which in turn also allowed for more ectoine to be secreted, the slower excretion rate could be compensated. In the end, for both transmembrane proteins, an increased ectoine titer of 57 – 70 % compared to the uninduced cultures was achieved.

When evaluating all experiments for the overexpression of *teaBC* together and each protein individually, it needs to be mentioned that there is some discrepancy in these batch experiments. While the ectoine content for one experiment is very reproducible within the replicates, in between different batches some variation is apparent. A comparison of the uninduced negative controls shows, that the ectoine production in the experiment for *teaBC* overexpression is noticeable higher than in the experiment, in which *teaB* and *teaC* are expressed separately. This is most likely also connected to the differences in growth rates. For the expression of the single genes, higher growth rates could be observed, in contrast to less ectoine content. To still allow an assessment of which strategy for ectoine secretion is the best, albeit these batch effects, the detected ectoine contents for the overexpression of *teaB*, *teaC*, and both proteins together were normed using the average ectoine content of all uninduced negative controls (Figure 4.38b).
After normalization, the expression of both transmembrane proteins together reached the same level as in the overexpression of only the small subunit TeaB ($p = 0.128$). The big subunit TeaC alone, on the other hand, facilitates almost 3 to 5 times the secretion achieved with either TeaB or TeaBC. Looking only at the amount of ectoine, the expression of *teaC* seems to be the best option. But the actual impact of the *teaC* overexpression on the membrane integrity and the vitality of these cultures still needs to be investigated. As mentioned above, the findings for the final ectoine titers suggest, that the overexpression of *teaC* might lead to cell lysis. If this is truly the case, expression of *teaB* or the combination *teaBC* are the preferable options during the cultivation since they seemingly do not interfere with cell vitality as adversely. However, from a biotechnological standpoint, the availability of a potential inducible cell lysis using the TeaC membrane protein is also a valuable application.

4.4 Metabolic Engineering of nitrogen assimilation

The synthesis of one molecule of ectoine requires the assimilation of two molecules of ammonia. Making this assimilation more efficient increases the theoretical yield of ectoine and can open the door for future improvements. There are two main pathways for the assimilation of nitrogen from ammonium in bacteria. It is taken up either via the high-affinity GS/GOGAT pathway, or via the low-affinity GDH pathway (Figure 2.8). These pathways show different affinities for NH_4^+ and have different energy requirements as well. The high-affinity pathway is able to scavenge nitrogen in environments of low availability but, in turn, uses one ATP for every ammonium that is incorporated. Also, the GS/GOGAT pathway creates a cycle made up of two reactions converting glutamate to glutamine and back which correspondingly needs two enzymes to operate. In contrast, the GDH pathway only needs one enzyme and no ATP but with the downside of a lower affinity [178, 215]. Based on calculations done by [162] using the GS/GOGAT pathway, the conversion of glucose to ectoine costs 2 ATP. In contrast, the GDH pathway is an ATP neutral alternative. In the *H. elongata* genome, genes for both pathways are annotated. Notably, the *gdh* (HELO_3049) was determined as a NADH-specific enzyme, which is usually linked to catabolic processes but in some species, an assimilating function has been reported [49, 84]. The activity of the *H. elongata* NADH-GDH *in vivo* could, therefore, be either assimilating or dissimilating. Maskow & Babel [137] deduced, that the conversion of glucose to ectoine is an ATP-neutral process using calorimetric experiments, which would be possible with an assimilating GDH.

Flux balance analysis (FBA) modeling in the *H. elongata* generally designates the GDH pathway to be the preferred route. Since both pathways are present in the *H. elongata* genome and the flux optimization is only dependent on the stoichiometric features, the additional ATP consumption in the GS/GOGAT pathway results in it being ignored in FBA simulations [190]. However, it has been shown before, that the switch from GS/GOGAT-mediated nitrogen uptake to the GDH pathway can lead to higher growth rates in media containing high concentrations of ammonia. At high concentrations the affinities are not as relevant. This was reported for a GOGAT-deficient mutant of *Methylophilus methylotrophus*. The overexpression of the *E. coli* GDH in this strain led to an increase in growth by 4 – 7 % [236].
To investigate the mode of function of the *H. elongata* NADH-dependent GDH and, thus, also the

potential to optimize the nitrogen uptake with regard to ectoine synthesis, a knockout mutant disrupting the GS/GOGAT cycle was generated.

4.4.1 Determining the main assimilation pathway: deletion of glutamate synthase

The *gltDB* operon (*gltD* HELO_3752, *gltB* HELO_3753) of the *H. elongata* wild type was completely replaced by a Sm^R resistance cassette using homologous recombination. The marker replacement mutant *H. elongata* Δ*gltDB*::Sm^R is referred to as "KHN1". With its disrupted GS/GOGAT pathway, KHN1 was unable to grow in minimal medium with ammonium as the sole nitrogen source (Figure 4.39), in which the wild type is growing well. The supplementation of the minimal medium with glutamate (E) restores growth for KHN1. The deletion strain is glutamate auxotrophic, which leads to the conclusion, that in *H. elongata* ammonium is solely taken up via the GS/GOGAT pathway and the NADH-dependent GDH found in the genome is not acting in an assimilating way.

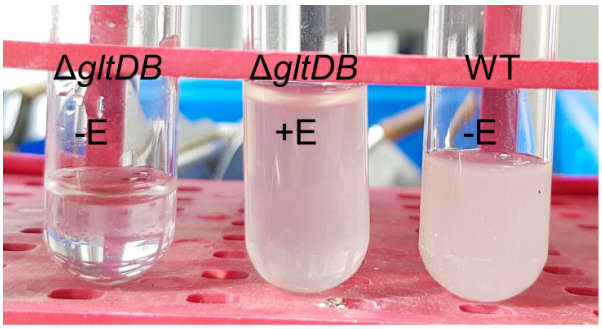

Figure 4.39: After the deletion of GOGAT, KHN1 is auxotrophic for glutamate in minimal medium (left), but with addition of glutamate growth is possible (middle). The wild type (right) shows no deficits in the same minimal medium, in which KHN1 is unable to grow.

4.4.2 Complementation of the glutamate synthase deletion

Complementation of KHN1 with the native *gltDB* operon

To link the observed glutamate auxotrophy of KHN1 directly to the loss of the glutamate synthase, encoded by *gltDB*, the previously deleted genome region was reintroduced into the modified strain. This was done using the inducible (XylS/Pm) complementation plasmid pSEVA388-*gltDB*. Subsequently, the complemented auxotrophic strain KHN1 was tested in minimal medium with ammonium as the sole nitrogen source. As shown in Figure 4.40a, the complemented strain, regained the ability to utilize ammonium as a nitrogen source. Even though the achieved growth rate of 0.291 ± 0.016 h^{-1} is about 40 % less than the wild type growth rate of 0.496 ± 0.027 h^{-1}, it shows that in *H. elongata* ammonium assimilation is solely dependent on the GS/GOGAT pathway. The auxotrophic strain without the reintroduced *gltDB* genes (KHN1) showed no signs of growth on ammonium, even after up to more than 30 h after inoculation. The reduced growth rate of the complemented strain can most likely be traced back to the disruption of the natural regulation of *gltDB* expression. Since the transcription levels and, thus, consequently, the levels of synthesized protein are altered, with no way of internal regulation adverse effects are to be expected. Furthermore, it was shown that the amount of protein, stemming from only the basal expression of the XylS/Pm promoter, is sufficient to facilitate growth with a growth rate of 0.103 ± 0.008 h^{-1}. The expression system XylS/Pm is considered to be tightly regulated due to the positive regulation of gene expression [28, 69] and has also been observed in *H. elongata* to show only minimal amounts of protein expression without inducer supplementation, using eGPF as a

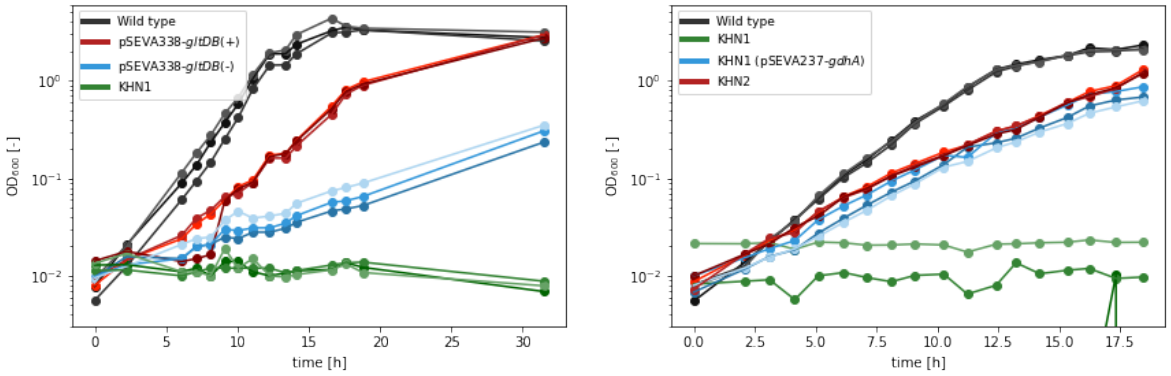

(a) Complementation with the native GOGAT

(b) Complementation with NADPH-GDH

Figure 4.40: Complementation of KHN1 in MM633 minimal medium with (a) the deleted *gltDB* operon or (b) the NADPH-GDH from *P. putida*. Wild type (black) and auxotrophic strain KHN1 (green) are compared to (a) the plasmid-based complementation with the native GOGAT, induced (red) and uninduced (blue) or (b) the plasmid-based complementation with NADPH-GDH (blue) and the genome-integrated version KHN2 (red). Both, the native GOGAT and NADPH-GDH from *P. putida* (plasmid-based and genome-integrated), reinstate the ability to grow.

signal protein (Chapter 4.1.6). A second experiment with five biological replicates illustrated the same findings. The complemented strain was able to achieve OD600 values of up to 1 in a time-frame of 70 h, while the control strain without pSEVA338-*gltDB* remained stagnant around OD600 0.01 throughout the experiment.

Complementation of KHN1 using an assimilating glutamate dehydrogenase

As a more energy-conserving alternative ammonium assimilation pathway to the disrupted native GS/GOGAT pathway, the functionality of uptake via a heterologous GDH was tested. It has been shown that even though *H. elongata* synthesizes compatible solutes, there are still some characteristics to its proteins showing a more acidic amino acid distribution [87] compared to many non-halophiles like *E. coli* [68]. Also, the overall GC content of 63.3 % of *H. elongata* [188] is much higher. Therefore, the NADPH-GDH steming from *P. putida* KT2440 with a similar average GC content of 61.6 % [228] was used (PP_0675) in order to lessen a possible negative impact on transcription and translation *in vivo*.
The introduction of the NADPH-GDH via plasmid pSEVA237-*gdhA* successfully restored the ability to utilize ammonium as the sole nitrogen source, as shown in Figure A.3 (appendix) on solid minimal medium. Next to the plasmid-based complementation, another approach, involving the introduction of *gdhA* into the *H. elongata* genome, was taken. Since plasmids can be lost without the respective selection pressure, the integration into the bacterial genome allows a more stable genotype and, also, the use of a complex medium without any supplementation of antibiotics. While using a plasmid, growth in complex medium would always bear the risk of plasmid loss. Together with the integration of the assimilatory NADPH-dependent GDH into the genome, at the same time the presumably dissimilatory NADH-dependent GDH native in *H. elongata* was removed to avoid potential adverse effects. Both enzymes potentially catalyze the same reaction in opposing directions. For this, the integration plasmid pSEVA511SC-*gdh*::*gdhA* for the substitution of *gdh* with *gdhA* was used. Also, in the genome integrated version, a second promoter σ^{38} for expression in the stationary phase next to the constitutive lacIp [223] which was used in pSEVA237-*gdhA* was introduced. The *gdhA* gene was oriented opposite to the native *gdh*. This new strain was called KHN2.
The growth rates of the GDH-complemented KHN1 on ammonium as the sole nitrogen substrate was assessed (Figure 4.40b). The wild type assimilates ammonium via the GS/GOGAT pathway and achieved a

growth rate of $0.477 \pm 0.005\ h^{-1}$. The strain KHN1 complemented with the plasmid pSEVA237-*gdhA* or via genome integration of NADPH-GDH (KHN2) grew considerably slower than the wild type. With an average growth rate of $0.276 \pm 0.005\ h^{-1}$ for the plasmid-based complementation and $0.266 \pm 0.005\ h^{-1}$ for the genome-integrated *gdhA* strain KHN2, they only reached approximately 60 % of the wild type growth rate. As a negative control KHN1 without the *gdhA* complementation was also inoculated but showed no growth up until the end of the experiment. Interestingly, both versions of complementation yielded very similar results. Even though a higher amount of GDH protein is expected to be available for the plasmid-based version because more than just one copy of the plasmid is present in the cell, the strains with the genome integrated *gdhA* (KHN2) grew just as fast. The promoters in both versions also differed slightly. The KHN2 strain had an additional σ^{38} to facilitate gene expression in the stationary phase. Furthermore, the native *gdh* encoding a dissimilatory GDH was removed to prevent any adversary effects of both glutamate dehydrogenases, working at the same time. Both adjustments could help to compensate the lesser amount of GDH protein compared to the plasmid-based complementation strain. However, it is rather unlikely that both approaches reach such similar growth rates by chance.

Auxotrophic complementation using NADPH-GDH as a selection marker

In large-scale high-density cultures, the uneven distribution of plasmid-based vectors during duplication is a major industrial problem. This problem of plasmid loss is even further reinforced by the increasing proportion of plasmid-free cells over time, not only due to the loss during duplication events, but also the faster growth of plasmid-free cells compared to plasmid-bearing ones. To avoid this, a positive selection needs to be set in place to prevent the growth of plasmid-free cells, making growth completely dependent on the maintenance of the plasmid. Traditionally, antibiotic resistance genes on the recombinant plasmid and the supplementation of the respective antibiotic in the culture medium have been used to ensure plasmid preservation of the host during cell division [59, 220].
However, in biotechnological production processes, the supplementation with an adequate amount of antibiotics is not only an additional cost factor but is also not an entirely impeccable practice. Most often during long term cultivation, the concentration of the antibiotic decreases because of dilution effects or degradation of the antibiotic by secreted enzymes, creating an environment, in which the growth of plasmid-free cells cannot be prevented. Additionally, the application of antibiotics is regarded as problematic in many areas of biotechnology, such as the production of therapeutics, where it may pose a risk to the patient's own microbiota and must be strictly removed. Furthermore, the excessive usage of antibiotics bears the risk of generating resistant strains through lateral gene transfer. This potential spreading of resistance genes is considered to be particularly dangerous to the environment [23, 211, 220].
As an alternative to the traditional antibiotics approach, the use of an auxotrophic selection marker has been reported in a variety of organisms, e.g. glycine synthesis in *E. coli*, lysine synthesis in *Mycobacterium bovis*, or histidine and tryptophan synthesis in *Physcomitrella patens*. Here, the inability to produce essential amino acids *de novo* is exploited. Auxotrophic strains unable to grow without the supplement of the respective compounds are complemented with the needed genes for the *de novo* synthesis on the recombinant plasmid. Like this, the plasmid is indispensable for growth in conditions at which the essential compounds are not supplemented. The need for maintenance of the plasmid is still given but no additional and potentially harmful additive needs to be supplied during cultivation [23, 59, 211, 220].

Similar to the mentioned complementations of amino acid auxotrophies, the strain KHN1 was complemented with a NADPH-GDH on the plasmid pSEVA237-*gdhA*. Connecting the survival of KHN1 to this plasmid allows its cultivation and recombinant production in antibiotic-free cultures. Since the *gdhA* gene can be used as selection pressure in minimal medium the kanamycin resistance cassette *neo* is not necessary in this strain and can be removed. The growth behavior of KHN1 complemented with pSEVA237-*gdhA* or pSEVA037-*gdhA*, for which the *neo* gene was removed, was screened on solid minimal medium (Figure A.5, appendix). Either plasmid allowed growth on minimal medium, however,

only pSEVA237-*gdhA* conferred growth in the presence of kanamycin.
To test the stability of plasmid inheritance and compare the use of an antibiotic resistance as a selective marker compared to the auxotrophic complementation, another plasmid pSEVA238-eGFP-*gdhA* derived from pSEVA237-*gdhA* was constructed. This plasmid harbors an inducible eGFP gene as a reporter for its presence and the quantity of plasmid-bearing cells. Initially, this was tested by growing KHN1 (pSEVA238-eGFP-*gdhA*) in a non-selective complex medium without any antibiotics until the stationary phase and, subsequently, plating an aliquot on non-selective plates. eGFP synthesis was induced in the liquid culture. The plasmid loss after growing in a non-selective liquid culture, followed by plating on non-selective solid medium, could visually be observed by fluorescent imaging of the non-selective plates (Figure A.4, appendix). eGFP-producing colonies showed higher intensities of the emission signal indicated by a darker color in the image. Furthermore, 50 single colonies of each of the three replicates were tested regarding their ability to grow on plates of minimal medium with ammonium as the sole nitrogen source. On average 11.3 ± 2.4 colonies (23 ± 5 %) lost the ability to assimilate ammonium, indicating the loss of *gdhA* and the plasmid.
The differences in stability of the plasmid perseverance for both antibiotic and auxotrophic selection markers were further determined in liquid cultures. First, an experiment applying both strategies together by using a minimal medium with ammonium (*gdhA* is needed) and kanamycin (*neo* is needed) was carried out to establish a baseline for a culture with the maximum amount of selection pressure possible and, thus, ideally no plasmid loss events.

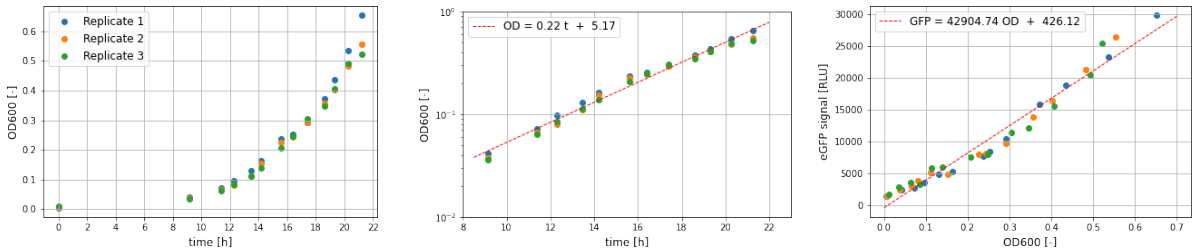

(a) Growth curves, linear (b) Growth curves, half-logarithmic (c) eGFP signal over OD600

Figure 4.41: Growth curves for three biological replicates in the baseline experiment with both selection pressures in linear (a) and half-logarithmic (b) depiction. The overall growth rate calculates to 0.22 h^{-1}, however, two distinct growth phases are apparent with a drop in growth speed after approximately 16 h. This is also reflected in the depiction of eGFP signal over OD600 (c) showing a nick at about OD600 0.3.

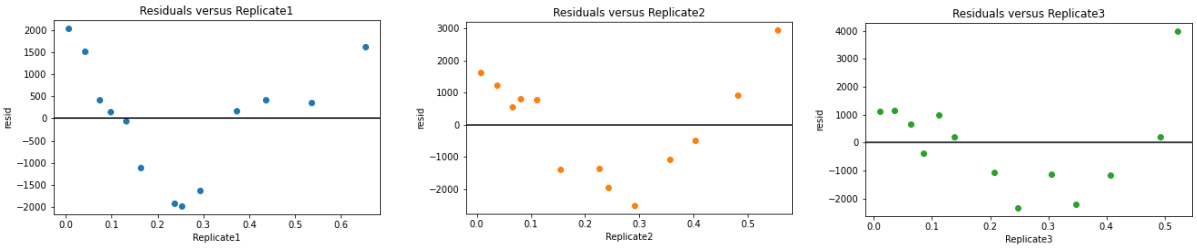

(a) Residual plot, Replicate 1 (b) Residual plot, Replicate 2 (c) Residual plot, Replicate 3

Figure 4.42: Residual plots for all three replicates (a, b, c) for the linear regression of eGFP signal over OD600 values. For all replicates the residuals form a parabola indicating a non-linear behavior.

The growth curves for all replicates in this medium showed a biphasic growth profile (Figure 4.41). This was more clearly recognizable by plotting the residuals of the linear regression for the eGFP singal

	Growth rate μ [h^{-1}]	**eGFP production rate q [RLU/ODh]**
Phase 1	0.272 ± 0.004	7754.73 ± 235.77
Phase 2	0.177 ± 0.018	10071.08 ± 558.79
Overall	0.223 ± 0.002	9551.03 ± 306.65

Table 4.6: Identification of different growth phases for the auxotrophic strain KHN1 complemented with NADPH-GDH and the determined eGFP production rate q.

over the OD600 values. In Figure 4.42 the residual plots depict a parabolic shape indicating that the data is does not behave linearly. After approximately 16 h at OD600 values of 0.25, a change in growth behavior was observed. Initially, the cultures showed a constant linear biomass evolution up until the nick at about 16 h. After this point, growth continued linearly with a reduced slope. The overall growth rate for all replicates over the entire process calculated to 0.223 ± 0.002 h^{-1}. However, before and after the change in growth speed, rates of 0.272 ± 0.004 h^{-1} and 0.177 ± 0.018 h^{-1} were obtained, respectively, showing a decrease of 35 % in between the growth phases. The reason for this is most likely linked to the depletion of ammonium over time. The assimilation using the low-affinity pathway via NADPH-GDH is less efficient at lower substrate concentrations. It seems that after 16 h, a certain threshold in ammonium concentration might be reached, where the reaction started to be limited and, thus, affected the growth rate. When plotting the OD600 values against the eGFP signal, the same effect is visible. Very consistently across all replicates, a nick around OD600 0.25 can be observed. However, here, the eGFP per OD600 signal continues with a considerably higher slope. This can be attributed to the increase of the eGFP per cell signal due to a lowered dilution. Hence, the drop in growth rate resulted in higher rates for eGFP per OD600, which is expressed in the eGFP production rates q with a rate of 7755 RLU/ODh before and an increased rate by 30 % of 10071 RLU/ODh after the shift. The differences in growth rate and eGFP production for both phases are depicted in detail in Table 4.6.

In a subsequent plasmid loss experiment, the biphasic growth was avoided by transferring an aliquot of

Selection marker	**Km supplementation**	**Glu supplementation**
None	-	+
Antibiotic	+	+
Auxotrophic	-	-
Both	+	-

Table 4.7: Overview of the different supplementations (kanamycin or/and glutamate) for the minimal medium to test each selective pressure: no selection, antibiotic selection, auxotrophic selection, and selection using both antibiotic and auxotrophic pressure.

the cultures into new medium after the critical OD600 value was reached, after which the growth started to slow down (details in Figure A.6). The quality of the markers was tested by inoculating the same three biological replicates with either only antibiotic, auxotrophic, or no selection pressure (Table 4.7).

After the initial transfer, all cultures regardless of medium composition showed very similar average growth rates. However, when grown without selection marker and with kanamycin a distinct increase in growth rate after the transfer into new medium was observed. This could be an indication of plasmid loss, since resources formerly used for plasmid replication, as well as the expression of eGFP are freed without it. Interestingly, the behavior with the antibiotic marker matched the cultures without selection marker, even though an antibiotic concentration deemed sufficient for plasmid maintenance in *H. elongata* so far was applied. However, it has been observed before, that after the regular use of kanamycin during continuous genetic modification, *H. elongata* showed growth in the presence of previously determined lethal doses of kanamycin and even at higher concentrations. It seems like *H. elongata* can tolerate kanamycin over time, which might be linked to a plasmid pMH1 that has been detected in various moderate halophiles [58, 217]. Repeated confrontation with antibiotics might cause

Selection marker	Growth rate μ [h^{-1}]	eGFP production rate q [RLU/ODh]
None	$\mu_{None,I}$=0.227 ± 0.007	$q_{None,I}$=3974.93 ± 414.84
None	$\mu_{None,II}$=0.275 ± 0.005	$q_{None,II}$=4525.87 ± 642.48
Antibiotic	$\mu_{Km^R,I}$=0.234 ± 0.021	$q_{Km^R,I}$=3759.84 ± 453.28
Antibiotic	$\mu_{Km^R,II}$=0.260 ± 0.015	$q_{Km^R,II}$=3508.37 ± 355.40
Auxotrophic	$\mu_{GDH,I}$=0.225 ± 0.012	$q_{GDH,I}$=6390.22 ± 637.59
Auxotrophic	$\mu_{GDH,II}$=0.232 ± 0.015	$q_{GDH,II}$=6346.79± 1012.60

Table 4.8: Growth rates μ and eGFP production rates q calculated for the plasmid loss experiment for all selection markers (No selection = None, Antibiotic selection = Km^R, Auxotrophic selection = GDH) and both growth cultures (I and II) (detailed description in appendix Figure A.6). No difference between no selection pressure and selection via kanamycin is observable. In contrast, the selection with GDH shows higher rates continuously in both cultures. Higher eGFP production rates are indicative of a higher number of plasmids containing the eGFP expression module.

resistance genes which are inactive under normal circumstances to be triggered.

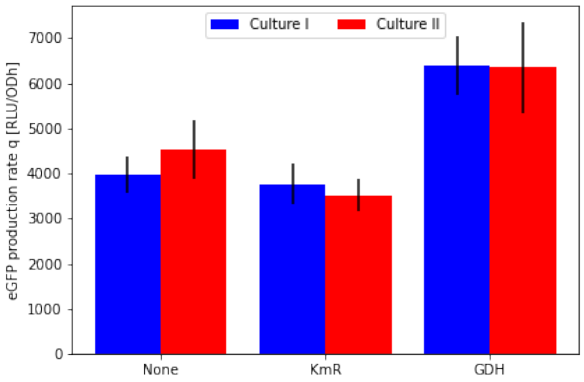

Figure 4.43: eGFP production rates q comparing the media without selection pressure (None), with antibiotic selection (Km^R), and auxotrophic selection (GDH) in the two consecutive cultures (I and II) (detailed description in appendix Figure A.6. No difference between no selection pressure and selection via kanamycin is observable. In contrast, the selection with GDH shows higher rates continuously in both cultures. Higher eGFP production rates are indicative of a higher number of plasmids containing the eGFP expression module.

A comparison of the eGFP production rates showed no statistical change for any selection marker regarding culture I and II (corresponding to the consecutive growth phases; culture I before and culture II after dilution with new medium) within the calculated standard deviations (Figure 4.43, Table 4.8). However, during the first culture at similar growth rates for all media compositions the eGFP production rate for marker GDH was far higher by approximately 60 – 70 %. Cultures without selection marker and the antibiotic marker Km were in the same range. This trend is continued, also, in the second growth phase. Statistically significant differences between the three selection pressures were determined ($p < 0.01$). The comparison of selection via GDH and no selection ($p < 0.01$) or Km resistance marker ($p < 0.01$) showed that using GDH yields a significantly higher eGFP production rate. Interestingly, no difference between the no marker and Km marker group was determined ($p > 0.05$).

4.4.3 Adaptive laboratory evolution of glutamate dehydrogenase mutants

To enhance the growth rates after exchanging the ammonium assimilation pathway from GS/GOGAT to NADPH-GDH, a adaptive laboratory evolution strategy was pursued to achieve a natural adaptation of the modified strains. For this, three of the KHN2 replicates (DE1, DE2, and DE8) were created by transferring the strains 15 - 20 times into new MM63 minimal medium with ammonium as the sole nitrogen source. In Figure 4.44a, their phylogenetic relationship is detailed. DE1 and DE8 are closer related with DE8 originating from a DE1. Basically, DE1 and DE2 are biological replicates of KHN2 which were immediately separated at the beginning of the evolution experiment. DE8 stems from DE1, which was plated in the initial phase of the experiment after only three transfers. One promising colony from this plate was further evolved separately from DE1 and DE2 creating the third strain line DE8.
The growth rates of these three evolved strains were subsequently determined and compared to the wild type growth in shake flask experiments. In the first experiment, two biological replicates of each evolved strain were compared to the wild type. This was followed up with a second growth experiment, with three biological replicates for each strain comparing the growth to the original modified strain KHN2, before the adaptation process by adaptive laboratory evolution. As shown in Figure 4.44b, DE1 with an overall average of 0.419 ± 0.019 h^{-1} in between both experiments, and DE2 with 0.403 ± 0.012 h^{-1} both grew just as fast as the wild type (0.398 ± 0.003 h^{-1}). DE8, growing with a rate of 0.383 ± 0.014 h^{-1} on average, seemed to be slightly slower than the other evolution strains. Both individual experiments showed that the growth rates of all evolved strains are the same as the wild type (p value > 0.05). In the second experiment with the original strain KHN2 as a reference (0.265 ± 0.010 h^{-1}), all strains are

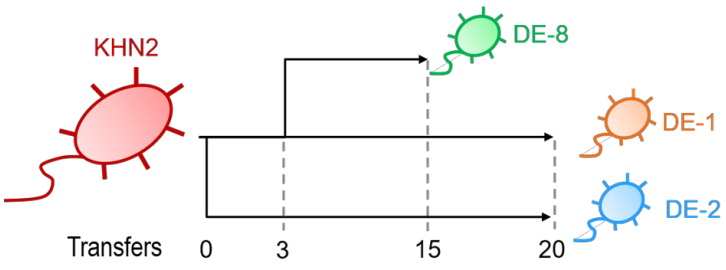

(a) Phylogenetic tree for adaptive laboratory evolution mutants

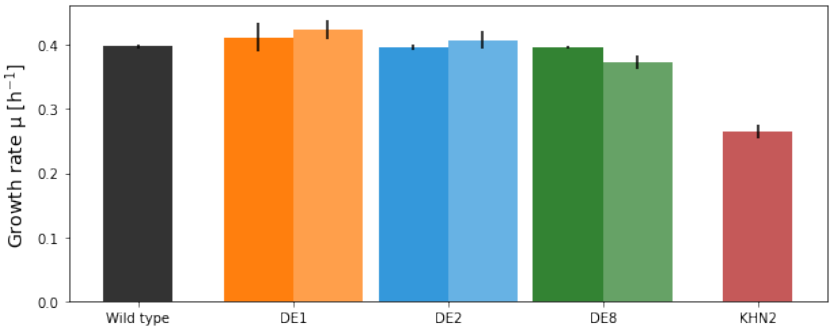

(b) Growth rates of adaptive laboratory evolution mutants

Figure 4.44: (a) Phyolgenetic tree for the evolved strains DE1, DE2 and DE8 leading back to their parental strain KHN2. (b) Growth rates of the three evolved strains. Two growth experiments were conducted: one comparing the new strains with the wild type and another one comparing them with the original strain KHN2. All evolved strains have significantly higher growth rates compared to KHN2. They are at the same level as the *H. elongata* wild type.
KHN2: *H. elongata gltDB*::Sm^R *gdh*::*gdhA*, DE1: laboratory evolution strain 1, DE8: laboratory evolution strain 2, DE1: laboratory evolution strain 3

clearly different from the common parent strain (p values < 0.01). In between the adaptive laboratory evolution mutant strains, for both experiments, no significant differences could be found (p value > 0.01). With further transfers it might be possible for the evolved mutants to eventually surpass the wild type growth rate. Within the measured standard deviations so far, however, the growth rates are considered the be at least the same.
The modified strain KHN2 (*H. elongata* Δ*gltDB*::Sm^R Δ*gdh*::*gdhA*), which is using the GDH pathway mediated by *gdhA* from *P. putida*, does not require ATP for the assimilation of ammonium. This modification led to a decreased growth rate by 40 % but the reduced growth rate was improved again by adaptive laboratory evolution, eventually, back to wild type levels in the strains DE1, DE2, and DE8. In order to determine if the reduction in growth was due to an excessive accumulation of ectoine synthesis intermediates, the strain was reconstructed with the background of the Leaky Mutant. Therefore, the modifications found in KHN1 and KHN2 were introduced in the Leaky Mutant. Initially, a glutamate auxotrophic Leaky Mutant was generated ("KHN3", *H. elongata* Δ*teaABC* Δ*doeA* Δ*gltDB*::Sm^R). Next, the substitution of the native *gdh* with *gdhA* from *P. putida* was done using two different integration plasmids. First, the same plasmid pSEVA511SC-*gdh*::*gdhA* as for KHN2 was used creating "KHN4" (*H. elongata* Δ*teaABC* Δ*doeA* Δ*gltDB*::Sm^R Δ*gdh*::*gdhA*). The same substitution was done with another plasmid based on pSEVA212S generating the strain "KHN5". Therefore, KHN5 should have the same genotype as KHN4. All modified strains created, while investigating and modifying the nitrogen assimilation, are summarized in Table 4.9. They were stored in the form of bacterial glycerol stocks at -80 °C for further analysis.

Strain	Derived from	Genotype
KHN1	Wild type	*gltDB*::Sm^R
KHN2	Wild type	*gltDB*::Sm^R *gdh*::*gdhA*
DE1	Wild type	*gltDB*::Sm^R *gdh*::*gdhA*, adaptive laboratory evolution
DE2	Wild type	*gltDB*::Sm^R *gdh*::*gdhA*, adaptive laboratory evolution
DE8	Wild type	*gltDB*::Sm^R *gdh*::*gdhA*, adaptive laboratory evolution
KHN3	Leaky mutant	Δ*teaABC* Δ*doeA* *gltDB*::Sm^R
KHN4	Leaky mutant	Δ*teaABC* Δ*doeA* *gltDB*::Sm^R *gdh*::*gdhA*
KHN5	Leaky mutant	Δ*teaABC* Δ*doeA* *gltDB*::Sm^R *gdh*::*gdhA*

Table 4.9: Summary of all generated mutant strains with modifications in the nitrogen assimilation.

4.5 Expanding the product range: Nγ-acetyl-L-2,4-diaminobutyric acid

Apart from its excellent performance as an ectoine producer, *H. elongata* has a lot of potential in other biotechnological applications. In an attempt to broaden the spectrum of valuable compounds synthesized by *H. elongata*, the intermediate Nγ-acetyl-L-2,4-diaminobutyric acid (γ-NADA) in the ectoine synthesis pathway was investigated further. γ-NADA is the direct precursor for ectoine. The ectoine synthase EctC condenses the linear γ-NADA molecule to form the cyclic ectoine. But there are two versions of this metabolite present in the *H. elongata* wild type. Depending on the location of the acetyl group, it is taking on either an α or γ form. While the γ version is the direct precursor metabolite for ectoine in the synthesis pathway, the α form is the product of ectoine hydrolysis by the ectoine hydrolase DoeA in the degradation pathway. The potential of γ-NADA as a novel product is not only limited to its activity as an osmolyte or protective agent. Ectoine shows outstanding properties in this regard, however, the differences in structure with γ-NADA being a linear molecule could potentially be more advantageous for some proteins. Furthermore, the linear structure potentially allows the polymerization of γ-NADA, which could open up a new spectrum of applications as a biopolymer.

In the following chapters, two modified strains for the production of γ-NADA are characterized

and evaluated for their potential to synthesize γ-NADA. The first strain, *H. elongata* Δ*ectC* – from here on referred to as Δ*ectC*, is based on the wild type with a single modification introduced by deletion of the ectoine synthase gene *ectC*. This abolishes the conversion of γ-NADA to ectoine similar to *C. salexigens* for which it was already reported, that blocking *ectC* led to an accumulation of γ-NADA [31]. The second strain, *H. elongata* Δ*ectC* σ^{38} RBS – from here on referred to as Δ*ectC* σ^{38} RBS – has additional modifications in the promoter and ribosomal binding site (RBS) of the ectoine operon. The sigma factor σ^{38} was added to ensure an increased transcription in the stationary phase and a synthetic RBS was introduced to optimize the translational activity. Both γ-NADA producer strains were constructed and kindly provided by the Federal Institute for Materials Research and Testing (BAM).

4.5.1 The salt tolerance of the γ-NADA producers

An initial screening with the γ-NADA producer strains in microtiter plate scale was carried out with the carbon substrate glucose. As always, the growth behavior in the salt range between 0.17 M and 2 M NaCl concentration was tested. For the lower salt concentrations, no differences between wild type and modified strains were observed. But starting at 1 M NaCl, decreased growth rates for both mutant strains were evident. With a growth rate of 0.372 ± 0.075 h^{-1}, the growth of *H. elongata* Δ*ectC* was distinctly slower than the wild type (0.721 ± 0.153 h^{-1}). But even though the growth rate in *H. elongata* Δ*ectC* σ^{38} RBS was also slightly reduced to 0.572 ± 0.066 h^{-1}, at 1 M NaCl, due to the high variance in the wild type, no clear difference from the wild type is shown. All in all, the high variance is a common problem of the microplate screenings. The growth rates for the wild type in this experiment, for instance, were also higher than in other screenings. Therefore, the growth data obtained are only compared within the experiment to determine qualitative changes between the strains. At the high salt condition 2 M, no growth for the γ-NADA producers up until 20 h of process time was detected. In Figure 4.45, the growth rates obtained in the screening are summarized. Since the high salt condition did not allow any growth for the γ-NADA producers, it was omitted.

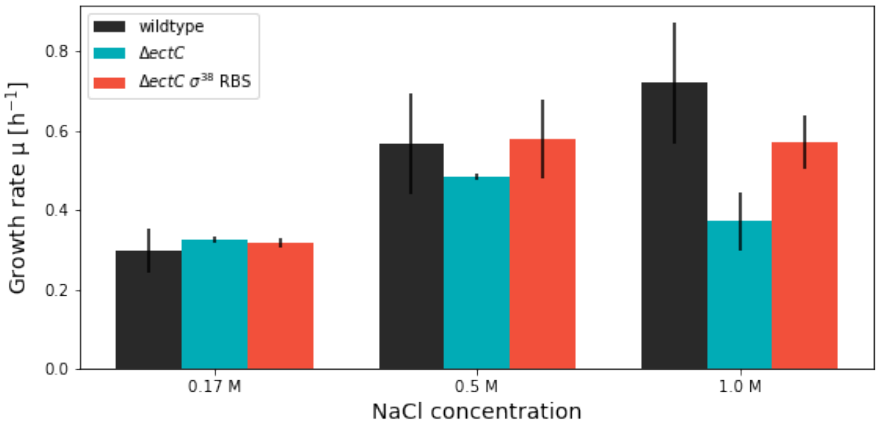

Figure 4.45: Achieved growth rates in the microtiter plate screening with glucose as substrate for the wild type (black), the Δ*ectC* mutant (turquoise), and the Δ*ectC* σ^{38} RBS mutant (light red). Only the wild type was able to grow at 2 M NaCl. Since no growth rates of the modified strains are available this data is not shown. Similar growth rates for all strains at low salinities were observed.

After the deletion of *ectC*, the salt tolerance in *H. elongata* was reduced to a lower tolerance range. Also, the salt optimum originally between approximately 0.5 M and 1 M NaCl, was lowered because a negative effect of the deletion on growth was already visible at 1 M NaCl. At low salt conditions, no impact could be observed. Since no compatible solutes were needed for growth at low salinity, this suggests, that the

adverse effect is solely linked to the loss of ectoine and γ-NADA cannot compensate as a compatible solute to the same level as ectoine. This was also observed by Cánovas *et al.* [31] in modified γ-NADA accumulating *C. salexigens* strain, in which γ-NADA was not able to confer the same NaCl tolerance as ectoine.

4.5.2 Quantifying the γ-NADA production

To verify the observations of the microtiter plate screening, the γ-NADA producer strains were further tested in shake flask experiments. Additionally, their capability as producer strains for γ-NADA was evaluated.

Accumulation of compatible solutes in 0.5 M NaCl

In the growth screening, no apparent differences from the wild type were found at 0.5 M NaCl. However, in the shake flasks the growth rates for both mutant strains *H. elongata* Δ*ectC* and *H. elongata* Δ*ectC* σ^{38} RBS with rates of 0.398 ± 0.002 h^{-1} and 0.376 ± 0.005 h^{-1}, respectively, compared to the wild type (0.432 ± 0.006 h^{-1}) were already slightly diminished. The wild type, therefore, already grows faster at a moderate salt concentration of 0.5 M NaCl. But between the mutant strains, no difference was found. For the detection of intracellularly accumulated compatible solutes, the content was normed using the dry weight, since the samples were taken at slightly different OD600 values. The presence of intra- and extracellular compatible solutes were investigated, but no extracellular ectoine for either γ-NADA producer could be detected. In Figure 4.46, the measurements for intracellular compatible solutes are visualized. For the wild type ectoine and for the mutant strains γ-NADA was measured. There are two measurements per strain at two time points, which are about one hour apart. Approximating a linear relation for the two time points resulted in slopes, which were far higher for the γ-NADA producers compared to the wild type. In the wild type, a content of 0.066 g/g for ectoine was determined. In Figure 4.46b. For the Δ*ectC* strain, a content of 0.186 g/g γ-NADA and for the second mutant strain Δ*ectC* σ^{38} RBS an even higher content of 0.280 g/g of γ-NADA was found. In the wild type, the intracellular ectoine content was at a stable level of 0.058 ± 0.002 g/gDW and 0.062 ± 0.001 g/gDW. This is reasonable because the intracellular ectoine levels in the wild type are strongly regulated and strictly adjusted to extracellular salt concentration. In general, for both γ-NADA producers (Δ*ectC*, Δ*ectC* σ^{38} RBS), the intracellular γ-NADA content was far higher compared to ectoine. Also, in contrast to the wild type, an increase in γ-NADA content for both strains from the first to second sampling time was observed. This increase was especially distinct for the additionally modified mutant Δ*ectC* σ^{38} RBS. While at the first time point in Δ*ectC* the γ-NADA content was higher (0.128 ± 0.007 g/gDW vs Δ*ectC* σ^{38} RBS with 0.106 ± 0.005 g/gDW), in the second time point only one hour later the strain Δ*ectC* σ^{38} RBS had caught up and even surpassed the sole Δ*ectC* mutant in γ-NADA content (0.156 ± 0.003 g/gDW for Δ*ectC* vs 0.168 ± 0.007 g/gDW for Δ*ectC* σ^{38} RBS). This was also apparent in the slopes for the for the linear approximation calculated for the compatible solute content per DW depicted in Figure 4.46a.

The Δ*ectC* σ^{38} RBS mutant possesses a modified promoter sequence in front of the ectoine operon with the sigma factor σ^{38}, activating transcription in the stationary phase. The increased γ-NADA production in the later time point hints towards a successful improvement of the production in the later growth phases due to this modification.
The differences in accumulation of compatible solutes observed in the wild type and the γ-NADA mutants, namely the overall higher content of γ-NADA per dry weight compared to ectoine, and the continuous increase only observed for the γ-NADA producers can most likely be traced back to problems in the regulation of compatible solute levels. It seems like the maintenance of a constant compatible solute level in the γ-NADA producers is not working properly. In the wild type, the compatible solute produced is ectoine which is not present in the modified strains. If the regulation is specifically linked to ectoine itself, as proposed by Grammann *et al.* [77] before, its removal would lead to the observed traits.

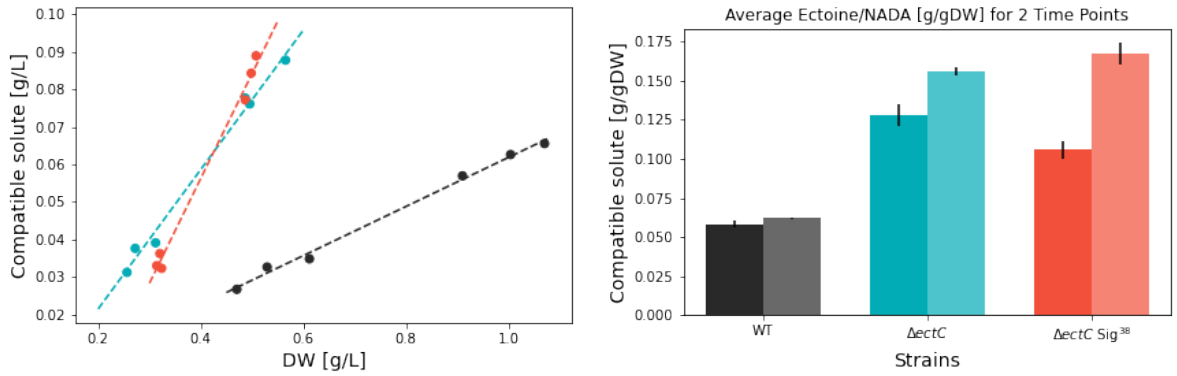

(a) Compatible solute content against dry weight

(b) Intracellular content in g/gDW

Figure 4.46: Amount of intracellular compatible solutes determined at 0.5 M NaCl for the wild type (black), the Δ*ectC* mutant (turquoise), and the Δ*ectC* σ^{38} RBS mutant (light red). (a) Two time points were sampled. The concentration of intracellular compatible solute is plotted against the dry weight. Using all data points a linear regression was performed to approximate the compatible solute content responding to the dry weight (dashed line) (b) Intracellular content of compatible solutes compared in g/gDW. The lighter and darker shades represent two separate consecutive time points of sampling. For the wild type, the ectoine content is constant. Both γ-NADA producers show an increase of γ-NADA over time.

Accumulation of compatible solutes in 1 M NaCl

The same experiment was repeated at a higher salt concentration of 1 M. In the screening experiment, for both mutant strains growth was still possible at this concentration even though with notably reduced growth rates especially for the Δ*ectC* strain. For the wild type, 1 M NaCl is still considered within the salt optimum. With growth rates of 0.432 ± 0.006 h^{-1} at 0.5 M NaCl and 0.430 ± 0.032 h^{-1} at 1 M NaCl achieved in the shake flasks, the wild type clearly showed a plateau in between this salt range with the growth rates at the same level. But in the γ-NADA producers, the growth rates at 1 M NaCl were severely reduced by 30 – 40 % compared to the rates at 0.5 M NaCl. At 1 M NaCl the growth rates were only at 0.241 ± 0.009 h^{-1} and 0.250 ± 0.004 h^{-1} for Δ*ectC* and Δ*ectC* σ^{38} RBS mutant, respectively. In contrast to the screening, the growth rates at 1 M for both γ-NADA producers were found to be the same in the flask experiments. However, it needs to be noted, that due to the considerably lower growth rates by almost half, the cultures of the γ-NADA producers only reached a fraction of the biomass compared to the wild type. Because the sigma factor σ^{38} is supposed to be active particularly in the stationary phase, its influence and advantages cannot be observed this early on. This also needs to be kept in mind for the following measurements of the compatible solutes.
Analogous to the compatible solute measurements at 0.5 M NaCl, the intracellular compatible solute content for all strains is depicted in Figure 4.47. The slopes for the linear approximation achieved for the compatible solute content per DW were much steeper for the γ-NADA producers. In contrast to the content for the wild type with 0.135 g/g, the content for the Δ*ectC* strain (0.372 g/g) and the Δ*ectC* σ^{38} RBS strain (0.317 g/g) were between 2 and 3 fold higher (Figure 4.47a). In Figure 4.47b, the compatible solute content is also shown normed by the amount of dry weight. The bar chart with the compatible solute content in g/gDW shows, that again, in the wild type the same ectoine content (0.121 ± 0.010 g/gDW) was maintained at both time points. Interestingly, comparing the average ectoine content at 0.5 M and 1 M NaCl, the content doubles from 0.5 M to 1 M NaCl similar to the doubling of the external salt concentration. In both γ-NADA producers, like in the experiment at 0.5 M NaCl, an increase in γ-NADA content with time was found. But here, the γ-NADA content in the Δ*ectC* σ^{38} RBS mutant was consistently lower than in the Δ*ectC* mutant. As mentioned before, this could

be due to sampling in the earlier stages of growth for the γ-NADA producers, and the advantages of the additional modifications in the Δ*ectC* σ^{38} RBS strain are expected to be particularly visible in the stationary phase. The results found for the external salt concentrations of 0.5 M and 1 M NaCl clearly

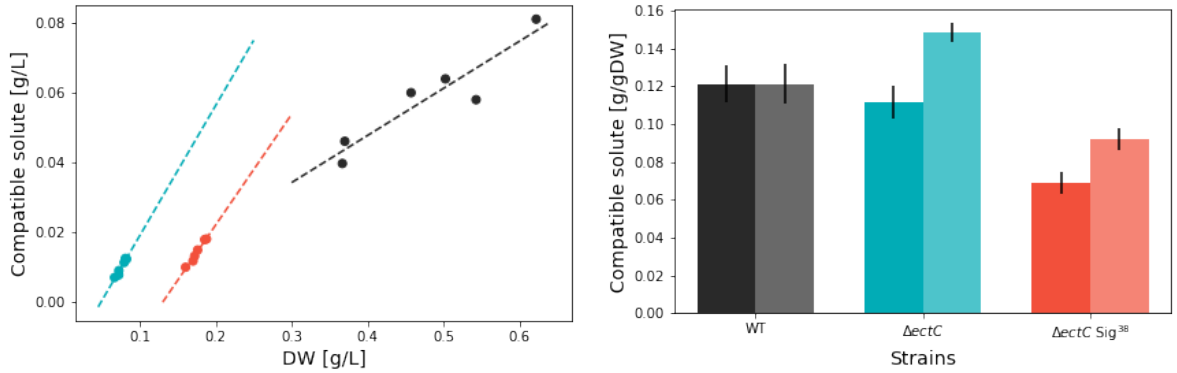

(a) Compatible solute content against dry weight

(b) Intracellular content in g/gDW

Figure 4.47: Amount of intracellular compatible solutes determined at 1 M NaCl for the wild type (black), the Δ*ectC* mutant (turquoise), and the Δ*ectC* σ^{38} RBS mutant (light red). (a) Two time points were sampled. The concentration of intracellular compatible solute is plotted over the dry weight. However, it has to be taken into consideration, that the biomass for the γ-NADA producers is very low and the strains are in different growth stages. Using all data points a linear regression was performed to approximate the compatible solute content responding to the dry weight (dashed line) (b) Intracellular content of compatible solutes compared in g/gDW. For the wild type, the ectoine content is constant. Both γ-NADA producers show an increase of γ-NADA over time.

demonstrated that γ-NADA is accumulated in a higher cytoplasmic concentration compared to ectoine. This can have different implications.
One possibility is simply the difference in the stabilizing effect of both molecules due to their different structures. If the turgor pressure in the cell is involved, a different compatible solute might lead to a different concentration, at which the turgor is stabilized. If the cyclic ectoine has better properties than the linear γ-NADA in this regard, less amount of compatible solute is needed. Another explanation is linked to the assumption that ectoine synthesis is directly regulated by the product ectoine itself. If this is the case, the regulation of the internal compatible solute content in the γ-NADA producers is defective after the removal of EctC. Since γ-NADA is continuously accumulated, in contrast to ectoine in the wild type, this hints towards such a regulation involving ectoine. If *ectC* is deleted and no ectoine but instead γ-NADA is synthesized, not only is the regulation disrupted, but most likely the absence of ectoine leads to a faulty feedback to increase compatible solute synthesis, ramping up the production artificially. Like this, the γ-NADA synthesis would be independent from the external salt concentration and experiments for γ-NADA production could be preferably carried out at 0.5 M NaCl, since the growth rates are considerably higher by 65 and 50 % for Δ*ectC* and Δ*ectC* σ^{38} RBS, respectively. In general, regarding the growth rates, the γ-NADA producers already showed an inhibition at 0.5 M NaCl and even more severely at 1 M NaCl compared to the wild type. Both mutant strains exhibited the same growth behavior for either salt concentration, however, an advantage of the additionally modified strain at 1 M cannot be discarded since the strains were not grown until the stationary phase, at which the effect of the sigma factor σ^{38} is to be expected and the exact cut-off regarding the salt concentration at which either strain ceases growth was not determined. In fact, a positive impact of the modifications in *H. elongata* Δ*ectC* σ^{38} RBS was consistently found in the γ-NADA production rate. Out of the two available producer strains, the additionally modified strain Δ*ectC* σ^{38} RBS has shown its potential in the late exponential phase as more advantageous, not necessarily regarding the growth rate but in γ-NADA production compared to the sole *ectC* knockout.

4.5.3 Batch cultivation of *H. elongata* Δ*ectC* σ38 RBS at 0.5 M NaCl

One of the γ-NADA producer strains, namely the additionally modified *H. elongata* Δ*ectC* σ^{38} RBS, was further characterized in a 2 L batch cultivation. Since the growth rates of the γ-NADA are already notably reduced at moderate external salt concentrations, the cultivation was carried out at 0.5 M NaCl. Like in the batch cultivation of the wild type at 1 M NaCl, an initial carbon source of 5 g/L glucose and a nitrogen source of 2 g/L ammonium sulfate was used. The process was monitored via the OD600 and the exhaust gases. Throughout 10 h, a biomass accumulation of 1.559 g/L with a growth rate of 0.390 h^{-1} was achieved. However, at this time point, the glucose substrate was not fully depleted with 0.968 g/L of glucose left for biomass and γ-NADA production. Using the growth rate and the glucose yield $Y_{\frac{X}{C}}$ (Table 4.10), the time, at which the substrate is completely consumed, was approximated (grey area in Figure 4.48a) to be at about 11 h of process time. The maximum amount of biomass after depletion of the substrate at 11 h is predicted to be 1.917 g/L. For a total working volume of 2 L, this makes up an overall biomass of 3.834 g. The biomass yield in this mutant strain with 0.327 gDW/gGlc was only half of the biomass yield, determined for the wild type growing at 1 M NaCl ($Y_{WT\,\frac{X}{C}}$ = 0.618 gDW/gGlc, Chapter 4.1.3). In the wild type, changes in osmolarity of the environment were shown to have no notable impact on the biomass yield [52, 163], suggesting the major difference is caused directly by the genetic modifications. Since it was indicated by previous experiments, that γ-NADA synthesis might be uncoupled from the regulation of ectoine synthesis and would be continuously accumulated, the reduction in biomass yield could be connected to the production of γ-NADA.

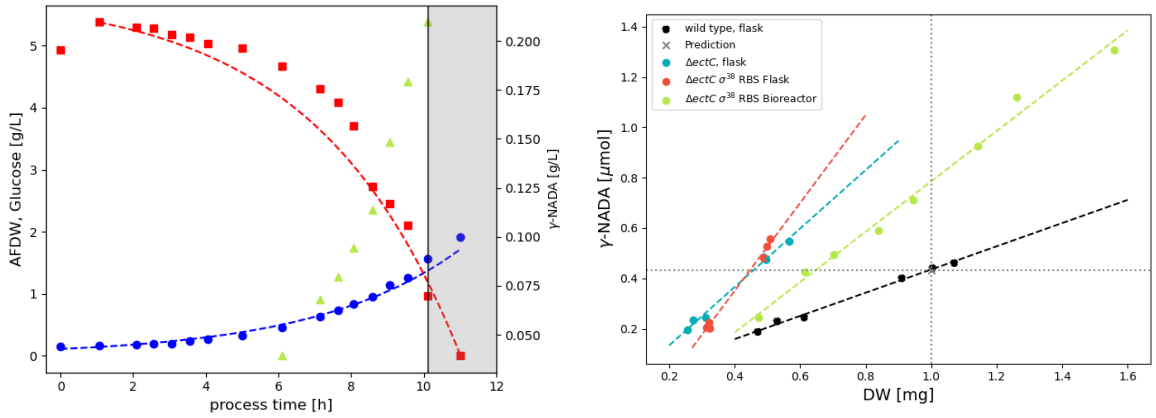

(a) Evolution of biomass, glucose, γ-NADA

(b) γ-NADA per biomass

Figure 4.48: (a) Experimental data and Monod model approximation for biomass formation (circles, blue) and glucose (squares, red) utilization during the batch cultivation of the γ-NADA producer *H. elongata* Δ*ectC* σ38 RBS. The γ-NADA shown in light green (triangles) was measured using HPLC for the latter part of the cultivation starting at about 7 h of process time. The last part (grey area) and the ending points of the cultivation after 10 h of process time was approximated using the Monod model (b) Comparison of the γ-NADA content achieved for the producer strains *H. elongata* Δ*ectC* (light blue) and *H. elongata* Δ*ectC* σ38 RBS (red or light green depending on the cultivation scale) at a moderate salinity of 0.5 M NaCl. Small scale flask data from Chapter 4.5.2. The biomass yield determined for the wild type (black) as a control coincides well with the theoretical approximation based on data from [52] (equation 2.4, grey). The yield determined in 2 L reactor scale with the strain *H. elongata* Δ*ectC* σ38 RBS (light green) detailed in equation 4.11 is slightly lower compared to the yield determined in flask scale for the same strain, thus, a scale impact regarding the γ-NADA yield is possible.

γ-NADA yield for strain *H. elongata* Δ*ectC* σ38 RBS at 2 L reactor scale:

$$\gamma\ NADA_{\,\Delta ectC\,\sigma^{38}\ RBS\ Bioreactor}\ [g/L] = DW\ [g/L]\ \cdot\ 1.000\ -\ 0.215 \tag{4.11}$$

For the later stage of the cultivation, after about 7 h of process time, additionally, the intracellular γ-NADA content was monitored over time. The γ-NADA product yields for the biomass and the glucose substrate were determined by linear regression. Similar to the extrapolation done for the biomass, the amount of γ-NADA at the end of the process was predicted using the product yield $Y_{\frac{NADA}{X}}$. In the end, a γ-NADA content of 0.142 g/gDW is expected. This translates to 0.545 g of γ-NADA for 3.834 g of total biomass.

Table 4.10: Growth yields determined for the γ-NADA producer *H. elongata* Δ*ectC* σ^{38} RBS in a 2 L batch cultivation (30 °C, 1000 rpm stirrer speed, 1.25 L/min) growing in MM63 minimal medium at 0.5 M NaCl with glucose as the sole carbon source.

Parameter	Unit	Experimental Data
Growth rate μ	h^{-1}	0.390
AFDW	g/L	1.917
Glucose Yield $Y_{\frac{X}{C}}$	g/g	0.327
O_2 Yield $Y_{\frac{X}{O2}}$	g/g	1.038
CO_2 Yield $Y_{\frac{X}{CO2}}$	g/g	0.831

All determined parameters for this cultivation of *H. elongata* Δ*ectC* σ38 RBS are summed up in Table 4.10. In order to compare the γ-NADA production in the bioreactor with the previous small scale shake flask experiment, the data for both experiments was plotted in the same figure (Figure 4.48b). The ectoine yields obtained by determining the linear correlation between γ-NADA and the dry weight were similar for the *H. elongata* γ-NADA producer strains compared to the wild type with a yield of 0.461 μmol/mgDW. For strain *H. elongata* Δ*ectC*, a yield of 1.162 μmol/mgDW was calculated. The yields for strain *H. elongata* Δ*ectC* σ38 RBS in flask and reactor scale differ notably. At flask scale a yield of 1.746 μmol/mgDW was determined, while at 2 L reactor scale the yield was only 1.000 μmol/mgDW suggesting a scale effect is likely.

5 Conclusions

5.1 Characterizing the wild type

5.1.1 Phenotypes.

In this work, the *H. elongata* wild type was characterized physiologically and metabolically as a starting point to develop a producer strain for compatible solutes. For glycolytic growth under optimal salt conditions at 1 M NaCl, an average intracellular ectoine content of 0.118 ± 0.003 g/gDW and an average growth rate of 0.453 ± 0.043 h^{-1} were determined. At 1 M NaCl, the OD600 to ash-free dry weight (AFDW) correlation published in Hobmeier *et al.* [86] predicts 0.488 g/L AFDW at OD600 1. The predicted ectoine content at 1 M NaCl was calculated in this work to be 0.121 g/gDW, making up about 12 % of the dry weight. Thus, for the AFDW correlation, at OD600 of 1 a ectoine content of 0.059 g/L is expected. The growth rate in MM63 minimal medium also corresponds well with the experimental data and predictions reported by Dötsch *et al.* [52], even though they consistently fall on the higher end in direct comparison.
The growth yield Y_X was determined as 0.587 gDW/gGlc for growing *H. elongata* in batch at 1 M NaCl. This is higher than the growth yields published by Dötsch *et al.* [52] for this bacterium growing in a similar medium. They established that with an increasing ectoine content the growth yield Y_X changes and increases as well which is due to the highly efficient conversion of glucose to ectoine being nearly energetically neutral. In contrast, biomass formation is more energy-intensive. If the share of ectoine in the biomass is higher, so is the yield. For cells without ectoine, Dötsch *et al.* [52] determined a theoretical growth yield Y_X of 0.466 ± 0.005 gDW/gGlc. With a prediction of the ectoine content of 0.121 g/gDW at 1 M NaCl, the theoretical growth yield Y_X for ectoine-containing cells at 1 M NaCl is estimated at 0.530 gDW/gGlc. Compared to the experimentally determined growth yield Y_X in this work, this makes up a deviation of about 10 %.
Overall, all key parameters are in good agreement with the range of previously reported data. The average ectoine content specifically fits perfectly with data adopted from Dötsch *et al.* [52]. A theoretical estimation of the ectoine content performed by linear approximation using measurements at different salinities predicts an ectoine content of 0.121 g/gDW. This equals approximately 12 % of the total dry weight.
Mathematical models predicting the growth rate for *H. elongata* with respect to the salinity of the environment describe the growth behavior based on substrate inhibition kinetics. In Figure 2.10a, one such model based on the formula defined by Yano & Koga [241] is visualized over the NaCl solubility range in water. With growth rates in minimal medium generally below 0.5 h^{-1}, *H. elongata* cultures are considered slow-growing cells. Growing on a complex LB medium with 1 M NaCl instead of the defined MM63 minimal medium supplied with the same salt concentration, approximately double the growth rate can be achieved (in this experiment: $\mu_{LB} = 0.878 \pm 0.022\ h^{-1}$ vs. $\mu_{MM63} = 0.479 \pm 0.027\ h^{-1}$). The difference here is that microbes in minimal medium need to synthesize all cellular components by themselves, whereas in complex media a variety of essential components are already present. The extra expense afforded to synthesize every component means a higher energy expenditure in minimal medium, which in turn leads to a poorer growth performance [250]. In any case, growing in minimal and complex media the growth rates of *H. elongata* are situated right around this critical point of 0.5 h^{-1} separating fast from slow-growing cells.
The *H. elongata* biomass was approximated using an OD600 to biomass correlation with an OD600 of 1 equating to 0.488 g/L AFDW. The melting temperature of ectoine at 280 °C is lower than that for the remaining biomass and can be clearly distinguished in the mass spectrometry (MS) signals. During combustion by STA, a small peak representing the release of CO_2 was observed at approximately 300 °C. This can be attributed to the combustion of ectoine. But the main portion of biomass is burned at much

higher temperatures around 500 °C, which was indicated in the MS signal with a much bigger release of CO_2. Since these combustion events can be clearly separated, the amount of ectoine contained in the biomass of a sample can potentially be determined using this method and potentially also the overall composition of the biomass sample.

5.1.2 Metabolic network.

In spite of its genome being sequenced and annotated, there are many open questions regarding the metabolism of *H. elongata*. Different analyses in this work have helped to fill some gaps and improve the metabolic reconstruction, as well as the behavior under different conditions of this organism.
The metabolic response to salt-related stress was studied using RNA-Seq. Further insight was obtained by comparison of transcriptomics between *H. elongata* and its close relative *C. salexigens* [182]. All in all, the transcriptomic response of both organisms to high osmolarity was very similar: upregulation of ectoine synthesis, upregulation of transporters for compatible solutes, and, simultaneously, the down-regulation of ectoine degradation. Both organisms also showed a much higher degree of transcription of all the genes related to flagellar function and chemotaxis when growing at high salinity. In a high-salt medium, the growth rate for *H. elongata* is limited due to more resources going into energy-intensive salt adaptation mechanisms [163].
The response to low salinity shows that both organisms face problems for energy acquisition, in spite not having to invest energy in salt adaptation mechanisms. For *C. salexigens* growing at low salt, Pastor *et al.* [165] described a metabolic overflow due to inflexible regulatory mechanisms at the lower end of its salt range. RNA-Seq analysis of *C. salexigens* by Salvador *et al.* [182] revealed, that the reduction in growth at low salt is tightly linked to changes in the Na^+ membrane gradient and the resulting sodium motive force, but the specific Na^+-dependent process responsible for this was not yet elucidated. In *H. elongata*, a similar picture was observed, with major issues exhibited within its respiratory chain especially at the stage of the electron transfer to the final electron acceptor. The *'default'* ETC used by *H. elongata* in the salt optimum involves a Na^+-translocating NADH:ubiquinone oxidoreductase NQR, a type II NADH:quinone oxidoreductase (NDH-2) without proton pumping activity, a succinate dehydrogenase – also non-pumping –, and the quinol oxidase bo' translocating protons (Figure 5.1). *H. elongata* creates both a Na^+ and H^+ gradient. Either could be used by the F-type ATP synthase to create ATP, however, sequence similarities with other F-type ATP synthases highly suggest that it is coupled to H^+ [87]. This same set-up is also found for growth at high salt with no striking differences in the transcriptome. Additionally, at high salinity no major protein folding or oxidative stress responses were found for *H. elongata*. However at low salt, major salt-related responses were observed hinting towards an inadequacy of this default set-up of the ETC in this condition. A variety of alternatives for the quinol oxidase bo' and an additional V-type ATPase, which could exert either ATP synthase or ATP-mediated pumping activity, were upregulated. In general, the redox homeostasis in *H. elongata* growing on low-salt medium seems to be disturbed, as indicated by the upregulation of the two-component system RegA/RegB, which is directly sensing the quinone/quinol pool.
Regarding the oxidoreductases in *H. elongata* no changes on a transcriptomic level could be observed, in contrast to what has been reported before in *C. salexigens* [182]. This might be due to differences in the organization of their ETCs. *C. salexigens* possesses an additional H^+-translocating NADH:quinone oxidoreductase (NDH-1), which is absent in *H. elongata*. This enables *C. salexigens* to build a sodium and proton gradients independently, while *H. elongata* has to build its proton gradient using Na^+ / H^+ exchangers. Moreover, *C. salexigens* only has one F-type ATP synthase, whereas in *H. elongata* the V-type ATPase is additionally expressed during low salt growth. It is not yet clear, where exactly the respiratory chain is failing. The evidence shown in this work, points at an inability to build the Na^+ and H^+ gradients. The overall expression profile in low salinity hints towards a detrimental reduction of the membrane potential which is strongly indicated with an increased expression of the UPF0057 family protein (HELO_2679) in low salt. These type of proteins are expressed with a falling membrane potential [123]. The fact that no signs of depolarisation was observed in the above mentioned studies with C. salexigens, is a further indication in this direction since its gradients are independent from each

other.

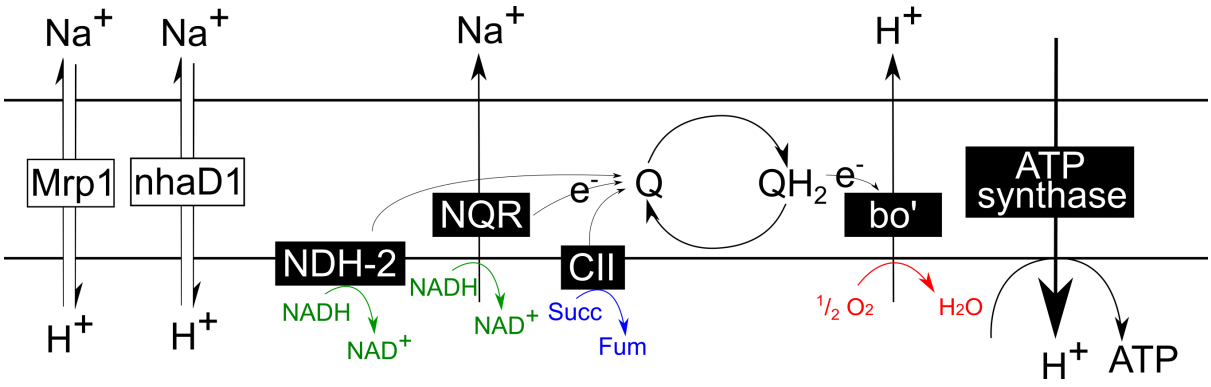

Figure 5.1: Default organization of the electron transport chain in *H. elongata* used in the salt optimum and at high salt conditions as revealed by RNA-Seq. There are two NADH dehydrogenases (NQR, NDH-2), a succinate dehydrogenase, and a quinol oxidase bo'. NQR is translocating Na^+ while the quinol oxidase bo' translocates H^+ transferring the electron to the final acceptor O_2. ATP is generated via a H^+-translocating F-type ATP synthase. The salt-regulated Na^+/H^+ antiporters Mrp1 and NhaD1 with different stoichiometries link the different gradients and top off the proton motive force (pmf).

Other than the modulation of respiratory chain processes, many more similarities between *H. elongata* and *C. salexigens* could be found. These include the scavenging for ion as well as the downregulation of chemotaxis and flagellar genes [182].
In this context, the behavior of the modified strain *H. elongata* Δ*teaABC* Δ*doeA*, showing key characteristics of the low salt stress response is of great interest. In this mutant, the distinct downregulation of a whole plethora of motility-related genes including flagellar synthesis and chemotaxis, was the most striking. Apart from this, the expression profile very closely resembled the wild type transcriptome even though two notable functions, ectoine transport and degradation, are disabled in *H. elongata* Δ*teaABC* Δ*doeA*.
Moreover, the transcriptome profiles with different carbon sources, comparing glycolytic and gluconeogenetic growth, substantiated the hypothesis that glycolytic carbon utilization in *H. elongata* happens exclusively through the ED pathway. This conclusion in combination with the hypothesis that the EMP pathway plays a role in gluconeogenetic growth was based on the reversibility of the *H. elongata* PP_i-dependent phosphofructokinase, as well as the similarities to its close relative *C. salexigens* [107, 165]. In the RNA-Seq analysis, all genes involved in the cytoplasmic glucose utilization pathway, branching towards the ED pathway via G6P dehydrogenase and the genes encoding the ED pathway themselves were strongly downregulated during gluconeogenetic growth. Even though the ED pathway has a lower ATP yield compared to the EMP pathway, its importance in the generation of NADPH reducing equivalents has been shown [35]. Also, it uses only two enzymes and, thus, fewer resources. In *E. coli*, a switch to the ED pathway at growth rates below 0.3 h^{-1} was suggested to work as a proteome saving strategy [144]. Within the transcriptomic analysis, no distinct role of the phosphofructokinase (*pfkA*) could be defined because neither the carbon source nor the different salt concentrations had an impact on its expression level.
A peculiarity was found for acetate utilization in *H. elongata* via acetyl-CoA synthetase. No changes in transcription levels for cells growing on acetate as the sole carbon source were observed. The use of acetate or gluconeogenetic substrates, might be regulated at a different point in the metabolism. One of the two isoenzymes for acetyl-CoA synthetase (HELO_2142) was found to be less expressed at high salt in particular, but not regulated regarding the substrate. The downregulation in high salinity could be linked to a decrease in flux through the ectoine degradation pathway, which involves the release of acetate during the conversion of α-NADA to DABA by DoeB.

Complementary to this, growth at low salt with different carbon sources resulted in citrate as the substrate facilitating the fastest growth compared to all other tested carbon sources. Citrate is a six-carbon compound and is involved in the first step of the TCA cycle. Normally, it is generated by the enzyme citrate synthase *gltA*, which fuses the acetyl group of acetyl-CoA with OAA and is known to be allosterically inhibited by NADH [231, 232]. With a deficient ETC at low salt, as indicated by the transcriptome analysis due to most likely a reduced membrane potential, the activity of citrate synthase is possibly inhibited. Consequently, the fluxes through the TCA cycle are stunted with the inhibition of the enzyme, catalyzing the first step. However, growing on citrate as a carbon source the inhibition of citrate synthase is not relevant. This could also explain the significantly less biomass that is accumulated for growth on citrate in these conditions since a higher flux through the TCA cycle would imply a bigger portion of the available carbon source is decarboxylated in the two oxidative decarboxylation steps releasing CO_2. On the other end, acetate and D-lactate facilitate the slowest growth rates for all tested carbon sources. Acetate utilization in *H. elongata* via acetate synthetase uses ATP and produces AMP. By utilizing a pyrophosphate (PP_i), this process is very energy-intensive and with an inefficient respiratory chain in low salinity, this energy-consuming reaction is even worse. Based on the genome annotation, it is not entirely clear how D-lactate is metabolized, but the most likely reaction is a D-lactate dehydrogenase (potentially HELO_1046) and the metabolization via PYR. Each conversion of lactate to PYR involves the reduction of one NAD^+ to NADH towards generating reducing equivalents. Therefore, this reaction might be unfavorable in an already reduced redox state of the cell during growth in low salt simply based on mass action.
Furthermore, it has been proposed, that the aspartate kinase LysC in *H. elongata* is not regulated by osmolarity [107]. This is supported by our findings. No distinct changes in the transcriptome regarding LysC were detected. However, for the suggested alternative point of regulation at the PEP-PYR-OAA node, only a clear connection to osmotic stress for the OAA decarboxylase, in particular *oadA*, was found. In [86], we demonstrated the shared action of PEP carboxylase and the membrane-bound OAA decarboxylase as anaplerotic enzymes, with the latter only active at high salt conditions. Anaplerosis is a critical part of the central metabolism, especially in *H. elongata* because it not only serves the amino acid demand but also provides material for ectoine synthesis. PEP carboxylase is always thermodynamically more favorable than OAA decarboxylase but has lower stoichiometric yields. OAA decarboxylase can carry the flux necessary for normal growth alone but only if the salt concentration is high enough. The co-existence of parallel pathways is frequent among bacteria and provides flexibility for different environmental conditions. In *H. elongata*, the salt dependence of one of the options makes sure, that in a high salinity environment at a higher ectoine demand, accordingly a higher flux through anaplerosis is achieved. With the upregulation of the first gene *oadA* in the encoding operon for OAA decarboxylase, this salt-dependent cooperation was backed by the transcriptomic analysis. Compared to PEP carboxylase and OAA decarboxylase, the glyoxylate shunt was suggested to be the worst option for anaplerosis and omitted at high salt [107], which was also apparent in the transcriptomic response. The glyoxylate shunt was downregulated, in particular at high salt. Since the carbon used in ectoine synthesis is withdrawn from the TCA cycle, as shown by the reduced CO_2 emission [163], the glyoxylate shunt at high salt is most likely downregulated to avoid material bypassing the catabolic reactions of the TCA cycle.

The overall picture drawn by the RNA-Seq analysis reveals, that outside of its salt optimum, the growth of *H. elongata* is stunted on either end of its salt range caused by difficulties in energy acquisition. On the low salt end, the ETC is impaired by membrane depolarization, while in high salinity the energy is reallocated in favor of salt adaptation mechanisms [87].

5.2 Metabolic Engineering to improve ectoine synthesis

5.2.1 Rerouting carbon flux

Increasing supply of precursors

The overall aim of this work was to modify the metabolic network in *H. elongata* in favor of ectoine production towards an optimized producer strain. The anaplerotic node constitutes a perfect target for the optimization of the metabolic fluxes due to its special role in this organism. One strategy to manipulate the flux distribution is the removal of competing pathways. This is the case for PEP carboxykinase, which decarboxylates OAA to PEP. Since this reaction, together with PEP carboxylase, forms a futile cycle that consumes ATP, its removal opens the way towards more efficient strains. The deletion of the *pckA* gene led to a higher extracellular ectoine titer in the secretion strain ($\Delta teaABC$ $\Delta doeA$) by approximately 45 % on glucose, implying that PEP carboxykinase is active during glycolytic growth. The impact on growth varied with the salt concentration and the carbon source used. At high salt, there was no difference in growth rate with either carbon source. But with a decreasing salt concentration the growth rate was negatively impacted, however, only with a glycolytic carbon source (glucose). On a gluconeogenic carbon source (acetate), the growth rate of the *pckA* deletion mutant was the same as its parental strain.
In *E. coli*, PEPCK and PEP synthase are two parallel reactions to convert intermediates from the TCA cycle to PEP [22, 97]. While PEPCK converts OAA in a single decarboxylation step to PEP, the alternative involves two steps with ME, converting MAL to PYR and, subsequently, Pps converting PYR to PEP. The deletion of either *pckA* or *ppsA* showed no phenotype during balanced growth in *E. coli*, whether on acetate or glucose. The parallel pathways seem redundant at a first glance. But even though no impact on growth in a steady state was demonstrated, a negative effect during carbon source transition from glucose to acetate was observed [97]. This shows that the function of a gene also needs to be assessed in dynamic environments in order to describe its whole range of metabolic functions.
In *H. elongata*, these alternative pathways described in *E. coli* are also present based on the genome annotation [188]. Thus after removal of PEPCK, the second option via ME and PEP synthase is still available. However, in contrast to *E. coli*, an impact on the growth rate is apparent in *H. elongata* during balanced growth on glucose after the disruption of PEPCK. In this organism, the futile cycle around the anaplerotic node between PEPC and PEPCK may play a special role due to OAA's role as an ectoine precursor. In general, OAA is an unstable compound and is believed to be present *in vivo* at only sub-micromolar concentrations [155]. Possibly, the futile cycle draining OAA is a mechanism to keep its concentration at a low level. The reaction for aspartate formation from OAA catalyzed by aspartate transaminase (*aspC*) is known to be controlled by mass action in *E. coli* [178]. An increase in OAA levels, therefore, also increases the levels of aspartate. But aspartate is at the same time used as a metabolic sensor for dicarboxylic acid availability and allosterically inhibits the formation of dicarboxylic acids from PEP. At high aspartate concentrations the conversion of dicarboxylic acids to PEP and PYR is even stimulated [178, 184]. These regulatory mechanisms might lead to a reduced flux through PEPC in *H. elongata*-PCK::Sm^R, which was, in fact, shown to be the case in an *E. coli* $\Delta pckA$ knockout by [240]. Additionally, malate dehydrogenase MDH is not a thermodynamically favorable reaction and even at normal physiological conditions, the concentrations of substrate MAL and product OAA are very important for this reaction. With the activation of malic enzymes NAD-ME and NADP-ME, due to high concentrations of aspartate and OAA [22], an increased rerouting of TCA intermediates towards PYR to circumvent OAA could take place. The conditions negatively affected by the deletion of PEPCK are particularly in low salt and salt optimum. At high salt, the growth rates are the same. This could indicate that indeed some type of feedback inhibition via aspartate is happening because at high salt condition the sodium-dependent OAD is reversed, working in an anaplerotic direction towards OAA carboxylation [86]. This could potentially compensate an adverse inhibiting effect on PEPC but due to its salt dependence this is only possible at high salt concentrations.
In *H. elongata*, as in *E. coli* [97], an alternative pathway towards PEP via ME and PEP synthase is

available. The additional deletion of the NADP-ME *maeB* lead to no changes in the growth rate but had an impact on the lag phase. The drastically increased lag phase observed for the single knockout of *pckA* was reduced by the removal of *maeB*. During the operation of the TCA cycle, the reaction via ME circumvents the thermodynamically unfavorable MAL dehydrogenase reaction. The genome annotation revealed the presence of two isoenzymes *maeA* and *maeB* with differing cofactor specificities. Even though no *in vitro* activity for *maeA* has been detected so far, it is possible that *in vivo* the isoenzyme is able to take over the needed flux. In *E. coli*, the regulation is tightly linked to acetate utilization and more specifically the reversible Pta-AckA pathway with the intermediate acetyl-phosphate [22, 55]. However, there is no annotated phosphate acetyltransferase (Pta) in *H. elongata*. The activity of both malic isoenzymes at the same time has been shown before in *E. coli* during acetate metabolism [22]. Generally, the $NADP^+$-dependent isoenzyme is used to generate NADPH from the decarboxylation reaction, while the NAD^+-dependent version is primarily associated with gluconeogenesis, but is not essential for it [184]. Also, it was shown that for a triple knockout mutant *E. coli* Δ*pckA* Δ*maeB* Δ*sfcA* growth on gluconeogenetic substrates is still not completely abolished [83]. Instead, the double knockout of PEPCK and PEP synthase generates this phenotype [73]. Thus, a possible explanation for the observed gluconeogenetic growth of *H. elongata*-PCK::Sm^R is that the second isoenzyme *maeA* shows activity *in vivo* and takes over the needed fluxes. The isoenzyme NAD-ME is activated by aspartate in *E. coli* [22]. Since aspartate is a precursor for ectoine and the flux towards the ectoine synthesis pathway is already brought up by the deletion of *pckA*, NAD-ME might be activated and redirect the flux towards PYR. Glycolytic growth was not negatively affected by the *maeB* deletion either, suggesting that no reverse flux towards anaplerosis is taking place. The adverse effects experienced in low salt growth, which was introduced by the PEPCK deletion, is alleviated in this double knockout mutant. It seems both PEPCK and NADP-ME show activity in glycolytic conditions in *H. elongata*. The compensation of the negative impact due to removal of PEPCK in the salt optimum by additional deletion of *maeB* could be related to a reduced MAL concentration. Apart from aspartate, MAL is also a known inhibitor for PEPC activity [37, 161]. and the removal of NADP-ME might reduce the MAL concentration to a point at which the inhibitory effect of MAL on PEPC is alleviated.
In an SO_4-limited medium, the growth behavior of the single PEPCK knockout mutant and double PEPCK and NADP-ME knockout mutant hints towards changes in the biomass composition or the OD600 to AFDW correlation established for the wild type. But next to this distinct effect on the biomass accumulation another important finding is the differences observed in the ectoine concentration in the cytoplasm for the deletion mutants *H. elongata*-PCK and *H. elongata*-PCKPPC with the first strain lacking only PEPCK and the latter both PEPCK and PEPC. Compared to the parental strain, the Leaky mutant, both modified strains have a higher ectoine content in the cytoplasm with *H. elongata*-PCK reaching the highest concentration.
Normally, intracellular ectoine levels are strictly regulated which by implication means that in these strains the regulation seems to be no longer functional. This most likely already includes the Leaky mutant itself. Also, this is in agreement with the already proposed hypothesis in the literature [115] that intracellular ectoine levels are controlled by a mechanism involving ectoine circulating from the cytoplasm to the periplasm.

Increasing ectoine excretion

An attempt to increase the flux towards ectoine synthesis would be expected to have negative effects due to metabolite feedback regulation inhibiting the pathway and slow down fluxes. This can be counteracted with concerted action. In concordance with a higher flux in the ectoine biosynthesis pathway, an increased "pull" on the product side can be applied by increasing ectoine excretion. Due to the excretion of ectoine into the extracellular space, ectoine production in the Leaky Mutant is already enhanced compared to the wild type. By increasing excretion, synthesis is also brought up to hold the same intracellular ectoine level. This was achieved by the overexpression of the genes *teaBC*, encoding the transmembrane proteins of the ectoine-specific TRAP transporter but without the respective substrate binding protein TeaA. The bigger subunit TeaC facilitates the release of a far higher amount of ectoine right after induction.

However, at the same time cell growth is stunted drastically, which could also be an indicator for cell lysis due to the overexpression. In contrast, TeaB or a combination of both transmembrane proteins releases less ectoine but has barely any growth deficiencies.
In this context, an interesting concept could be the overexpression of *teaB* during the cultivation of *H. elongata* to increase ectoine secretion in the growth phase. After depletion of the substrate, the expression of TeaC membrane channels could be employed to induce cell lysis. The complete release of the product into the medium makes the following downstream processing steps easier. Even if both transmembrane proteins are expressed together at some point, no detrimental effect is to be expected, since the expression of TeaBC was shown to behave like TeaB. But to make this concept work, the expression of *teaB* needs to be blocked tightly enough to allow cell lysis via TeaC. For example, a genetic organization as depicted in Figure 5.2 could be used. TeaB is expressed constitutively during the cultivation to boost ectoine secretion. After the desired biomass is reached or the substrate is depleted, the expression of *teaC* is induced for cell lysis. Together with *teaC* a repressor for the *teaB* promoter could be transcribed to prevent the concomitant expression of both genes.

5.2.2 Improving ectoine synthesis: Re-engineering nitrogen assimilation.

Ammonium uptake in *H. elongata* was shown to proceed solely via the GS/GOGAT high-affinity pathway. This could be determined by disrupting the pathway by removal of the glutamate synthase GOGAT, which leads to an auxotrophic strain for glutamate. By employing the GS/GOGAT pathway, the conversion of glucose to ectoine consumes 2 ATP [52, 162]. Two nitrogen atoms are incorporated into one ectoine molecule and for the assimilation of each ammonium one ATP is needed. Based on calorimetric measurements by Maskow & Babel [137], the efficiency of glucose to ectoine conversion, however, is approximately 100 %, suggesting it to be ATP neutral. But the ATP-expensive GS/GOGAT was determined as the only available ammonium assimilation pathway in *H. elongata*. The ability to grow using ammonium as the sole nitrogen source is restored by complementation with the native genes *gltDB*, encoding the glutamate synthase GOGAT, or an assimilatory NADPH-dependent glutamate dehydrogenase *gdhA* from *P. putida*. The role of its native NADH-dependent glutamate dehydrogenase *gdh* remains unclear, but most likely a dissimilatory function can be accredited. This allows the opportunity to engineer a modified strain with a different ammonium uptake strategy via NADPH-GDH. The switch from GS/GOGAT to NADPH-GDH allows the nitrogen uptake to be energetically cheaper essentially reducing the ATP cost for each synthesized ectoine molecule by a half. The ATP saved through these changes can be used in other processes [162, 188].
However, a modified strain taking up ammonium solely via NADPH-GDH from *P. putida* (Δ*gltDB*::SmR Δ*gdh*::*gdhA*, KHN2) showed a considerably reduced growth rate by about 40 % compared to the wild type. Similar to Richard Lenski's long term *E. coli* evolution experiment [20], an evolution experiment was performed to try and recover the reduction in growth rate using directed evolution [39]. Because already a major change in the metabolic network was undertaken, the new available fluxes first need to be adjusted. This was done by growing the new strain facing the very conditions, in which these genomic changes are most profound, in this case with ammonium as the sole nitrogen source. Naturally, occurring mutations advantageous for the new metabolic framework were selected based on an improvement in growth rate and in only a 15 to 20 transfers a growth rate equal to that in the wild type could be achieved again for three different evolution lines termed DE1, DE2, and DE8. Further mutation of these lines could potentially even surpass the maximum growth rate of the wild type. In any case, the increased efficiency in nitrogen assimilation further paves the way for improvements on ectoine productivity.

5.3 *H. elongata* as an industrial platform organism

The industrial application of *H. elongata*, up to this point, is mainly limited to ectoine production, but its potential clearly goes beyond. *H. elongata* combines highly unusual metabolic capabilities with the completely standard genetics of a Gram-negative bacterium. The transfer of genetic constructs like promoters or genes from other organisms, like *E. coli* and *P. putida*, posed no problems. An example of

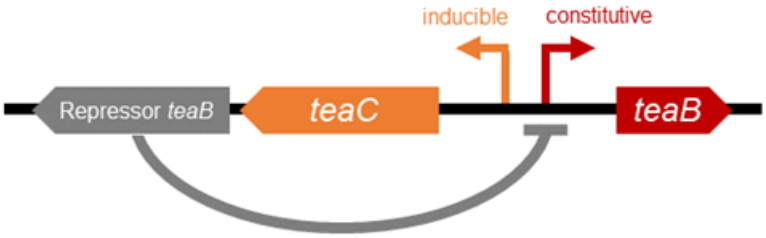

Figure 5.2: Example for a possible application of the TeaBC-mediated excretion of ectoine: the transcription unit includes *teaB* (red), which can be overexpressed constitutively during growth. After depletion of the carbon source, expression of *teaC* (orange) can be induced to completely release the intracellular ectoine content through cell lysis. To avoid co-transcription which would impair lysis via TeaC, the expression of *teaB* needs to be repressed at this stage. Therefore, a repressor could be co-transcribed together with *teaC* in order to inhibit transcription of *teaB*.

this, is the XylS/Pm promoter originally from the *P. putida* TOL plasmid, which showed similar traits in *H. elongata* as in its origin strain. In particular, the very low basal expression observed is noteworthy, since the uninduced expression of proteins that are detrimental to cell vitality is commonly known to be a major setback in the production of heterologous proteins. Additionally, the presence of compatible solutes in the *H. elongata* cytoplasm could enhance the folding of proteins during heterologous overexpression based on the preferential exclusion effect. Some proteins are known to be extremely hard to produce as soluble proteins, like kinases or phosphatases [205], which could benefit from the stabilizing effects.
The glutamate auxotrophic *H. elongata* strain developed in this work shows potential, especially in combination with the auxotrophic complementation plasmid pSEVA037-*gdhA* to facilitate the expression of heterologous genes. By using a plasmid-based expression, a far higher copy number for the gene in question is available and, therefore, a higher transcription can be achieved. At the same time, no antibiotics are needed for the maintenance of the plasmid since the NADPH-GDH vital for growth with ammonium as the sole nitrogen source is located on the plasmid. But in case it needs to be cured, this can also be done in complex medium, in which the uptake of ammonium is not essential.
A first step towards expanding the product spectrum of *H. elongata* has already been made in this work. By deleting the gene *ectC*, encoding for the last step in the ectoine biosynthesis, the synthesis is halted prematurely at the precursor γ-NADA. The direct consequences for these strains are the reduction of salt tolerance, which manifests itself by a reduced growth rate with increasing salt concentration compared to the wild type. The optimal salt range for the wild type was determined in between 0.5 and 1 M NaCl. For the new Δ*ectC* mutants at the lower end (0.5 M NaCl) only a negligible reduction of the growth rate by 8 – 13 % was observed. However, at 1 M NaCl the growth rate drops drastically by 30 – 40 %, whereas in the wild type at both salt concentrations the growth rates are the same. This single knockout also impacts the OD600 to biomass correlation. For both NADA producers, much lower ratios were found. The intracellular ectoine content in the wild type is strictly regulated and is constant over time. With an increase in the salt concentration, the intracellular ectoine content is also increased, which appears fairly linear with a doubling of the ectoine content going from 0.5 to 1 M NaCl. In contrast, in the NADA producers, the intracellular NADA content increases with time. This could be hinting at a disturbance of the regulation in these strains. If the cells continue to accumulate NADA without regulation, a hypotonic environment might be created with the cells facing an increasing turgor pressure. This could explain the drastically different OD600 to biomass ratio, as the the influx of water would change the size and/or shape of the cells. Different shape or size distributions of cells due to different growth conditions are known to produce different standard curves [109]. However, no extracellular γ-NADA was detected. In a hypotonic environment with high turgor pressure the mechano-sensitive channels would open to avoid

rupturing of the cells. Another possibility is that the properties of ectoine as an osmolyte are distinctly different compared to its precursor and a lesser amount is needed to achieve the same effect.
H. elongata also shows potential for the production of bulk products [242]. As a natural PHB producer there is still potential for this product, especially in open and continuous processes as done in other members of this genus *Halomonas* [246], or even a co-production of both ectoine and PHB [81, 146] in an industrial sense. Furthermore, in the course of this work, *H. elongata* has proven itself to be genomically accessible and well applicable with established molecular methods.
Furthermore, some special properties characteristic to *H. elongata* further could be taken advantage of for the expression of heterologous proteins. With ectoine naturally occurring in the cytoplasm, its positive effects as a stabilizer in protein folding could benefit the expression of proteins prone to denaturation. Also, the bacterial milking strategy developed by Sauer & Galinski [183] for the release of ectoine might be applicable to other components of the cytoplasm as well. Mechano-sensitive channels are not substrate-specific. The efflux is activated prompted by an increased turgor pressure in the cell. Like this, there are several promising ways for *H. elongata* to become a potential workhorse for not only elucidating osmo-adaptive mechanisms as a model organism or specifically the production of ectoine but also as an industrial platform organism for other applications in biotechnological processes.

Bibliography

1. Abramov, O. & Mojzsis, S. J. Microbial habitability of the Hadean Earth during the late heavy bombardment. *Nature* **459,** 419–422 (2009).
2. Ahn, S., Jung, J., Jang, I.-A., Madsen, E. L. & Park, W. Role of Glyoxylate Shunt in Oxidative Stress Response. *The Journal of biological chemistry* **291,** 11928–11938. ISSN: 0021-9258 (2016).
3. Alam, A., Bröms, J. E., Kumar, R. & Sjöstedt, A. The Role of ClpB in Bacterial Stress Responses and Virulence. *Frontiers in molecular biosciences* **8,** 668910. ISSN: 2296-889X (2021).
4. Anantharaman, V. & Aravind, L. Evolutionary history, structural features and biochemical diversity of the NlpC/P60 superfamily of enzymes. *Genome biology* **4,** R11 (2003).
5. Aon, M. A., Cortassa, S. & O'Rourke, B. Redox-optimized ROS balance: a unifying hypothesis. *Biochimica et biophysica acta* **1797,** 865–877. ISSN: 0006-3002 (2010).
6. Aslan, S., Noor, E. & Bar-Even, A. Holistic bioengineering: rewiring central metabolism for enhanced bioproduction. *The Biochemical journal* **474,** 3935–3950 (2017).
7. Bannantine, J. P. *et al.* NlpC/P60 domain-containing proteins of *Mycobacterium avium* subspecies *paratuberculosis* that differentially bind and hydrolyze peptidoglycan. *Protein science : a publication of the Protein Society* **25,** 840–851 (2016).
8. Barquera, B. The sodium pumping NADH:quinone oxidoreductase (Na^+-NQR), a unique redox-driven ion pump. *Journal of bioenergetics and biomembranes* **46,** 289–298. ISSN: 0145-479X (2014).
9. Basan, M. *et al.* Overflow metabolism in *Escherichia coli* results from efficient proteome allocation. *Nature* **528,** 99–104 (2015).
10. Batista, M. B. *et al.* PHB Biosynthesis Counteracts Redox Stress in *Herbaspirillum seropedicae*. *Frontiers in microbiology* **9,** 472. ISSN: 1664-302X (2018).
11. Battley, E. H. Calculation of the heat of growth of *Escherichia coli* K-12 on succinic acid. *Biotechnology and bioengineering* **37,** 334–343 (1991).
12. Beardmore-Gray, M. & Anthony, C. The oxidation of glucose by *Acinetobacter calcoaceticus*: interaction of the quinoprotein glucose dehydrogenase with the electron transport chain. *Journal of general microbiology* **132,** 1257–1268. ISSN: 0022-1287 (1986).
13. Becher, B. & Müller, V. Delta mu Na^+ drives the synthesis of ATP via an delta mu Na^+-translocating F1F0-ATP synthase in membrane vesicles of the archaeon *Methanosarcina mazei* Gö1. *Journal of bacteriology* **176,** 2543–2550. ISSN: 0021-9193 (1994).
14. Benziman, M., Russo, A., Hochman, S. & Weinhouse, H. Purification and Regulatory Properties of the Oxaloacetate Decarboxylase of *Acetobacter xylinum*. *Journal of bacteriology* **134,** 1–9. ISSN: 0021-9193 (1978).
15. Bhattacharya, S. in *Response Surface Methodology in Engineering Science [Working Title]* (IntechOpen, 2021). doi:10.5772/intechopen.95835.
16. Bilstein, A., Heinrich, A., Rybachuk, A. & Mösges, R. Ectoine in the treatment of irritations and inflammations of the eye surface. *BioMed Research International* **2021** (2021).
17. Bitop AG. *Fight against Coronavirus:* https://www.bitop.de/application/files/5915/9110/1179/200602_Ectoin_vs._SARS-CoV-2_summary_14.05.20.pdf (2022).
18. Blacker, T. S. & Duchen, M. R. Investigating mitochondrial redox state using NADH and NADPH autofluorescence. *Free radical biology & medicine* **100,** 53–65 (2016).
19. Bligh, E. G. & Dyer, W. J. A rapid method of total lipid extraction and purification. *Canadian journal of biochemistry and physiology* **37,** 911–917 (1959).

20. Blount, Z. D. *et al.* Genomic and phenotypic evolution of *Escherichia coli* in a novel citrate-only resource environment. *eLife* **9.** doi:10.7554/eLife.55414 (2020).
21. Bolen, D. W. & Baskakov, I. V. The osmophobic effect: natural selection of a thermodynamic force in protein folding. *Journal of molecular biology* **310,** 955–963. ISSN: 0022-2836 (2001).
22. Bologna, F. P., Andreo, C. S. & Drincovich, M. F. *Escherichia coli* malic enzymes: two isoforms with substantial differences in kinetic properties, metabolic regulation, and structure. *Journal of bacteriology* **189,** 5937–5946. ISSN: 0021-9193 (2007).
23. Borsuk, S. *et al.* Auxotrophic complementation as a selectable marker for stable expression of foreign antigens in *Mycobacterium bovis* BCG. *Tuberculosis (Edinburgh, Scotland)* **87,** 474–480. ISSN: 1472-9792 (2007).
24. Boyer, H. W. & Roulland-dussoix, D. A complementation analysis of the restriction and modification of DNA in *Escherichia coli*. *Journal of molecular biology* **41,** 459–472. ISSN: 0022-2836 (1969).
25. Boyle, P. M. & Silver, P. A. Parts plus pipes: synthetic biology approaches to metabolic engineering. *Metabolic engineering* **14,** 223–232 (2012).
26. Braatsch, S., Helmark, S., Kranz, H., Koebmann, B. & Jensen, P. R. *Escherichia coli* strains with promoter libraries constructed by Red/ET recombination pave the way for transcriptional fine-tuning. *BioTechniques* **45,** 335–337. ISSN: 0736-6205 (2008).
27. Brämer, C. O. & Steinbüchel, A. The malate dehydrogenase of *Ralstonia eutropha* and functionality of the C(3)/C(4) metabolism in a Tn5-induced *mdh* mutant. *FEMS microbiology letters* **212,** 159–164. ISSN: 0378-1097 (2002).
28. Brautaset, T., Lale, R. & Valla, S. Positively regulated bacterial expression systems. *Microbial Biotechnology* **2,** 15–30. ISSN: 17517915 (2009).
29. Brock, T. D. & Freeze, H. Thermus aquaticus gen. n. and sp. n., a nonsporulating extreme thermophile. *Journal of bacteriology* **98,** 289–297 (1969).
30. Bylund, G. O., Wipemo, L. C., Lundberg, L. A. & Wikström, P. M. RimM and RbfA are essential for efficient processing of 16S rRNA in *Escherichia coli*. *Journal of bacteriology* **180,** 73–82. ISSN: 0021-9193 (1998).
31. Cánovas, D. *et al.* Isolation and characterization of salt-sensitive mutants of the moderate halophile *Halomonas elongata* and cloning of the ectoine synthesis genes. *The Journal of biological chemistry* **272,** 25794–25801. ISSN: 0021-9258 (1997).
32. Chao, Y. P. & Liao, J. C. Metabolic responses to substrate futile cycling in *Escherichia coli*. *The Journal of biological chemistry* **269,** 5122–5126. ISSN: 0021-9258 (1994).
33. Chao, Y. P., Patnaik, R., Roof, W. D., Young, R. F. & Liao, J. C. Control of gluconeogenic growth by *pps* and *pck* in *Escherichia coli*. *Journal of bacteriology* **175,** 6939–6944. ISSN: 0021-9193 (1993).
34. Chavarría, M., Kleijn, R. J., Sauer, U., Pflüger-Grau, K. & de Lorenzo, V. Regulatory tasks of the phosphoenolpyruvate-phosphotransferase system of *Pseudomonas putida* in central carbon metabolism. *mBio* **3.** doi:10.1128/mBio.00028-12 (2012).
35. Chavarría, M., Nikel, P. I., Pérez-Pantoja, D. & de Lorenzo, V. The Entner-Doudoroff pathway empowers *Pseudomonas putida* KT2440 with a high tolerance to oxidative stress. *Environmental microbiology* **15,** 1772–1785 (2013).
36. Chen, Y.-H., Lu, C.-W., Shyu, Y.-T. & Lin, S.-S. Revealing the Saline Adaptation Strategies of the Halophilic Bacterium *Halomonas beimenensis* through High-throughput Omics and Transposon Mutagenesis Approaches. *Scientific reports* **7,** 13037 (2017).
37. Chen, Z., Bommareddy, R. R., Frank, D., Rappert, S. & Zeng, A.-P. Deregulation of feedback inhibition of phosphoenolpyruvate carboxylase for improved lysine production in *Corynebacterium glutamicum*. *Applied and environmental microbiology* **80,** 1388–1393 (2014).

38. Chung, C. T., Niemela, S. L. & Miller, R. H. One-step preparation of competent *Escherichia coli*: transformation and storage of bacterial cells in the same solution. *Proceedings of the National Academy of Sciences of the United States of America* **86,** 2172–2175. ISSN: 0027-8424 (1989).
39. Cobb, R. E., Chao, R. & Zhao, H. Directed Evolution: Past, Present and Future. *AIChE journal. American Institute of Chemical Engineers* **59,** 1432–1440. ISSN: 0001-1541 (2013).
40. Conesa, A. *et al.* A survey of best practices for RNA-seq data analysis. *Genome biology* **17,** 13 (2016).
41. Constantinidou, C. *et al.* A reassessment of the FNR regulon and transcriptomic analysis of the effects of nitrate, nitrite, NarXL, and NarQP as *Escherichia coli* K12 adapts from aerobic to anaerobic growth. *The Journal of biological chemistry* **281,** 4802–4815. ISSN: 0021-9258 (2006).
42. Corkins, M. E., Wilson, S., Cocuron, J.-C., Alonso, A. P. & Bird, A. J. The gluconate shunt is an alternative route for directing glucose into the pentose phosphate pathway in fission yeast. *The Journal of biological chemistry* **292,** 13823–13832. ISSN: 0021-9258 (2017).
43. Czech, L. *et al.* Role of the extremolytes ectoine and hydroxyectoine as stress protectants and nutrients: genetics, phylogenomics, biochemistry, and structural analysis. *Genes* **9,** 177 (2018).
44. Dabney, J., Meyer, M. & Pääbo, S. Ancient DNA damage. *Cold Spring Harbor perspectives in biology* **5,** a012567 (2013).
45. Dai, X. *et al.* Reduction of translating ribosomes enables *Escherichia coli* to maintain elongation rates during slow growth. *Nature microbiology* **2,** 16231 (2016).
46. Dammel, C. S. & Noller, H. F. Suppression of a cold-sensitive mutation in 16S rRNA by overexpression of a novel ribosome-binding factor, RbfA. *Genes & development* **9,** 626–637. ISSN: 0890-9369 (1995).
47. Davidson, V. L. in *Encyclopedia of biophysics* (ed Roberts, G. C. K.) 2166–2168 (Springer, Berlin, 2013). ISBN: 978-3-642-16711-9. doi:10.1007/978-3-642-16712-6{\textunderscore}46.
48. Denkel, L. A. *et al.* Methionine sulfoxide reductases are essential for virulence of *Salmonella typhimurium*. *PloS one* **6,** e26974 (2011).
49. Díaz, S., Pérez-Pomares, F., Pire, C., Ferrer, J. & Bonete, M.-J. Gene cloning, heterologous overexpression and optimized refolding of the NAD-glutamate dehydrogenase from *Haloferax mediterranei*. *Extremophiles : life under extreme conditions* **10,** 105–115 (2006).
50. Dimroth, P. & Hilpert, W. Carboxylation of pyruvate and acetyl coenzyme A by reversal of the sodium pumps oxaloacetate decarboxylase and methylmalonyl-CoA decarboxylase. *Biochemistry* **23,** 5360–5366 (1984).
51. D'Mello, R., Hill, S. & Poole, R. K. The oxygen affinity of cytochrome bo' in *Escherichia coli* determined by the deoxygenation of oxyleghemoglobin and oxymyoglobin: Km values for oxygen are in the submicromolar range. *Journal of bacteriology* **177,** 867–870. ISSN: 0021-9193 (1995).
52. Dötsch, A., Severin, J., Alt, W., Galinski, E. A. & Kreft, J.-U. A mathematical model for growth and osmoregulation in halophilic bacteria. *Microbiology (Reading, England)* **154,** 2956–2969. ISSN: 1350-0872 (2008).
53. Du, D. *et al.* Structure of the AcrAB-TolC multidrug efflux pump. *Nature* **509,** 512–515 (2014).
54. Elias, M. *et al.* C-terminal periplasmic domain of *Escherichia coli* quinoprotein glucose dehydrogenase transfers electrons to ubiquinone. *The Journal of biological chemistry* **276,** 48356–48361. ISSN: 0021-9258 (2001).
55. Enjalbert, B., Millard, P., Dinclaux, M., Portais, J.-C. & Létisse, F. Acetate fluxes in *Escherichia coli* are determined by the thermodynamic control of the Pta-AckA pathway. *Scientific reports* **7,** 42135 (2017).
56. Ezraty, B., Aussel, L. & Barras, F. Methionine sulfoxide reductases in prokaryotes. *Biochimica et biophysica acta* **1703,** 221–229. ISSN: 0006-3002 (2005).

57. Fallet, C., Rohe, P. & Franco-Lara, E. Process optimization of the integrated synthesis and secretion of ectoine and hydroxyectoine under hyper/hypo-osmotic stress. *Biotechnology and Bioengineering* **107,** 124–133. ISSN: 0006-3592 (2010).

58. Fernandez-Castillo, R., Vargas, C., Nieto, J. J., Ventosa, A. & Ruiz-Berraquero, F. Characterization of a plasmid from moderately halophilic eubacteria. *Journal of general microbiology* **138,** 1133–1137. ISSN: 0022-1287 (1992).

59. Fiedler, M. & Skerra, A. *proBA* complementation of an auxotrophic *E. coli* strain improves plasmid stability and expression yield during fermenter production of a recombinant antibody fragment. *Gene* **274,** 111–118. ISSN: 0378-1119 (2001).

60. Follonier, S., Panke, S. & Zinn, M. A reduction in growth rate of *Pseudomonas putida* KT2442 counteracts productivity advances in medium-chain-length polyhydroxyalkanoate production from gluconate. *Microbial cell factories* **10,** 25 (2011).

61. Forward, J. A., Behrendt, M. C., Wyborn, N. R., Cross, R. & Kelly, D. J. TRAP transporters: a new family of periplasmic solute transport systems encoded by the *dctPQM* genes of *Rhodobacter capsulatus* and by homologs in diverse gram-negative bacteria. *Journal of bacteriology* **179,** 5482–5493. ISSN: 0021-9193 (1997).

62. Fraile, R., Sánchez-Mir, L. & Hidalgo, E. A new adaptation strategy to glucose starvation: modulation of the gluconate shunt and pentose phosphate pathway by the transcriptional repressor Rsv1. *The FEBS journal* **287,** 874–877 (2020).

63. Frenkel, R. Regulation and physiological functions of malic enzymes. *Current topics in cellular regulation* **9,** 157–181. ISSN: 0070-2137 (1975).

64. Fu, X.-Z. *et al.* Development of *Halomonas* TD01 as a host for open production of chemicals. *Metabolic engineering* **23,** 78–91 (2014).

65. Galinski, E. A. in *Advances in Microbial Physiology Volume 37* 273–328 (Elsevier, 1995). ISBN: 9780120277377. doi:10.1016/S0065-2911(08)60148-4.

66. Galinski, E. A., Pfeiffer, H. P. & Trüper, H. G. 1,4,5,6-Tetrahydro-2-methyl-4-pyrimidinecarboxylic acid. A novel cyclic amino acid from halophilic phototrophic bacteria of the genus *Ectothiorhodospira*. *European journal of biochemistry* **149,** 135–139. ISSN: 0014-2956 (1985).

67. Galinski, E. A. & Herzog, R. M. The role of trehalose as a substitute for nitrogen-containing compatible solutes (*Ectothiorhodospira halochloris*). *Archives of microbiology* **153,** 607–613. ISSN: 0302-8933 (1990).

68. Gandbhir, M., Rasched, I., Marlière, P. & Mutzel, R. Convergent evolution of amino acid usage in archaebacterial and eubacterial lineages adapted to high salt. *Research in Microbiology* **146,** 113–120. ISSN: 09232508 (1995).

69. Gawin, A., Valla, S. & Brautaset, T. The XylS/Pm regulator/promoter system and its use in fundamental studies of bacterial gene expression, recombinant protein production and metabolic engineering. *Microbial Biotechnology* **10,** 702–718. ISSN: 17517915 (2017).

70. Geisel, N. Constitutive versus responsive gene expression strategies for growth in changing environments. *PloS one* **6,** e27033 (2011).

71. Gibson, D. G. *et al.* Enzymatic assembly of DNA molecules up to several hundred kilobases. *Nature Methods* **6,** 343–345. ISSN: 1548-7105 (2009).

72. Giuffrè, A., Borisov, V. B., Arese, M., Sarti, P. & Forte, E. Cytochrome bd oxidase and bacterial tolerance to oxidative and nitrosative stress. *Biochimica et biophysica acta* **1837,** 1178–1187. ISSN: 0006-3002 (2014).

73. Goldie, A. H. & Sanwal, B. D. Genetic and physiological characterization of Escherichia coli mutants deficient in phosphoenolpyruvate carboxykinase activity. *Journal of bacteriology* **141,** 1115–1121. ISSN: 0021-9193 (1980).

74. Göller, K., Ofer, A. & Galinski, E. A. Construction and characterization of an NaCl-sensitive mutant of *Halomonas elongata* impaired in ectoine biosynthesis. *FEMS microbiology letters* **161,** 293–300. ISSN: 0378-1097 (1998).

75. Gorenflo, V., Steinbüchel, A., Marose, S., Rieseberg, M. & Scheper, T. Quantification of bacterial polyhydroxyalkanoic acids by Nile red staining. *Applied microbiology and biotechnology* **51,** 765–772 (1999).

76. Goto, S., Kato, S., Kimura, T., Muto, A. & Himeno, H. RsgA releases RbfA from 30S ribosome during a late stage of ribosome biosynthesis. *The EMBO journal* **30,** 104–114 (2011).

77. Grammann, K., Volke, A. & Kunte, H. J. New type of osmoregulated solute transporter identified in halophilic members of the bacteria domain: TRAP transporter TeaABC mediates uptake of ectoine and hydroxyectoine in *Halomonas elongata* DSM 2581^T. *Journal of bacteriology* **184,** 3078–3085. ISSN: 0021-9193 (2002).

78. Grant, S. G., Jessee, J., Bloom, F. R. & Hanahan, D. Differential plasmid rescue from transgenic mouse DNAs into *Escherichia coli* methylation-restriction mutants. *Proceedings of the National Academy of Sciences of the United States of America* **87,** 4645–4649. ISSN: 0027-8424 (1990).

79. Green, J. & Paget, M. S. Bacterial redox sensors. *Nature reviews. Microbiology* **2,** 954–966 (2004).

80. Gunsalus, R. P. Control of electron flow in *Escherichia coli*: coordinated transcription of respiratory pathway genes. *Journal of bacteriology* **174,** 7069–7074. ISSN: 0021-9193 (1992).

81. Guzmán, H., Van-Thuoc, D., Martín, J., Hatti-Kaul, R. & Quillaguamán, J. A process for the production of ectoine and poly(3-hydroxybutyrate) by *Halomonas boliviensis*. *Applied microbiology and biotechnology* **84,** 1069–1077 (2009).

82. Hahn, M. B. *et al.* DNA protection by ectoine from ionizing radiation: molecular mechanisms. *Physical chemistry chemical physics : PCCP* **19,** 25717–25722 (2017).

83. Hansen, E. J. & Juni, E. Isolation of mutants of *Escherichia coli* lacking NAD- and NADP-linked malic. *Biochemical and biophysical research communications* **65,** 559–566. ISSN: 0006-291X (1975).

84. Harper, C. J., Hayward, D., Kidd, M., Wiid, I. & van Helden, P. Glutamate dehydrogenase and glutamine synthetase are regulated in response to nitrogen availability in *Myocbacterium smegmatis*. *BMC microbiology* **10,** 138 (2010).

85. Harris, J. R., Lundgren, B. R., Grzeskowiak, B. R., Mizuno, K. & Nomura, C. T. A rapid and efficient electroporation method for transformation of *Halomonas* sp. O-1. *Journal of microbiological methods* **129,** 127–132 (2016).

86. Hobmeier, K. *et al.* Anaplerotic Pathways in *Halomonas elongata*: The Role of the Sodium Gradient. *Frontiers in microbiology* **11,** 561800. ISSN: 1664-302X (2020).

87. Hobmeier, K. *et al.* Adaptation to Varying Salinity in *Halomonas elongata*: Much More Than Ectoine Accumulation. *Frontiers in Microbiology* **13,** 1–19 (2022).

88. Hobmeier, K. *et al.* Metabolic engineering of Halomonas elongata: Ectoine secretion is increased by demand and supply driven approaches. *Frontiers in Microbiology, 2022, vol. 13* (2022).

89. Hui, S. *et al.* Quantitative proteomic analysis reveals a simple strategy of global resource allocation in bacteria. *Molecular systems biology* **11,** 784 (2015).

90. Huisman, G. W., de Leeuw, O., Eggink, G. & Witholt, B. Synthesis of poly-3-hydroxyalkanoates is a common feature of fluorescent pseudomonads. *Applied and environmental microbiology* **55,** 1949–1954 (1989).

91. Inuzuka, M. & Helinski, D. R. Requirement of a plasmid-encoded protein for replication *in vitro* of plasmid R6K. *Proceedings of the National Academy of Sciences of the United States of America* **75,** 5381–5385. ISSN: 0027-8424 (1978).

92. Iuchi, S. & Lin, E. C. Adaptation of *Escherichia coli* to redox environments by gene expression. *Molecular microbiology* **9,** 9–15. ISSN: 0950-382X (1993).

93. Jacobs, M. H., van der Heide, T., Driessen, A. J. & Konings, W. N. Glutamate transport in *Rhodobacter sphaeroides* is mediated by a novel binding protein-dependent secondary transport system. *Proceedings of the National Academy of Sciences of the United States of America* **93,** 12786–12790. ISSN: 0027-8424 (1996).

94. Johnson, K., Jiang, Y., Kleerebezem, R., Muyzer, G. & van Loosdrecht, M. C. M. Enrichment of a mixed bacterial culture with a high polyhydroxyalkanoate storage capacity. *Biomacromolecules* **10,** 670–676 (2009).

95. Jorge, C. D., Borges, N., Bagyan, I., Bilstein, A. & Santos, H. Potential applications of stress solutes from extremophiles in protein folding diseases and healthcare. *Extremophiles* **20,** 251–259 (2016).

96. Kaila, V. R. I. & Wikström, M. Architecture of bacterial respiratory chains. *Nature reviews. Microbiology* **19,** 319–330 (2021).

97. Kao, K. C., Tran, L. M. & Liao, J. C. A global regulatory role of gluconeogenic genes in *Escherichia coli* revealed by transcriptome network analysis. *The Journal of biological chemistry* **280,** 36079–36087. ISSN: 0021-9258 (2005).

98. Kapfhammer, D., Karatan, E., Pflughoeft, K. J. & Watnick, P. I. Role for glycine betaine transport in *Vibrio cholerae* osmoadaptation and biofilm formation within microbial communities. *Applied and environmental microbiology* **71,** 3840–3847 (2005).

99. Karr, D. B., Waters, J. K. & Emerich, D. W. Analysis of Poly-beta-Hydroxybutyrate in *Rhizobium japonicum* Bacteroids by Ion-Exclusion High-Pressure Liquid Chromatography and UV Detection. *Applied and environmental microbiology* **46,** 1339–1344 (1983).

100. Kato, O. *et al.* Quinone-dependent D-lactate dehydrogenase Dld (Cg1027) is essential for growth of Corynebacterium glutamicum on D-lactate. *BMC microbiology* **10,** 321 (2010).

101. Kawakami, T., Kuroki, M., Ishii, M., Igarashi, Y. & Arai, H. Differential expression of multiple terminal oxidases for aerobic respiration in *Pseudomonas aeruginosa*. *Environmental microbiology* **12,** 1399–1412 (2010).

102. Kennedy, C. J., Boyle, P. M., Waks, Z. & Silver, P. A. Systems-Level Engineering of Nonfermentative Metabolism in Yeast. *Genetics* **183,** 385–397. ISSN: 0016-6731 (2009).

103. Kerscher, S., Dröse, S., Zickermann, V. & Brandt, U. The three families of respiratory NADH dehydrogenases. *Results and problems in cell differentiation* **45,** 185–222. ISSN: 0080-1844 (2008).

104. Kessler, B., de Lorenzo, V. & Timmis, K. N. A general system to integrate *lacZ* fusions into the chromosomes of gram-negative eubacteria: regulation of the Pm promoter of the TOL plasmid studied with all controlling elements in monocopy. *Molecular and General Genetics MGG* **233,** 293–301. ISSN: 0026-8925 (1992).

105. Kessler, B., Timmis, K. N. & de Lorenzo, V. The organization of the Pm promoter of the TOL plasmid reflects the structure of its cognate activator protein XylS. *Molecular and General Genetics MGG* **244,** 596–605. ISSN: 0026-8925 (1994).

106. Khosla, C. & Keasling, J. D. Metabolic engineering for drug discovery and development. *Nature reviews. Drug discovery* **2,** 1019–1025. ISSN: 1474-1776 (2003).

107. Kindzierski, V. *et al.* Osmoregulation in the Halophilic Bacterium *Halomonas elongata*: A Case Study for Integrative Systems Biology. *PloS one* **12,** e0168818 (2017).

108. Kita-Tsukamoto, K., Wada, M., Yao, K., Nishino, T. & Kogure, K. Flagellar motors of marine bacteria *Halomonas* are driven by both protons and sodium ions. *Canadian journal of microbiology* **50,** 369–374. ISSN: 0008-4166 (2004).

109. Koch, A. L. Turbidity measurements of bacterial cultures in some available commercial instruments. *Analytical Biochemistry* **38,** 252–259. ISSN: 00032697 (1970).

110. Koffas, M., Roberge, C., Lee, K. & Stephanopoulos, G. Metabolic engineering. *Annual review of biomedical engineering* **1,** 535–557. ISSN: 1523-9829 (1999).

111. Korge, P., Calmettes, G. & Weiss, J. N. Increased reactive oxygen species production during reductive stress: The roles of mitochondrial glutathione and thioredoxin reductases. *Biochimica et biophysica acta* **1847,** 514–525. ISSN: 0006-3002 (2015).

112. Kraegeloh, A. & Kunte, H. J. Novel insights into the role of potassium for osmoregulation in *Halomonas elongata*. *Extremophiles : life under extreme conditions* **6,** 453–462 (2002).

113. Krampitz, L. O. & Werkman, C. H. The enzymic decarboxylation of oxaloacetate. *The Biochemical journal* **35,** 595–602 (1941).

114. Kuhlmann, A. U. & Bremer, E. Osmotically regulated synthesis of the compatible solute ectoine in *Bacillus pasteurii* and related *Bacillus* spp. *Applied and environmental microbiology* **68,** 772–783 (2002).

115. Kuhlmann, S. I., van Terwisscha Scheltinga, A. C., Bienert, R., Kunte, H.-J. & Ziegler, C. 1.55 A structure of the ectoine binding protein TeaA of the osmoregulated TRAP-transporter TeaABC from *Halomonas elongata*. *Biochemistry* **47,** 9475–9485 (2008).

116. Kumari, S. *et al.* Regulation of acetyl coenzyme A synthetase in *Escherichia coli*. *Journal of bacteriology* **182,** 4173–4179. ISSN: 0021-9193 (2000).

117. Kunte, H. J. & Galinski, E. A. Transposon mutagenesis in halophilic eubacteria: conjugal transfer and insertion of transposon Tn5 and Tn1732 in *Halomonas elongata*. *FEMS microbiology letters* **128,** 293–299. ISSN: 0378-1097 (1995).

118. Kunte, H. J. Osmoregulation in Bacteria: Compatible Solute Accumulation and Osmosensing. *Environmental Chemistry* **3,** 94. ISSN: 1448-2517 (2006).

119. Kunte, H. J., Trüper, H. G. & Stan-Lotter, H. in *Astrobiology* (eds Horneck, G. & Baumstark-Khan, C.) 185–200 (Springer Berlin Heidelberg, Berlin, Heidelberg, 2002). ISBN: 978-3-642-63957-9. doi:10.1007/978-3-642-59381-9{\textunderscore}13.

120. Kunte, H., Lentzen, G. & Galinski, E. Industrial Production of the Cell Protectant Ectoine: Protection Mechanisms, Processes, and Products. *Current Biotechnology* **3,** 10–25. ISSN: 22115501 (2014).

121. Kurnasov, O. *et al.* NAD biosynthesis: identification of the tryptophan to quinolinate pathway in bacteria. *Chemistry & biology* **10,** 1195–1204. ISSN: 1074-5521 (2003).

122. Kurz, M., Brünig, A. N. S. & Galinski, E. A. NhaD type sodium/proton-antiporter of *Halomonas elongata*: a salt stress response mechanism in marine habitats? *Saline systems* **2,** 10 (2006).

123. Kwok, A. C. *et al.* Functional responses between PMP3 small membrane proteins and membrane potential. *Environmental Microbiology* **22,** 3066–3080 (2020).

124. Laivenieks, M., Vieille, C. & Zeikus, J. G. Cloning, sequencing, and overexpression of the *Anaerobiospirillum succiniciproducens* phosphoenolpyruvate carboxykinase (*pckA*) gene. *Applied and environmental microbiology* **63,** 2273–2280 (1997).

125. Lambert, L. A., Abshire, K., Blankenhorn, D. & Slonczewski, J. L. Proteins induced in *Escherichia coli* by benzoic acid. *Journal of bacteriology* **179,** 7595–7599. ISSN: 0021-9193 (1997).

126. Larsen, P. I., Sydnes, L. K., Landfald, B. & Strøm, A. R. Osmoregulation in *Escherichia coli* by accumulation of organic osmolytes: betaines, glutamic acid, and trehalose. *Archives of microbiology* **147,** 1–7. ISSN: 0302-8933 (1987).

127. Layer, G., Verfürth, K., Mahlitz, E. & Jahn, D. Oxygen-independent coproporphyrinogen-III oxidase HemN from *Escherichia coli*. *The Journal of biological chemistry* **277,** 34136–34142. ISSN: 0021-9258 (2002).

128. Lazazzera, B. A., Bates, D. M. & Kiley, P. J. The activity of the *Escherichia coli* transcription factor FNR is regulated by a change in oligomeric state. *Genes & development* **7,** 1993–2005. ISSN: 0890-9369 (1993).

129. Lee, P. Y. & Chen, C. Y. Toxicity and quantitative structure-activity relationships of benzoic acids to *Pseudokirchneriella subcapitata*. *Journal of hazardous materials* **165,** 156–161 (2009).

130. Li, B. & Dewey, C. N. RSEM: accurate transcript quantification from RNA-Seq data with or without a reference genome. *BMC bioinformatics* **12,** 323 (2011).

131. Liss, I. N-acetyldiaminobuttersäure, eine neue aminosäure aus dem latex von *Euphorbia pulcherrima* willd ex klotzsch. *Phytochemistry* **1,** 87–88. ISSN: 00319422 (1962).

132. Liu, M. *et al.* Microbial production of ectoine and hydroxyectoine as high-value chemicals. *Microbial Cell Factories* **20,** 1–11 (2021).

133. Liu, R. & Ochman, H. Stepwise formation of the bacterial flagellar system. *Proceedings of the National Academy of Sciences of the United States of America* **104,** 7116–7121. ISSN: 0027-8424 (2007).

134. Madison, L. L. & Huisman, G. W. Metabolic engineering of poly(3-hydroxyalkanoates): from DNA to plastic. *Microbiology and molecular biology reviews : MMBR* **63,** 21–53. ISSN: 1092-2172 (1999).

135. Marin, S. A., Plfüger, G. K., Hobmeier, K. & Kremling, A. EP3608404 (A1) (2020).

136. Martínez-García, E. & de Lorenzo, V. Engineering multiple genomic deletions in Gram-negative bacteria: analysis of the multi-resistant antibiotic profile of *Pseudomonas putida* KT2440. *Environmental microbiology* **13,** 2702–2716 (2011).

137. Maskow, T. & Babel, W. Calorimetrically obtained information about the efficiency of ectoine synthesis from glucose in *Halomonas elongata*. *Biochimica et Biophysica Acta (BBA) - General Subjects* **1527,** 4–10. ISSN: 03044165 (2001).

138. Matsuno, T. & Yumoto, I. Bioenergetics and the role of soluble cytochromes C for alkaline adaptation in gram-negative alkaliphilic *Pseudomonas*. *BioMed research international* **2015,** 847945 (2015).

139. Matsushita, K., Shinagawa, E. & Ameyama, M. in *Carbohydrate Metabolism - Part D* 187–193 (Elsevier, 1982). ISBN: 9780121819897. doi:10.1016/S0076-6879(82)89033-2.

140. Mertens, E. Pyrophosphate-dependent phosphofructokinase, an anaerobic glycolytic enzyme? *FEBS Letters* **285,** 1–5. ISSN: 00145793 (1991).

141. Miller, J. H. *Experiments in molecular genetics* 11. print. ISBN: 0879691069 (Cold Spring Harbor Laboratory, Cold Spring Harbor, NY, 1992).

142. Miller, R. E. & Stadtman, E. R. Glutamate synthase from *Escherichia coli*. An iron-sulfide flavoprotein. *The Journal of biological chemistry* **247,** 7407–7419. ISSN: 0021-9258 (1972).

143. Minato, Y., Fassio, S. R., Reddekopp, R. L. & Häse, C. C. Inhibition of the sodium-translocating NADH-ubiquinone oxidoreductase Na^+-NQR decreases cholera toxin production in *Vibrio cholerae* O1 at the late exponential growth phase. *Microbial pathogenesis* **66,** 36–39 (2014).

144. Mori, M., Hwa, T., Martin, O. C., de Martino, A. & Marinari, E. Constrained Allocation Flux Balance Analysis. *PLoS Computational Biology* **12,** e1004913. ISSN: 1553-734X (2016).

145. Mortazavi, A., Williams, B. A., McCue, K., Schaeffer, L. & Wold, B. Mapping and quantifying mammalian transcriptomes by RNA-Seq. *Nature Methods* **5,** 621–628. ISSN: 1548-7105 (2008).

146. Mothes, G., Schubert, T., Harms, H. & Maskow, T. Biotechnological Coproduction of Compatible Solutes and Polyhydroxyalkanoates using the Genus *Halomonas*. *Engineering in Life Sciences* **8,** 658–662. ISSN: 16180240 (2008).

147. Murai, T., Tokushige, M., Nagai, J. & Katsuki, H. Studies on regulatory functions of malic enzymes. I. Metabolic functions of NAD- and NADP-linked malic enzymes in *Escherichia coli*. *Journal of biochemistry* **71,** 1015–1028. ISSN: 0021-924X (1972).

148. Murata, T., Kawano, M., Igarashi, K., Yamato, I. & Kakinuma, Y. Catalytic properties of Na^+-translocating V-ATPase in *Enterococcus hirae*. *Biochimica et Biophysica Acta (BBA) - Bioenergetics* **1505,** 75–81. ISSN: 00052728 (2001).

149. Nakano, M. *et al.* ATP hydrolysis and synthesis of a rotary motor V-ATPase from *Thermus thermophilus*. *The Journal of biological chemistry* **283,** 20789–20796. ISSN: 0021-9258 (2008).

150. *Escherichia coli and Salmonella: Cellular and molecular biology* 2nd ed. (eds Neidhardt, F. C. & Curtiss, R.) ISBN: 1555810845 (ASM Press, Washington, D.C, 1996).

151. Nelson, K. E. *et al.* Complete genome sequence and comparative analysis of the metabolically versatile *Pseudomonas putida* KT2440. *Environmental microbiology* **4,** 799–808 (2002).

152. Nguyen, Q. A. *Characterization of nitrogen assimilation and PHB accumulation in Halomonas elongata* MA thesis (TU München, 2018).

153. Nicolet, Y. Structure–function relationships of radical SAM enzymes. *Nature Catalysis* **3,** 337–350 (2020).

154. Nikel, P. I., Chavarría, M., Fuhrer, T., Sauer, U. & de Lorenzo, V. *Pseudomonas putida* KT2440 Strain Metabolizes Glucose through a Cycle Formed by Enzymes of the Entner-Doudoroff, Embden-Meyerhof-Parnas, and Pentose Phosphate Pathways. *The Journal of biological chemistry* **290,** 25920–25932. ISSN: 0021-9258 (2015).

155. Noor, E. *et al.* Pathway Thermodynamics Highlights Kinetic Obstacles in Central Metabolism. *PLoS Computational Biology* **10.** ISSN: 1553-734X. doi:10.1371/journal.pcbi.1003483 (2014).

156. O'Brien, R., Chuang, D. T., Taylor, B. L. & Utter, M. F. Novel enzymic machinery for the metabolism of oxalacetate, phosphoenolpyruvate, and pyruvate in *Pseudomonas citronellolis*. *The Journal of biological chemistry* **252,** 1257–1263. ISSN: 0021-9258 (1977).

157. Oh, M.-K., Rohlin, L., Kao, K. C. & Liao, J. C. Global expression profiling of acetate-grown *Escherichia coli*. *The Journal of biological chemistry* **277,** 13175–13183. ISSN: 0021-9258 (2002).

158. Ongagna-Yhombi, S. Y. & Boyd, E. F. Biosynthesis of the osmoprotectant ectoine, but not glycine betaine, is critical for survival of osmotically stressed *Vibrio parahaemolyticus* cells. *Applied and environmental microbiology* **79,** 5038–5049 (2013).

159. Ono, H. *et al.* Characterization of Biosynthetic Enzymes for Ectoine as a Compatible Solute in a Moderately Halophilic Eubacterium, *Halomonas elongata*. *Journal of bacteriology* **181,** 91–99. ISSN: 0021-9193 (1999).

160. Opperman, M. C. *Disruption of Gluconeogenesis in Halomonas elongata: Production and Characterization of a ΔppsA mutant strain* MA thesis (TU München, 2020).

161. O'Regan, M. *et al.* Cloning and nucleotide sequence of the phosphoenolpyruvate carboxylase-coding gene of *Corynebacterium glutamicum* ATCC13032. *Gene* **77,** 237–251 (1989).

162. Oren, A. Bioenergetic aspects of halophilism. *Microbiology and molecular biology reviews : MMBR* **63,** 334–348. ISSN: 1092-2172 (1999).

163. Oren, A. Thermodynamic limits to microbial life at high salt concentrations. *Environmental microbiology* **13,** 1908–1923 (2011).

164. Overton, T. W. Recombinant protein production in bacterial hosts. *Drug discovery today* **19,** 590–601 (2014).

165. Pastor, J. M. *et al.* Role of central metabolism in the osmoadaptation of the halophilic bacterium *Chromohalobacter salexigens*. *The Journal of biological chemistry* **288,** 17769–17781. ISSN: 0021-9258 (2013).

166. Pastor, J. M. *et al.* Fructose metabolism in *Chromohalobacter salexigens*: interplay between the Embden-Meyerhof-Parnas and Entner-Doudoroff pathways. *Microbial cell factories* **18,** 134 (2019).

167. Patra, M. *et al.* Under the influence of alcohol: the effect of ethanol and methanol on lipid bilayers. *Biophysical Journal* **90,** 1121–1135. ISSN: 00063495 (2006).

168. Pereira, J. B. *Integrated analysis of salt tolerance in Halomonas elongata from fermentation data* MA thesis (TU München, 2017).

169. Peters, P., Galinski, E. A. & Trüper, H. G. The biosynthesis of ectoine. *FEMS microbiology letters* **71,** 157–162. ISSN: 0378-1097 (1990).

170. Petri, J. *et al.* Structure of the NDH-2 - HQNO inhibited complex provides molecular insight into quinone-binding site inhibitors. *Biochimica et Biophysica Acta (BBA) - Bioenergetics* **1859,** 482–490. ISSN: 00052728 (2018).

171. Pfeiffer, F. *et al.* Revision and reannotation of the *Halomonas elongata* DSM 2581^T genome. *MicrobiologyOpen* **6.** doi:10.1002/mbo3.465 (2017).

172. Phadtare, S., Alsina, J. & Inouye, M. Cold-shock response and cold-shock proteins. *Current opinion in microbiology* **2,** 175–180. ISSN: 1369-5274 (1999).

173. Prieto, A. *et al.* A holistic view of polyhydroxyalkanoate metabolism in *Pseudomonas putida*. *Environmental microbiology* **18,** 341–357 (2016).

174. Prossliner, T., Skovbo Winther, K., Sørensen, M. A. & Gerdes, K. Ribosome Hibernation. *Annual review of genetics* **52,** 321–348 (2018).

175. Qin, Q. *et al.* CRISPR/Cas9 editing genome of extremophile *Halomonas* spp. *Metabolic engineering* **47,** 219–229 (2018).

176. Quax, T. E. F., Claassens, N. J., Söll, D. & van der Oost, J. Codon Bias as a Means to Fine-Tune Gene Expression. *Molecular cell* **59,** 149–161 (2015).

177. Ran, F. A. *et al.* Genome engineering using the CRISPR-Cas9 system. *Nature protocols* **8,** 2281–2308 (2013).

178. Reitzer, L. in *Reference Module in Biomedical Sciences* (Elsevier, 2014). ISBN: 9780128012383. doi:10.1016/B978-0-12-801238-3.02427-2.

179. Ridley-Thomas, C. I., Austin, A., Lucey, W. P. & Clark, M. Variability in the determination of ash free dry weight for periphyton communities: A call for a standard method. *Water Research* **23,** 667–670. ISSN: 00431354 (1989).

180. Rosa, L. T., Bianconi, M. E., Thomas, G. H. & Kelly, D. J. Tripartite ATP-Independent Periplasmic (TRAP) Transporters and Tripartite Tricarboxylate Transporters (TTT): From Uptake to Pathogenicity. *Frontiers in cellular and infection microbiology* **8,** 33 (2018).

181. Salapatek, A. M. *et al.* Effects of ectoine containing nasal spray and eye drops on symptoms of seasonal allergic rhinoconjunctivitis. *Clinical and translational allergy* **11,** e12006 (2021).

182. Salvador, M. *et al.* Quantitative RNA-seq Analysis Unveils Osmotic and Thermal Adaptation Mechanisms Relevant for Ectoine Production in *Chromohalobacter salexigens*. *Frontiers in microbiology* **9,** 1845. ISSN: 1664-302X (2018).

183. Sauer, T. & Galinski, E. A. Bacterial milking: A novel bioprocess for production of compatible solutes. *Biotechnology and Bioengineering* **57,** 306–313. ISSN: 0006-3592 (1998).

184. Sauer, U. & Eikmanns, B. J. The PEP-pyruvate-oxaloacetate node as the switch point for carbon flux distribution in bacteria. *FEMS microbiology reviews* **29,** 765–794. ISSN: 0168-6445 (2005).

185. Schröter, M.-A. *et al.* Ectoine protects DNA from damage by ionizing radiation. *Scientific reports* **7,** 1–7 (2017).

186. Schweikhard, E. S., Kuhlmann, S. I., Kunte, H.-J., Grammann, K. & Ziegler, C. M. Structure and function of the universal stress protein TeaD and its role in regulating the ectoine transporter TeaABC of *Halomonas elongata* DSM 2581^T. *Biochemistry* **49,** 2194–2204 (2010).

187. Schwentner, A. *et al.* Modular systems metabolic engineering enables balancing of relevant pathways for l-histidine production with *Corynebacterium glutamicum*. *Biotechnology for biofuels* **12,** 65. ISSN: 1754-6834 (2019).

188. Schwibbert, K. *et al.* A blueprint of ectoine metabolism from the genome of the industrial producer *Halomonas elongata* DSM 2581^T. *Environmental microbiology* **13,** 1973–1994 (2011).

189. Scott, M., Gunderson, C. W., Mateescu, E. M., Zhang, Z. & Hwa, T. Interdependence of cell growth and gene expression: origins and consequences. *Science* **330,** 1099–1102. ISSN: 0036-8075 (2010).

190. Sehr, C., Kremling, A. & Marin-Sanguino, A. Design Principles as a Guide for Constraint Based and Dynamic Modeling: Towards an Integrative Workflow. *Metabolites* **5,** 601–635. ISSN: 2218-1989 (2015).

191. Sevilla, E., Bes, M. T., González, A., Peleato, M. L. & Fillat, M. F. Redox-Based Transcriptional Regulation in Prokaryotes: Revisiting Model Mechanisms. *Antioxidants & redox signaling* **30,** 1651–1696 (2019).

192. Shepherd, M. & Poole, R. K. in *Encyclopedia of biophysics* (ed Roberts, G. C. K.) 172–177 (Springer, Berlin, 2013). ISBN: 978-3-642-16711-9. doi:10 . 1007 / 978 - 3 - 642 - 16712 - 6{\textunderscore}30.

193. Siebers, B., Klenk, H. P. & Hensel, R. PP$_i$-dependent phosphofructokinase from *Thermoproteus tenax*, an archaeal descendant of an ancient line in phosphofructokinase evolution. *Journal of bacteriology* **180,** 2137–2143. ISSN: 0021-9193 (1998).

194. Silva-Rocha, R. *et al.* The Standard European Vector Architecture (SEVA): a coherent platform for the analysis and deployment of complex prokaryotic phenotypes. *Nucleic acids research* **41,** D666–75 (2013).

195. Singh, V. K., Singh, K. & Baum, K. The Role of Methionine Sulfoxide Reductases in Oxidative Stress Tolerance and Virulence of *Staphylococcus aureus* and Other Bacteria. *Antioxidants (Basel, Switzerland)* **7.** ISSN: 2076-3921. doi:10.3390/antiox7100128 (2018).

196. *Principles of Bioenergetics* (eds Skulachev, V. P., Bogachev, A. V. & Kasparinsky, F. O.) ISBN: 978-3-642-33429-0. doi:10.1007/978-3-642-33430-6 (Springer Berlin Heidelberg, Berlin, Heidelberg, 2013).

197. Søltoft-Jensen, J. & Hansen, F. in *Emerging Technologies for Food Processing* 387–416 (Elsevier, 2005). ISBN: 9780126767575. doi:10.1016/B978-012676757-5/50017-7.

198. Stalker, D. M., Kolter, R. & Helinski, D. R. Plasmid R6K DNA replication. *Journal of molecular biology* **161,** 33–43. ISSN: 0022-2836 (1982).

199. Stratford, M. & Eklund, T. in *Food Preservatives* (eds Russell, N. J. & Gould, G. W.) 48–84 (Springer US, Boston, MA, 2003). ISBN: 978-1-4757-1006-9. doi:10.1007/978-0-387-30042-9_4.

200. Strigul, N., Dette, H. & Melas, V. B. A practical guide for optimal designs of experiments in the Monod model. *Environmental Modelling & Software* **24,** 1019–1026. ISSN: 13648152 (2009).

201. Swartz, T. H., Ikewada, S., Ishikawa, O., Ito, M. & Krulwich, T. A. The Mrp system: a giant among monovalent cation/proton antiporters? *Extremophiles : life under extreme conditions* **9,** 345–354 (2005).

202. Sweeney, T. E. & Beuchat, C. A. Limitations of methods of osmometry: measuring the osmolality of biological fluids. *The American journal of physiology* **264,** R469–80. ISSN: 0002-9513 (1993).

203. Szenk, M., Dill, K. A. & de Graff, A. M. R. Why Do Fast-Growing Bacteria Enter Overflow Metabolism? Testing the Membrane Real Estate Hypothesis. *Cell systems* **5,** 95–104. ISSN: 2405-4712 (2017).

204. Takase, K., Yamato, I. & Kakinuma, Y. Cloning and sequencing of the genes coding for the A and B subunits of vacuolar-type Na^+-ATPase from *Enterococcus hirae*. Coexistence of vacuolar- and F0F1-type ATPases in one bacterial cell. *The Journal of biological chemistry* **268,** 11610–11616. ISSN: 0021-9258 (1993).

205. Tokunaga, H., Arakawa, T. & Tokunaga, M. Novel soluble expression technologies derived from unique properties of halophilic proteins. *Applied microbiology and biotechnology* **88,** 1223–1231 (2010).

206. Toyama, H. *et al.* Membrane-bound, 2-keto-D-gluconate-yielding D-gluconate dehydrogenase from "*Gluconobacter dioxyacetonicus*" IFO 3271: molecular properties and gene disruption. *Applied and environmental microbiology* **73,** 6551–6556 (2007).

207. Tribelli, P. M., Nikel, P. I., Oppezzo, O. J. & López, N. I. Anr, the anaerobic global regulator, modulates the redox state and oxidative stress resistance in *Pseudomonas extremaustralis*. *Microbiology (Reading, England)* **159,** 259–268. ISSN: 1350-0872 (2013).

208. Tromans, D. Modeling Oxygen Solubility in Water and Electrolyte Solutions. *Industrial & Engineering Chemistry Research* **39,** 805–812. ISSN: 0888-5885 (2000).

209. Trösch, R. & Willmund, F. The conserved theme of ribosome hibernation: from bacteria to chloroplasts of plants. *Biological chemistry* **400,** 879–893 (2019).

210. Ueta, M. *et al.* Role of HPF (hibernation promoting factor) in translational activity in *Escherichia coli*. *Journal of biochemistry* **143,** 425–433. ISSN: 0021-924X (2008).

211. Ulfstedt, M., Hu, G.-Z., Johansson, M. & Ronne, H. Testing of Auxotrophic Selection Markers for Use in the Moss *Physcomitrella* Provides New Insights into the Mechanisms of Targeted Recombination. *Frontiers in plant science* **8,** 1850. ISSN: 1664-462X (2017).

212. Unden, G. & Bongaerts, J. Alternative respiratory pathways of *Escherichia coli*: energetics and transcriptional regulation in response to electron acceptors. *Biochimica et Biophysica Acta (BBA) - Bioenergetics* **1320,** 217–234. ISSN: 00052728 (1997).

213. Unden, G. *et al.* Control of FNR function of *Escherichia coli* by O2 and reducing conditions. *Journal of molecular microbiology and biotechnology* **4,** 263–268. ISSN: 1464-1801 (2002).

214. Van der Valk, T. *et al.* Million-year-old DNA sheds light on the genomic history of mammoths. *Nature* **591,** 265–269 (2021).

215. van Heeswijk, W. C., Westerhoff, H. V. & Boogerd, F. C. Nitrogen assimilation in *Escherichia coli*: putting molecular data into a systems perspective. *Microbiology and molecular biology reviews : MMBR* **77,** 628–695. ISSN: 1092-2172 (2013).

216. Vandrich, J., Pfeiffer, F., Alfaro-Espinoza, G. & Kunte, H. J. Contribution of mechanosensitive channels to osmoadaptation and ectoine excretion in Halomonas elongata. *Extremophiles : life under extreme conditions* **24,** 421–432 (2020).

217. Vargas, C., Fernández-Castillo, R., Cánovas, D., Ventosa, A. & Nieto, J. J. Isolation of cryptic plasmids from moderately halophilic eubacteria of the genus *Halomonas*. Characterization of a small plasmid from *H. elongata* and its use for shuttle vector construction. *Molecular and General Genetics MGG* **246,** 411–418. ISSN: 0026-8925 (1995).

218. Vemuri, G. N., Eiteman, M. A., McEwen, J. E., Olsson, L. & Nielsen, J. Increasing NADH oxidation reduces overflow metabolism in *Saccharomyces cerevisiae*. *Proceedings of the National Academy of Sciences of the United States of America* **104,** 2402–2407. ISSN: 0027-8424 (2007).

219. Ventosa, A., Nieto, J. J. & Oren, A. Biology of moderately halophilic aerobic bacteria. *Microbiology and molecular biology reviews : MMBR* **62,** 504–544. ISSN: 1092-2172 (1998).

220. Vidal, L., Pinsach, J., Striedner, G., Caminal, G. & Ferrer, P. Development of an antibiotic-free plasmid selection system based on glycine auxotrophy for recombinant protein overproduction in *Escherichia coli*. *Journal of biotechnology* **134,** 127–136. ISSN: 0168-1656 (2008).

221. Vreeland, R. H., Litchfield, C. D., Martin, E. L. & Elliot, E. *Halomonas elongata*, a New Genus and Species of Extremely Salt-Tolerant Bacteria. *International Journal of Systematic Bacteriology* **30,** 485–495. ISSN: 0020-7713 (1980).

222. Wagner, G. P., Kin, K. & Lynch, V. J. Measurement of mRNA abundance using RNA-seq data: RPKM measure is inconsistent among samples. *Theory in biosciences = Theorie in den Biowissenschaften* **131,** 281–285 (2012).

223. Wagner, S. G. *Systematische Analyse der heterologen Expression in Escherichia coli* PhD thesis (2019).

224. Wakai, S. Biochemical and thermodynamic analyses of energy conversion in extremophiles. *Bioscience, biotechnology, and biochemistry* **83,** 49–64 (2019).

225. Wang, D.-M. *et al.* A Membrane-Bound Gluconate Dehydrogenase from 2-Keto-D-Gluconic Acid Industrial Producing Strain *Pseudomonas plecoglossicida* JUIM01: Purification, Characterization, and Gene Identification. *Applied biochemistry and biotechnology* **188,** 897–913 (2019).

226. Wang, Q. & Nomura, C. T. Monitoring differences in gene expression levels and polyhydroxyalkanoate (PHA) production in *Pseudomonas putida* KT2440 grown on different carbon sources. *Journal of Bioscience and Bioengineering* **110,** 653–659. ISSN: 1389-1723 (2010).

227. Waschina, S., D'Souza, G., Kost, C. & Kaleta, C. Metabolic network architecture and carbon source determine metabolite production costs. *The FEBS journal* **283,** 2149–2163 (2016).

228. Weinel, C., Nelson, K. E. & Tümmler, B. Global features of the *Pseudomonas putida* KT2440 genome sequence. *Environmental microbiology* **4,** 809–818 (2002).

229. Weissbach, H. *et al.* Peptide methionine sulfoxide reductase: structure, mechanism of action, and biological function. *Archives of biochemistry and biophysics* **397,** 172–178. ISSN: 0003-9861 (2002).

230. Weissman, S. A. & Anderson, N. G. Design of Experiments (DoE) and Process Optimization. A Review of Recent Publications. *Organic Process Research & Development* **19,** 1605–1633. ISSN: 1083-6160 (2015).

231. Weitzman, P. Regulation of citrate synthase activity in *Escherichia coli*. *Biochimica et Biophysica Acta (BBA) - Enzymology and Biological Oxidation* **128,** 213–215. ISSN: 09266593 (1966).

232. Weitzman, P. Allosteric fine control of citrate synthase in *Escherichia coli*. *Biochimica et Biophysica Acta (BBA) - Enzymology* **139,** 526–528. ISSN: 00052744 (1967).

233. Werner, C., Doenst, T. & Schwarzer, M. in *The Scientist's Guide to Cardiac Metabolism* 39–55 (Elsevier, 2016). ISBN: 9780128023945. doi:10.1016/B978-0-12-802394-5.00004-2.

234. Wifling, K. & Dimroth, P. Isolation and characterization of oxaloacetate decarboxylase of *Salmonella typhimurium*, a sodium ion pump. *Archives of microbiology* **152,** 584–588. ISSN: 0302-8933 (1989).

235. Wikström, M. & Hummer, G. Stoichiometry of proton translocation by respiratory complex I and its mechanistic implications. *Proceedings of the National Academy of Sciences of the United States of America* **109,** 4431–4436. ISSN: 0027-8424 (2012).

236. Windass, J. D. *et al.* Improved conversion of methanol to single-cell protein by *Methylophilus methylotrophus*. *Nature* **287,** 396–401 (1980).

237. Wolf, A., Krämer, R. & Morbach, S. Three pathways for trehalose metabolism in *Corynebacterium glutamicum* ATCC13032 and their significance in response to osmotic stress. *Molecular microbiology* **49,** 1119–1134. ISSN: 0950-382X (2003).

238. Wood, H. G. & Utter, M. F. The role of CO2 fixation in metabolism. *Essays in biochemistry* **1,** 1–27. ISSN: 0071-1365 (1965).

239. Xu, C. *et al.* Proteomic analysis on the expression of outer membrane proteins of *Vibrio alginolyticus* at different sodium concentrations. *Proteomics* **5,** 3142–3152. ISSN: 1615-9853 (2005).

240. Yang, C., Hua, Q., Baba, T., Mori, H. & Shimizu, K. Analysis of *Escherichia coli* anaplerotic metabolism and its regulation mechanisms from the metabolic responses to altered dilution rates and phosphoenolpyruvate carboxykinase knockout. *Biotechnology and Bioengineering* **84,** 129–144. ISSN: 0006-3592 (2003).

241. Yano, T. & Koga, S. Dynamic behavior of the chemostat subject to substrate inhibition. *Biotechnology and Bioengineering* **11,** 139–153. ISSN: 0006-3592 (1969).

242. Ye, J.-W. & Chen, G.-Q. *Halomonas* as a chassis. *Essays in Biochemistry* **65,** 393–403 (2021).

243. Yin, J., Chen, J.-C., Wu, Q. & Chen, G.-Q. Halophiles, coming stars for industrial biotechnology. *Biotechnology advances* **33,** 1433–1442 (2015).

244. Ying, W. NAD^+/NADH and $NADP^+$/NADPH in cellular functions and cell death: regulation and biological consequences. *Antioxidants & redox signaling* **10,** 179–206 (2008).

245. Yudkin, M. D. & Moses, V. Carabolite repression of the *lac* operon. Repression of translation. *The Biochemical journal* **113,** 423–428 (1969).

246. Yue, H. *et al.* A seawater-based open and continuous process for polyhydroxyalkanoates production by recombinant *Halomonas campaniensis* LS21 grown in mixed substrates. *Biotechnology for biofuels* **7.** ISSN: 1754-6834. doi:10.1186/1754-6834-7-108 (2014).

247. Zaccai, G. *et al.* Neutrons describe ectoine effects on water H-bonding and hydration around a soluble protein and a cell membrane. *Scientific reports* **6,** 31434 (2016).

248. Zamboni, N., Maaheimo, H., Szyperski, T., Hohmann, H.-P. & Sauer, U. The phosphoenolpyruvate carboxykinase also catalyzes C3 carboxylation at the interface of glycolysis and the TCA cycle of *Bacillus subtilis*. *Metabolic engineering* **6,** 277–284 (2004).

249. Zelcbuch, L. *et al.* Spanning high-dimensional expression space using ribosome-binding site combinatorics. *Nucleic acids research* **41,** e98 (2013).

250. Zhang, J. & Greasham, R. Chemically defined media for commercial fermentations. *Applied microbiology and biotechnology* **51,** 407–421 (1999).

251. Zhang, L.-h., Lang, Y.-j. & Nagata, S. Efficient production of ectoine using ectoine-excreting strain. *Extremophiles : life under extreme conditions* **13,** 717–724 (2009).

252. Zhao, S., Ye, Z. & Stanton, R. Misuse of RPKM or TPM normalization when comparing across samples and sequencing protocols. *RNA (New York, N.Y.)* **26,** 903–909 (2020).

253. Zhao, S. *et al.* Comparison of stranded and non-stranded RNA-seq transcriptome profiling and investigation of gene overlap. *BMC genomics* **16,** 675 (2015).

254. Zhu, M. & Dai, X. Growth suppression by altered (p)ppGpp levels results from non-optimal resource allocation in *Escherichia coli*. *Nucleic acids research* **47,** 4684–4693 (2019).

A Supplementary material

A.1 Supplementary figures

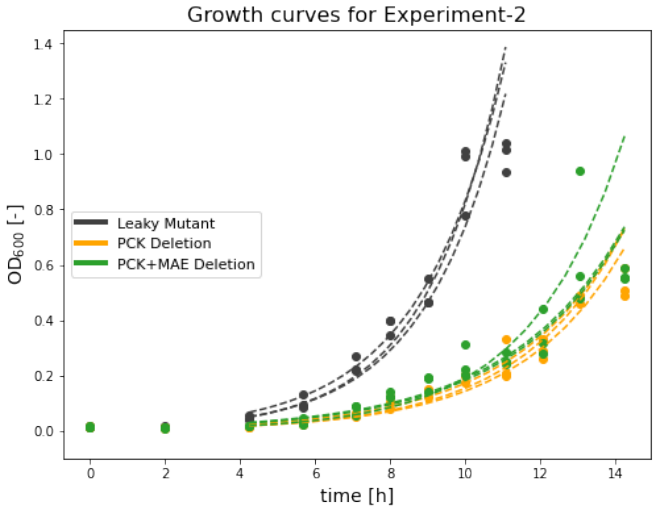

(a) Growth curves for batch experiment 2

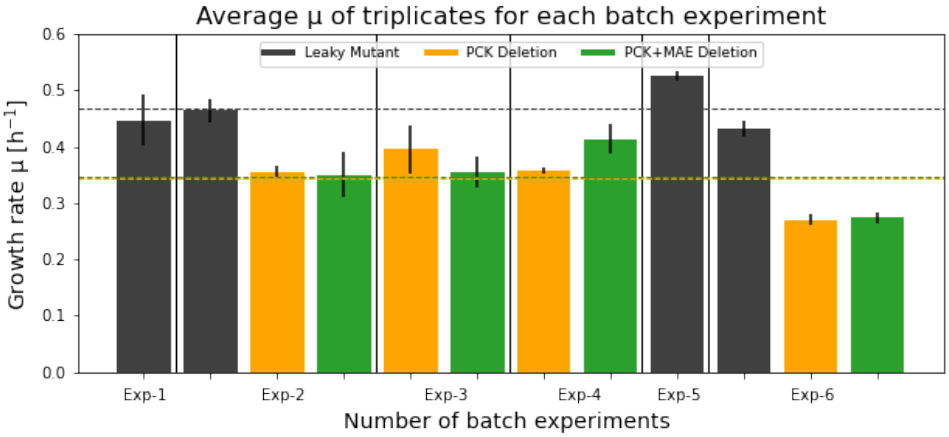

(b) Growth curves for all shake flask experiments

Figure A.1: Overview of all growth rates observed in the experiments performed in shaking flasks with the Leaky Mutant (black) and the modified strains *H. elongata*-PCK (orange) and *H. elongata*-PCKMAE (green). All experiments were carried out at 1 M NaCl and with glucose as the sole substrate. Different batches are shown by vertical lines and the numeration of experiments. The overall averages are depicted as dashed lines in the respective colors. Growth curves observed in batch experiment 2 with all three strains growing in the same experiment. The Leaky Mutant clearly shows an adavantage over the modified strains.

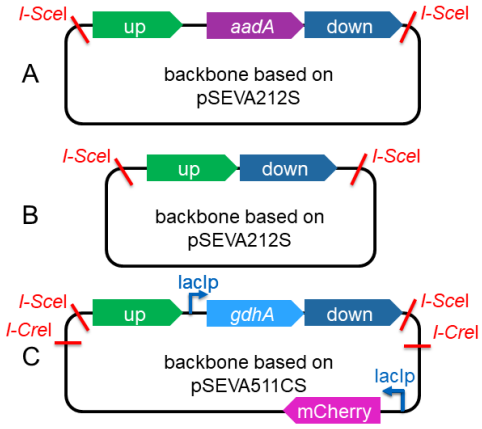

(a) Backbones for the integration vectors

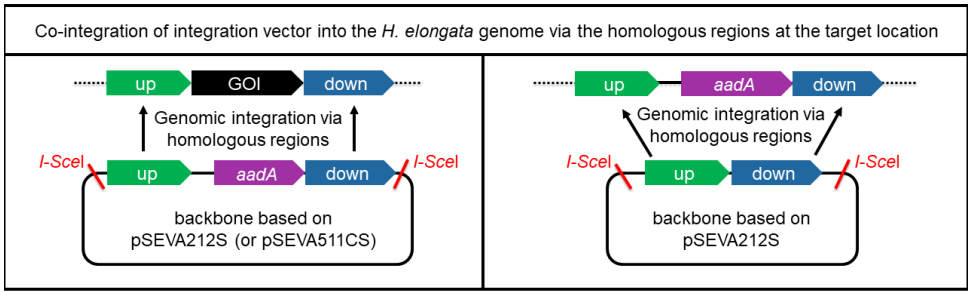

(b) Genome integration of the substitution (left) or deletion (right) vector

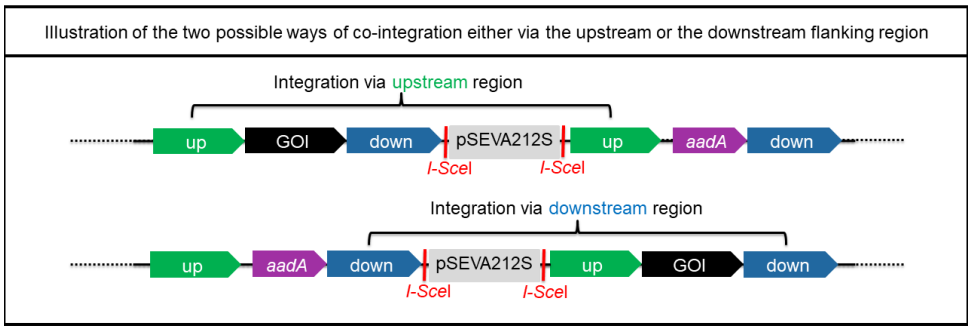

(c) The two possible orientations of co-integration

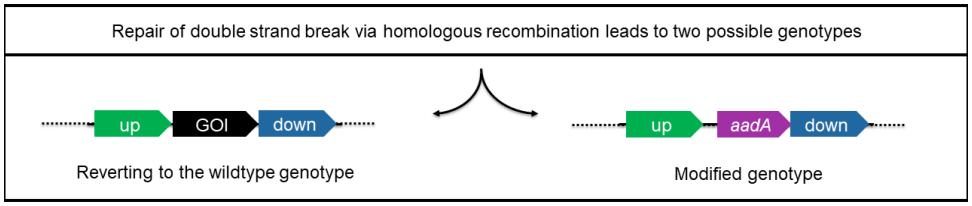

(d) Possible genotypes after homologous recombination

Figure A.2: Illustration of the workflow for genome modifications via homologous recombination as described in Hobmeier *et al.* [86] adapted from Martínez-García & de Lorenzo [136].

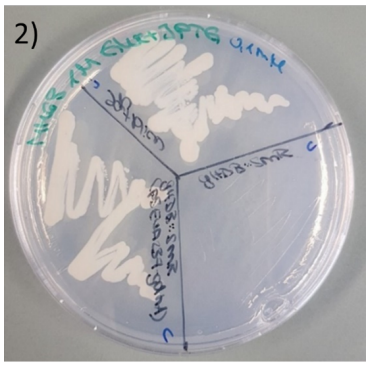

Figure A.3: Pre-experiment on solid minimal medium shows that NADPH-GDH from *P. putida* confers the ability to the auxotrophic *H. elongata* strain KHN1 to utilize ammonia again. Plated on the left (*gltDB*::Sm^R (pSEVA237-*gdhA*)) is KHN1 (pSEVA237-*gdhA*). The *H. elongata* wild type (top) and the auxotrophic strain KHN1 (right, *gltDB*::Sm^R) are added as controls.

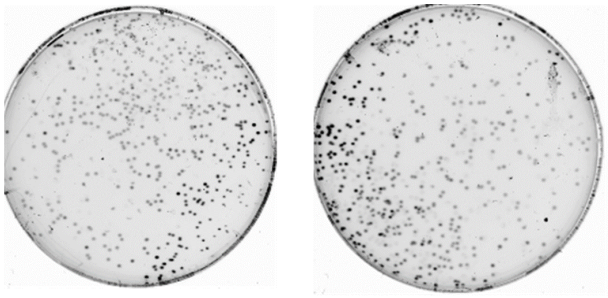

Figure A.4: Fluorescent eGFP imaging in single colonies: shown are non-selective LB agar plates with KHN1 (pSEVA238-eGFP/*lacIp-gdhA*) colonies after cultivation without selection pressure in liquid complex medium grown up to the stationary phase. The cultures were induced to produce eGFP in the liquid culture. Plasmid loss is indicated by the abscence of eGFP fluorescence which is shown in this imaging by the intensity of the color. Colonies with high amounts of eGFP fluorescence appear darker, almost black, depending on the amount of eGFP protein. On these plates it is overt that a lot of colonies appear more grey and, thus, show no eGFP fluorescence indicating a plasmid loss for many of the colony-forming units.

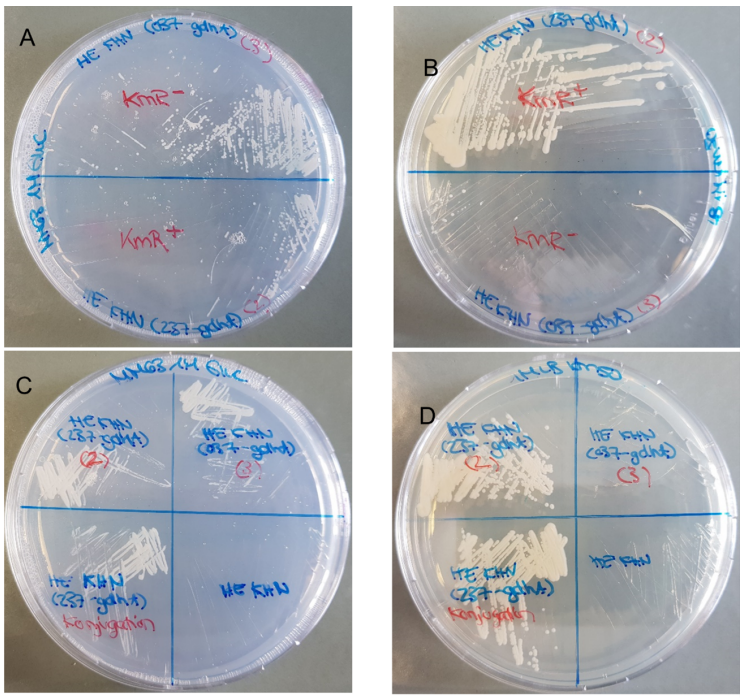

Figure A.5: Phenotypes of plasmid bearing auxotrophic strain *H. elongata*-GLT (also called KHN1 or simply KHN). A Comparison of the plasmids pSEVA237-*gdhA* and the auxotrophic plasmid pSEVA037-*gdhA* with the KmR cassette removed. On a MM63 minimal medium plate with Glucose as carbon and Ammonium as nitrogen source but without Km^R, both strains can grow. **B** Same setup as **A** but with supplementation of Km. Only the strain with pSEVA237-*gdhA* is able to grow. **C** Comparison of the auxotrophic strain KHN (bottom right) unable to grow on minimal medium with plasmid bearing KHN strains. Top right: pSEVA037-*gdhA*, top left and bottom left: pSEVA237-*gdhA*. Both plasmids facilitate growth on minimal medium. **D** Same setup as **C** but tested is growth in complex medium with supplementation of Km. Here, only the strains harboring the plasmid pSEVA237-*gdhA* can grow. The plasmid without kanamycin resistance pSEVA037-*gdhA* and the auxotrophic strain both cannot grow.

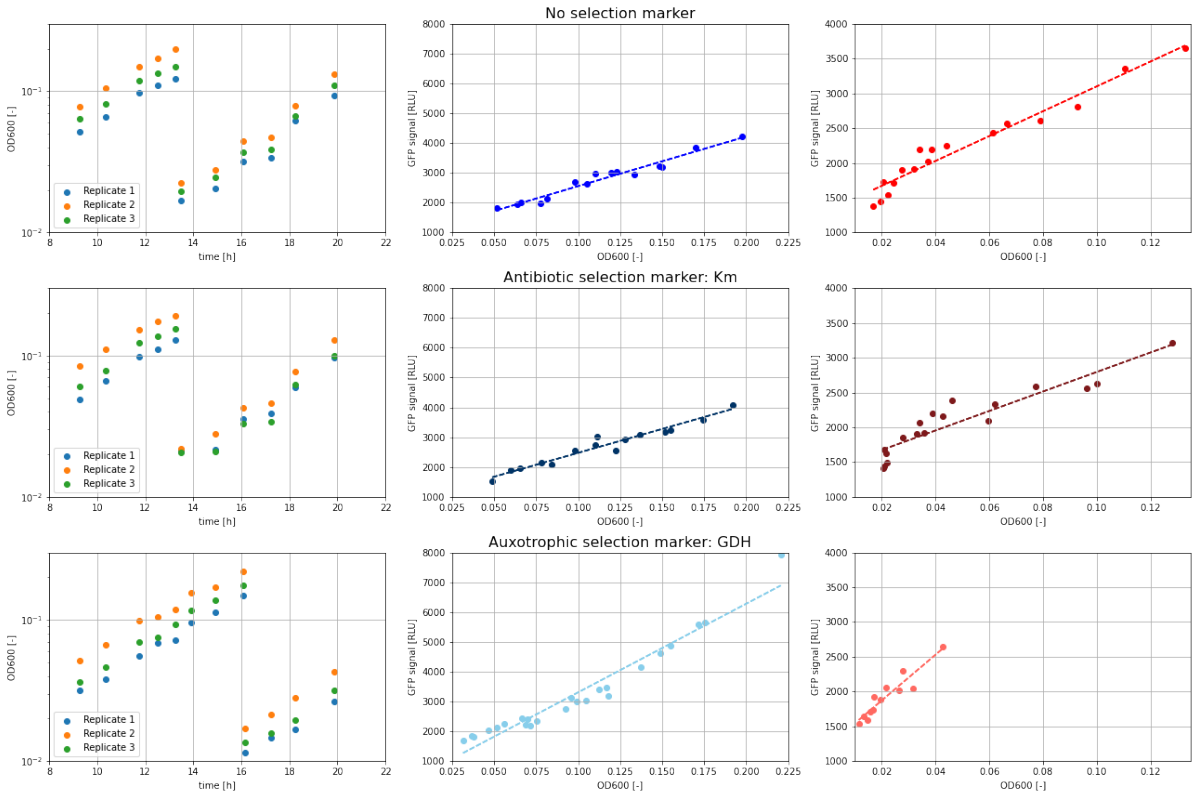

Figure A.6: Detailed analysis of the plasmid loss experiment in KHN1 with the plasmid pSEVA238-eGFP/*lacIp-gdhA* which inducibly produces eGFP. The OD600 values are shown in the first column for three biological replicates for each medium (rows), triggering different selection pressures for plasmid maintenance. The different selection pressures are organized in the rows with the first row representing medium with no selection, the second row representing an antibiotic selection using kanamycin, and the third row representing the auxotrophic selection via GDH. The OD600 values in the first column show two growth phases. After reaching an OD600 of approximately 0.25 the cultures were diluted to avoid a reduction in growth rate which was observed for higher OD600 values in this strain. The second column depicts the eGFP singal per OD600 values in the first growth phase (blue colors) and the third column depicts the same for the second growth phase (red colors). A linear regression was performed for the eGFP signal in both growth phases, indicated by the dashed regression lines. Differences in the slopes show the amount of eGFP per OD600 indicating the amount of plasmids present in the strain for each medium. A steeper slope suggests that there is more fluorophore at less biomass indicative for a higher number of plasmids.

A.2 Supplementary tables

Table A.1: Overview of the used bacterial strains including the genetic modifications, the names which are used in this work and the respective references to their origin.

Strain	Modifications	Name in this work	Reference
H. elongata DSM 2581		Wild type, WT	[221]
H. elongata DSM 2581	Δ*teaABC*Δ*doeA*	Leaky Mutant, LM, KB2.13	[119]
H. elongata DSM 2581	Δ*teaABC*Δ*doeA* Δ*ppc*::Sm	*H. elongata*-PPC::Sm	[86]
H. elongata DSM 2581	Δ*teaABC*Δ*doeA* Δ*ppc*	*H. elongata*-PPC	[86]
H. elongata DSM 2581	Δ*teaABC*Δ*doeA* Δ*oad*::Sm	*H. elongata*-OAD::Sm	[86]
H. elongata DSM 2581	Δ*teaABC*Δ*doeA* Δ*oad*	*H. elongata*-OAD	[86]
H. elongata DSM 2581	Δ*teaABC*Δ*doeA* Δ*pckA*::Sm	*H. elongata*-PCK::Sm	[135]
H. elongata DSM 2581	Δ*teaABC*Δ*doeA* Δ*pckA*	*H. elongata*-PCK	[135]
H. elongata DSM 2581	Δ*teaABC*Δ*doeA* Δ*pckA*Δ*maeB*::Sm	*H. elongata*-PCKMAE::Sm	[135]
H. elongata DSM 2581	Δ*teaABC*Δ*doeA* Δ*pckA*Δ*maeB*	*H. elongata*-PCKMAE	[135]
H. elongata DSM 2581	Δ*teaABC*Δ*doeA* Δ*pckA*Δ*ppc*	*H. elongata*-PCKPPC	This work
H. elongata DSM 2581	Δ*gltDB*::Sm	*H. elongata*-GLT, KHN1	This work
H. elongata DSM 2581	Δ*gltDB*::Sm Δ*gdh*::*gdhA*	KHN2	This work
H. elongata DSM 2581	Δ*teaABC*Δ*doeA* Δ*gltDB*::Sm	KHN3	This work
H. elongata DSM 2581	Δ*teaABC*Δ*doeA* Δ*gltDB*::Sm Δ*gdh*::*gdhA*	KHN4, KHN5	This work
H. elongata DSM 2581	Δ*ectC*	*H. elongata* Δ*ectC*	BAM
H. elongata DSM 2581	Δ*ectC*σ^{38} RBS	*H. elongata* Δ*ectC*σ^{38} RBS	BAM
P. putida KT2440		*P. putida*	[151]
E. coli DH5α *λpir*		*E. coli* DH5α *λpir*	[78]
E. coli HB101		*E. coli* HB101	[24]

Table A.2: All used antibiotics and the applied concentrations depending on the microbe.

Antibiotic	Abbreviation	Working Concentration [μg/mL]
Ampicillin	Am, AmR	*H. elongata*: 500, *E. coli*: 100
Kanamycin	Km, KmR	*H. elongata*: 50, *E. coli*: 50
Gentamicin	Gm, GmR	*H. elongata*: 50, *E. coli*: 10
Streptomycin	Sm, SmR	*H. elongata*: 200, *E. coli*: 200
Tetracycline	Tc, TcR	*H. elongata*: 10, *E. coli*: 10
Chloramphenicol	Cm, CmR	*H. elongata*: 34, *E. coli*: 34

Table A.3: Overview of all plasmids used which were already pre-existing and were not cloned in the course of this work.

Plasmid	ABR	Description	Reference
pRK600	Cm	Helper plasmid for plasmid mobilization during bacterial mating	[104]
pSEVA237R-31	Km	Plasmid for constitutive expression of mCherry via the *lacIp* promoter	[223]
pSEVA237R-32	Km	Plasmid for constitutive expression of eGFP via the *lacIp* promoter	[223]
pSEVA438	Sm	Cloning vector in pSEVA line, harbors the inducible XylS/Pm promoter system	[194]
pSEVA212S	Km	Cloning vector in pSEVA line, harbors two I-SceI recognition sites around the multiple cloning site, used in homologous recombination	[136]
pSEVA434	Sm	Cloning vector used as a template for the SmR cassette	[194]
pSW-2	Gm	Expression vector for I-SceI endonuclease	[136]
pSEVA212S-Δ*ppc*	Km	Integration vector for PEPC deletion in *H. elongata*	[86]
pSEVA338	Cm	Cloning vector in pSEVA line, harbors the inducible XylS/Pm promoter system	[194]
pSEVA411	Sm	Cloning vector in pSEVA line	[194]

Table A.4: Overview of all cloned plasmids throughout this work with the respective cloning method, either via traditional restriction/ligation cloning or via Gibson Assembly.

Plasmid	ABR	Description	[bp]	Method
pSEVA438-eGFP	Sm	Expression plasmid for eGFP via XylS/Pm	5830	Restriction, Ligation
pSEVA438-mCherry	Sm	Expression plasmid for mCherry via XylS/Pm	5833	Restriction, Ligation
pSEVA212S-$\Delta pckA$::Sm^R	Km, Sm	Integration vector for substitution of *pckA* with a Sm cassette in *H. elongata*	4815	Gibson Assembly
pSEVA212S-$\Delta pckA$	Km	Integration vector for deletion of *pckA* in *H. elongata*	3826	Gibson Assembly
pSEVA212S-$\Delta maeB$::Sm^R	Km, Sm	Integration vector for substitution of *maeB* with a Sm cassette in *H. elongata*	4980	Gibson Assembly
pSEVA212S-$\Delta maeB$	Km	Integration vector for deletion of *maeB* in *H. elongata*	3991	Gibson Assembly
pSEVA438-*teaBC*	Sm	Expression plasmid for *teaBC* via XylS/Pm	7009	Gibson Assembly
pSEVA438-*teaB*	Sm	Expression plasmid for *teaB* via XylS/Pm	5707	Gibson Assembly
pSEVA438-*teaC*	Sm	Expression plasmid for *teaC* via XylS/Pm	6397	Gibson Assembly
pSEVA212S-Δ *gltDB*::Sm^R	Km, Sm	Integration vector for substitution of *gltDB* with a Sm cassette in *H. elongata*	4999	Gibson Assembly
pSEVA338-*gltDB*	Cm	Expression plasmid for *gltDB* via XylS/Pm	10811	Gibson Assembly
pSEVA237-*gdhA*	Km	Expression plasmid for *gdhA* from *P. putida* via *lacIp*	4515	Gibson Assembly
pSEVA511CS	Tc	Backbone for the construction of integration plasmids, harbors I-SceI and I-CreI recognition sites	3229	Restriction, Ligation
pSEVA211CS	Km	Backbone for the construction of integration plasmids, harbors I-SceI and I-CreI recognition sites	2966	Restriction, Ligation
pSEVA511CS-Δgdh :: *gdhA*	Tc	Integration plasmid for the substitution of *gdh* with *gdhA* from*P. putida* in *H. elongata*	5938	Gibson Assembly
pSEVA212-Δgdh :: *gdhA*	Km	Integration plasmid for the substitution of *gdh* with *gdhA* from*P. putida* in *H. elongata*	5006	Restriction, Ligation
pSEVA037-*gdhA*	None	Expression plasmid for *gdhA* from *P. putida* via *lacIp* without ABR cassette	3503	Restriction, Ligation
pSEVA238-eGFP/*lacIp-gdhA*	Km	Expression plasmid for *gdhA* from *P. putida* (*lacIp*) and eGFP (XylS/Pm)	7219	Restriction, Ligation

Table A.5: Oligonucleotides used for polymerase chain reactions. The primers annealing to the template are given in black lower case letters. In case a synthetic ribosomal binding site is inserted it is indicated in grey. Recognition sites for general restriction enzymes are underlined in black, the recognition site of the I-SceI homing endonuclease is underlined in grey, and the recognition site of the I-CreI homing endonuclease is underlined in blue. Gibson Assembly overhangs are written in upper case. Bases in parenthesis are added next to restriction sites in order to increase the surface for an improved binding of the restriction enzyme to the DNA. The annealing temperatures were determined using the *NEB Tm Calculator* tool.

Oligonucleotide	**Sequence 5′ → 3′**
Gibson Assembly cloning of pSEVA438-*teaBC*, pSEVA438-*teaB*, pSEVA438-*teaC*	
438 *teaBC* fwdP	GCCGCGCGAATTCgagctcaggaggcttcatatgaccgacgaagaagaag
438 *teaBC* revP	CAGTCACGACGCGGCCGCaagcttttacctgaaacgcagatcg
438 *teaB* revP	GCGGCCGCAAGCTTGCATGCctgcagtcagacttccgtttccgtatcc
438 *teaC* fwdP	CCGCGCGAATTCgagctcaggaggcttcatatgacgacaataatggttgc
Gibson Assembly cloning of pSEVA511SC and pSEVA211SC	
SP Cre-Sce MCS FWD	(TTTT)ttaattaacaaaacgtcgtgagacagtttggtattaccctgttatccctaagcggataacaatttcacacag
SP MCS Cre-Sce REV	ccctaaccaaactgtctcacgacgttttgcgccagggttttcccag
SP Cre Spe 31/32 FWD	tgagacagtttggttagggataacagggtaatgcggataacaatttcac
SP 31/32 Spe REV	(AAAA)actagtttacttgtacagctcgtc
Gibson Assembly clonging of pSEV237-*gdhA*	
237 *gdhA* NEB fwd	GGGTGGTGCTGCAGGCATGCgagctcaggaggaaaaacatatgtctaccatgatcgaatctgtcg
237 *gdhA* NEB rev	TCTATCAACAGGAGTCCAAGtcagaccacgccctgagc
Removal of the Km^R cassette from pSEV237-*gdhA*	
SynthP_ Hind_ F	ctcaaaatctctgatgttacattgaagctt(TTTT)
SynthP_ Hind_ R	(TTTT)aagcttgttcgtgtagactttccttg
Integration plasmid for the marker replacement of PEPCK with a Sm^R cassette	
pckA-pSEVA212S-F	ATCCCCGGGTACCGAGCTCGgatgtctggaagattacttcagc
pckA-up-R	GTCAAGGTTCgtcgattcctgggccttg
pckA-SmR-F	AGGAATCGACgaaccttgaccgaacgcag
pckA-SmR-R	CTCGGCAGGCttatttgccgactaccttggtg
pckA-down-F	CGGCAAATAAgcctgccgagggcgacaac
pckA-pSEVA212S-R	AGGGATAACAGGGTAATCTGcaggtccagatgatcgcgacaagg
Integration plasmid for the in-frame deletion of PEPCK	
pckA-up-Del-R	CTCGGCAGGCtcgattcctgggccttg
pckA-down-Del-F	AGGAATCGACgcctgccgagggcgacaac
Sequencing primers around the PEPCK gene in *H. elongata*	
SeqP_ DelpckA_ fwd	gaagggcagatcaccatcac

Continued on next page

Table A.5 – continued from previous page

Oligonucleotide	Sequence $5' \rightarrow 3'$
SeqP_ DelpckA_ rev	gtcgagcagttccacggtag
Integration plasmid for the marker replacement of NADPH-ME (*maeB*) with a Sm^R cassette	
Del-maeB up-pSEVA F	ATCCCCGGGTACCGAGCtcgtccgaagggtacgcgtaccc
Del-maeB up-Sm R	GTCAAGGTTCgctgaggatccgatctgcgattc
Del-maeB up-Sm F	GATCCTCAGCgaaccttgaccgaacgcagc
Del-maeB Sm-down R	TTAAGCAGTAttatttgccgactaccttggtg
Del-maeB Sm-down F	CGGCAAATAAtactgcttaaatgcctgcacgtgc
Del-maeB down-pSEVA R	AGGGATAACAGGGTAATCTGctgcgcggcgagatacgtca
Del-maeB up-down R	TTAAGCAGTAgctgaggatccgatctgcgattc
Del-maeB up-down F	GATCCTCAGCtactgcttaaatgcctgcacgtg
Sequencing primers around the NADPH-ME (*maeB*) gene in *H. elongata*	
gHe_ M_ F	ttggacagcgggagttcg
gHe_ M_ R	aacaccgacagccagacatt
Sequencing primers around the PEPC gene in *H. elongata*	
Seq_ gHe_ P_ F	tcaccgccaagatgctcaag
Seq_ gHe_ P_ R	ctgatccaggacgacattcc
Integration plasmid for the marker replacement of GOGAT (*gltDB* genes) with a Sm^R cassette	
gltDB-pSEVA212S-F	attaccctgttatccctagaagcttTCTGGCGAATCGACTCGAG
gltDB-up-R	ggtcaaggttGTCCTGAACGTTGTTCAGG
gltDB-SmR-F	cgttcaggacAACCTTGACCGAACGCAG
gltDB-SmR-R	aggcacgtccTTATTTGCCGACTACCTTGG
gltDB-down-F	cggcaaataaGGACGTGCCTCAGCTACG
gltDB-pSEVA212S-R	gggtaatctgaattcgagctcACGCCATCGAAACCCATC
Sequencing primers around the GOGAT (**gltDB**) genes in *H. elongata*	
gHe_ GLT_ F	gaacgcagttccttgacgctg
gHe_ GLT_ R	ctcgatggcggtcgtcaa
Complementation plasmid for the *gltDB* Knockout	
338-gltDB-F	ACCTGCAGGCATGCaagcttaggaggcttcatatgaaccgaggtctccac
338-gltDB-R	TCTATCAACAGGAGTCCAAGactagtttacacatccagatagtcgagga
Integration plasmid for the replacement of GDH from *H. elongata* with *gdhA* from *P. putida*	
Sub 237gdhA - 511 F (1)	CACAGGAGGCCGCCTAGGCCcgacgaagaagaagacctcttcgccc
Sub 237ghdA - down R (2)	TAATAGAAAATTATAGCCCACTCCCCAGGCCGCGTATGTAGCGGATCCacgtgacgggcgcctccc
Sub 237-gdhA F (3)	GAGTGGGCTATAATTTTCTATTATGGAAtggcgcaaaacctttcgc
Sub 237-gdhA R (4)	GAGGTGATTGtcagaccacgccctgagc

Continued on next page

Table A.5 – continued from previous page

Oligonucleotide	Sequence $5' \rightarrow 3'$
Sub 237-gdhA up F (5)	CGTGGTCTGAcaatcacctcgactgccg
Sub 237-gdhA 511 R (6)	AGGGTTTTCCCAGTCACGACcttgtcgagctgtattgcg
Sequencing primers around the GDH gene in *H. elongata*	
Seq_ gdh_ F	catgctcacctgggcaagggatg
Seq_ gdh_ F_ new	ccagcaggtcgagaacagcttc
Seq_ gdh_ R	cgtcgacgtgattcgcgagaac
Seq_ gdh_ R_ new	gaccatgaagtcccgcgatg
Used for cloning fragments into pSEVA511CS and pSEVA211CS	
X11-31 y rev	(AAAA)cctaggattaccctgttatccctaacca
Used to determine the orientation of the cointegrates	
orient_ primer	cgccagggttttcccagtcac
Used to check for the presence of pSW-2	
pSW_ F	ggacgcttcgctgaaaacta
pSW_ R	aacgtcgtgactgggaaaac
Primers around the MCS of the pSEVA vectors	
SW16	gcctttcgttttatttgatgcct
SW17	ggatctatcaacaggagtccaag
SW18	ggctatctctagtaaggcctac
Primers around the *doeA* gene	
doeA_ fwdP	cgatattggccggtaattg
doeA_ revP	gaccacggtgacaggaatcatc
Primers around the *teaABC* operon	
teaABC_ fwdP	catctttggccctgggaac
teaABC_ revP	gtgcttgaacacgcagagg
Primers around the *ectC* gene	
ectC F	atcatcgaaaccagcggtca
ectC R	gctgcgaacaacgaaagagc

Table A.6: General composition of the MM63 minimal medium used in all growth experiments for *H. elongata* cultures. Unless stated otherwise the default components were used.

Medium component	Concentration [mM]	Condition was
KH_2PO_4, MM63 salt	100	fixed
$(NH_4)_2SO_4$, MM63 salt	15	fixed
KOH, MM63 salt	75	fixed
NaCl, MM63 salt	1000 (default)	variable
Glucose, carbon source (default)	27.75	variable
$MgSO_4 \cdot 7H_2O$, trace element	1	fixed
$FeSO_4 \cdot 7H_2O$, trace element	0.004	fixed

Table A.7: Composition of the SO_4-limited MM63 minimal medium used in the experiment comparing the ectoine production of the Leaky Mutant, *H. elongata*-PCK, and *H. elongata*-PCKMAE described in Chapter 4.2.3.

Medium component	Concentration [mM]
KH_2PO_4, MM63 salt	100
$(NH_4)_2SO_4$, MM63 salt	0.3
NH_4Cl, nitrogen source	30
KOH, MM63 salt	75
NaCl, MM63 salt	1000
Glucose, carbon source	27.75
$MgSO_4 \cdot 7H_2O$, trace element	1
$FeSO_4 \cdot 7H_2O$, trace element	0.004

Table A.8: Composition of the 15 media used for the statistical design of experiments examining the growth rate and maximum OD600 depending on NaCl, NH_4, and PO_4 concentration described in Chapter 4.1.2.

Medium	Effect	NaCl [M]	NH_4 [mM]	PO_4 [mM]	Growth rate μ [h^{-1}]	$OD600_{max}$
M1	+∗B	1.085	4.0	40.85	0.512 ± 0.030	0.335 ± 0.010
M2	center	1.085	2.33	40.85	0.502 ± 0.059	0.244 ± 0.003
M3	AC	1.629	1.34	58.18	0.480 ± 0.040	0.179 ± 0.004
M4	C	0.540	1.34	58.18	0.520 ± 0.063	0.163 ± 0.015
M5	-∗B	1.085	0.66	40.85	0.501 ± 0.030	0.095 ± 0.005
M6	-∗C	1.085	2.33	11.7	0.591 ± 0.018	0.254 ± 0.013
M7	+∗C	1.085	2.33	70.0	0.555 ± 0.053	0.219 ± 0.020
M8	ABC	1.629	3.32	58.18	0.400 ± 0.039	0.338 ± 0.009
M9	+∗A	2.0	2.33	40.85	0.469 ± 0.021	0.276 ± 0.005
M10	A	1.629	1.34	23.52	0.304 ± 0.055	0.151 ± 0.003
M11	base	0.540	1.34	23.52	0.545 ± 0.041	0.204 ± 0.011
M12	AB	1.629	3.32	23.52	0.604 ± 0.095	0.371 ± 0.008
M13	BC	0.540	3.32	58.18	0.542 ± 0.025	0.335 ± 0.008
M14	-∗A	0.17	2.33	40.85	0.332 ± 0.035	0.230 ± 0.016
M15	B	0.540	3.32	23.52	0.604 ± 0.017	0.351 ± 0.012

A.3 Basic calculations and RNA-Seq data

A.3.1 Linear regression code, ANOVA analysis, and Michaelis-Menten fit in Python

The maximum specific growth rate μ_{max} in the exponential growth phase was routinely determined by linear regression in Python. The natural logarithm ln of the *OD600 data* was fitted linearly over the process *time data* using statsmodels. The resulting slope represents μ_{max}.

```
import statsmodels.api as sm
import numpy as np
X= time data
X= sm.add_constant(X)
Y= np.log(OD600 data)
mod= sm.OLS(Y,X)
res= mod.fit()
slope= res.params[1]
intercept= res.params[0]
Rsq= res.rsquared
```

ANOVA analysis was applied to determine statistical differences between datasets. A certain *parameter* is tested within a *category* in the overall *data set*.

```
import statsmodels.api as sm
from statsmodels.formula.api import ols
import scipy.stats as stats
model= ols('parameter   C(category)',data=data set).fit()
sm.stats.anova_lm(model, typ=2)
```

A Michealis-Menten fit was performed for the saturation of *inducer concentration* (3-MB) of the XylS/Pm promoter using the scipy curve fit function.

```
import numpy as np
import scipy
x= np.array([0.0, 0.1, 1.0, 2.0]) :inducer concentration
y= :fluorescence signal
def mm_model (x,vM,kM):
return vM*x/(x+kM)
parameters, covar= scipy.optimize.curve_fit(mm_model,x,y)

def mm_model_YK (x,vM,kM,k2):
return vM*(x/(kM+x+((x*x*x)/(k2*k2))))
parameters, covar= scipy.optimize.curve_fit(mm_model_YK,x,y)
```

A.3.2 Statistical design of experiment: linear model fitting with R

The central composite design experiment was analyzed using R. A linear fit for the *growth rate data* and the *maximum OD600 data* was performed and the respective coefficients for each factor and their interactions were determined. The actual data for the growth rates and the maximum OD600 used for the fits are shown below in the source code.

```
A <- B <- C <- c(-1, +1)
design <- expand.grid(A=A, B=B, C=C)
A <- design$A
B <- design$B
C <- design$C
y <- c(0.545009,0.304367,0.603677,0.603839,0.519986,0.479886,0.542172,0.399878)
```
:growth rate data
```
y <- c(0.203544,0.150182,0.350628,0.371231,0.163377,0.17908,0.335385,0.337504)
```
:maximum OD600 data
```
linearmodel <- lm(y   A + B + C + A*B + A*C + B*C + A*B*C)
summary(linearmodel)
```

A.3.3 RNA-Seq data availability

All RNA-Seq raw FASTQ files generated in this work were uploaded to SRA (https://www.ncbi.nlm.nih.gov/sra) and can be accessed under the accession number PRJNA803715. The analysed data sets can be found in Hobmeier *et al.* [87].